Analysis of chromosomal protein-linked break repair in zebrafish and mammalian models

A thesis submitted to the University of Sheffield

for the degree of Doctor of Philosophy

By

Ringailė Zakšauskaitė

November 2017

Declaration

I hereby declare that this thesis has not been and will not be, submitted in whole or in part to another University for the award of any other degree.

Ringailė Zakšauskaitė

Acknowledgements

First, I would like thank my supervisor Prof. Sherif El-Khamisy, who managed to keep my morale high even after bad science days and was always there for me to ask any question, big or small. He inspired me throughout my PhD and helped me gain confidence as an independent scientist. I am also indebted to my co-supervisor Dr. Fredericus van Eeden, who was never too busy to help me or answer any zebrafish-related questions, and trained me in many techniques. His experience and enthusiasm have been invaluable to me during my time as a PhD student.

I would also like to express my gratitude to members of the El-Khamisy and van Eeden labs for being great and friendly teams. I would especially like to thank Jude Chiang, who has been an incredible help throughout my whole PhD, training me in many techniques, providing advice and proofreading this thesis; Ryan Beveridge, Swagat Ray, Chunyan Liao, Eleanor Markham and Stone Elworthy, who didn't mind being bombarded with my endless questions and went out of their way to help me. In addition, I would like to thank for all the help and training I received from Prof. Mark Dickman and his lab with mass spectrometry; members of the Department of Molecular Biology and Biotechnology, the Bateson Centre, the Medical School and Sheffield Institute of Translational Neurosciences, especially from Mirinda Tattan, who continued characterization of the *atm*$^{-/-}$ zebrafish model and kindly shared her results with me to use in this thesis.

I would like to thank my mum, dad and grandparents, who have always been supportive and never stopped believing in me, even when I didn't; Eric and Martin for being amazing little brothers and my friends for the patience to listen to me and for keeping my life fun and exciting throughout those years. Last but not least, I would like to thank Alex Moore for being incredible all along and helping me become a better person, professionally and personally.

Abstract

Tyrosyl-DNA phosphodiesterase 1 (TDP1) is a DNA repair enzyme, which processes damaged 3' termini arising at a variety of DNA breakage events. The most notable damaged termini are topoisomerase I cleavage complexes (TOP1-CCs). They arise when topoisomerase 1, which normally transiently nicks the DNA to relieve torsional stresses, becomes trapped on the DNA. Accumulation of such protein-linked DNA breaks (PDBs) has been linked to a number of neurodegenerative diseases, including spinocerebellar ataxia with axonal neuropathy 1 (SCAN1), ataxia telangiectasia and amyotrophic lateral sclerosis. SCAN1 results from a hypomorphic mutation of TDP1 and manifests predominantly in progressive degeneration of the cerebellum.

Tdp1$^{-/-}$ mice were generated, but did not sufficiently recapitulate the SCAN1 phenotype, leaving many questions about the mechanisms of the disease and the pathogenicity of TOP1-CCs unanswered. The main aim of this project therefore was to investigate the impact of PDB accumulation at the whole organismal level by generating and characterizing a humanized zebrafish model of SCAN1 and a *tdp1* knockout zebrafish. The *tdp1* knockout zebrafish showed a trend of locomotor deficits and a trend of topotecan hypersensitivity as adults, whereas embryos surprisingly did not exhibit either of these traits and did not have increased levels of DNA damage. In addition, my colleagues and I generated several double mutants in conjunction with *tdp1* knockout in order to study the loss of Tdp1 in an environment with increased genomic instability. We found that *tdp1*$^{-/-}$; *atm*$^{-/-}$, *tdp1*$^{-/-}$; *rnaseh2a*$^{-/-}$, *tdp1*$^{-/-}$; tg(*SOD1*^{G93R})$^{-/+}$ and *tdp1*$^{-/-}$*; tg(c9orf72*$^{(G4C2)102}$*)*$^{-/+}$ fish were viable and that *tdp1*$^{-/-}$; *atm*$^{-/-}$ fish exhibited possible female-to-male sex reversal and infertility. Finally, I studied the post-translational regulation of human TDP1 via its N-terminus. Our lab has previously identified a SUMOylation site in the N-terminus of TDP1, which promotes its accumulation at DNA damage sites. It was speculated that potential phosphorylation sites may be interacting with the nearby SUMO1 site, thus providing an extra layer of regulation. I did indeed identify such phosphorylation sites, which were suppressing the SUMOylation and interaction with LIG3 and PNK.

Table of Contents

List of Figures

List of Tables

Abbreviations

-/-	homozygous mutant
-/+	heterozygous mutant
+/+	wild-type
53BP1	p53-binding protein 1
6-4PP	6-4 photoproducts
ABC	ammonium bicarbonate
ACN	acetonitrile
AGS	Aicardi-Goutières Syndrome
ALS	amyotrophic lateral sclerosis
alt-NHEJ	alternative non homologous end-joining
amp	ampicillin
AOS1	activator of SUMO 1
AP	apurinic/apyrimidinic or abasic site
APE1	apurinic/apyrimidinic endonuclease 1
APS	ammonium persulphate
APTX	aprataxin
A-T	ataxia telangiectasia
ATLD	ataxia telangiectasia-like disorder
ATM	ataxia telangiectasia mutated
ATR	ataxia telangiectasia and rad3-related kinase
AU	arbitrary units
BER	base excision repair
BFP	blue fluorescent protein
BLM	Bloom syndrome protein
bp	base pairs
BRCA1	breast cancer-associated protein
BSA	bovine serum albumin
C9orf72	chromosome 9 open reading frame 72
Cas	CRISPR-associated protein
Cas9	CRISPR-associated protein 9
cdkI	cyclin-dependent kinase inhibitor protein
cDNA	complementary DNA
CENT2	centrin 2
ChIP	chromatin immunoprecipitation
chk1	checkpoint kinase 1
chk2	checkpoint kinase 2
CHX	cyclohexamide
CK2	casein kinase 2
c-NHEJ	canonical non homologous end-joining
CNS	central nervous system
CPD	cyclobutane-pyrimidine dimers
CPT	camptothecin

CPT-11	irinotecan (camptothecin-11) – see IRI
CRISPR	clustered regularly interspaced short palindromic repeats
crRNA	CRISPR-associated RNA
CtIP	C-terminal binding protein 1
cyclinG1	cyclin G1
D. rerio	*Danio rerio*
DAPI	4`6-diamino-2-phenylindole
dCAPS	derived cleaved amplified polymorphic sequences
ddb2	damage-specific DNA binding protein 2
ddH2O	Double-distilled water
DDR	DNA damage response
df	degrees of freedom
dH2O	Deionized water
DMEM	Dulbecco's modified Eagle's medium
DMSO	dimethylsulphoxide
DNA	deoxyribonucleic acid
DNase	deoxyribonuclease
dNTP	Deoxynucleotide triphosphate
dpf	days post-fertilization
DR	direct reversal
dRP	deoxyribosephosphate
DSB	double-strand break
DSBR	double-strand break repair
dsRED	red fluorescent protein
DTT	dithiothreitol
DUB	deubiquitinase
E.coli	*Escherichia coli*
E3	zebrafish embryo growth medium
ECL	enhanced chemiluminescence
EDTA	ethylenediaminetetracetic acid
eme1	essential meiotic structure-specific endonuclease
ENU	N-ethyl-N-nitrosourea
Exo1	Exonuclease 1
F1	first filial generation (offspring of generation 0)
F2	second filial generation (offspring of F1)
F3	third filial generation (offspring of F2)
FAT	FRAP/ATM/TRRAP domain
FATC	C-terminal FRAP/ATM/TRRAP domain
FBS	foetal bovine serum
g	relative centrifugal force
G0	generation 0
gadd45a	growth arrest and DNA damage inducible alpha
GAPDH	glyceraldehyde 3-phosphate dehydrogenase
gDNA	genomic DNA
gen1	Holliday junction 5' flap endonuclease
GFP	green fluorescent protein
GG-NER	global genome nucleotide excision repair

gkt	glaikit
gRNA	guide ribonucleic acid
Gy	gray
Gy	greys
H&E	haematoxylin and eosin
H493R	histidine 493 mutated to arginine
HEK293	human embryonic kidney 293 cell line
His	histidine
HKD	an amino acid sequence motif (HxxxxxxxKxD)
HNPCC	hereditary nonpolyposis colorectal carcinoma
hpf	hours post-fertilization
HR	homologous recombination
hsp70	heat-shock protein 70
ICL	interstrand crosslink
IDL	insertion/deletion loop
IF	immunofluorescence
IP	immunoprecipitation
IR	ionizing radiation
IRI	irinotecan – see CPT-11
IVT	in vitro transcription
K111R	lysine 111 mutated to arginine
kan	kanamycin
Kb	kilobases
KD	knockdown
kDa	kilodaltons
KO	knockout
LB	Luria-Bertani bacterial medium
LIG3	ligase 3
LP-BER	long patch base excision repair
LWT	London wild-type
MCS	multiple cloning site
MEM	minimum essential medium
MgCl2	magnesium chloride
MGMT	methyl-guanine methyltransferase
miRNA	microRNA
MMR	mismatch repair
MO	morpholino
MRE11	double-strand break repair protein MRE11
MRN	MRE11-RAD50-NBS1 complex
mRNA	messenger ribonucleic acid
MSI	microsatellite instability
MUS81	crossover junction endonuclease MUS81
myc	proto-oncogene protein myc
MYH	Mutyh
NEM	n-ethylmaleimide
NER	nucleotide excision repair
NHEJ	non-homologous end joining

NLS	nuclear localization signal
NMD	nonsense mediated decay
NRE	nucleotide repeat expansions
N-terminus	amino terminus
OD	optical density
OGG1	8-oxoguanine DNA glycosylase 1
P53	tumour protein 53
p97	ubiquitin-dependent protein segregase p97
PAGE	polyacrylamide gel electrophoresis
PAM	protospacer adjacent motif (NGG)
PARP	poly(ADP-ribose) polymerase
PARylate	Addition of a PAR moiety
PBS	phosphate-buffered saline
PCNA	proliferating cell nuclear agent
PCR	polymerase chain reaction
PDB	protein-linked DNA break
PDBR	protein-linked DNA break repair
PEI	polyethylenimine
PER	photoenzymatic repair
PG	phosphoglycolate
pH	potential of hydrogen
PHR	deoxyribodipyrimidine photolyase
PI3KK	phosphatidylinositol 3 kinase-like kinase
PI3K-like	phosphatidylinositol 3 kinase domain
PMR	photomotor response
PNK	polynucleotide kinase
Pol	polymerase
PP2Ac	protein phosphatase 2A, catalytic subunit
PTM	post-translational modification
PTU	phenylthiourea
PY	phosphotyrosyl
qPCR	quantitative polymerase chain reaction
RAD23B	Nucleotide Excision Repair Protein RAD23 Homolog B
RAD51	DNA repair protein RAD51 homolog 1
rDNA	ribosomal DNA
R-loop	DNA/RNA hybrid
RNase	ribonuclease
Rnh2a	ribonuclease H2, subunit a
RPA	replication protein A
rpm	revolutions per minute
rSAP	recombinant shrimp alkaline phosphatase
S.D.	standard deviation
S.E.M	standard error of the mean
SAM	S-adenosyl-methionine
SCAN1	spinocerebellar ataxia with axonal neuropathy 1
SDS	sodium dodecyl sulphate
SENP	Sentrin/SUMO-specific protease

shRNA	short-hairpin RNA
siRNA	silencing RNA
SMA	spinal muscular atrophy
SMUG1	single-strand selective monofunctional uracil-DNA glycosylase 1
SP-BER	short patch base excision repair
SPRTN	spartan
SSB	single-strand break
SSBR	single-strand break repair
ssDNA	single-stranded DNA
SXXA	serine XX mutated to alanine
SXXD	serine XX mutated to aspartate
T7	T7 RNA polymerase or T7 endonuclease 1
TALE	transcription activator-like effector
TALEN	transcription activator-like effector nuclease
TBB	4,5,6,7-tetrabromo-2-azabenzimidazole
TBS	tris-buffered saline
TC-NER	transcription-coupled nucleotide excision repair
TDP1	tyrosyl-DNA phosphodiesterase
TDRD3	Tudor domain-containing protein 3
TEMED	N,N,N',N'' – tetramethylethylendiamine
T_i	time elapsed at fatigue flow rate
T_{ii}	time increment
TILLING	targeting induced local lesions in genomes
TOP1	topoisomerase 1
TOP1-CC	topoisomerase 1 cleavage complexes
TPT	topotecan
TR	targeting-resistant
tracRNA	trans-acting antisense RNA
Tris	trishydroxyaminomethane
Triton X-100	polyethylene glycol octylphenyl ether
Tween-20	polyoxyethylene sorbitanmonolaurate
U	units
UBA2	ubiquitin-like modifier-activating enzyme 2
UBC9	ubiquitin- like modifier-conjugating enzyme 9
U_{crit}	critical swimming speed
U_i	highest flow rate sustained for a whole increment
U_{ii}	flow rate increment
UNG	uracil-DNA glycosylase
USP11	ubiquitin carboxy-terminal hydrolase
UV	ultra-violet
V(D)J	variable, diversity and joining recombination
WCE	whole-cell extract
WISH	whole-mount *in situ* hybridization
WT	wild-type
X^2	chi squared
XFE	XPF-ERCC1 syndrome
XLF	XRCC4-like factor

XP	xeroderma pigmentosum
XPC	Xeroderma pigmentosum, complementation group C
XPF	DNA repair endonuclease XPF
XRCC1	X-ray repair cross-complementing protein 1
γH2AX	phosphorylated histone H2A variant H2AX

1

Introduction

1.1. Introduction to genomic stability

Each living cell is constantly under attack by various genotoxins, both from external factors and from the processes within the cell itself. Cellular processes that may directly cause mutations are transcription and replication. Other vital processes, such as respiration, result in byproducts that chemically react with DNA. Environmental genotoxins can be physical, for example UV light and ionizing radiation from the sun, or chemical, such as cigarette smoke and pollutants.

Higher organisms depend on faithful transmission and maintenance of their genetic material for their development, reproduction, survival and longevity. To combat these threats and maintain genomic integrity eukaryotes have evolved sophisticated DNA damage response (DDR) mechanisms. DDR is a complex network of many different pathways involved in sensing DNA damage, activating signalling cascades, orchestrating DNA repair and cellular processes, such as DNA transactions, chromatin remodelling, cell cycle, autophagy and apoptosis (Jackson and Bartek, 2009). Defects in these processes can lead to cell death, radiosensitivity, tumorigenesis, immunodeficiency and premature ageing, which is evident from multiple diseases these deficiencies cause (Caldecott, 2008; Ciccia and Elledge, 2010; Rass et al., 2007).

This thesis will primarily focus on protein-linked chromosomal breaks, which arise from aberrant activity of DNA topoisomerases. However, a broad outline of different types and sources of DNA damage, the pathways specialized to repair them, and the diseases that arise if such repair is deficient will also be discussed.

1.2. Sources and types of DNA damage

Different sources can cause different types of damage to our genetic material, depending on the site and chemical nature of the modification. The DNA molecule can be altered in any part of its structure: the sugar phosphate backbone, bases or the glycosidic bonds between the two. Lesions on the sugar phosphate backbone can occur on one or both strands. This results in single-stranded (SSBs) or double-stranded breaks (DSBs), respectively. The most common types of DNA damage **(figure 1.1)** and the sources that cause them will be outlined in this section.

1.2.1. Base damage or loss

1.2.1.1. Oxidation

Aerobic organisms produce reactive oxygen species (ROS) as a by-product during respiration (Cooke et al., 2003). ROS are estimated to generate 50,000 lesions per cell per day (Swenberg et al., 2011). Generation of energy by oxygen reduction creates superoxide and hydroxyl radicals, hydrogen peroxide and singlet oxygen species. ROS can also be released by phagocytes during natural processes of defence against pathogens or by peroxisomes in certain circumstances. External sources of ROS include ionizing and ultraviolet radiation. The latter activates small molecules, such as tryptophan, which can then generate ROS (McCormick et al., 1976). ROS can interact with various molecules in the cell, including DNA, changing their chemical structure and properties. As well as other types of DNA damage, over 20 distinct base modifications

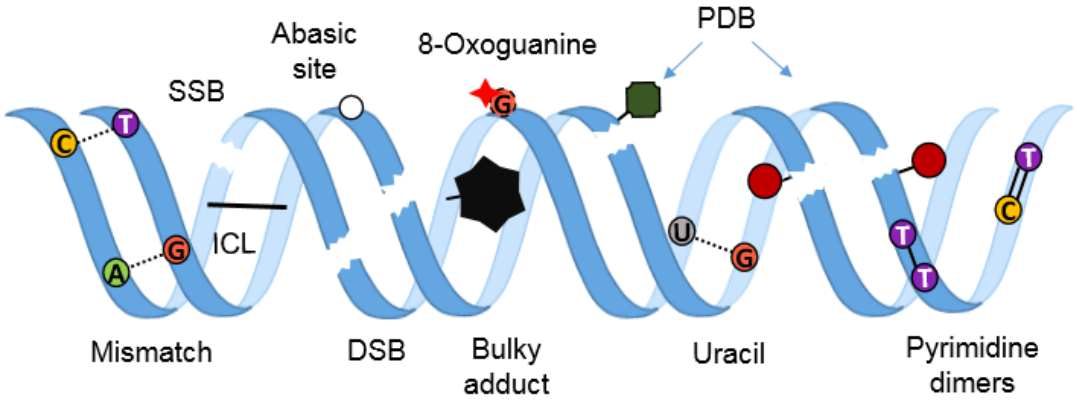

Figure 1.1. Types of DNA damage. Deviations from Watson-Crick pairing can arise during replication, when a polymerase inserts an incorrect base, or due to spontaneous deamination of cytosine (C→U), induced by UV. UV radiation can create photoproducts, such as pyrimidine dimers (T-T and C=T). Bases can be modified by oxidation (8-oxoguanine), as a result of reactive oxygen species (ROS), or methylation (bulky adduct, abasic site). Inter-strand crosslinks (ICLs) can be caused by intercalating agents, e.g. cisplatin. Single-stranded breaks (SSBs) can arise during programmed repair or enzymatic processes, which give rise to protein-linked DNA breaks (PDBs), but also as a result of ROS-induced spontaneous sugar disintegration. Enzymatic activity by proteins, such as topoisomerase 2 (TOP2), can also result in double-stranded PDBs. Another source of double-stranded breaks (DSBs) is close proximity of two antiparallel SSBs.

have been associated with oxidation, the most notable of which is 8-hydroxyguanine (Lindahl, 1993). Guanine modified in such a way preferentially pairs with adenine rather than cytosine. This can lead to the permanent replacement of 8-hydroxyguanine with a thymidine after replication, called a transversion mutation. Oxidative DNA damage has been linked to cancer, neurodegeneration, cardiovascular disease, cancer and ageing (Cooke et al., 2003).

1.2.1.2. Methylation

Another source of DNA base modification is methylation (Lindahl, 1993). S-adenosyl-methionine (SAM) is a major cofactor in enzymatic transmethylation reactions, where it acts as a methyl group donor. Such reactions occur endogenously to regulate expression of DNA by methylation of cytosine bases. SAM is intrinsically a weak alkylating agent as slow non-enzymatic transfer of its methyl group to nucleophile groups on DNA also occurs. As opposed to the enzymatic reaction, which always methylates the C5 position on cytosine (Moore et al., 2013), the non-enzymatic reaction can result in aberrant methylation of all 4 bases (Lindahl, 1993). 7-methylguanine and 3-methyladenine are the most abundant modifications. 7-methylguanine is prone to spontaneous hydrolysis, which can lead to an abasic (AP) site (Park and Ames, 1988). The methyl group in 3-methyladenine acts as a bulky lesion, blocking replication, and thus is highly cytotoxic (Rydberg and Lindahl, 1982).

1.2.1.3. Photochemical reactions

UV radiation induces photochemical lesions in two adjacent pyrimidine bases (Sinha and Hader, 2002). Cyclobutane-pyrimidine dimers (CPDs), 6-4 photoproducts (6-4PPs) and their photoisomerization products, Dewar isomers, account for all UV-induced damage. They occur at a frequency of ~75 % and ~25 % of all photoproducts (Mitchell and Nairn, 1989), respectively, and can block DNA replication and transcription (Ikehata and Ono, 2011; Sinha and Hader, 2002). In addition, CPDs containing one or two cytosines are prone to spontaneous deamination, which leads to mutagenic uracil CPDs (Ikehata and Ono, 2011). Defects in nucleotide excision repair (NER), which repairs UV-induced damage, lead to extreme photosensitivity in patients (Ciccia and Elledge, 2010).

1.2.1.4. Replication errors

Faithful eukaryotic DNA replication is attributed to the combination of DNA polymerases and mismatch repair (MMR) (McCulloch and Kunkel, 2008). In order to carry out replication with maximum precision DNA polymerases α, δ and ε have evolved high selectivity for correct base-pairing. In addition DNA polymerases δ and ε have 3'→5' exonuclease activity, which allows excision of incorrect nucleotides in parallel with replication. Most remaining misincorporated nucleotides will then be repaired by MMR. Nevertheless, incorrect bases are reported at a rate of approximately one in 3.3×10^8 per cell division (Lynch et al., 2008).

Another source of mismatches are microsatellites, which are sites that contain multiple repeated short sequences. During replication of such sequences the primer

can slip, generating heteroduplex DNA with different numbers of repeated sequences on antiparallel strands (Kunkel, 1993). This phenomenon is known as microsatellite instability (MSI) and the resulting heteroduplexes are called insertion/deletion loops (IDLs) as unpaired nucleotides can be partially extrahelical.

1.2.2. N-glycosidic bond hydrolysis

The N-glycosidic bond between the base and sugar of DNA can be cleaved by glycosylases during DNA repair, but also destabilized under certain conditions, such as heat or non-enzymatic methylation (Lindahl, 1993). Hydrolysis of this bond results in an apurinic/apyrimidinic (AP) site, which can be mutagenic and interfere with replication and transcription if unrepaired (Guillet and Boiteux, 2002; Loeb and Preston, 1986; Yu et al., 2003). Apurinic sites occur 20 times more frequently than apyrimidinic sites (Lindahl and Karlstrom, 1973). Together they are among the most common DNA lesions (Lindahl, 1993).

1.2.3. DNA backbone damage

1.2.3.1. Single-stranded breaks (SSBs)

ROS are also a major source of single-stranded breaks (SSBs) (Caldecott, 2008). ROS can either directly promote breaks in the DNA backbone by oxidizing the sugar, or indirectly through base excision repair (BER) of oxidized bases. Other base lesions can also result in SSBs through the action of BER. Another source of SSBs is aberrant topoisomerase I (TOP1) activity. TOP1 nicks one strand of DNA in order to unwind it and relieve torsional stresses during replication and transcription. The nick is created by the generation of transient covalent cleavage complexes between TOP1 and the

3’ end of DNA (TOP1-CCs). In the event of collision with transcription machinery, nearby bulky lesions or chemical inhibition TOP1-CCs can become persistent, leading to single-stranded protein-linked DNA breaks (PDBs).

SSBs arising directly from ROS have a one base gap between the broken strands (Caldecott, 2008). BER can create a gap of one to several bases as an intermediate repair product, whereas TOP1 breaks have no gap. Most SSBs have damaged termini, particularly the 3’ end. SSBs can block transcription and during replication can be converted into double-strand breaks (DSBs) due to collision with replication forks (Kuzminov, 2001). In addition, SSBs can over-activate PARP1, which depletes the cellular pool of NAD^+ and ATP, and leads to cell death (Virag and Szabo, 2002).

1.2.3.2. Double-stranded breaks (DSBs)

DSBs are produced either by the close proximity of two antiparallel SSBs within one helical turn of DNA (Hanai et al., 1998; Van Der Schans, 1978), or by collapse of replication forks due to a single SSB or other lesions. Hence, DNA damaging agents that cause a high number of SSBs along with base modifications, such as ROS and IR, are also major sources of DSBs. Programmed DSBs occur during recombination in meiosis (Keeney and Neale, 2006), during V(D)J recombination, immunoglobulin class switching and somatic hypermutations in lymphocytes (Dudley et al., 2005; Wu et al., 2003) or due to topoisomerase 2 (TOP2) activity (Nitiss, 2009). Such events are tightly controlled, but can sometimes lead to permanent DSB formation (Jackson, 2002).

The two ends of a DSB often have damaged bases and termini, and can physically dissociate (Jackson, 2002). This complicates repair and promotes inappropriate

invasion of other genomic sites, leading to chromosomal abnormalities, such as deletions, translocations and aneuploidy (Hoeijmakers, 2001; Jackson, 2002; van Gent et al., 2001). DSBs are thus the most cytotoxic out of all DNA lesions and pose a huge threat to genomic stability by promoting tumorigenesis and cell death.

1.3. DNA damage response (DDR)

1.3.1. Signal transduction

With such abundance of different types of DNA damage comes a requirement for efficient and specialized repair. A big variety of enzymes are involved in repair processes: nucleases, glycosylases, phosphatases, kinases, ligases, topoisomerases and polymerases, to name just a few (Ciccia and Elledge, 2010). The activities of all repair factors require tight regulation due to their potential to cause harm to the DNA. Complex signal transduction pathways provide such regulation with phosphatidylinositol 3 kinase-like kinase (PIKK) and poly(ADP)ribose polymerase (PARP) family proteins at the very core.

PARP proteins are activated by SSBs resulting from IR, ROS or BER (Caldecott, 2008). PARP1 senses SSBs and DSBs through three of its zinc-finger DNA binding motifs and together with PARP2 uses NAD^+ to generate PAR chains on its substrates within seconds of DNA damage (Ciccia and Elledge, 2010; Rouleau et al., 2010). Targets of PARP1 and PARP2 include histones H1 and H2B, PARylation of which promotes recruitment of chromatin remodelling and DNA repair factors, and PARP1 itself (Ciccia and Elledge, 2010). PAR chains act as temporary docking stations for localization of required factors before their disassembly by PAR hydrolyzing enzyme

PARG. Although less is known about other PARP family proteins, PARP3 has been implicated in DSB repair (Rulten et al., 2011), telomere maintenance and mitotic spindle stabilization (Beck et al., 2014; Boehler et al., 2011).

PIKK family kinases involved in DDR are Ataxia Telangiectasia Mutated (ATM), Ataxia Telangiectasia and Rad3-related kinase (ATR) and DNA-dependent protein kinase (DNA-PK). ATM is a highly pleiotropic kinase with hundreds of substrates, whereas DNA-PK mainly phosphorylates factors in the DSB end-joining pathway. Both ATM and DNA-PK are activated by genotoxins, which generate DSBs (Harper and Elledge, 2007; Meek et al., 2008). ATM is first recruited to replication protein A (RPA)-coated single-stranded DNA (ssDNA) at stalled replication forks and DSBs and then activated. ATM and ATR are involved in non-homologous end joining (NHEJ), homologous recombination (HR), interstrand crosslink (ICL) repair, nucleotide excision repair (NER) and maintenance of replication forks during replication stress and normal conditions. ATM also regulates TDP1-mediated SSBR by phosphorylating TDP1 and promoting repair of TOP1-CCs through a TDP1-independent mechanism (Alagoz et al., 2013; Chiang et al., 2010; Das et al., 2009; Katyal et al., 2014). Phosphorylation of targets is achieved either directly by ATM/ATR, or indirectly through different kinases, including checkpoint kinase 1 (CHK1), checkpoint kinase 2 (CHK2) and casein kinase 2 (CK2) (Ciccia and Elledge, 2010).

In addition to PARylation and phosphorylation, DDR utilizes other post-translational modifications (PTMs), including ubiquitination, SUMOylation, acetylation and methylation (Dantuma and van Attikum, 2016). PTMs are the primary mechanism of DDR regulation due to its quick effects, but transcriptional regulation is also used

(Ciccia and Elledge, 2010). The most documented example of transcriptional regulation is through the p53 transcription factor. P53 is phosphorylated by ATM and CHK2 in response to DSBs and promotes cell cycle arrest, senescence or apoptosis. It can also activate DNA repair, for example the NER pathway. Utilizing a vast array of PTMs and transcription factors, DDR orchestrates not only DNA repair, but also apoptosis, cell-cycle arrest, differentiation, immunity and melanin production (Ciccia and Elledge, 2010; Shiloh, 2003).

Defective DDR signalling can be highly detrimental. For example, mutations of ATM in humans cause ataxia telangiectasia (A-T), a syndrome with progressive neurodegeneration, immunodeficiency, radiosensitivity and predisposition to cancer (Khanna et al., 2001).

1.3.2. DNA repair

1.3.2.1. Mismatch repair (MMR)

As discussed in section **1.2.1.4**, deviations from Watson-Crick base pairing can occur due to incorrect insertion of bases by DNA polymerases or microsatellite instability (MSI) during replication. Such mismatches in newly synthesized DNA are normally removed by mismatch repair (MMR) proteins to allow polymerases another chance at correct template synthesis (Jiricny, 2006). MMR largely increases the fidelity of replication as mismatches are often mutagenic, which has led to high conservation of its mechanisms across species.

Mismatched bases create distortions in the helical structure of DNA, which in mammals are sensed by the MutSα (MSH2-MSH6) or MutSβ (MSH2-MSH3)

heterodimer (Kunkel and Erie, 2005). Recruitment of MutSα to the mismatch is promoted by the interaction of MSH2 with PCNA and replication factor C (RFC) (Lau and Kolodner, 2003). Binding of MutS to the mismatch recruits MutL12 heterodimer MutLα (MLH1-PMS2), MutLβ (MLH1-PMS1) or MutLγ (MLH1-MLH3) (Kunkel and Erie, 2005). MutLα nicks the faulty strand on either side of the mismatch. PCNA and RFC also interact with MutLα, promoting its endonuclease activity. Exonuclease 1 (Exo1) carries out resection until the mismatch is removed in both 5'→3' and 3'→5' direction (Genschel et al., 2002), but the latter also requires PCNA (Guo et al., 2004). The resulting ssDNA is then covered with RPA, displacing the MMR proteins MutSα and MutLα (Jiricny, 2006; Lau and Kolodner, 2003). This in turn promotes gap-filling by Polδ and ligation by DNA ligase 1 (LIG1) (Zhang et al., 2005). It is thought that single base Watson-Crick and IDL mismatches are primarily repaired by MutSα, whereas longer IDLs with up to 16 additional nucleotides are mostly repaired by MutSβ (Kunkel and Erie, 2005).

MMR is important in meiosis and mitosis, DDR signalling, apoptosis, class-switch recombination and somatic hypermutation (Jiricny, 2006). Deficiencies in MMR cause microsatellite instability and hereditary nonpolyposis colorectal carcinoma (HNPCC) in humans (Ciccia and Elledge, 2010; Jiricny, 2006).

1.3.2.2. Nucleotide excision repair (NER)

The NER pathway is responsible for the repair of a wide array of structurally unrelated bulky lesions, including CPDs and 4-6PP photoproducts, ICLs and cyclopurines, induced by ROS (Marteijn et al., 2014). Such versatility in NER is achieved by recognition of common features between these lesions rather than the

differences. Bulky lesions can distort the DNA helix in transcriptionally silent genomic sites and block RNA polymerases during transcription. This has led to two distinct NER pathways: global genome NER (GG-NER), which scans the whole genome for such lesions, and transcription-coupled NER (TC-NER), which is activated by stalled RNA polymerase 2 (RNA Pol2).

The main differences between GG-NER and TC-NER happen at the damage recognition level (Marteijn et al., 2014). Distortions of the helical structure in GG-NER are recognized by XPC, RAD23B and centrin 2 (CENT2) complex. XPC probes the DNA and binds an ssDNA gap, a result of the distorted DNA helix antiparallel to the lesion. In TC-NER, on the other hand, stalled RNA Pol2 is recognized by its interaction with CSB, CDSA and XAB2. After the recognition step, GG-NER and TC-NER converge, both recruiting the transcription factor II H (TFIIH) complex. The DNA helix around the lesion is then opened up bidirectionally by helicases XPB and XPD, which are part of the TFIIH complex and have 3'→5' and 5'→3' activity, respectively. RPA coats the intact strand, but is later displaced together with TFIIH complex by XPA. XPA recruits XPF-ERCC1 (5') and XPG endonucleases (3') for excision of 22 – 30 nucleotides around the lesion. The remaining gap is filled and sealed by Polδ, Polε or Polκ and LIG1 or XRCC1-LIG3 with the help of PCNA and RFC.

Defects in NER genes cause Cockayne syndrome, xeroderma pigmentosum, XPF-ERCC1 (XFE) syndrome and trichothiodystrophy (Ciccia and Elledge, 2010; Marteijn et al., 2014). Symptoms generally include photosensitivity, premature ageing and neurological problems, such as neurodegeneration, hypomyelination and microcephaly.

1.3.2.3. Base excision repair (BER)

Small base modifications, such as oxidation or methylation, which do not distort the DNA double helix are usually repaired by the base excision repair pathway (BER) (Dianov et al., 2017). BER has two sub-pathways, depending on the number of nucleotides being replaced (Hakem, 2008). Short-patch BER (SP-BER) usually corrects a single nucleotide, whereas 2 – 13 nucleotides are replaced in long-patch BER (LP-BER). It is thought that SP-BER is the preferred mechanism.

Base modifications are recognized and removed by 11 different damage-specific glycosylases, such as 8-oxoguanine DNA glycosylase 1 (OGG1) and Mutyh (Myh) **(figure 1.2)** (Dianov et al., 2017). Glycosylases can be mono- or bifunctional. Monofunctional glycosylases can only remove the damaged base, whereas bifunctional glycosylases can also incise the backbone. If the glycosylase does not generate a nick, it recruits apurinic/apyrimidinic endonuclease 1 (APE1) in complex with X-ray cross-complementing protein 1 (XRCC1) to fulfil this function. A single-stranded break with damaged termini is thus generated. APE1 generates 3'-hydroxyl (3'-OH) and 5'-deoxyribosephosphate (5'-dRP) termini, whereas cleavage by bifunctional glycosylases with or without β-lyase activity leaves 3'-α, β unsaturated aldehyde or 3'-P ends, respectively. At this point its repair converges with the SSB repair (SSBR) pathway, discussed in the next section.

It is thought that mechanisms for combatting ROS-induced DNA damage, such as BER, become less efficient with age (Wallace, 2014). This in turn leads to accumulation of damage, transcription problems and eventually age-related diseases, such as cancer and neurodegeneration. It was indeed found that OGG1

activity declines in an age-related fashion in human lymphocytes (Chen et al., 2003b) and that several BER factors had decreased expression and activity in Alzheimer's patients (Jacob et al., 2013; Sliwinska et al., 2017; Weissman et al., 2007). In agreement with these findings, *Ogg1*$^{-/-}$ mice accumulated oxidative DNA damage in their liver over time (Osterod et al., 2017). Lymphomas were also observed in aged uracil-DNA glycosylase (UNG) deficient mice, which were exacerbated by the additional deletion of single-strand selective monofunctional uracil-DNA glycosylase 1 (SMUG1) (Wallace, 2014).

1.3.2.4. Single-strand break repair (SSBR)

PARP1 senses SSBs, as discussed in **section 1.3.1**, and recruits end-processing factors together with the XRCC1 scaffold protein **(figure 1.2)** (Caldecott, 2008; Dianov et al., 2017). SSBs, resulting from base excision, TOP1 cleavage or directly from ROS insult, have a variety of damaged ends. Such DNA ends first require processing into a 5'-phosphate (5'-P) and 3'-OH groups before gap filling and ligation can commence.

There are 5 known end-processing factors: APE1, PNK, POLβ, TDP1 and APTX, some of which have overlapping functions. For example, APE1 can process both 3'-α, β unsaturated aldehyde and 3'-P termini, arising from BER, as well as ROS-induced 3'-phosphoglycolate (3'-PG) ends (Izumi et al., 2000). Polynucleotide kinase/phosphatase (PNK) repairs 3'-P ends (Habraken and Verly, 1988; Jilani et al., 1999), which can arise during BER, but also from spontaneous hydrolysis of oxidized bases or during TOP1-CC processing. APE1-generated 3'-OH and 5'-dRP termini are removed by POLβ (Podlutsky et al., 2001). In addition, tyrosyl-DNA phosphodiesterase 1 (TDP1) can process 3'-phosphotyrosyl (3'-PY), 3'-PG and 3'-dRP

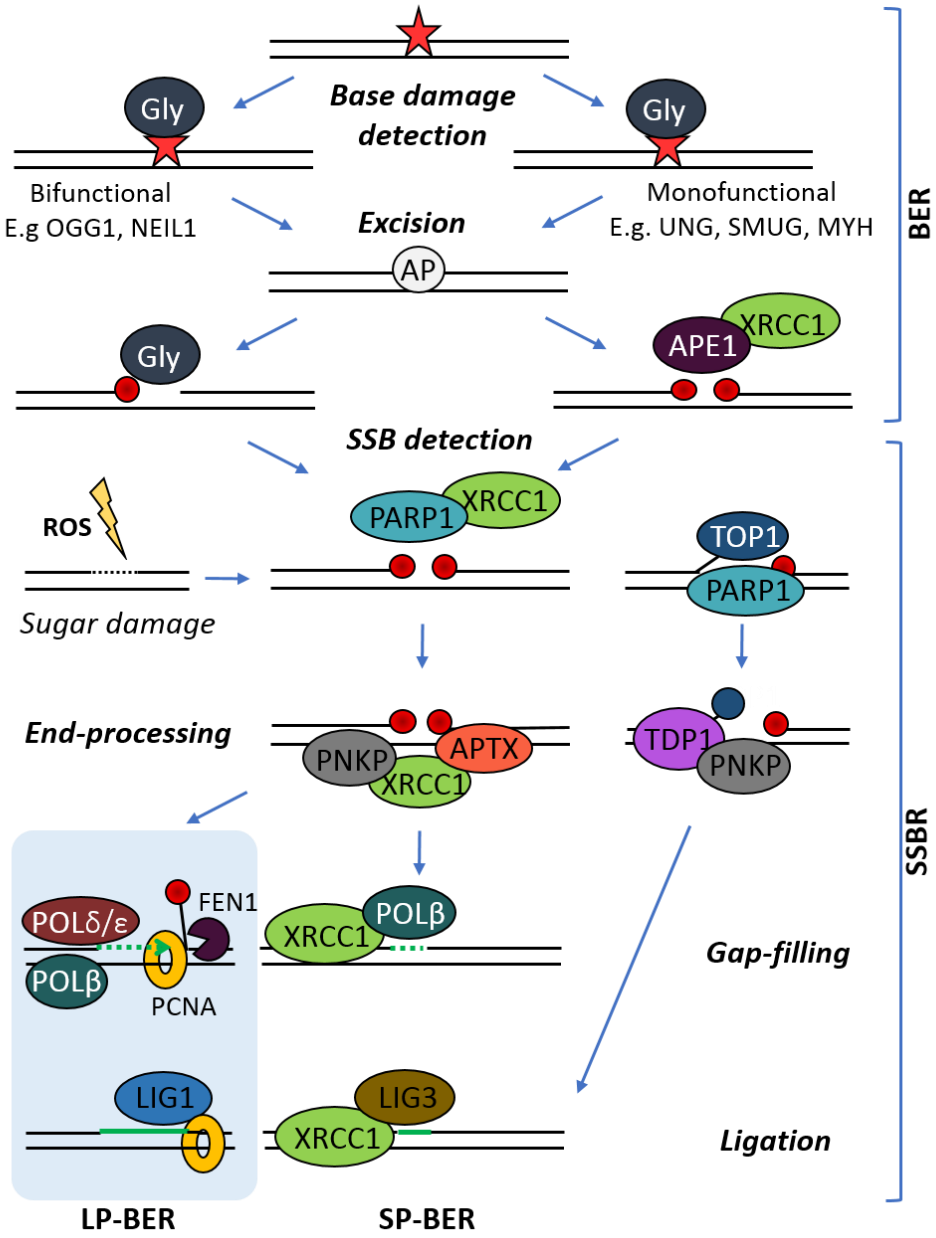

Figure 1.2. Base excision repair and single-strand break repair pathways. A non-bulky damaged base (red star) is detected and excised by glycosylases, leaving an abasic (AP) site. Bifunctional glycosylases (left) then nick the DNA backbone to create a single strand break with a damaged 3' terminus (red circle). Monofunctional glycosylases recruit APE1-XRCC1 complex to nick the DNA backbone, leaving both termini damaged. PARP1, in complex with XRCC1 then detects these BER-induced SSBs along with ROS-induced direct SSBs, resulting from disintegration of oxidized deoxyribose, and TOP1-induced SSBs. End-processing by PNKP, APTX and TDP1 (in the case of TOP1-SSBs) takes place, producing 5'-P and 3'-OH groups, suitable for extension by POLβ and ligation by LIG3 during short-patch BER (SP-BER). If 5' ends are resistant to POLβ lyase activity, long-patch BER (LP-BER) is initiated by 5'→3' synthesis (POLβ, δ and/or ε) of 2-12 nucleotides, creating a 5' flap structure. FEN1 cleaves the flap with the help of PCNA and PARP1. Adapted from Caldecott, 2008 and Dianov and Hubscher, 2013.

moieties into 3'-P (Davies et al., 2002; Interthal et al., 2005a; Lebedeva et al., 2011; Murai et al., 2012; Zhou et al., 2005), which are then suitable for final repair by PNK. In a similar fashion, aprataxin (APTX) can remove 5'-AMP ends, which arise due to abortive DNA ligation and can interfere with replication and transcription (Ahel et al., 2006).

If the termini have been processed, gap-filling of a single nucleotide by POLβ (SP-BER) then takes place (Caldecott, 2008). If the 5'dRP is resistant to lyase activity of POLβ due to oxidization, LP-BER is initiated by POLβ, POLδ and/or POLε. Extra 2-12 nucleotides are synthesized in 5'→3' direction to create a flap structure, which is then removed by flap endonuclease 1 (FEN1) with the help of PARP1 and PCNA. LP could also be preferentially chosen during S-phase (Mjelle et al., 2015). Finally, the two ends are ligated by LIG3α after SP-BER or, usually, by LIG1 after LP-BER (Caldecott, 2008).

In contrast to defects in BER-specific factors, which have been linked to neurodegeneration, cancer and ageing **(section 1.3.5)**, defects in TDP1, PNK and APTX cause predominantly neurological phenotypes (Ciccia and Elledge, 2010; Dumitrache and McKinnon, 2017). In humans, mutations of *TDP1* and *APTX* lead to spinocerebellar ataxia with axonal neuropathy 1 (SCAN1) (El-Khamisy et al., 2005; Interthal et al., 2005b; Takashima et al., 2002) and ataxia oculomotor apraxia 1 (AOA1) (Date et al., 2001; Moreira et al., 2001), respectively. Mutations of *PNKP* in different loci lead to MCSZ (microcephaly, early onset, intractable seizures and developmental delay) syndrome (Reynolds et al., 2012; Shen et al., 2010), microcephaly with neurodegeneration and polyneuropathy (Poulton et al., 2013) or

ataxia oculomotor apraxia 4 (AOA4) (Bras et al., 2015; Dumitrache and McKinnon, 2017).

1.3.2.5. Double-strand break repair (DSBR)

Repair of DSBs is more complex than repair of other lesions, as in a DSB two DNA molecules are involved, which may physically dissociate from each other (Chiruvella et al., 2013). In addition, there is a danger of inappropriate coupling of such ends, which can lead to mutations and rearrangements.

There are two major DSBR pathways: non-homologous end joining (NHEJ) and homologous recombination (HR) (Jackson, 2002). As suggested in the titles, the choice of pathway depends on the availability of homologous DNA. DNA is replicated in the S-phase of the cell cycle, providing a homologous sister chromatid for HR through to the end of the G2-phase, until mitosis is initiated. During the rest of the cell cycle and in post-mitotic cells NHEJ is the only mechanism available for DSBR. Nevertheless, during late S and G2-phases, when both pathways are available, the complexity of damage and the local chromatin structure can determine the pathway choice (Kakarougkas and Jeggo, 2014).

1.3.2.5.1. Non-homologous end joining (NHEJ)

In mammalian cells, over 90 % of DSBs are thought to be repaired by NHEJ (Hakem, 2008). In addition, NHEJ factors are required for V(D)J recombination and class-switch recombination (CSR) (Chiruvella et al., 2013).

There are three main steps of NHEJ: DSB end tethering, end-processing and ligation (Lees-Miller and Meek, 2003). In canonical NHEJ (c-NHEJ) Ku70/Ku80 heterodimer

binds, stabilizes and aligns the two ends of the DSB. Ku70/Ku80 then recruits DNA-PK by interaction with its catalytic subunit DNA-PKcs. DNA-PK stabilizes the break by binding the DSB ends and prevents endonucleolytic cleavage. End-processing factors, such as artemis, are then recruited to prepare end compatible for ligation by Xrcc4-Lig4 and Xrcc4-like factor (XLF).

Although c-NHEJ can promote small deletions due to the potential requirement for end resection, an alternative NHEJ (alt-NHEJ) has emerged, which is more error-prone (Chiruvella et al., 2013). It has been suggested that alt-NHEJ may be the primary source of genomic translocations in mammals (Simsek and Jasin, 2010).

C-NHEJ defects in humans compromise V(D)J recombination and CSR in lymphocytes, leading to severe immunological deficiencies, and cause hypersensitivity to genotoxins, such as IR (Kasparek and Humphrey, 2011). In addition, alt-NHEJ is increased, which leads to aberrant end joining and mutagenic translocations.

1.3.2.5.2. Homologous recombination (HR)

DSBs arising in late S2 and G2-phases are sensed and stabilized by the MRN complex, consisting of MRE11, RAD50 and NBS1 **(figure 1.3)** (Ciccia and Elledge, 2010). MRE11 binds both ends of the DNA, displacing Ku70/80 to prevent NHEJ, while RAD50 tethers the ends. NBS1 causes ATM autophosphorylation, which activates the kinase. ATM first phosphorylates histone H2AX and multiple other downstream targets, including 53BP1 and BRCA1, promoting recruitment of DSBR factors and chromatin reorganization. ATM signalling also initiates 5'→3' DNA end resection by MRE11, C-terminal-binding protein-interacting protein (CtIP), DNA2 nuclease/helicase, Bloom syndrome helicase (BLM) and EXO1 (Liu and Huang, 2016). During resection RPA

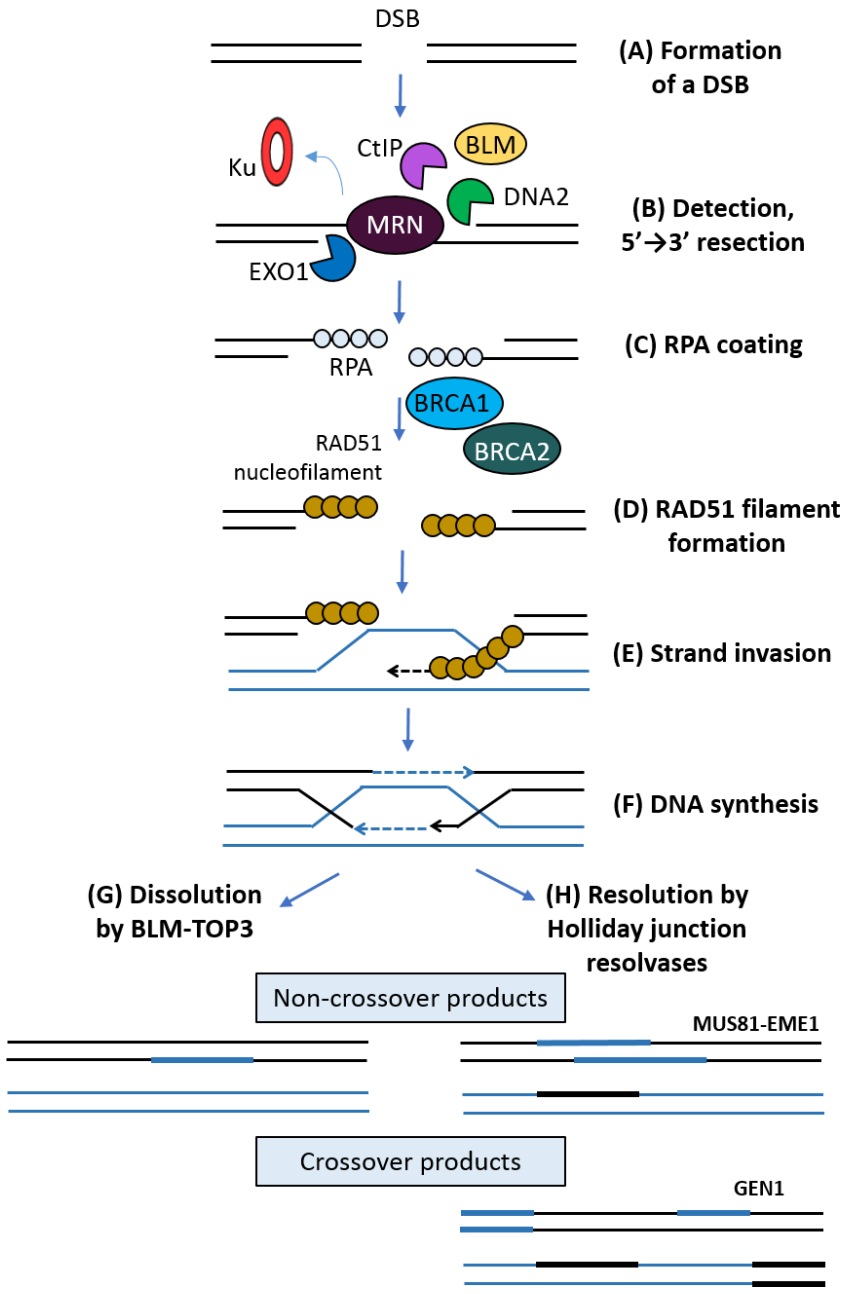

Figure 1.3. Double-strand break repair (DSBR) by homologous recombination (HR). (A) The DSB is formed by the proximity of two SSBs or due to the collapse of replication machinery. **(B)** The lesion is sensed by the MRN (MRE11-RAD50-NBS1) complex, which binds both DNA ends through MRE11 displacing NHEJ factor Ku. NBS1 then activates ATM (not shown), which then initiates DDR signalling and promotes recruitment of downstream factors. 5'→3' resection is carried out by EXO1, CtIP, DNA2 and BLM. **(C)** RPA coats 3' ssDNA overhangs. **(D)** RAD51 nucleofilament is formed with the help of mediator proteins, such as BRCA1 and BRCA2. **(E)** RAD51 nucleofilament initiates homology searching and strand invasion, forming a D-loop structure. **(F)** DNA polymerases synthesize missing DNA using sister chromatids as templates. D-loop is either resolved by BLM-TOP3 into non-crossover products **(G)** or resolved by resolvases into non-crossover (by crossover junction endonuclease MUS81 and essential meiotic structure-specific endonuclease 1 (EME1) complex) or crossover (by Holliday junction 5' flap endonuclease (GEN1))

coats the exposed ssDNA to prevent the formation of secondary structures and initiates homology searching (Ciccia and Elledge, 2010). RAD54 together with RAD51 nucleofilaments facilitate strand invasion, which results in Holliday junction formation. Repair is then carried out by DNA polymerases, using the sister chromatid as a template. LIG1 ligates the nicks, creating a double Holliday junction. Finally, the double Holliday junction is either resolved into crossover products by a resolvase (meiosis) or dissolved into noncrossover products by the BLM/TOP3 complex (mitosis). HR leads to error-free repair (Heyer et al., 2010).

HR repairs only ~10 % of DSBs in mammals (Hakem, 2008). Nevertheless, defects in the MRN complex lead to severe implications for human health, such as AT-like disorder (ATLD) and Nijmegen breakage syndrome (NBS). ATLD results from hypomorphicmutations of MRE11 and manifests in immunodeficiency and progressive neurodegeneration, similarly to AT (Delia et al., 2004). However, ATLD symptoms are milder than those of AT and do not include telangiectasia of the eye.

1.4. DNA Topoisomerases

Most cellular processes that manipulate DNA, such as replication, transcription, recombination and chromatin remodelling, create supercoiling of the intertwined double helical structure (Ashour et al., 2015). DNA topoisomerases are enzymes, which resolve such topological entanglements and allow cellular processes to continue. They are able to carry out this function by transiently nicking one strand of the DNA backbone, which allows the passage of one strand against the other, or by creating a DSB, which allows duplex DNA to pass through (Champoux, 2001).

Topoisomerases are conserved from prokaryotes to eukaryotes and essential to life in vertebrates and flies (Forterre et al., 2007; Pommier et al., 2006).

Some topoisomerases can relieve only negative supercoiling, whereas some can relax supercoiling of both directions (positive and negative) (Champoux, 2001). There are also topoisomerases, which can create supercoils of either direction.

Three different types of topoisomerases are found in humans: type IA (TOP3α and TOP3β), IB (nuclear and mitochondrial TOP1) and IIA (TOP2α and TOP2β) (Pommier et al., 2016). Type I enzymes cleave one DNA strand, while both strands are broken by members of the type IIA group. They are further classified, depending on whether they break DNA by forming a covalent linkage with its 5' (type IA and IIA) or 3' (type IB) end.

1.4.1. Topoisomerase mechanism of action

Topoisomerases bind DNA and their active site tyrosine residue initiates nucleophilic attack of the scissile phosphate residue of the DNA in a transesterification reaction (Champoux, 2001). This breaks the DNA backbone and creates a covalent phosphodiester bond between the tyrosine residue of the enzyme and phosphate residue of the DNA. The generated gaps in the DNA allow passage or rotation of DNA strands or duplexes. The topoisomerase is released when the hydroxyl group, generated on the other side of the nick by the transesterification reaction, deprotonates the phosphotyrosine and restores phosphodiester linkage of the DNA backbone.

1.4.2. Topoisomerase functions

As transcription machinery passes along DNA, it generates positive supercoils downstream and negative supercoils upstream (Wu et al., 1988). Positive supercoiling reduces the speed at which RNA polymerases can travel. On the other hand, negative supercoiling of DNA may cause it to hybridize to the nascent RNA, leading to a hybrid of two DNA strands (template and displaced strand) and one RNA strand, called an R-loop (Aguilera and Garcia-Muse, 2012). Highly repetitive long genes, such as those coding for ribosomal DNA (rDNA), may be especially prone to this phenomenon (Garg et al., 1987). R-loops interfere with RNA elongation and replication fork progression, posing a threat to genome stability, causing mutations and chromosome rearrangements or loss (Ashour et al., 2015). Both TOP1 and TOP2 were implicated in ensuring successful transcription of rDNA genes by preventing R-loop formation (El Hage et al., 2010; French et al., 2011). In addition, TOP3β together with Tudor domain-containing protein 3 (TDRD3) was shown to suppress R-loop formation and reduce chromosomal translocations (Yang et al., 2014). In addition, topoisomerases play a crucial in driving the expression of long genes (Ashour et al., 2015).

As well as being major players in transcription, topoisomerases are also important in relieving DNA replication-related supercoiling, replication initiation and chromatin remodeling (Pommier et al., 2016).

The main function of DNA topoisomerases is to facilitate topological changes in DNA through breaking and resealing DNA strands in all cells. In contrast SPO11, a type IIB topoisomerase homologue, is expressed only in germ cells with the function of

generating programmed DSBs to facilitate recombination in meiosis (Pommier et al., 2016). Recently a couple more non-canonical roles of topoisomerases have emerged. TOP3β was shown to also serve as an RNA topoisomerase and has been found in polyribosomes (Ahmad et al., 2016; Stoll et al., 2013; Xu et al., 2013). Although the physiological significance of these findings remains unclear, it is thought it may be important for processing long RNA transcripts and relieve torsional stresses during translation. It was also found that TOP1 cleaves ribonucleotides, misincorporated into DNA. Such enzymatic cleavage could serve as a signal for the MMR pathway, but this function is up to debate (Pommier et al., 2016).

1.5. Tyrosyl-DNA phosphodiesterase 1 (TDP1)

Although normally a transient event, TOP1-mediated SSBs can become permanent if they collide with replication or transcription machinery or are close to DNA lesions **(figure 1.4)** (El-Khamisy and Caldecott, 2006). This results in TOP1 cleavage complexes (TOP1-CCs), which interfere with transcription and replication. TOP1-CCs can be repaired by TDP1, an SSBR end-processing factor capable of cleaving the phosphodiester bond joining TOP1 and DNA.

TDP1 is a member of the phospholipase D family, bearing two catalytic HKD (HXK(X)4D(X)6GSXN) motifs (Interthal et al., 2001). To resolve TOP1-CCs human TDP1 first utilizes histidine 263 to initiate nucleophilic attack of the scissile phosphate and histidine 493 to protonate the tyrosyl group (Davies et al., 2003; Interthal et al., 2001). This results in the release of TOP1 from the DNA and a temporary TDP1-DNA complex joined via a phosphohistidine (H263) bond. Next, the H493R residue

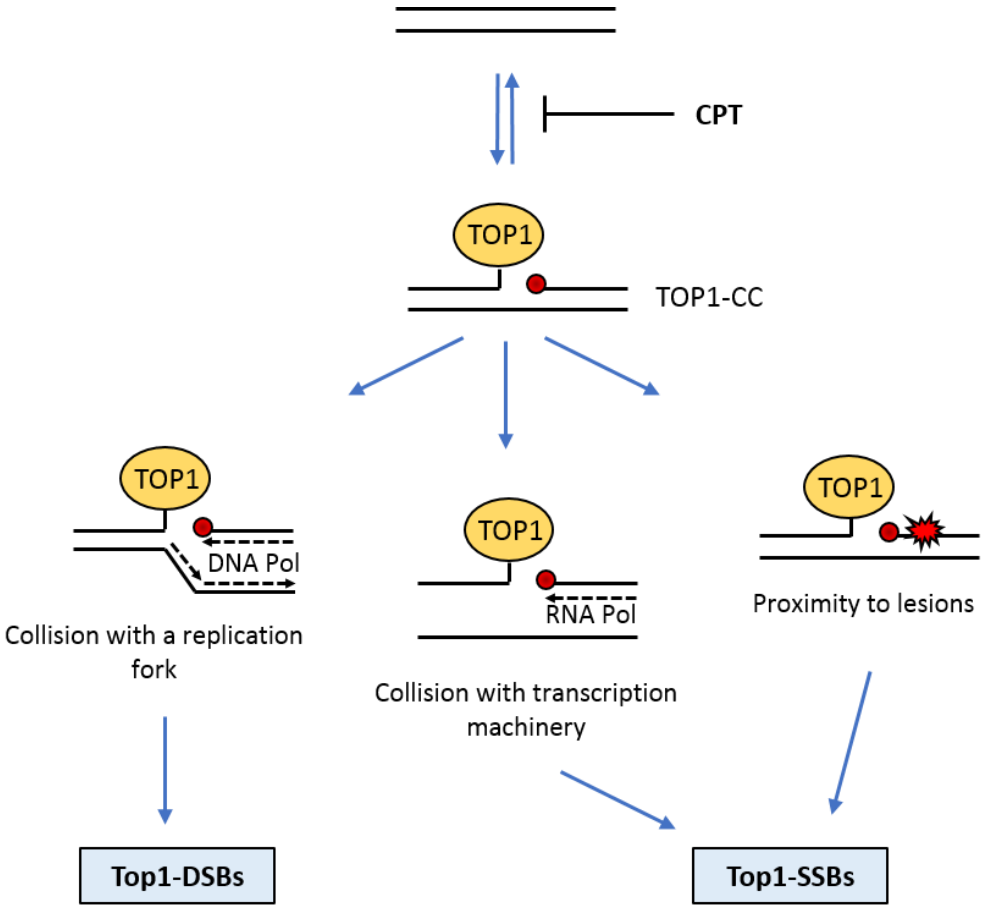

Figure 1.4. Model for generation of SSBs and DSBs from TOP1-CCs. TOP1 transiently nicks the DNA to relieve topological entanglements by creating a transient reversible TOP1 cleavage complex (TOP1-CC). TOP1-CCs can become irreversible due to TOP1 poisons, such as camptothecin (CPT), which inhibit the ligation step, due to collision with replication or transcription machinery, or due to proximity of TOP1-CC to lesions, such as SSBs or abasic sites. Adapted from El-Khamisy and Caldecott, 2006.

activates a water molecule, which promotes hydrolysis of the phosphohistidine linkage and frees TDP1 from DNA.

In addition to removing 3'-phosphotyrosyl (3'-PY) moieties, TDP1 has also been shown to process oxidation-induced 3'-PG, alkylation-induced 3'-dRP termini and 3'-phosphoamide termini, such as those resulting from TDP1-mediated TOP1-CC repair (Inamdar et al., 2002; Interthal et al., 2005a; Zhou et al., 2009). Moreover, TDP1 exhibits limited 3'-exonuclease activity for both DNA and RNA substrates (Interthal et al., 2005a). It can promote the removal of one nucleotide from the 3'-OH terminus.

1.5.1. Spinocerebellar ataxia with axonal neuropathy 1 (SCAN1)

A recessive mutation of *TDP1* active site histidine 493 into arginine has been found in patients with spinocerebellar ataxia with axonal neuropathy 1 (SCAN1) (Takashima et al., 2002). SCAN1 is a late childhood onset progressive neurodegenerative disease. It predominantly affects the cerebellum and peripheral nerves, resulting in a gradual onset of ataxic gait and loss of sensation in the extremities, such as touch, pain and vibration sensation. As neurodegeneration progresses it manifests in areflexia (loss of reflexes), nystagmus (uncontrollable eye movements), dysarthria (speech impediment) and *pes cavus* (high arched feet), which eventually leads to loss of walking ability. Borderline hypoalbuminemia, mild hypercholesterolaemia and seizures have also been observed (Takashima et al., 2002).

TDP1^{H493R} mutation not only reduces TDP1 activity by approximately 25-fold, but also causes TDP1 to become trapped on DNA as it attempts to repair TOP1-CCs through a covalent TDP1-DNA intermediate with a half-life of 13 minutes (Hirano et al., 2007;

Interthal et al., 2005b). Wild-type TDP1 is capable of cleaving the phosphoamide linkage between TDP1^{H493R} and DNA, which means two alleles of the *TDP1^{H493R}* are required for pathogenicity (Interthal et al., 2005b).

Unlike other DNA damage repair diseases, SCAN1 does not lead to immunodeficiency, mental retardation, predisposition to cancer or photosensitivity (de Boer and Hoeijmakers, 2000; Takashima et al., 2002). SCAN1 was the first disease associated with protein-linked DNA breaks (PDBs), but since more neurodegenerative diseases have been shown to accumulate PDBs, such as ataxia telangiectasia (A-T) (Katyal et al., 2014), amyotrophic lateral sclerosis (ALS) (Walker et al., 2017) and spinal muscular atrophy (SMA) (Karyka and El-Khamisy, unpublished). Although PDBs are clearly pathogenic, it is not known whether they are causative of the neurological demise, or whether they are just a secondary pathology.

1.5.2. Neuroprotective role of TDP1

When *TDP1^{H493R}* mutation was first discovered in SCAN1 patients, it was thought that loss of TDP1 function was the causative factor in the disease. Since, *Tdp1$^{-/-}$* mice have been generated exhibiting little to no phenotype at all, prompting to reconsider this hypothesis (Hawkins et al., 2009; Hirano et al., 2007; Katyal et al., 2007). Although the role of TDP1 in processing TOP1-CCs is undisputed, the physiological consequences of TDP1 loss appear to be minimal in unperturbed conditions. It is thus now thought that either the TDP1-DNA complexes alone contribute to SCAN1 pathology (Hirano et al., 2007) or together with the unrepaired TOP1-CCs, due to reduced TDP1 activity **(figure 1.4)** (Interthal et al., 2005b).

1.5.3. Clinical significance of TDP1

Topoisomerase 1 poisons, such as topotecan and irinotecan, are widely used in chemotherapy. However, some cancer cells can upregulate TDP1 activity or expression, which complicates treatment using TOP1 inhibitors (Jakobsen et al., 2015; Liu et al., 2007). The apparent lack of toxicity in unperturbed TDP1 deficient cells and animal models makes TDP1 an attractive target for inhibition along with TOP1 (Alagoz et al., 2014; Hawkins et al., 2009; Hirano et al., 2007; Katyal et al., 2007). Additional inhibition of TDP1 should potentiate the effect of TOP1 poisons in cancerous cells due to the negative effect of increased TOP1-CCs on replication, whilst being less harmful to healthy more slowly dividing cells (Pommier et al., 2016). Multiple attempts have been made to generate TDP1 inhibitors, such as vanadate, but they have been either not sufficiently specific or effective to reach clinical trial stage (Ashour et al., 2015; Huang et al., 2011b).

1.6. Zebrafish as a model organism

The zebrafish, *Danio rerio*, is a vertebrate increasingly used in all fields of research, including developmental, cardiovascular, cancer and neurological studies (Amsterdam et al., 2004; Santhakumar et al., 2012; Stainier et al., 1996; Ziv et al., 2013). It is a freshwater teleost fish, native to the Himalayan region (Mayden et al., 2007). Zebrafish offer many advantages over traditional models, such as cost-effectiveness, high fecundity, small larval size and transparency and rapid external development, allowing the observation of morphogenesis (Bandmann and Burton, 2010). They have a longer life span than mice, facilitating studies of aging and age-related diseases (Yu et al., 2006; Zhdanova et al., 2008). Moreover, it is relatively easy

and cheap to house large colonies of zebrafish. A wealth of information and resources has been accumulated by researchers working with this model, including the genomic sequence, gene expression data, anatomical atlases and multiple transgenic and knockout lines (Bryson-Richardson et al., 2007; Howe et al., 2018; Howe et al., 2013). In addition, a multitude of methods have been developed and optimized for use in zebrafish, including visualization of fluorescent reporters *in vivo*, forward or reverse genetics techniques **(section 1.6.3)** and behaviour analysis **(section 1.6.4)** (Finley et al., 2001; Jim et al., 2016; Kwan et al., 2007; Liu et al., 2017; Lu and DeSmidt, 2013; Norton and Bally-Cuif, 2010; Reyon et al., 2012; Suster et al., 2009; Watanabe et al., 2010). High-throughput small molecule screening can be performed with zebrafish larvae in 96-well plates to identify compounds that induce or alleviate known phenotypes (Baxendale et al., 2012; Kari et al., 2007; Kithcart and MacRae, 2017; Kokel et al., 2010; Kokel and Peterson, 2008; Ordas et al., 2015; Wang et al., 2015). Using already FDA-approved drug libraries can speed up the process of applying any hits in clinical trials.

Due to the high homology between zebrafish and human genomes, zebrafish have orthologues of genes involved in all DNA damage repair pathways and there is also a high degree of conservation among genes involved in neurodegeneration (Bandmann and Burton, 2010; Pei and Strauss, 2013). Nevertheless, before studying any zebrafish gene, the sequence similarity, synteny conservation and gene expression pattern should be compared with the human orthologue. This is due to the fact that the teleost fish ancestor underwent a whole-genome duplication event (Amores et al., 1998; Christoffels et al., 2018; Meyer and Van de Peer, 2005; Taylor

et al., 2003; Taylor et al., 2001). Most gene duplications were then rapidly lost, however, about 14 -24 % were retained, depending on the function. The remaining duplicates could have survived the selective pressures due to gaining new functions (neofunctionalization) in addition to the original ones, or by partitioning the ancestral function between the two paralogues (subfunctionalization). The possible interaction between the paralogues should also be taken into consideration (Hewamadduma et al., 2018; Schmid et al., 2013).

Another limitation of zebrafish is the low tolerance of inbreeding, which means there are less well-characterized inbred zebrafish lines than, for example, mouse lines (Kalueff et al., 2014). In addition, the delivery of water-insoluble drugs via water immersion can be problematic, although they can be injected, delivered by gavage or solubilized in a vehicle solution, such as DMSO (Dang et al., 2016; Samaee et al., 2017). Directly translating drug dosages from humans or rodents is also not always possible due to differences in physiology and there are species-specific differences in the blood-brain barrier, which may affect brain accessibility to the drug (Fleming et al., 2013; Jeong et al., 2008; Xie et al., 2010).

1.6.1. Zebrafish as a model for neurological disease

The organization of the zebrafish central nervous system (CNS) is similar to other vertebrates with a forebrain, midbrain, hindbrain and spinal cord **(figure 1.5A)** (Panula et al., 2010; Sager et al., 2010). Although the overall scale and structure of human and zebrafish CNS are quite different, the key areas relevant to human disease show high degrees of conservation. For instance, the zebrafish cerebellum has molecular, Purkinje and granular cell layers as those observed in the human

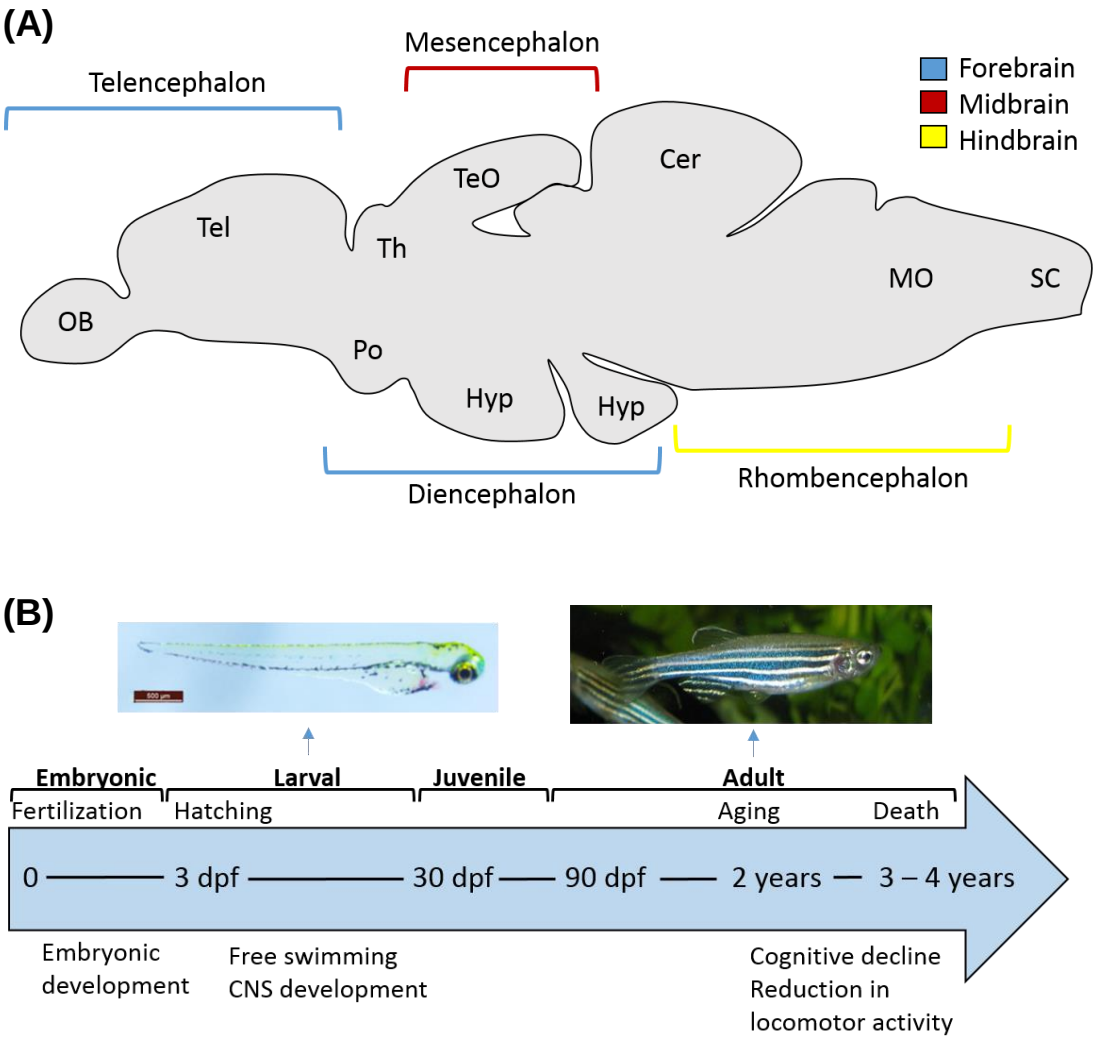

Figure 1.5. Zebrafish as an animal model for neurodegeneration. (A) The brain structures of adult zebrafish. OB – olfactory bulb, Tel – telencephalon, Po – preoptic region, Th – thalamus, TeO – optic tectum, Hyp – hypothalamus, Cer – cerebellum, MO – medulla oblongata, SC – spinal cord. Adapted from Gaspar and Lillesaar, 2012. **(B)** Life cycle of Danio rerio. Once the egg has been fertilized, it enters the embryonic stage (0 – 72 hpf). The larval stage begins at 72 hpf after hatching up to 30 dpf, when zebrafish enter the juvenile stage. Zebrafish are considered adult once they reach sexual maturity at approximately 90 dpf and start to exhibit ageing from approximately 2 years onwards until their death at 4 – 5 years of age. Adapted from Stewart et al., 2014. Adult zebrafish image: Copyright Azul. Reproduced under Creative Commons license from Wikimedia: http://commons.wikimedia.org/wiki/File:Tape_measures_-_centymetr.jpg

cerebellar cortex (Bae et al., 2009). The cell types found in each of these layers are similar to those found in humans with comparable inputs and synaptic connections. In addition, they express similar markers and genes. Eurydendroid cells are the zebrafish equivalent of deep cerebellar nuclei, but in contrast to mammals, where deep nuclei are embedded in the white matter at the core of the cerebellum, the eurydendroid cell bodies lie in the granule cell layer (Bae et al., 2009). There is structural homology of the zebrafish hypothalamus, medulla, optic and olfactory systems, spinal cord and cranial nerves to the human counterparts (Sager et al., 2010). Like humans, zebrafish also have enteric and peripheral nervous systems. Differences include the duplication of the tyrosine hydroxylase and the presence of only one, rather than two monoamine oxidase genes (Candy and Collet, 2005; Panula et al., 2010; Setini et al., 2005).

So far manipulation of zebrafish paralogues of human genes involved in neurodegeneration, such as Parkinson's, ALS and cerebellar ataxias, has successfully provoked comparable phenotypes (Bae et al., 2009; Bandmann and Burton, 2010; Kawahara and Hayashi, 2016; Mahmood et al., 2013; Watchon et al., 2017). In addition, aging zebrafish start showing natural cognitive and circadian rhythm decline, and reduced locomotor activity, similar to late stages of human life **(figure 1.5B)** (Gilbert et al., 2014; Ruhl et al., 2016; Stewart et al., 2014; Yu et al., 2006; Zhdanova et al., 2008). This means it may be possible to recapitulate human phenotypes in a much shorter time-frame. However, the onset of most neurodegenerative diseases is late in life and occurs due to accumulation of pathologies in the neurons (Johnson, 2000; Katyal et al., 2014; Kiernan et al., 2011;

Takashima et al., 2002). It also becomes more difficult to identify subtle phenotypes and perform imaging as the fish age. In addition, unlike humans, zebrafish exhibit high regenerative capacity of their neurons, which might complicate studies of neurodegenerative diseases (Adolf et al., 2006; Arvidsson et al., 2002; Grandel et al., 2006; Kishimoto et al., 2012).

1.6.2. Zebrafish as a model for DNA repair

Zebrafish have orthologues of most genes involved in all DNA damage repair pathways, including direct reversal (DR), MMR, NER, BER, NHEJ, HR and translesion synthesis (Feitsma et al., 2008b; Fortier et al., 2009; Imamura and Kishi, 2005; Pei and Strauss, 2013; Zeng et al., 2009). In addition, the zebrafish genome contains genes required for p53-mediated damage recognition and apoptosis (Inohara and Nunez, 2000; Lee et al., 2008). Investigation of different DNA damage repair pathways will be discussed here. However, to date most studies in zebrafish have been limited to investigating the effects of toxic compounds on DDR and systematic studies of such pathways have not been carried out (Ku-Centurion et al., 2016; Sasagawa et al., 2016).

1.6.2.1. Direct Reversal

Direct reversal is a pathway, which reverses DNA damage directly without breaking the phosphodiester bond. For example, Methyl-Guanine Methyltransferase (MGMT) repairs alkylation damage by removing the methyl group from methyl-guanine (Olsson and Lindahl, 1980). An orthologue of MGMT is present in the zebrafish genome, but it has not been studied (Pei and Strauss, 2013). Interestingly, however,

zebrafish possess a distinct pathway of direct reversal not present in placental mammals, called photoenzymatic repair (PER) (Dong et al., 2007; Tamai et al., 2004). This pathway is activated by long wavelength UVA and visible light, which generate CPDs and oxidative damage (Kelner, 1949; Kobayashi et al., 2000; Sancar, 2003). CPDs are induced by UV-B and UV-C rays and can be reversed by a single light-dependent reaction, catalysed by deoxyribodipyrimidine photolyase (Phr) (Hirayama et al., 2009; Sinha and Hader, 2002). In mammals, on the other hand, such damage is repaired less efficiently by NER (Lucas-Lledó et al., 2018).

1.6.2.2. NER

NER can repair both types of pyrimidine dimers, CPDs and 6, 4-PPs **(section 1.3.2.2.)** and is found in all organisms (Pei and Strauss, 2013). Several groups have studied the effects of UV irradiation on zebrafish or their liver cells and the role of NER genes, such as *p53*, *cyclinG1*, *ddb2*, *xpc*, *cdkI* and *gadd45a*, in response to UV-induced damage (Notch and Mayer, 2009; Notch et al., 2007; O'Reilly-Pol and Johnson, 2008; Zeng et al., 2009). It has been shown that different developmental stages have distinct expression patterns/levels of NER factors and that they are also differentially sensitive to DNA damaging agents (Notch and Mayer, 2009; Silva et al., 2012). For example, embryos at 12 hpf were the most sensitive to UV-A and UV-B treatment (Dong et al., 2007). No studies have been carried out to distinguish TC-NER and GG-NER in zebrafish, however the balance is likely to be affected by the presence of PER (Pei and Strauss, 2013).

1.6.2.3. BER

As described in section **1.3.2.3**, BER repairs small lesions, such as 8-oxoguanine, uracil or AP sites. Among studied zebrafish BER enzymes are Apex1 (APE1 orthologue) and PolB (Ishido et al., 2011; Wang et al., 2006). The zebrafish Apex1 protein is highly homologous to its mammalian orthologue and the *apex1* gene has two copies: *apex1a* and *apex1b* (Wang et al., 2006). Zebrafish embryos, injected with morpholinos against apex1, die at the midblastula transition, whereas partial knockdown or rescue with the human APE1 mRNA gives rise to embryos with abnormalities in the heart, blood cells, notochord, eyes and brain.

Unfertilized zebrafish eggs and early stage embryos can, as a minimum, carry out the first three BER steps (Wang et al., 2006). However, up to 12 - 13 hpf, zebrafish BER has a few unusual features, likely owing to the high cell proliferation rates. Mg^{2+}-dependent endonucleases act as a backup for Apex1 in coping with excess oxidative damage. In addition, Polβ is not yet expressed at this stage and thus BER is dependent on aphidicolin-sensitive polymerase(s) (Ishido et al., 2011). Normal BER is initiated once the embryo has hatched from the chorion and is exposed to normal oxidative stress (Fortier et al., 2009).

1.6.2.4. MMR

Wrongly incorporated DNA bases are repaired by MMR **(section 1.3.2.1.)**. Several zebrafish MMR genes, including *msh6*, *msh2* and *mlh1,* have been cloned and their expression has been analysed (Yeh et al., 2004; Yeh et al., 2003). *Msh6* was shown to be differentially expressed in relation to msh2 through developmental stages, while

msh2 was differentially distributed in tissues (Yeh et al., 2003). At 120 hpf the relative expression is stabilized (Yeh et al., 2004). In 12 dpf – 48 dpf embryos, *msh2* mRNA was found in the brain, the fourth ventricle and the eyes (Yeh et al., 2004). In contrast, *mlh1* localized to distal regions of synaptonemal complexes (Moens, 2006). Loss of *mlh1* lead to infertility in zebrafish males as meiosis was arrested at metaphase I stage (Feitsma et al., 2007). However, some of the germ cells successfully completed meiosis (Leal et al., 2008). In addition, *msh6*$^{-/-}$, *msh2*$^{-/-}$ and *mlh1*$^{-/-}$ zebrafish developed tumours, especially neurofibromas in the abdomen and eye (Feitsma et al., 2008b). Surprisingly, loss of these genes did not enhance mutagenesis caused by exogenous genotoxins. For example, ethylnitrosourea failed to increase the mutation rate in *msh6*$^{-/-}$ zebrafish germline (Feitsma et al., 2008a). Although BER is the primary mechanism for alkylation damage repair, zebrafish embryos that were treated with alkylating agents showed chromosomal instability and cell death due to MMR-induced stalled replication forks (Feitsma et al., 2018).

1.6.2.5. NHEJ

As discussed in **section 1.3.2.5.1.**, NHEJ is an error-prone pathway that repairs DSBS, arising from UV and IR. Zebrafish NHEJ factors *ku70* and *ku80* have been cloned and they were both shown to be maternally provided to the embryo (Bladen et al., 2005; Bladen et al., 2007). *Ku80* promotes cell survival after IR damage in embryos (Bladen et al., 2005). In *ku80* knockdown zebrafish, IR-induced apoptosis was suppressed by the additional knockdown of *p53*, suggesting that such apoptosis is *p53*-dependent (Bladen et al., 2005). Moreover, zygotic *ku70* mRNA is found in neural tissue, such as the retina and the brain (Bladen et al., 2007). It protects the developing nervous

system against IR-induced DNA damage, although it is not required for development in the absence of genotoxic insult. As in mammalian cells, in zebrafish embryos NHEJ is also the primary pathway for DSBR out of the three available pathways: HR, SSA and NHEJ (Dai et al., 2010). In addition, NHEJ is the predominant mechanism for integration of exogenous DNA in zebrafish, which is utilized in genome editing techniques, such as CRISPR/Cas9 and transcription activator-like effector nucleases (TALENs) **(section 1.6.3.)** (Liu et al., 2012).

1.6.2.6. HR

Homologous recombination (HR) is an error-free pathway for repairing DSBs (section 1.3.2.5.2). HR activity has been documented in early stage zebrafish embryos and zebrafish embryonic stem cells (Fan et al., 2006; Hagmann et al., 1998). *Brca2*$^{-/-}$ zebrafish and their cells showed defects in HR and genomic instability (Rodriguez-Mari et al., 2011). In addition, oocytes in juvenile *brca2*$^{-/-}$ zebrafish failed to complete meiosis, leading to female-to-male sex reversal. The spermatocytes in these males arrested during meiosis and died by apoptosis, rendering the fish sterile. In turn, the somatic cells in the gonads of *brca2*$^{-/-}$ fish showed neoplastic proliferation (Rodriguez-Mari et al., 2011; van Eeden, unpublished). Additional mutation of *p53* rescued sex reversal, giving rise to infertile females with an increased risk of ovarian tumours and only giving rise to abnormal embryos. These studies identified a novel role for Brca2 in either the maintenance or establishment of oocyte nuclear architecture and also suggests its importance in zebrafish spermatogenesis. Another study has confirmed the conservation of the role of Brca2 in zebrafish by showing that *brca2* knockdown and knockout fish almost completely fail to form IR-induced

Rad51 foci (Vierstraete et al., 2017). Attempts have been made to harness zebrafish HR for genome editing, however, they have not been successful to date (Liao and Essner, 2011; Takahashi et al., 2005b).

1.6.3. Genetic tools for generating zebrafish models

1.6.3.1. Generating zebrafish knockdowns

Temporary silencing of zebrafish genes, or a knockdown (KO), can be achieved via the use of antisense oligonucleotides, called morpholinos (MOs) (Draper et al., 2001; Nasevicius and Ekker, 2000). MOs can be targeted against the start codon of an mRNA or a splice site of a pre-mRNA, preventing either transcription or splicing. MOs are nuclease-resistant and thus very stable (Hudziak et al., 1996). They are injected into single-cell stage embryos, just after fertilization, and can knockdown the target mRNA very efficiently. Knockdown (KD) efficiency can then be assessed by western blotting or RT-qPCR, depending on whether the MO was designed against a start codon or a splice site, respectively. This technique is a lot quicker than generating knockouts and can be used in high throughput experiments, but has some limitations.

The KD is indeed very transient and starts losing efficiency from 3 dpf until the complete recovery of gene expression at 5 dpf (Bandmann and Burton, 2010). Hence, modelling diseases with a late onset is impossible. In addition, MOs have been shown to induce non-specific phenotypes, such as small head and eyes, craniofacial defects and somite and notochord abnormalities, due to the activation of the p53 pathway (Bandmann and Burton, 2010; Robu et al., 2007; Wright et al., 2004). Another non-specific effect is neuronal cell death at 24 hpf, which can obscure modelling

neurodegenerative disease (Robu et al., 2007). Although control MOs can be used to account for non-specific phenotypes, they have been shown to sometimes induce quite severe off-target effects (Bandmann and Burton, 2010). Moreover, rescue of the phenotype by the additional injection of wild-type mRNA for the protein of interest or the protein of interest itself can increase confidence in a morpholino, as well as a careful comparison with any available knockout models. Additional insight can also be gained by comparing the phenotypes between wild-type or mutant versions and by performing the rescue using recombinant human protein of interest. The latter is especially useful if mRNA injection is producing a non-specific toxic effect, which has been reported with some mRNAs (Bandmann and Burton, 2010). When modelling neurodegenerative disease, confidence in the specificity of the phenotype can be gained by observing the death of MO-specific neurons, but not others. Such limitations of using MOs have generated a need for more advanced genome editing techniques, which introduce more stable changes that can be passed on through generations. Nevertheless, a recent study has shown that while some KOs induce genetic compensation, this is not the case with MOs (Rossi et al., 2015).

1.6.3.2. TILLING

Random mutagenesis in zebrafish can be carried out using N-ethyl-N-nitrosourea (ENU) and TILLING (Targeting Induced Local Lesions in Genomes). ENU is a potent mutagen that introduces various single-base alkylation lesions throughout the genome, although some loci are more likely to be affected (Bandmann and Burton, 2010; Russell et al., 1979). TILLING is a high-throughput mutation screening technique that was first developed in *Arabidopsis thaliana*, but has since been

adapted in zebrafish (Draper et al., 2004; McCallum et al., 2000; Stemple, 2004; Wienholds et al., 2003). First, F_0 generation males are chemically mutagenized, then outcrossed to females to produce the F_1 generation. Genetic regions of interest are then directly sequenced from adult F_1 fish to identify point mutation carriers. Although valuable stable mutant lines can be generated using this approach, it is laborious, inefficient and more expensive than other methods (Bandmann and Burton, 2010).

1.6.3.3. Site-specific endonucleases

Site-specific endonucleases are an invaluable tool in animal research. They allow the generation of random or specific mutations and insertions at chosen sites by generating a double-strand break. There are three commonly used classes of site-specific endonucleases: zinc-finger endonucleases (ZFNs), transcription activator-like effector endonucleases (TALENs) and CRISPR/Cas9 (clustered regularly interspaced short palindromic repeats (CRISPR)/ CRISPR-associated protein 9 (Cas9)) endonucleases. (Doyon et al., 2008; Ekker, 2008; Hruscha et al., 2013; Huang et al., 2011a; Hwang et al., 2013; Hwang et al., 2014; Meng et al., 2008; Sander et al., 2011; Wood et al., 2011a).

ZFNs were the first to be utilized for genome editing (Bibikova et al., 2003; Bibikova et al., 2001; Bibikova et al., 2002; Doyon et al., 2008; Foley et al., 2009; Kim et al., 1996; Meng et al., 2008). They are chimeric proteins, generated by fusing several zinc-finger domains with the endonuclease domain of Fok1 (Kim et al., 1996). Zinc-finger domains typically recognize trinucleotide motifs, allowing some customization

of the target sequence. To reduce off target effects ZFNs that require heterodimerization prior to DNA cleavage have been generated (Miller et al., 2007).

TALENS are also fusion proteins, composed of Fok1 catalytic and site-specific DNA-binding domains (Miller et al., 2011; Zhang et al., 2011a). TALENs use tandem 32 – 35 amino acid transcription activator-like effector (TALE) sequences for DNA binding, each of which recognize a different nucleotide (Boch et al., 2009). This allows the engineering of a nuclease with a completely custom site specificity.

CRISPR/Cas9 is the most recent method, employing an anti-viral immune mechanism from *Streptococcus pyogenes* (Jinek et al., 2012). Hypervariable CRISPR loci, which incorporate short sequences of genetic material from invading viruses, are present in many prokaryotes (Barrangou et al., 2007). These loci are then expressed as CRISPR-derived RNA (crRNA) and together with trans-acting antisense RNA (tracRNA) form an active complex with a Cas nuclease and guide it to the corresponding viral DNA to destroy it **(figure 1.6A)** (Gasiunas et al., 2012; Jinek et al., 2012). The two RNA species, crRNA and tracRNA, were combined into a single guide RNA (gRNA) for use in the CRISPR/Cas9 system (Jinek et al., 2012). The gRNA is first designed as a DNA ultramer with the tracRNA scaffolding sequence at the 5' end, T7 RNA polymerase promoter site at the 3' end and the ~20 nucleotide tracRNA targeting sequence in the middle, and then *in vitro* transcribed for injection with Cas9 mRNA into single cell embryos **(figure 1.6B)** (Hruscha et al., 2013; Hwang et al., 2013; Mali et al., 2013b).

Although all three site-specific endonucleases can perform efficient genome editing, they differ in off-target effects, sequence constrictions and ease of construction (Ata et al., 2016). Highly efficient Cas nucleases are the easiest to assemble, whereas ZFNs

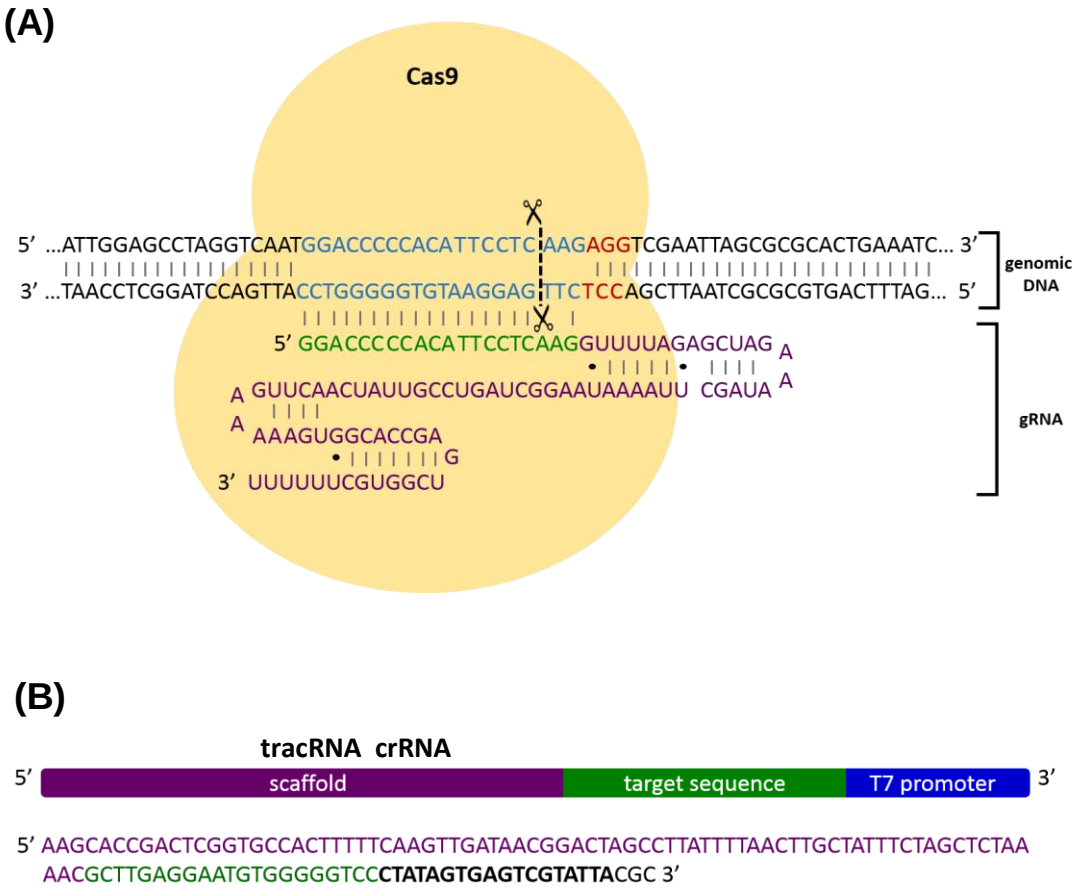

Figure 1.6. Schematic representation of CRISPR-Cas9 system. (A) Cas9 is guided by the gRNA to the target site in the genome, where it makes a double-strand break 3 bp upstream of the PAM sequence. **(B)** Structure of DNA template ultramer for gRNA transcription (adapted from Ran et al, 2013)

are the most difficult. Not all trinucleotide combinations are available for ZFNs and it is not always possible to precisely define the specificity, which can be affected by proximal domains of the protein (Isalan et al., 1997; Sander et al., 2011). While both CRISPR/Cas9 and TALENs can elicit very high on-target effects, a few studies have reported that the CRISPR/Cas9 method may also give rise to high off-target effects (Hsu et al., 2013; Mali et al., 2013a; Pattanayak et al., 2013). As ZFNs are quite restricted for available targetingsequences and CRISPR/Cas9 system requires the presence of the protospacer adjacent motif (PAM) (NGG) three base pairs downstream of the cleavage site, TALENs have the broadest target sequence range and are able to target almost any sequence. (Reyon et al., 2012). However, TALENs are sensitive to methylation, a property that is difficult to overcome, whereas Cas9 is not (Chen et al., 2013; Valton et al., 2012; Yaung et al., 2014). When considering a suitable target site, polymorphisms in the zebrafish colony and highly repetitive sequences should be avoided with all three methods.

1.6.3.4. Generating transgenic zebrafish

The introduction of zebrafish or human genes, harbouring deleterious mutations into a zebrafish genome, is a powerful method to dissect the mechanisms by which dominant negative and gain-of-function mutations give rise to disease. Genomic insertions can be made both in wild-type and mutant backgrounds and multiple copies of the gene can be inserted if an overexpression phenotype is being studied. There is a vast array of fluorescent reporters and promoters available to add to the transgenic construct. This allows transgenes to be visualised, whilst their

spatiotemporal expression is being carefully regulated. Fluorescent imaging in larvae is facilitated by their transparency, particularly the ability to perform live imaging.

A simple and commonly used method for generating transient transgenic zebrafish is the microinjection of mRNA for the protein of interest into one-cell stage embryos (Bandmann and Burton, 2010). Linearized plasmid DNA can also be injected, however, it results in the formation of concatemers (Culp et al., 1991; Kawakami, 2005; Stuart et al., 1988). In addition, the distribution of the concatemers is uneven and integration is inefficient. This leads to high mosaicism and rare integration, posing the requirement for many fish to be screened in order to identify founders. A few improvements to this basic technique have been made, including the I-sceI meganuclease and Tol2 transposase systems (Jacquier and Dujon, 1985; Suster et al., 2009). I-sceI is derived from *Saccharomyces cerevisiae* and recognizes and cleaves an 18 bp sequence, not found in the zebrafish genome. When the transgenic construct, flanked by such sequences, isinjected into one-cell stage embryos alongside I-sceI enzyme, it is integrated at higher efficiency and with less mosaicism than linearized plasmid DNA (Thermes et al., 2002). The germline transmission rate is also much higher using the I-sceI meganuclease. Only one or few copies of the transgene integrate in tandem into a single integration site and thus the transgene is passed on in mendelian ratios, facilitating the generation of double transgenics (Bai et al., 2009). *Tol2*, on the other hand, is a transposon that was discovered in the medaka fish. The open reading frame of the transposase was deleted from *Tol2* transposable elements and thus integration events of such element-flanked transgene can only occur when the *Tol2* transposase is co-injected (Kawakami, 2005; Kawakami et al.,

2000). Integration efficiency of this method is high enough to allow relatively low numbers of fish to be screened in order to identify suitable founders.

1.6.4. Examining motor function and behaviour in zebrafish

1.6.4.1. Analysis of motor capacity and balance in adult zebrafish

Studies of zebrafish models of amyotrophic lateral sclerosis (ALS) demonstrate the use of the swim tunnel in determination of motor capacity (Ramesh et al., 2010) and trout cerebellectomy studies show it can facilitate investigation of cerebellar function in fish (Roberts et al., 1992). Individual zebrafish are placed in a water tunnel (Plaut, 2000; Ramesh et al., 2010) and the water flow rate is gradually increased until the fish exhaust. Premature exhaustion may be a sign of multiple abnormalities, including muscle weakness (Ramesh et al., 2010) and lack of cerebellar function (Roberts et al., 1992).

Another way to assess the balance capacity of a fish is by using a drop test, where the fish are dropped into a deep tank of water from ~10 cm of height above the water surface, to cause a brief disorientation of the vestibular apparatus (Detrich et al., 2016). The movements, speeds, total distance travelled and preferred tank areas of the fish are then recorded using a camera system. Healthy fish usually pause at the bottom of the tank, then start exploring the bottom third of the tank and eventually rise to the top. Any alterations to normal behaviour may signal problems with balance, the motor pathways of which are coordinated by the cooperation of the cerebellum and the vestibular system (Morton and Bastian, 2004). The camera system can also be utilized to monitor normal movement of fish without any additional challenges.

1.6.4.2. Photomotor response in embryonic zebrafish

A highly robust response to short light and dark intervals, called the photomotor response (PMR), has been previously reported in zebrafish larvae (Colon-Cruz et al., 2017; Kristofco et al., 2016; Rihel and Schier, 2012; Sun et al., 2016; Truong et al., 2012). Normally zebrafish embryos are more active in the dark, which is thought to provide cover from predators. Impairment in this response can signify neurodevelopmental abnormalities (Rihel and Schier, 2012; Sun et al., 2016; Truong et al., 2012) or abnormalities in movement and sight, which can affect the visual or physical responses to the light. The molecular mechanisms behind this response are not well understood. Nevertheless, it has been widely used as a phenotypic readout for multiple compound toxicity studies and retroactive drug screening (Rihel and Schier, 2012; Sun et al., 2016; Truong et al., 2012).

1.7. Aims and objectives

- Generate *tdp1*$^{-/-}$ zebrafish and characterise the model in embryonic stages and in adulthood using biochemical, immunohistochemical and behavioural analyses with high animal numbers.
- Determine the mechanism by which TDP1^{H493R} causes SCAN1 by generating and characterizing a humanized TDP1^{H493R} zebrafish model in *tdp1*$^{-/-}$ background.
- Investigate the function of Tdp1 in environments with increased oxidative stress and/or Top1-CCs by generating *tdp1*$^{-/-}$*; atm*$^{-/-}$, *tdp1*$^{-/-}$; *tg(SOD1*^{G93R}*)*$^{-/+}$ and *tdp1*$^{-/-}$*; tg(C9orf72*^{102xG4C2}*).*

- Investigate the role of Tdp1 in the repair of non-Top1-mediated DNA damage by generating *tdp1*$^{-/-}$*; top1*$^{-/-}$ zebrafish.
- Elucidate any interactions between the characterized SUMOylation at lysine 111 and putative Casein Kinase 2 (CK2) phosphorylation sites in the N-terminus of human TDP1.
- Confirm N-terminal TDP1 phosphorylation *in vivo* by generating phosphomutant and phosphomimetic variants of putative phosphorylation sites via site-directed mutagenesis and identify the relevant kinase and phosphatase.
- Determine any DNA repair phenotypes, resulting from site-directed mutagenesis of putative phosphorylation sites in TDP1 N-terminus, especially phenotypes that are a direct consequence of interaction with SUMOylation at K111.

2

Materials and Methods

2.1. Materials

Unless otherwise stated, all materials were obtained from the following vendors. Chemicals were obtained from Sigma-Aldrich or Fisher Scientific and restriction enzymes from New England Biolabs or Roche Diagnostic. All DNA oligonucleotides were synthesized by Integrated DNA Technologies (Leuven, Belgium) and RNA oligonucleotides by Dharmacon™ or Eurofins MWG Operon (Ebersberg, Germany). Tissue culture medium and nutritional supplements were supplied by Gibco® Invitrogen or Sigma Aldrich. Foetal bovine serum (FBS) was obtained from PAN-Biotech (Aidenbach, Germany) or Sigma Aldrich (F6524) and tetracycline-free FBS was sourced from Labtech (FB1001T/500). All tissue culture plastic-ware was obtained from Corning or Nunc™.

2.1.1. DNA plasmids

All DNA plasmids used in this thesis are listed in **tables 2.1** and **2.2**. For CRISPR/Cas9, pCS2-nCas9n (Addgene, 47929) plasmid was used to synthesize Cas9 mRNA. It contains Cas9 cDNA, codon-optimized for zebrafish and under the SP6 promoter for *in vitro* transcription. For propagation in bacterial culture, it contains an ampicillin resistance under the AmpR promoter.

For Tol2 transposase transgenesis, the pCS2-Cre plasmid (Langenau et al., 2005) and

Tol2 (Kwan et al., 2007) kit was used with several amendments. It will be discussed in more detail in **chapter 4**.

Plasmid construct	Source/Reference
p3E-lxP-mCherrypA	Dr. Henry Roehl
p3E-lxP-TDP1^{H493R}pA	This thesis
p3E-lxP-TDP1pA	This thesis
pCI-puro-Myc-TDP1	Dr. Shih-Chieh Chiang (Chiang et al., 2010)
pCI-puro-Myc-TDP1^{K111R}	Dr. Jessica Hudson (Hudson et al. 2012)
pCS2-Cre	Antonio Jacinto (Langenau et al., 2005)
pCS2FA-Tol2	Dr. Henry Roehl (Kwan et al., 2007)
pCS2-nCas9n	Dr. Freek Van Eeden (Addgene, 47929)
pDestTol2CG2	Dr. Henry Roehl (Kwan et al., 2007)
pDestTol2CG2-ubi-lxP-BFP-lxP-TDP1	This thesis
pDestTol2CG2-ubi-lxP-BFP-lxP-TDP1^{H493R}	This thesis
pENTR5'_ubi	Dr. Henry Roehl (Addgene, 27230)
pME-lxP-BFP	Dr. Stone Elworthy

Table 2.1. Genome editing constructs. Names and sources of DNA constructs used for CRISPR/Cas9 and Tol2 transgenesis.

Plasmid construct	Source/Reference
pcDNA5-FRT-miTDP1	Dr. Shih-Chieh Chiang (Chiang et al., 2017)
pcDNA5-FRT-TDP1-miTDP1	Dr. Shih-Chieh Chiang (Chiang et al., 2017)
pcDNA5-FRT-TDP1$_{TR}$ $^{S13\text{-}15A,S90\text{-}92A}$-	This thesis
pcDNA5-FRT-TDP1$_{TR}$ $^{S13\text{-}15D,S90\text{-}92D}$-	This thesis
pcDNA5-FRT-TDP1$_{TR}$ $^{S90\text{-}92A}$-miTDP1	This thesis
pcDNA5-FRT-TDP1$_{TR}$ $^{S90\text{-}92D}$-miTDP1	This thesis
pcDNA5-FRT-TDP1$_{TR}$-miScr	Dr. Shih-Chieh Chiang (Chiang et al., 2017)
pcDNA5-FRT-TDP1$_{TR}$-miTDP1	Dr. Shih-Chieh Chiang (Chiang et al., 2017)
pCI-puro-Myc	Prof. Keith Caldecott
pCI-puro-Myc-TDP1	Dr. Shih-Chieh Chiang (Chiang et al., 2010)
pCI-puro-Myc-TDP1$^{1\text{-}150}$	Dr. Shih-Chieh Chiang (Chiang et al., 2010)
pCI-puro-Myc-TDP1$^{1\text{-}150,\ S13\text{-}15A}$	This thesis
pCI-puro-Myc-TDP1$^{1\text{-}150,\ S13\text{-}15A,S90\text{-}92A}$	This thesis
pCI-puro-Myc-TDP1$^{1\text{-}150,\ S90\text{-}92A}$	This thesis
pCI-puro-Myc-TDP1$^{1\text{-}150,K111R}$	This thesis
pCI-puro-Myc-TDP1^{K111R}	Dr Jessica Hudson (Hudson et al., 2012)
pCI-puro-Myc-TDP1^{K111R}	This thesis
pCI-puro-Myc-TDP1$^{S13\text{-}15A,S90\text{-}92A}$	This thesis
pCI-puro-Myc-TDP1$^{S13\text{-}15D,S90\text{-}92D}$	This thesis
pCI-puro-Myc-TDP1$^{S90\text{-}92D}$	This thesis
pEGFP-C3	Addgene (6082-1)
pEGFP-C3-SUMO1	Prof. Alan Lehmann
pEGFP-N1-Myc-TDP1	Kirsty Liversidge
pEGFP-N1-Myc-TDP1$^{S13\text{-}15A,S90\text{-}92A}$	This thesis
pEGFP-N1-Myc-TDP1$^{S13\text{-}15D,S90\text{-}92D}$	This thesis
pEGFP-N1-Myc-TDP1$^{S90\text{-}92A}$	This thesis
pEGFP-N1-Myc-TDP1$^{S90\text{-}92D}$	This thesis
pPGKFLP	Prof. Stuart Wilson
pRC/CMV-CK2α	Addgene (27086)
pRC/CMV-CK2α^{K68M} (kinase-dead)	Addgene (27089)

Table 2.2. Mammalian expression vectors. Names and sources of mammalian expression constructs used in this thesis.

For protein expression in mammalian cell culture pCI-puro-Myc (Promega, E1731), pcDNA5-FRT, pEGFP-N1 (Addgene, 6085-1) and pEGFP-C3 (Addgene, 6082-1) vectors were used. The pCI-puro-Myc vector carries a c-Myc tag upstream of the multiple coning site (MCS), which can be used to pull down proteins in co-immunoprecipitation (Co-IP) experiments. The CMV promoter/enhancer sequence drives constitutional expression of the fusion protein. In addition, the vector contains SV40-driven puromycin resistance for selection in mammalian cells and an ampicillin resistance cassette for propagation in *E. coli* cells.

The pcDNA5-FRT vector was used for stable cell line generation in Flp-In™ 293 Trex cells.

In this vector gCMV/2x TetO2 promoter/enhancer sequence drives expression of the gene of interest and a Flp Recombinase Target (FRT) site is found upstream of a hygromycin resistance gene. The antibiotic resistance is activated upon integration into the host genome mediated by the Flp recombinase.

The pEGFP-N1 and pEGFP-C3 vectors both contain the CMV promoter driving the EGPF-gene fusion expression, and the kanamycin resistance gene. In the pEGFP-N1 vector, the pEGFP tag is downstream of the MCS, giving rise to a C-terminal EGFP tag. In pEGFP-C3, the tag is upstream of the MCS, producing an N-terminal EGFP tag.

2.2. Molecular biology techniques

2.2.1. DNA plasmid propagation and maintenance

2.2.1.1. DNA transformation

After slowly thawing 50 µL of chemically competent DH5α *E.coli* cells on ice, they were incubated with 100-500 ng of plasmid DNA for 15-20 minutes on ice. Cells were then heat-shocked at 42°C for 45 seconds and returned to ice for 1-2 minutes. 200 µL of LB broth was added and the cells were shaken at 225 rpm and 37°C for 1 hour. 50 µL of the total volume were spread onto selective LB agar plates, which were incubated at 37°C overnight. Selective plates were made with 50 µg/mL of antibiotic (ampicillin or kanamycin).

2.2.1.2. Liquid bacterial culture and DNA extraction

Once a single transformant colony was obtained, it was inoculated into 5 mL or 100 mL of selective LB broth (50 µg/mL antibiotic) and shaken overnight at 225 rpm and 37°C. The 5 mL or 100 mL liquid culture was then used for DNA extraction with the QIAprep® Spin Miniprep or Plasmid Plus Midi kit (Qiagen, 27104, 12943), respectively, according to the manufacturer's protocol.

2.2.1.3. Glycerol stocks

Combine 750 mL of liquid culture and 250 mL 70% glycerol in a vial and freeze at -80°C.

2.2.2. DNA agarose gel electrophoresis

Unless otherwise stated, 100 mL of 1 % w/v agarose in 1 x TBE buffer (89 mM Tris, 89 mM boric acid, 2 mM EDTA pH 8.0) with 2 µg/mL ethidium bromide was set in a gel tray with a comb. The comb was removed and DNA samples in 1 x DNA loading buffer (39 % glycerol, 25 mM EDTA, 0.2 % w/v bromophenol blue, 0.2 % w/v xylene cyanol) were loaded into wells alongside 5 µg of 2-Log DNA ladder (New England Biolabs, N3200L). The samples were electrophoresed for 1 hour at 100 V in 1 x TBE and DNA bands were visualized by UV transillumination in the ChemiDoc MP imaging system (Bio-Rad, 1708280).

2.2.3. RNA agarose gel electrophoresis

100 mL or 200 mL of 1 % w/v agarose in 1 x TBE buffer (89 mM Tris, 89 mM boric acid, 2 mM EDTA pH 8.0) with 2 µg/mL ethidium bromide was set in a gel tray with a comb. The comb was removed and RNA samples in 1 x DNA loading buffer (39 % glycerol, 25 mM EDTA, 0.2 % w/v bromophenol blue, 0.2 % w/v xylene cyanol) were loaded into wells alongside 5 µg of 100 bp ladder (NEB, N3231S). The samples were electrophoresed for approximately 10 minutes at 100 V in 1 x TBE and RNA bands were visualized by UV transillumination in the ChemiDoc MP imaging system (Bio-Rad, 1708280).

2.2.4. Quantification of nucleic acid concentration

DNA concentration was quantified using the NanoDrop ND-Spectrophotometer at 260 nm or by gel electrophoresis. For quantification by gel electrophoresis 1 µL of DNA was diluted in 9 µL of 15 % w/v ficoll in DNA loading buffer. 6 µL, 3 µL and 1 µL

of the dilution alongside 1 µg, 2 µg, 5 µg and 10 µg of DNA ladder were then run on a 1 % w/v agarose gel at 100 V for 1 hour. The DNA bands were visualized and a sample band closest in brightness to one of the ladder bands of a similar size was chosen. As the total DNA amount was known for each of the ladder bands, the concentration of sample DNA could be determined proportionately. RNA concentration was determined by NanoDrop only at a wavelength of 260 nm.

2.2.5. DNA sequencing

DNA was sequenced using the GATC Biotech (Cologne, Germany) LightRun Sanger sequencing service. Custom primers were designed using Primer 3 v 4.0 (http://primer3.ut.ee/).

2.2.6. DNA restriction digestion and DNA fragment purification

Unless specified otherwise, 0.2 – 5 µg of DNA was digested using 1 – 5 U of restriction enzyme in 1 x appropriate buffer in a total volume of 20 µL. The optimal digestion temperature and time were determined following the restriction enzyme manufacturer's instructions. Complete digestion was determined by electrophoresis of the digested sample alongside an undigested control. When required, DNA fragments were cut out of the gel and purified using the QIAquick® Gel Extraction Kit (Qiagen, 28704), according to manufacturer's instructions.

2.2.7. Phenol/chloroform DNA extraction

One equal volume of phenol: chloroform: isoamyl alcohol (25:24:1, VWR, A0944.0100) was added to the sample and gently mixed. The sample was then centrifuged for 5 minutes at 13,300 rpm and the resulting aqueous layer carefully

moved into a fresh tube. Subsequently, one equal volume of chloroform: isoamyl alcohol was added to the aqueous layer and the mixture was centrifuged at 13,300 rpm for 2 minutes. The aqueous layer containing DNA was once again collected into a fresh tube. To precipitate the DNA, sodium acetate was added to a final concentration of 0.3 M, followed by 2 volumes of ethanol and 20 µg glycogen. The precipitation was carried out either for 30 minutes at -80ºC or overnight at -20ºC and the DNA was pelleted at 4ºC and 13,300 rpm for 30 minutes. The pellet was washed twice with 750 µL 70 % ethanol and spun down for 2 minutes at 13,300 rpm. To avoid disturbing the pellet, the supernatant was removed very carefully. The pellet was air-dried until translucent and resuspended in double-distilled water (ddH_2O) or TE buffer (10 mM Tris, 1 mM EDTA, pH 8).

2.2.8. Total RNA extraction using TRIzol reagent

50 zebrafish embryos were anaesthetized in tricaine **(section 2.3.4)** and homogenized in 250 µL of TRIzol reagent until tissue was sufficiently disrupted. Another 750 µL of TRIzol reagent were added and the sample was incubated at room temperature for 5 minutes. 200 µL of chloroform were added and the tube was inverted a few times to mix. The sample was incubated for 2 minutes at room temperature and centrifuged at 12,000 x g for 15 minutes at 4°C. The aqueous layer was carefully transferred into a fresh tube using a trimmed 200 µL pipette tip. To precipitate the RNA 500 µL of isopropanol were added and the sample was incubated for 10 minutes at room temperature. The sample was then centrifuged at 12,000 x g for 10 minutes at 4°C and supernatant was carefully removed. The RNA pellet was washed in 1 mL of 75 % ethanol and mixed by

gentle inversion. The sample was centrifuged at 7,500 x g for 5 minutes at 4°C. The ethanol was removed and the pellet was left to air-dry for 10 minutes. The pellet was then resuspended in 100 µL of nuclease-free H_2O at 55°C for 10 minutes with frequent vortexing.

2.2.9. Ammonium acetate RNA precipitation

The reaction was made up to 100 µL with ddH_20 and mRNA precipitated by the addition of ammonium acetate and ethanol to a final concentration of 0.3M and 70 %, respectively. The precipitation was carried out either for 30 minutes at -80ºC or overnight at -20ºC and the DNA was pelleted at 4ºC and 13,300 rpm for 30 minutes. To remove salts, the pellet was washed with 500 µL of 70 % ethanol and centrifuged at 4ºC at 13,300 rpm for 10 minutes. The pellet was air-dried until translucent and resuspended in ddH_2O.

2.2.10. Synthesis of capped RNA

2.2.10.1. Template plasmid linearization

10 µg of template DNA plasmid were digested with 30-60 U of a single-cutting restriction endonuclease that cuts after the cDNA (Not1 or Not1-HF) in the appropriate buffer in a total volume of 30 µL for 3 hours and run on an agarose gel alongside an undigested control to confirm complete digestion. Once complete digestion was achieved, the DNA was purified from the linearization reaction using the MinElute PCR Purification Kit (Qiagen, 28004) according to the manufacturer's instructions and quantified **(section 2.2.4)**.

2.2.10.2. *In vitro* transcription

1 – 2 µg of linearized plasmid was used as a template for *in vitro* mRNA synthesis with the mMESSAGE mMACHINE® SP6 kit (Life Technologies, AM1340) according to the manufacturer's high-yield protocol. Once the reaction was complete, template DNA was digested by 2 U of the supplied TURBO DNase for 15 minutes at 37°C. RNA was precipitated as described in **section 2.2.9**.

2.2.11. Polymerase Chain Reaction

Unless specified otherwise, all PCR reactions were carried out in Techne TC 300G or BioRad T100™ thermal cyclers using Reddymix or Dreamtaq Green (Thermo Fisher Scientific, 11540344, K1081) PCR master mixes, according to the manufacturer's instructions.

2.2.12. PCR purification

All PCR reactions were purified either by using the QIAquick® or MinElute® PCR Purification Kits (Qiagen, 28104, 28004) according to the manufacturer's instructions or by exonuclease 1 (Exo1) (Thermo Fisher Scientific, 15513677) – shrimp alkaline phosphatase (SAP) purification (NEB, M0371S).

2.2.13. Site-directed mutagenesis

Site directed-mutagenesis was carried out using the QuickChange XL Site-directed mutagenesis kit (Agilent Technologies, 200521) or the KOD Hot Start DNA polymerase (Merck, 71086). Primers were designed using the QuickChange primer

design facility[1] and are listed in table 2.3. The 25 µL QuickChange XL Site-directed mutagenesis reaction was set up according to manufacturer's instruction, except 400 – 500 ng template DNA was used. The 25 µL KOD Hot Start DNA polymerase reaction contained 1 x KOD buffer, 15 µM forward and reverse primer, 2 mM dNTPs, 20 ng template, 25 mM MgSO4, 0.04 % PCR-grade DMSO and 0.5 U polymerase. PCR was carried out in a Techne TC-3000X thermal cycler under these conditions: initial denaturation at 95°C for 5 minutes; 18 - 25 cycles of 95°C for 1 minute, annealing for 1 minute (temperatures noted in **table 2.3**), extension at 68°C for 1 minute/kb template; and final extension at 68°C for 7 - 10 minutes. 5 µL of the reaction were run on an agarose gel to determine if the reaction was successful and a specific PCR product was synthesized. The remainder of the reaction was treated with Dpn1 for 1 hour at 37°C to digest the methylated un-mutated template DNA. 10 µL of the reaction were then diluted in a total volume of 50 µL ddH_2O to reduce toxicity to the cells during transformation. 50 µL of diluted DNA were gently mixed with 50 µL of chemically-competent DH5α cells as described in **section 2.2.1.1**. If low transformation rate was expected, the cell plating step was amended as follows. The full 200 µL of cells in LB were centrifuged at 3,000 rpm for 2 minutes and the supernatant was removed. The cells were resuspended in 50 µL of LB broth and plated onto selective plates. Single colonies were inoculated into 5 mL of LB broth for growth and subsequent DNA extraction as described in section **2.2.1.2** and sequenced to confirm mutagenesis.

[1] www.genomics.agilent.com/primerDesignProgram.jsp?toggle=uploadTrans&mutate=true&_requestid=12768

Primer name	Sequence	F/R	Ta (°C)
TDP1^{K111R} (F)	GTGGTGATCAGAAAGGAGAAAG	F	50
TDP1^{K111R} (R)	CTTTCTCCTTTCTGATCACCAC	R	50
TDP1$^{S13\text{-}15A}$ (F)	GAAGGCGATTATGGGAGGTGGACCATAGCTGCTGCTGA TGAAAGTGAGGAAGAAAAGCC	F	70
TDP1$^{S13\text{-}15A}$ (R)	GGCTTTTCTTCCTCACTTTCATCAGCAGCAGCTATGGTCC ACCTCCCATAATCGCCTTC	R	70
TDP1$^{S13\text{-}15D}$ (F)	CTCAGGAAGGCGATTATGGGAGGTGGACCATAGATGAT GATGATGAAAGTGAGGAAGAAAAGCCAAAAC	F	64.3
TDP1$^{S13\text{-}15D}$ (R)	GTTTTGGCTTTTCTTCCTCACTTTCATCATCATCATCTATG GTCCACCTCCCATAATCGCCTTCCTGAG	R	64.3
TDP1$^{S90\text{-}91A}$ (F)	GGCTGGTGTCTGGCCGCCAGTGATGATGAGCT	F	63
TDP1$^{S90\text{-}91A}$ (R)	AGCTCATCATCACTGGCGGCCAGACACCAGC	R	63
TDP1$^{S90\text{-}92A}$ (F)	GGTGTCTGGCCGCCGCTGATGATGAGCTG	F	63
TDP1$^{S90\text{-}92A}$ (R)	GCAGCTCATCATCAGCGGCGGCCAGACACC	R	63
TDP1$^{S90\text{-}92D}$ (F)	CAGGAGGACCTCGGCTGGTGTCTGGACGACGATGATG ATGAGCTGCAACCAGAAAT	F	67
TDP1$^{S90\text{-}92D}$ (R)	ATTTCTGGTTGCAGCTCATCATCATCGTCGTCCAGACAC CAGCCGAGGTCCTCCTG	R	67
TDP1^{S90A} (F)	CTCGGCTGGTGTCTGGCCAGCAGTGATGATG	F	63
TDP1^{S90A} (R)	CATCATCACTGCTGGCCAGACACCAGCCGAG	R	63
TDP1$_{TR}^{S13\text{-}15A}$ (F)	GAAGGCGATTATGGGAGGTTCACGATAGCAGCCGCCG ACGAAAGTGAGGAAGAAA	F	64.3
TDP1$_{TR}^{S13\text{-}15A}$ (R)	TTTCTTCCTCACTTTCGTCGGCGGCTGCTATCGTGAACCT CCCATAATCGCCTTC	R	64.3
TDP1$_{TR}^{S13\text{-}15D}$ (F)	GTCTCAGGAAGGCGATTATGGGAGGTTCACGATAGATG ACGACGACGAAAGTGAGGAAGAAAAGCCAAA	F	65.4
TDP1$_{TR}^{S13\text{-}15D}$ (R)	TTTGGCTTTTCTTCCTCACTTTCGTCGTCGTCATCTATCGT GAACCTCCCATAATCGCCTTCCTGAGAC	R	65.4
TDP1$_{TR}^{S90\text{-}92A}$ (F)	GACCTCGGCTTCTGCCTCGCAGCTGCCGACGATGAGCT	F	69.2
TDP1$_{TR}^{S90\text{-}92A}$ (R)	GGTTGCAGCTCATCGTCGGCAGCTGCGAGGCAGAAGCC	R	69.2
TDP1$_{TR}^{S90\text{-}92D}$ (F)	CAGGAGGACCTCGGCTGGTGTCTGGACGACGATGATG ATGAGCTGCAACCAGAAAT	F	67
TDP1$_{TR}^{S90\text{-}92D}$ (R)	ATTTCTGGTTGCAGCTCATCATCATCGTCGTCCAGACAC CAGCCGAGGTCCTCCTG	R	67

Table 2.3. Sequences and annealing temperatures of site-directed mutagenesis primers used in this thesis. Mutagenic bases are in red.

2.2.14. Gibson assembly

To clone the mutagenized N-terminus of *TDP1* (from vector pCI-puro-Myc-TDP1$^{1\text{-}150,\ S13\text{-}15A,\ S90\text{-}92A}$) into a full-length *TDP1* plasmid (pCI-puro-Myc-TDP1), overlapping primers (table 2.4.) were designed using the NEBuilder® Assembly Tool (https://nebuilder.neb.com/). The insert and backbone were amplified using these primers with the KOD Hot Start DNA polymerase (Merck, 71086). The 50 µL reaction was set up according to manufacturer's instructions using 5-10 ng of template DNA. DMSO was added to a final concentration of 4 % into the backbone PCR reaction to disrupt secondary structures in the template. The PCR reaction was carried out in a Techne TC-3000X thermal cycler under these conditions: initial denaturation at 95°C for 2 minutes; 35-40 cycles of 95°C for 20 seconds, annealing for 10 seconds at 62°C (backbone) or 65°C (insert), extension at 70°C for 7 minutes (backbone) or 30 seconds (insert); and final extension at 70°C for 7 - 10 minutes. The whole reactions were subjected to agarose gel electrophoresis and gel extraction using the QIAquick® Gel Extraction Kit (Qiagen, 28704), according to manufacturer's instructions. Gibson assembly was carried out on the purified DNA fragments using the Gibson Assembly Cloning Kit (NEB, E5510). The reaction was set up according to the manufacturer's protocol using 80 ng of backbone and 8.4 ng insert at a 1:3 backbone to insert ratio and incubated at 50°C for 30 minutes. 2 µL of the assembly reaction were transformed into NEB5α chemically-competent cells, according to the Gibson Assembly Chemical Transformation Protocol. Single colonies were inoculated into 5 mL of selective LB media for growth and subsequent DNA extraction as described in section 2.2.1.2. Correct insertion and its orientation was determined by restriction

Overlaps	Oligo (Uppercase = gene-specific primer)	Anneals	F/R	Ta (°C)
-	CTCGAGAGTCTCCTCTGAATTC	pCI-myc-TDP1	R	64.9
pCI-myc-TDP1	tcagaggagactctcgagATGTCTCAGGAAGGCGATTATG	pCI-myc-TDP1$^{1-150}$	F	62.1
pCI-myc-TDP1	ccgtcattgggagcaGAGATGTCTTTCTCCTTTTTGATC	pCI-myc-TDP1$^{1-150}$	R	62.1
-	TGCTCCCAATGACGGCAC	pCI-myc-TDP1	F	64.9

Table 2.4. Gibson assembly cloning primers. Uppercase bases denote gene-specific primers during amplification. Target plasmid is shown in the 'anneals' column. Lowercase bases denote overhangs which overlap pCI-myc-TDP1 plasmid during Gibson assembly.

digestion with EcoR1 and EcoRV. Selected colonies were sequenced to confirm successful cloning.

2.3. General Zebrafish techniques

2.3.1. Zebrafish husbandry

All adult zebrafish work was carried out in the Bateson Center aquaria at the University of Sheffield. The zebrafish facilities were maintained at a constant temperature of 28°C on a 14:10 hour light:dark cycle. The fish were kept in tanks at a density of 4 animals per 1 L or less and fed artemia or dry food (GEMMA Micro, SKRETTING) twice a day.

Experimental procedures were carried out in accordance with the UK Home Office Animals (Scientific Procedures) Act 1986 under project licenses 40/3641 and 40/3738 issued to Dr. Fredericus Van Eeden and personal license I023015BA issued to Ringaile Zaksauskaite.

2.3.2. Zebrafish strains and lines

All wild-type (WT) zebrafish used are either London wild-type (LWT) or nacre. All mutant lines and their WT siblings were generated from LWT fish and out-crossed to nacre fish at the generation 0 (G0) stage. All mutant lines were generated using the CRISPR/Cas9 system as described in the relevant chapters. Transgenic fish from Dr. Tennore Ramesh lab were generated in AB background.

2.3.3. Zebrafish embryo collection and maintenance

Multiple pairs of males and females were set up in tanks with dividers overnight. The dividers were pulled out in the morning as required to allow mating stimulated by the start of the light cycle. Occasionally, instead of pair-mating, marble trays with a mesh were placed inside the tanks overnight for embryo collection in the morning. Once the embryos were laid, they were collected using a fine sieve and washed with aquaria water and incubated in 1 x E3 medium (500 µM NaCl, 17 µM KCl, 33µM $CaCl_2$, 33 µM $MgSO_4$) with 0.0001 % methylene blue at 28°C. The embryos were kept in approximately 40 mL of E3 medium in 10 cm petri dishes at a density of maximum 60 embryos per dish. The plates were monitored for any unfertilized, dead or abnormal embryos, which were removed and medium was replaced when required to keep the healthy embryos clean. Animals were kept no longer than 5.2 dpf, unless they were raised to adulthood, according to the UK Home Office Animals (Scientific Procedures) Act 1986.

2.3.4. Zebrafish anaesthesia

Embryos were anaesthetized in 1 mL/petri dish of 0.4% w/v tricaine (PharmaQ, Hampshire) for ease of manipulation. If embryos were to be kept afterwards, the plate was replaced with fresh E3 media. Adults were anaesthetized in 0.017% tricaine in aquarium water and monitored in recovery.

2.3.5. Zebrafish fin clipping

Adult zebrafish (≥ 2 months of age) were anaesthetized in a beaker in 200 mL of diluted tricaine one fish at a time. As soon as they were unresponsive, the animals

were gently fished out with a spoon. If the fish started moving at this point, they were returned into the beaker to continue anesthesia and fished out again. No more than a third of the tail fin was clipped using scissors washed in 70 % ethanol and aquarium water. The zebrafish were returned to the tank for recovery and monitoring and the fin-clip was transferred with fine tweezers into a 96-well plate (StarLab, E1403-6200) on ice for genomic DNA extraction. If re-clipping was required, it was carried out no sooner than 2 months after the previous fin-clip to allow regeneration and no more than 3 times per fish.

If genotyping was required prior to raising, the larvae were fin-clipped at 3 dpf. They were anaesthetized and 10 µL of Tween-20 was added per plate. The fish were transferred onto a petri dish lid with masking tape and excess media removed to set the embryos in place. A scalpel was used to cut the tail fin at the break in the pigment line to avoid cutting off the circulation **(figure 2.1.)**. The tail fragment was transferred to a 96-well plate (StarLab, E1403-6200) using a Pasteur pipette for genomic DNA extraction. To confirm the expulsion of the tail fragment, the pipette was washed out onto the lid with a large volume of media. The corresponding fish were transferred into a 24-well plate (Corning™, 10732552) in 3 mL of E3 medium and checked at the end of 3 and 4 dpf.

2.3.6. Intraperitoneal drug injections

Zebrafish were maintained in groups of 7-9, weighed and fasted for 24 hours prior to injection. They were anaesthetized (section 2.3.4) and placed in a tricaine pre-wetted sponge with the pelvic fins facing upwards. A final concentration of 45 mg/kg Topotecan or 30 % DMSO in a total volume of 10 µL of Hank's buffered solution

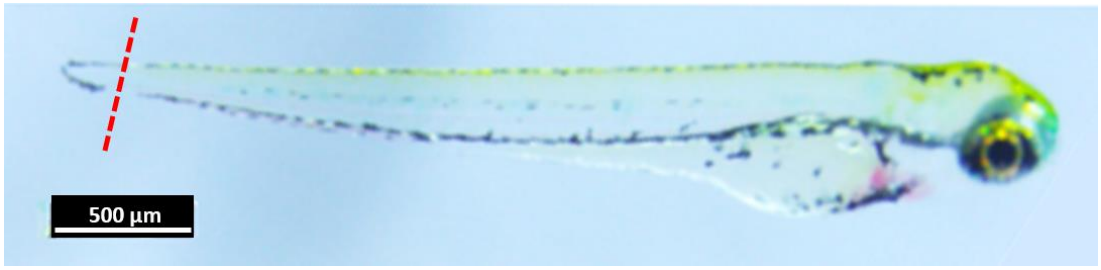

Figure 2.1. 3 dpf embryo fin-clips. The tail fin of larvae is cut at the gap in the pigment line (red line) and used for genomic DNA extraction.

(Gibco, 11530476) were injected into the intraperitoneal space using an insulin syringe with a 30G needle (Bunzl Healthcare, 324826) in two daily injections. The fish were recovered and monitored daily using the Adult ViewPoint zebrafish behaviour system in the Sheffield Zebrafish Screening Unit. They were culled 5 days post-injection by immersion fixation **(section 2.6.1)**.

2.3.7. Microinjection of embryos

Prior to injection, injection plates were prepared by pouring ~30 mL of 2 % w/v agarose in 1x E3 (500 µM NaCl, 17 µM KCl, 33µM $CaCl_2$, 33 µM $MgSO_4$) into a 10 cm petri dish and creating a ladder effect **(Figure 2.2.)**. Injection needles were pulled from thin-wall single-barrel borosilicate glass capillaries (World Precision Instruments, TW120-4) in a micropipette puller (P-97, Sutter Instrument Co., Novato, USA). Injection solution was prepared in 10 – 20 % phenol red in nuclease-free H_2O to aid injection.

Once preparations were made, the microloader pipette tip (Eppendorf, 930001007) was used to fill the injection needle with the solution. The needle was secured into the PV820 Pneumatic Pico-Pump injector (World Precision Instruments) and the tip of the needle was broken off with extra-fine tweezers (Agar Scientific, T5130). The needle was then immersed into mineral oil on top of a 10 mm graticule and the injection volume adjusted to 0.1 mm (0.5 nL) by changing the 'period' setting on the injector in 'timed' mode. The needle was kept immersed whilst 1-cell stage embryos were collected and aligned on the injection plate and any liquid is removed. The required volume was then injected into the yolk or the cell of the embryos.

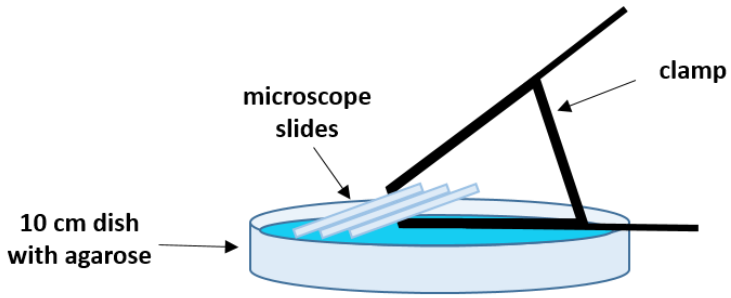

Figure 2.2. Microinjection plate preparation. 3 clamped microscope slides (Thermo Fisher Scientific, 10144633BF) were placed on the surface of 30 mL 2 % w/v agarose at an angle with the clamp resting on the dish. This allows for a few rows of embryos to be aligned for injection in one dish.

After injection, extra care was taken to remove any abnormal or dead embryos as injection can increase their incidence.

2.3.8. Zebrafish genomic DNA extraction

Embryos above 24 hpf and embryonic or adult fin clips were lysed in 50, 15 and 100 µL of DNA extraction buffer (10 mM Tris-HCl pH8, 1 mM EDTA, 0.3% Tween-20, 0.3% Triton), respectively. The samples were boiled for 10 minutes at 98ºC in a thermocycler and cooled down to 55ºC before adding 2 µL of 25 mg/mL proteinase K. Proteinase K digestion was carried out for 1-3 hours at 55ºC, then the enzyme was inactivated at 98ºC for 10 minutes. The digestion reaction was diluted by adding 100 µL of ddH_2O, except in the case of 3 dpf fin clips, where no water was added. The tissue debris was pelleted by centrifugation at 13,300 rpm for approximately 4 minutes and 1.5 – 5 µL of the supernatant was used in PCR (as described in section 2.3.9).

2.3.9. Genotyping

Big genomic deletions were identified by PCR and electrophoresis **(section 2.3.2)** alone. Small deletions were identified either by sequencing or restriction digest followed by electrophoresis. When very fine resolution of DNA fragments was required, a 3 % w/v agarose (1.5 % MetaPhor agarose (Lonza, LZ50181), 1.5 % agarose) gel was set. Samples were then subjected to 150 V electrophoresis for 30 minutes.

2.3.9.1. Genotyping by restriction digest

15 µL of the PCR reaction was digested for 2 – 3 hours at the appropriate temperature with 2.5 – 10 U of restriction enzyme in a total volume of 20 µL without added buffer. The extra time and enzyme were crucial to ensure complete digestion and therefore correct genotyping.

2.3.9.2. Derived cleaved amplified polymorphic sequences (dCAPS)

When a flanking restriction site was not available near the mutation, in some cases it was possible to take advantage of the dCAPS method. This method introduces a restriction site into the PCR product by using mismatched primers **(Figure 2.3.)**.

2.4. Zebrafish genome editing

A simplified overview of zebrafish genome editing can be found in **figure 2.4.** It focuses on the CRISPR/Cas9 system, but the process for Tol2 transgenesis is very similar.

2.4.1. CRISPR/Cas9 system

2.4.1.1. Guide RNA (gRNA) oligonucleotide design

DNA template oligonucleotides for guide RNA (gRNA) transcription were designed to contain a scaffolding sequence, a specific target site and a T7 polymerase promoter site. The targeting sequence was complementary to a 20 bp stretch of genomic DNA, immediately followed by an endogenous PAM motif (NGG), which the Cas9 nuclease recognizes. Preferably, the target sequence had an internal or flanking restriction site

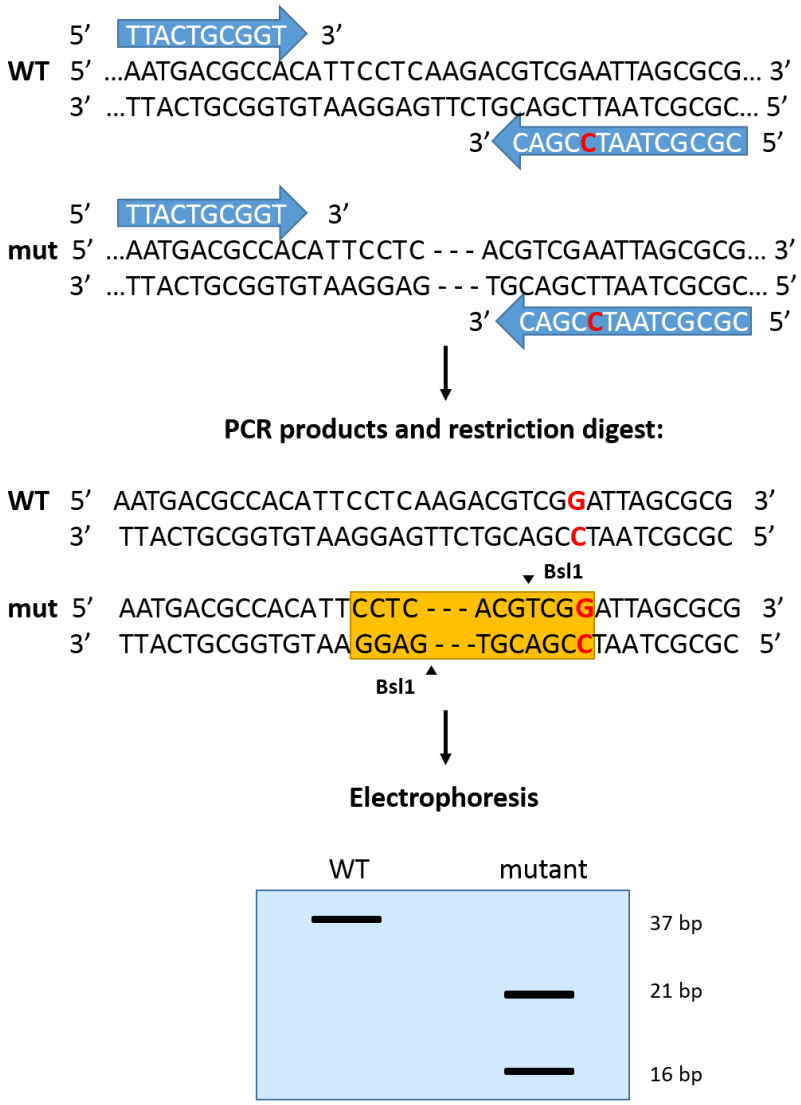

Figure 2.3. Diagram of derived cleaved amplified polymorphic sequences (dCAPS). PCR primers are designed in a way to introduce a mutation in the PCR product, which results in a restriction site in either the wild-type or the mutant sequence. Then after restriction digestion and electrophoresis of the PCR product, the sequences can be discriminated. In the diagram an adenine is mutated into a guanine (red), which results in a Bsl1 restriction site in the mutant PCR only (Bsl1 consensus sequence CCNNNNN/NNGG, yellow box). After digestion with Bsl1, the mutant PCR results in a 21 and a 16 bp band, and wild-type PCR remains undigested at 37 bp in length.

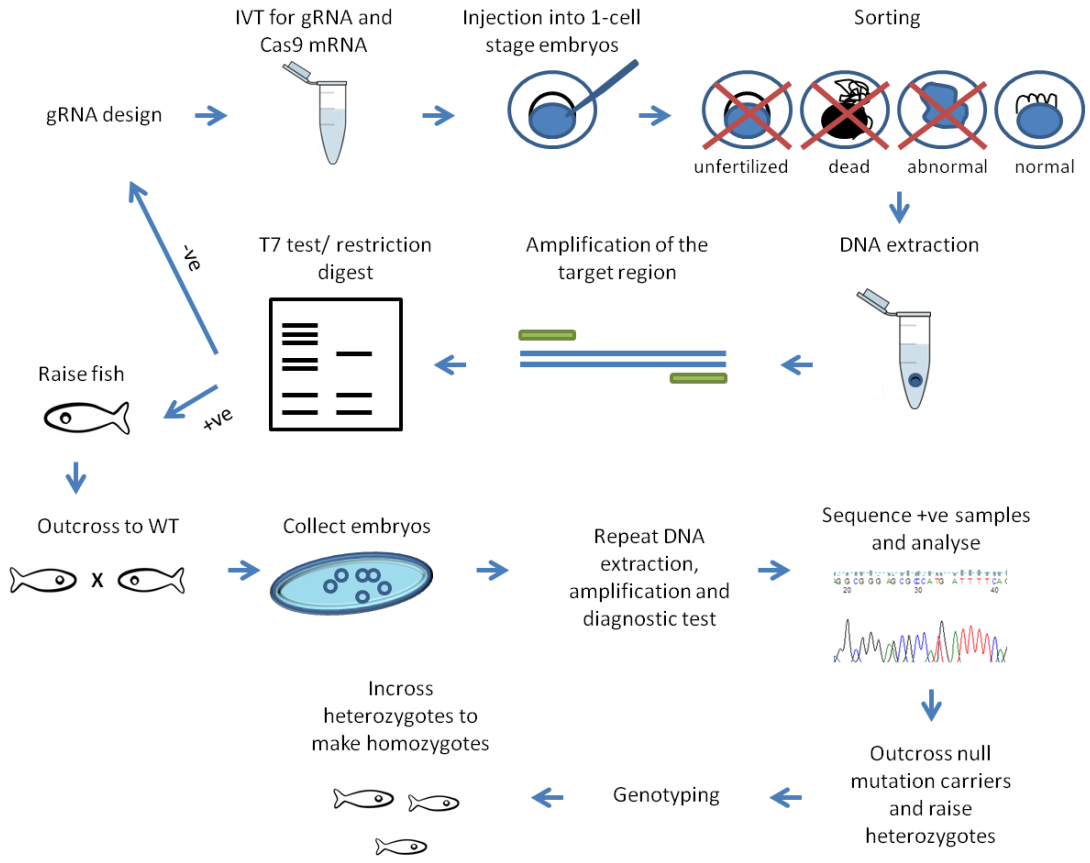

Figure 2.4. Null-allele generation using CRISPR/Cas9. Firstly, guide RNA is designed. It is then transcribed *in vitro* along with Cas9 mRNA, both of which are injected into 1-cell stage wild-type zebrafish embryos into the blastoderm or the yolk. A few hours after injection unfertilized, dead and abnormal embryos are removed. Genomic DNA is extracted from 24 hpf – 4 dpf embryos and used to amplify the region of interest, where Cas9 is expected to cut. The efficiency of the gRNA is determined by either a restriction digest or a T7 endonuclease test, depending on whether the target region contains a restriction site. If the test is positive, the embryos are raised. Once they have sexually matured, they are outcrossed to WT fish to determine the rate of germline transmission. This is done by DNA extraction, amplification of region of interest and diagnostic test, as described above. All positive samples are sequenced in order to determine the exact mutation. If it does not result in a frameshift and a null allele, the whole process is repeated. If it does, the null mutation carriers are outcrossed to raise heterozygotes, which then have to be confirmed by genotyping and incrossed to generate homozygote mutants.

to aid genotyping and started with GG to facilitate *in vitro* transcription of gRNA. In some cases, where an endogenous GG start was not available, it was artificially tagged onto the 3' of the targeting sequence in the oligonucleotide. In addition, it was aimed to find a suitable gRNA in the first few exons to increase the chance of nonsense-mediated decay (NMD) of mRNA.

2.4.1.2. *In vitro* transcription of gRNA

5 µM of T7 primer and 5 µM of template DNA in a total volume of 20 µL were denatured at 95°C in a thermocycler for 5 minutes. The thermocycler was left on with the sample inside for 5 hours or overnight, so that the primer and the template could anneal by slowly cooling. 5 µM of annealed template was then used for *in vitro* transcription of gRNA with the MEGAshortscript™ T7 Transcription Kit (Life

Technologies, AM1354), according to the manufacturer's instructions. The reaction was terminated by adding 115 µL of nuclease-free H_2O and 15 µL of ammonium acetate stop solution provided with the kit. The RNA was then precipitated by adding two volumes of ethanol and incubation for at least 15 minutes at -20°C. To pellet the gRNA, the sample was centrifuged at 4°C and 13,300 rpm for 15 minutes. The supernatant was removed and the pellet was resuspended in 15 µL of nuclease-free H_2O. Successful gRNA synthesis and purification was determined by running 1 µL of the reaction on a 2.5 % w/v agarose for approximately 10 minutes before and after ethanol precipitation.

2.4.1.3. *In vitro* transcription of Cas9 messenger RNA (mRNA)

pCS2-nCas9n plasmid (Addgene, 47929) was linearized at 37°C with NotI-HF and *in vitro* transcribed as described in section 2.3.8.

2.4.1.4. Co-microinjection of gRNA and mRNA

Cas9 mRNA and gRNA were injected into embryos (as described in section 2.4.6) at a concentration of 2.4 µg and 0.4 µg/µL, respectively (Hruscha et al., 2013).

2.4.1.5. Determination of CRISPR-Cas9 efficiency

24 hours post-injection genomic DNA was extracted **(section 2.4.7)** from 6 embryos per injection plate and 6 uninjected controls, and used for PCR **(section 2.3.9)** of CRISPR target region. In the case of big deletions, changes could already be seen solely after PCR and electrophoresis, but an additional method was required for smaller deletions. For the latter, if a flanking restriction site was available, then the appropriate restriction digest was carried out (section 2.4.8.1). When the CRISPR-Cas9 was working efficiently, a different digestion pattern would emerge. If a restriction site was not available, T7 endonuclease assay was utilized.

2.4.1.5.1. T7 endonuclease 1 assay

5 – 10 µL of PCR product in 1 x NEB2 buffer in a total volume of 15 – 20 µL was denatured for 5 minutes at 95°C and re-annealed by dropping the temperature by -2°C/second for 5 seconds, then by 0.1°C/second for 600 seconds. 1 U of T7 endonuclease 1 was then added for digestion at 37°C for 2 – 15 minutes. If mutations were present in a part of the cells, denaturing and annealing the DNA would form heteroduplexes, which were in turn digested by the T7 endonuclease 1 **(figure 2.5.)**.

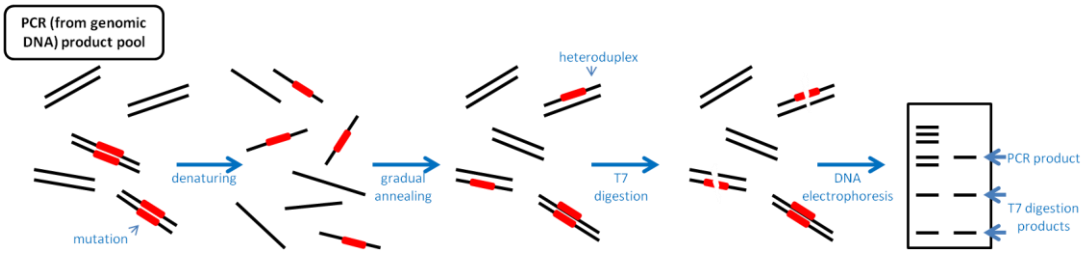

Figure 2.5. T7 endonuclease assay diagram. PCR product pool containing mutations is denatured and slowly reannealed to form heteroduplexes. T7 endonuclease 1 recognizes and cuts these heteroduplexes into two parts, which run further on an agarose gel than the original PCR product. The more efficiently the CRISPR-Cas9 system works, the more of these heteroduplexes are created and the brighter the lower two bands become.

After electrophoresis (section 2.3.2), the intensity of the digested DNA positively correlates with CRISPR efficiency.

2.4.1.6. Determination of germ-line transmission of desired mutations

Once the injected fish started laying (at approximately 2 months), they were out-crossed to wild-type fish and 7 embryos per cross were genotyped **(section 2.4.8)**. The embryos that showed a different pattern after electrophoresis were then sequenced to determine the exact mutation and whether there is a resulting frame-shift.

2.4.2. Tol2 transgenesis

Tol2 transgenesis was carried out with the help of the Tol2 Kit (Kwan et al., 2007) with vectors kindly donated by the Dr. Henry Roehl and Dr. Freek Van Eeden labs.

2.4.2.1. Transgene cloning into entry vector

Primer 3 v. 4.0 (http://primer3.ut.ee/) was used to design primers **(table 2.5)** close to the ends of the gene. Primers matching the 5' and 3' ends of the gene were designed with an extraneous Age1 restriction site and a few extra base pairs on the 5' of the forward primer and half of an extraneous SnaB1 restriction site on the 5' of the reverse primer **(table 2.5A)**. The target genes, *TDP1* and *TDP1*^{H493R} were amplified from the pCI and pcDNA5 plasmids **(table 2.1)** with these primers using KOD Hot Start polymerase (Merck, 71086) via a touchdown PCR reaction. Initial denaturation was carried out for 1 minute at 95°C, then 25 cycles of 50 second denaturation at 95°C, 10 second annealing, gradually decreasing by -0.2°C/cycle from 58°C to 53°C and 2 minute extension at 68°C, finished by a single cycle of 5 minutes at 68°C for final

(A)

Target	Oligo (Uppercase = gene-specific primer)	F/R	Ta (°C)
TDP1	cgac**accggt**cgccaccATGTCTCAGGAAGGCGATTATGGGAGG	F	71.8
TDP1	**gta**TCAGGAGGGCACCCACATGTTCCCAT	R	65

(B)

Target	Oligo	F/R	Ta (°C)
TDP1	AGGAAGGCGATTATGGGAGG	F	56.6
TDP1	GGCACCCACATGTTCCCAT	R	58.2

Table 2.5. Primers used in transgene cloning. (A) Primers used for cloning of transgenes into 3' entry vectors. Uppercase base pairs denote the gene-specific part of the primer. Age1 restriction site (in red) was added onto the 5' of the forward primers and half of SnaB1 restriction site (in blue) was added to the 5' of reverse primers. Full SnaB1 restriction site – TAC/GTA). **(B)** Primers generated using Primer 3 v. 4.0 and used for sequencing clones.

extension. The amplicons were purified using the Qiaquick® PCR Purification Kit (Qiagen, 28104), according to manufacturer's instructions. The purified PCR products were digested with 5 U of Age1, and 4 µg of the p3E-lxP-mCherry backbone were digested with 5 U of Age1 and 10 U of SnaB1 for hour at 37°C in a total volume of 100 µL. The restriction enzyme was heat inactivated at 80°C for 20 minutes to prevent further cutting and the required DNA fragments were extracted using the QIAquick® Gel Extraction Kit (Qiagen, 28704), according to manufacturer's instructions. The DNA concentration was quantified using the gel quantification method as described in section 2.2.2. Inserts were then cloned into the multiple cloning site (MCS) of the backbone at a 3 : 1 insert to vector ratio using a total amount of 100 ng of DNA with the Quick Ligation™ kit (New England Biolabs, M2200S) and transformed into NEB5α cells, according to the manufacturer's instructions. 20 µL and 50 µL were spread onto agar plates with 50 µg/mL kanamycin and incubated at 37°C overnight. Colonies were picked and cultured overnight at 37°C in 5 mL of 50 µg/mL kanamycin in LB media. DNA was extracted using the QIAprep® Spin Miniprep kit (Qiagen, 27104), according to manufacturer's instructions. To determine correct insertion size and orientation, a double restriction digest with Age1 and SnaB1 and agarose gel electrophoresis was carried out as described in **sections 2.2.3** and **2.2.6**. The correct clones were sequenced using the GATC Biotech (Cologne, Germany) LightRun Sanger sequencing service and DNA concentration was determined using the gel quantification method, as described in section 2.2.2. Two 3'-entry constructs were generated: p3E-lxP-TDP1pA and p3E-lxP-TDP1^{H493R}pA **(table 2.1)**.

2.4.2.2. Multi-gateway cloning

Multi-gateway cloning takes advantage of LR recombination, where the LR clonase transfers DNA fragments between different vectors using attL and attR sites. In my effort to generate transgenic zebrafish lines I used a destination vector with Tol2 recognition sequences and 3 entry vectors: 5'-entry vector with a ubiquitin promoter, middle entry vector with a loxP-BFP-STOP cassette and a 3'-entry vector with a loxP site **(section 2.4.7.2)** and a transgene of interest. After the LR reaction, the content of all entry vectors is inserted to the destination vector in the required order and in frame.

20 fmol of each plasmid: destination vector pDestTol2CG2, pENTR5'_ubi, pME-lxP-BFP and one of the 3'-entry vectors, were combined in 1 x TE buffer (10 mM Tris, 1 mM EDTA, pH 8) with 2 µL of LR Clonase™ 2 Plus (Invitrogen, 12538120) in a total volume of 10 µL. The sample was briefly vortexed twice and incubated for 20 hours. 2 µg of Proteinase K (Invitrogen, 12538120) were added and the sample was incubated for 10 minutes at 37°C to stop the recombination reaction. 3 µL of the reaction were then transformed into NEB10β cells (New England Biolabs, 30191), according to manufacturer's protocol, plated onto 100 mg/mL carbenicillin-resistance agar plates and incubated at 37°C overnight. 6 translucent colonies were picked for each construct, then streaked onto selective plates with 100 mg/mL carbenicillin and incubated in 5 mL LB with 50 mg/ml ampicillin at 37 °C overnight. DNA was extracted using the QIAprep® Spin Miniprep kit (Qiagen, 27104), according to manufacturer's instructions, and its concentration was quantified with the NanoDrop ND-Spectrophotometer. A diagnostic digest was carried out using Xho1 to

cut out the insert **(section 2.2.6)** and fractionating the sample on a 0.7 % w/v agarose gel **(section 2.2.4)**. Clones with correct insert size were sequenced to confirm correct clonase recombination reaction. Colonies from the streaked plates were then grown in 100 mL LB with 50 mg/ml ampicillin at 37 °C overnight and used for DNA extraction with the Plasmid Plus Midi Kit (Qiagen, 12943). Two transgene constructs were generated: pDestTol2CG2-ubi-lxP-BFP-lxP-TDP1 and pDestTol2CG2-ubi-lxP-BFP-lxP-TDP1^{H493R} **(table 2.1)**.

2.4.2.3. Injection of transgenes

Tol2 transposase mRNA was synthesized from the Not1-linearized pCS2FA-Tol2 vector as described in section 2.2.8. 5 µL of injection solution were prepared, containing 50 ng/µL Tol2 mRNA, 50 ng/µL pDestTol2CG2-ubi-lxP-BFP-lxP-transgene construct in 20 % phenol red. A range of volumes (0.5 – 2.5 nl) was injected into 1-cell stage embryos from a *tdp1*$^{SH475/SH476}$ incross, as described in section 2.3.6.

2.4.2.4. Determination of injection efficiency

At 24 hours post-injection embryos were sorted for GFP expression in the heart (*cmlc2*:EGFP) and at 48 hours post-injection for ubiquitous BFP expression using the Zeiss AxioZoom.V16 dissecting microscope. The embryos with the highest levels of BFP expression were raised.

2.4.2.5. Selection of transgenic lines

Once the fish were laying at approximately 3 months post-fertilization, the injected G_0 fish were outcrossed to *tdp1*$^{-/-}$ zebrafish. Only GFP-expressing embryos were

selected at 24 hpf and at 48 hpf the most highly BFP-expressing embryos were raised for the F_1 generation. The F_1 zebrafish should stably express BFP.

2.4.2.6. Cre-Lox recombination

To remove the BFP-STOP cassette and allow expression of the transgenes, Cre-Lox recombination was used. The pCS2-Cre.zf1 plasmid was linearized with Not1 and used to synthesize Cre mRNA as described in section 2.2.8. 300 ng of Cre mRNA were injected into one-cell stage embryos as described in section 2.3.6. Embryos were then screened for loss of BFP expression and at 5 dpf harvested **(section 2.7.1)** for western blotting to confirm expression of the transgenes **(section 2.7.6)**.

2.5. Zebrafish gene expression analysis

2.5.1. Real-time quantitative PCR (RT-qPCR)

Total RNA was prepared using TRIzol reagent extraction, as described in section 2.2.8, and the concentration was quantified using the NanoDrop ND-Spectrophotometer at 260 nm. Up to 5 µg of total RNA were reverse transcribed with the Tetro cDNA synthesis Kit (Bioline, BIO-65042), according to manufacturer's instructions. Primers were designed to be 18 – 30 bp long and free of primer dimers, to have a GC content of 40 – 60 % and a melting temperature of 55 – 60°C, and to produce amplicons of 75 – 200 bp **(table 2.6)**.

5 µL of a 1:10 dilution of cDNA and 5 µM of primers in 1 x SensiMix SYBR Hi-ROX master mix (Bioline, QT605-05) were used to set up an RT-qPCR reaction. To generate the standard curve, equal volumes of each of the cDNA samples were mixed and 100 %, 10 %, 1% and 0.1 % dilutions were used as a template for each primer pair.

Target	Oligo	F/R	Tm (°C)	GC (%)	Product size (bp)
CtIP	TTCTGGGAGGTGGGATTTCC	F	56.8	55	165
CtIP	TGTGAACAGCTCGACTCAGT	R	56	50	165
GAPDH	GTGGAGTCTACTGGTGTCTTC	F	54.4	52	173
GAPDH	GTGCAGGAGGCATTGCTTACA	R	58.1	52	173
Mre11	CGGTCCGTAATGAACAGCAG	F	56	55	235
Mre11	TTGAGCATGGTGTTGGGTTG	R	56.1	50	235
Mus81	CACATTATTCTGCCGCTCCC	F	56.2	55	200
Mus81	CGGCTGCTTTATCACCAGAC	R	56.1	55	200
Tdp2	ACCAATCCCAGGAGAGAACG	F	56.6	55	178
Tdp2	TCTTGTTTGCCCAGCTGTTC	R	56	50	178
Xpf	CCTTCACTTCTGCATCGACG	F	59.9	55	217
Xpf	AGAATGGTTTAGCGGGGTCA	R	56.4	50	217

Table 2.6. Primers used in RT-qPCR. The target, sequence, direction, melting temperature (Tm), GC content and product size of primers used in RT-qPCR.

The reaction was run in triplicate in a Rotor-Gene 6000 real-time thermocycler (Corbett Research) under these conditions: 95°C for 10 minutes, followed by 45 cycles of 95°C for 15 seconds, 55°C for 15 seconds, and 72°C for 30 seconds.

2.5.2. Whole-mount *in situ* hybridization

Whole mount *in situ* hybridization was carried out according to Wilkinson lab protocol. Probes of 800 – 1000 bp were amplified from either wild-type zebrafish cDNA or genomic DNA using primers listed in **table 2.7** with KOD Hot Start DNA polymerase (Merck, 71086), according to the manufacturer's instructions. The thermocycling conditions were as follows: 95°C for 3 minutes, followed by 30 cycles of 95°C for 20 seconds, 53°C for 10 seconds, and 70°C for 45 seconds; finished with 5 minutes at 70°C. The products were subjected to electrophoresis on a 2 % w/v agarose gel and specific bands were extracted using the QIAquick® Gel Extraction Kit (Qiagen, 28704), according to manufacturer's instructions. A second round of PCRwas carried out on the extracts to increase the DNA concentration using the same primers, except for zgc:173742, for which nested primers were used **(table 2.7)**. 2 µL of the final PCR product were used in a 20 µL transcription reaction with 1 x DIG-UTP labelling mix (Roche, 000000011277073910) 10 U of T7 or T3 RNA polymerase (Promega, P207B, P208C), 1 x provided polymerase buffer and 40 U of RnaseOUT™ Rnase inhibitor (Invitrogen, 10777019). The reaction was incubated at 37°C for 2 hours. 1 µL was removed and stored on ice. DNA was digested with 2 U of TURBO DNase (Life Technologies, AM1354) for 20 minutes at 37°C. To confirm whether an intact full-length transcript has been synthesized, 1 µL of the reaction was removed and subjected to electrophoresis **(section 2.2.4)** alongside the 1 µL removed

Target	Oligo (Uppercase = gene-specific primer)	F/R	Tm (°C)	Template	Product size (bp)
Tdp1	taatacgactcactatagggAGCAGTATCC GCCAGAATTT	F	64.6	cDNA	1030
Tdp1	aattaaccctcactaaaggTGGTCTCAGCA GCTCAAGAA	R	64.9	cDNA	1030
Tdp2b	taatacgactcactatagggAAACGTGC CGTCAGCTACTT	F	64.9	cDNA	806
Tdp2b	aattaaccctcactaaaggTCATCTGGA AAGATGGTGTGA	R	63.5	cDNA	806
Top1	taatacgactcactatagggTGCGATTA GCTCATTTCACG	F	63.1	gDNA	927
Top1	aattaaccctcactaaaggGCCGCTGTATC AATGGTTTT	R	64.4	gDNA	927
Top1l	taatacgactcactatagggAGTTCGGCAT CCCGATAGAG	F	64.4	gDNA	879
Top1l	aattaaccctcactaaaggGGAATTCACAT TCTGCATGTTT	R	63.2	gDNA	879
Top1mt	taatacgactcactatagggTTCTCTGCGT GTGGAGCAC	F	65.3	cDNA	851
Top1mt	aattaaccctcactaaaggCACAACACAAC AGATGAGCAGA	R	64.9	cDNA	851
Zgc:173742	taatacgactcactatagggATGAAGT GGCCCGTAAACTG	F	55.3	cDNA	932
Zgc:173742	aattaaccctcactaaaggCCAGGCAA ACTTATCCCTCA	R	54.6	cDNA	932
Zgc:173742 (nested)	taatacgactcactatagggAGTGGCCC GTAAACTGAAGA	F	64.5	PCR	870
Zgc:173742 (nested)	aattaaccctcactaaaggTTCTTACAC CAGGCCACACT	R	64.9	PCR	870

Table 2.7. Primers used for WISH probe synthesis. The target, sequence, direction and melting temperature (Tm) of the primers is denoted as well as the template DNA the primers are used on (cDNA, gDNA or PCR) and resulting probe length in base pairs. T7 polymerase primer site (in red) and two guanine bases (underlined) were added onto the 5' of the forward primer and T3 polymerase primer site (in blue) was added onto the 5' of the reverse primer. As a required concentration of a specific PCR producy

previously. RNA was precipitated as described in section 2.2.9, except the precipitation was carried out for 2 hours at -20°C. The pellet was resuspended in 100 µL ddH_2O and stored at -80°C.

24 hpf embryos were dechorionated and fixed in 4 % w/v PFA in PBS at 4°C overnight. They were washed in PBSTw (0.1 Tween-20 in PBS) 3 times for 5 minutes. The embryos were subjected to a methanol in PBSTw series of 5 minutes each in 25 %, 50 %, 75 % and 100 % methanol in PBSTw and stored at -20°C overnight. The embryos were rehydrated back into PBSTw through another series of 5 minute washes: 75 %, 50 %, 25% MeOH in PBSTw and then washed 4 times for 5 minutes in PBSTw. The embryos were treated with 10 µg/µL of proteinase K for 20 minutes, then proteinase K was quenched by washing twice with 2 mg/mL glycine in PBSTw for 5 minutes. Embryos were re-fixed in 4 % w/v PFA in PBSTw for 20 minutes at room temperature and washed 5 times for 5 minutes in PBSTw with shaking. Embryos were washed in50 % Hybe-/- (50 % formamide, 5 x SSC (ChemCruz, SC296419), 9.2 mM citric acid, 0.1 % Tween-20, pH 6) in PBSTw for 5 minutes and pre-hybridized in Hybe+/+ (50 % formamide, 5 x SSC, 9.2 mM citric acid, 0.1 % Tween-20, 0.5 mg/mL tRNA (Invitrogen, 15401029), 0.05 mg/mL heparin) for at least one hour at 65°C. The pre-hybe was then replaced with Hybe+/+ containing a 1:200 dilution of the probe and the sample was incubated at 65°C overnight. The Hybe solution was removed whilst keeping the tubes in the hot block. The following 10 minute washes were carried out at 65°C: 100 % Hybe-/-, 75% Hybe in 2 x SSCTw (0.1 % Tween-20 in 2x SSC), 50 % Hybe in 2 x SSCTw, 25% Hybe in 2 x SSCTw and 100 % 2 x SSCTw. The embryos were then washed 4 times for 15 minutes in 0.2 x SSCTw. The following 5 minute washes were carried

out: 75 % 0.2 x SSC in MABTw (0.1M maleic acid, 0.15 M NaCl, 0.1 % Tween-20, pH 7.5), 50 % 0.2 x SSC in MABTw, 25 % 0.2 x SSC in MABTw and 100 % MABTw. The embryos were blocked in 2 % Blocking Reagent (Roche, 11096176001) in MABTw for at least 1 hour at room temperature with gentle shaking. The blocking buffer was replaced with a 1:5000 dilution of α-DIG antibody (Roche, 11093274910) in blocking buffer and the sample was incubated overnight with gentle rocking at 4 °C. Sample was rocked for 1 hour at room temperature to allow the antibody reaction to reach completion. The sample was washed 8 times for 15 minutes in MABTw with gentle rocking. Embryos were equilibrated in BCL3 developing buffer (100 mM Tris pH 9.5, 100 mM NaCl, 50 mM $MgCl_2$, 0.1 % Tween-20) 3 times for 5 minutes at room temperature. The developing buffer was then replaced with 50 % BM Purple (Roche, 11442074001) in BCL3. The staining was developed by gently rocking at room temperature in tubes wrapped in foil until desired levels of staining were achieved (1 hour – 2.5 days). The reaction was stopped by washing in BCL3 buffer, then fixing in 4% PFA in PBS at least overnight at 4°C or 3 hours at room temperature. For imaging embryos were washed in a series of 5 minute washes: 3 times in PBSTw, once in 25 % glycerol (Invitrogen, 15514-011) in PBSTw, once in 50 % glycerol in PBSTw and once in 70 % glycerol in PBSTw. They were imaged on the Leica M165FC dissecting microscope with Leica Application Suite v.4.3.0.

2.6. Zebrafish behaviour analysis

All zebrafish behaviour analysis was carried out in the Sheffield Zebrafish Screening Facility.

2.6.1. Photomotor response (PMR) analysis

5 dpf embryos were washed in E3 media (500 µM NaCl, 17 µM KCl, 33µM $CaCl_2$, 33 µM $MgSO_4$) and transferred into a 96-well plate in E3. 100 µL of media was taken out of the last column of the plate and replaced with 100 µL of tricaine 0.4 % w/v. This group served as an immotile negative control. The fish were left to acclimatize for 30 minutes. The light in the Zebrabox ViewPoint system was left to warm up for 30 minutes at 10 % intensity. The 96-well plate was placed into the system and habituated in 10 % light for 30 minutes. The zebrafish were then subjected to 3 cycles of 5 minutes darkness (0 % intensity light) and 5 minutes light (10 % intensity light) and total distance moved in each light and dark phase was measured. Data was analysed in MicroSoft Office Excel 2016.

2.6.2. Analysis of adult zebrafish locomotion

Up to 10 tanks with single sibling fish (approximately half were controls) were imaged at any one time in the Adult ViewPoint for 3 – 8 hours total. The first 30 minutes – 1 hour were discounted as habituation time. Various parameters, including total distance moved, were analyzed in MicroSoft Office Excel 2016.

2.6.3. Swim tunnel analysis

Zebrafish were withheld food on the day of experiment and habituated in the experiment room for 1 hour. Individual zebrafish were placed in a 2.54 cm tunnel (AccuScan Instruments Inc.) (Plaut, 2000; Ramesh et al., 2010) and the water flow rate was gradually increased to 6.58 cm/sec. The fish were subjected to this flow rate for 5 minutes, then the current was increased in 6.58 cm/sec increments for 5 minutes each time, until the fish fell into a mesh net at the end of the tunnel. To

avoid false positives, the timer was paused and the current was reduced and gradually increased to allow re-entry into the highest achieved flow rate. The time of the second exhaustion was recorded. The critical swimming speed was calculated using the following formula: $U_{crit}=U_i + (U_{ii}*T_i/T_{ii})$, where U_i is the highest flow rate sustained for a whole interval (cm/sec), U_{ii} is the flow rate increment (6.58 cm/sec), T_i is the time elapsed at fatigue flow rate (in minutes) and T_{ii} is the time increment (5 minutes) (Brett, 1964; Plaut, 2000; Ramesh et al., 2010).

2.6.4. Drop test

Zebrafish were acclimatized in the analysis room for 30 minutes, then dropped into tall water tanks from 10 cm above the water level as described by Detrich *et al.* and monitored using the Adult ViewPoint system. Various parameters, including total distance moved, were analyzed in MicroSoft Office Excel 2016. Freezing time was recorded manually by starting the stopwatch every time fish were frozen for more than 1 second.

2.7. Zebrafish histology

2.7.1. Immersion fixation and decalcification

The fish were culled by immersion in concentrated tricaine for terminal anesthesia, followed by immersion in 50 mL cold neutral buffered 10 % formalin as soon as the fish are non-responsive. The tissue was fixed at 4°C for 48 hours with rotation and then moved to 50 mL of 0.5M EDTA for 3 – 4 days for decalcification.

2.7.2. Paraffin embedding and sectioning of tissue

The tissue was embedded into paraffin blocks using Dr. Catarina Henriques' protocol by staff in The University of Sheffield Medical School Bone Analysis laboratory (DU14) (Carneiro et al., 2016). The tissue was processed in a Leica TP1020 tissue processor using a series of washes: 10 minutes and then 50 minutes in neutral buffered 10 % formalin, 1 hour in 50 % ethanol, 1 hour in 70 % ethanol, 1.5 hours in 95 % ethanol, 2 hours and 2.5 hours in 100 % ethanol, 1.5 hours in 50 % Xilol in ethanol, 3 hours twice in xylene, 3 and 4.5 hours in Histosec® pastilles paraffin (Merck, 1116092504). The tissue was then embedded into paraffin blocks, according to their regular protocol. The paraffin blocks were sectioned transversely into 4 µm sections by the histology service in Sheffield Institute of Translational Neurosciences, according to their protocol.

2.7.3. Haematoxylin and eosin staining

The sections were prepared as described in sections 2.6.1 and 2.6.2 and then stained by the histology service in Sheffield Institute of Translational Neurosciences, according to their protocol. The sections were imaged using the Olympus BX60 microscope with an air objective and Q-Capture pro 7.0 software.

2.8. Mammalian cell culture

2.8.1. Cell line maintenance

Human embryonic kidney 293 (HEK293) and Flp-In™ 293 T-Rex (Thermo Fisher, R780-07) cell lines were grown as monolayers in T75 flasks at 5 % CO_2 and a constant temperature of 37°C in humidified incubators for no more than 20 passages. HEK293

cells were grown in MEM media with 10 % FBS, 2 mM L-glutamine, 100 U/mL penicillin and 100 µg/mL streptomycin. Flp-In™ 293 T-Rex cells were grown in DMEM media with 10 % TET-free FBS, 2 mM L-glutamine, 100 U/mL penicillin, 100 µg/mL streptomycin, 100 µg/ml Hygromycin B (InvivoGen, 31282-04-9) and 10 µg/mL blasticidin (InvivoGen, ant-bl-1). For long-term storage cells were cooled gradually to -80°C in 10 % DMSO in FBS and then transferred to liquid nitrogen. To re-establish the cell line, the cells were briefly thawed at 37°C, resuspended in warm media and centrifuged at 1000 rpm for 5 minutes. The supernatant with residual DMSO was removed and cells were grown in fresh media for at least two passages before use in experiments.

2.8.2. Nucleic acid transfection

2.8.2.1. Calcium phosphate transfection

Mammalian expression vectors (table 2.1B) were prepared for transfection using the Plasmid Plus Midi Kit (Qiagen, 12943). HEK293 were plated at a density of 1.6 x 10^6 cells per 10 cm petri dish and incubated at 37°C overnight. 1 hour – 30 minutes before transfection media was replaced. Whilst continuously bubbling with a Pasteur pipette attached to a pipette-gun (Integra, 155 021), 500 µL of 10 µg DNA in 245 mM $CaCl_2$ was added drop-wise to 500 µL of 2 x hepes-buffered saline (275 mM NaCl, 1.5 mM Na_2HPO_4, 55 mM Hepes). The resulting transfection solution was then added to the plates in a drop-wise fashion to avoid precipitation of $CaCl_2$. Cells were incubated at 37°C overnight, then the transfection reagent was washed off with 2 x 10 mL warm PBS washes. The media was replaced and the cells were harvested after a total of 48 hours.

2.8.2.2. Polyethylenimine transfection

Mammalian expression vectors (table 2.1B) were prepared for transfection using the Plasmid Plus Midi Kit (Qiagen, 12943). HEK293 and Flp-In™ 293 T-Rex cells were plated at a density of 1.6 x 10^6 cells and 4 x 10^6 cells per 10 cm dish. Flp-In™ 293 T-Rex cells were induced with 1 µg/mL doxycycline and both cell lines were left to adhere overnight at 37°C. 1 hour – 30 minutes before transfection media was replaced. 1 mL of OptiMEM medium (Gibco, 31985062) was combined with 10 µg of plasmid DNA and 50 µL of 1 mg/mL pH 7 polyethylenimine (PEI) (Polysciences, 23966-1) at a ratio of 1:5 DNA to PEI. The transfection solution was mixed by vortexing, incubated for 20 minutes at room temperature and added drop-wise onto the cells. Cells were incubated at 37°C overnight, then the transfection reagent was washed off with 2 x 10 mL warm PBS washes. The media was replaced and the cells were harvested after a total of 48 hours.

2.8.2.3. Lipid-based transfection of DNA

3 x 10^5 Flp-In™ 293 T-Rex cells were plated in a 6-well dish and left to adhere at 37°C overnight. 1 hour – 30 minutes before transfection media was replaced. In one tube 1 µg of DNA was mixed with 100 µL of OptiMEM. In another tube 3 µL of GeneJuice® transfection reagent (Merck, 70967-3) and 100 µL of OptiMEM were mixed. Both tubes were incubated at room temperature for 5 minutes, then the DNA mixture was added to the transfection reagent mixture. The sample was incubated at room temperature for 30 minutes and added drop-wise onto the cells. Cells were incubated at 37°C overnight, then the transfection reagent was washed off with 2 x 1 mL warm PBS washes. The media was replaced and the cells were either harvested

after a total of 48 hours or further grown in antibiotic selection for stable cell line generation.

2.8.2.4. Lipid-based transfection of RNA

siRNAs listed in table 2.8 were first ordered as a SMARTpool® from Dharmacon (L-003598-01-0005) and then separately from Eurofins (Leuven, Belgium). 3 x 10^5 Flp-In™ 293 T-Rex cells were plated in a 6-well dish and left to adhere at 37°C overnight. 1 hour – 30 minutes before transfection media was replaced. In one tube siRNA (50 nM final volume) was mixed with 100 µL of OptiMEM. In another tube 3 µL of DharmaFECT 1 transfection reagent (Dharmacon, T-2001) and 100 µL of OptiMEM were mixed. Both tubes were incubated at room temperature for 5 minutes, then the siRNA mixture was added to the transfection reagent mixture. The sample was incubated at room temperature for 20 minutes and added drop-wise onto the cells. Cells were incubated at 37°C overnight, then the transfection reagent was washed off with 2 x 1 mL warm PBS washes. The media was replaced and the cells were harvested after a total of 48 hours.

2.8.2.5. Co-transfection of DNA and si-RNA

Mammalian expression vectors (table 2.1B) were prepared for transfection using the Plasmid Plus Midi Kit (Qiagen, 12943). siRNAs listed in **table 2.8** were first ordered as a SMARTpool® from Dharmacon and then separately from Eurofins (Leuven, Belgium). HEK293 cells were plated at a density of 2 – 3 x 10^5 cells in a 6-well dish and left to adhere at 37°C overnight. siRNA was transfected as described in section 2.6.2.3 and incubated at 37°C overnight. The transfection reagent was washed off

Target	Sequence
PP2AC	CCGGAAUGUAGUAACGAUU
	ACAUUAACACCUCGUGAAU
	UCAUGGAACUUGACGAUAC
	CAGGUAGAGCUUAAACUAA

Table 2.8. Sequences of all siRNA oligonucleotides used in this thesis. A pool of 4 different siRNAs was used to knock-down the expression of the catalytic subunit of PP2A.

with 2 x 1 mL warm PBS washes and new media was added. The cells were incubated at 37°C overnight and media was replaced 1 hour – 30 minutes before DNA transfection. In one tube 2 µg of DNA was mixed with 100 µL of OptiMEM. In another tube 5 µL of Lipofectamine® 2000 transfection reagent (Thermo Fisher Scientific, 11668027) and 100 µL of OptiMEM were mixed. Both tubes were incubated at room temperature for 5 minutes, then the DNA mixture was added to the transfection reagent mixture. The sample was incubated at room temperature for 20 minutes and added drop-wise onto the cells. Cells were incubated at 37°C overnight and the transfection reagent was washed off with 2 x 1 mL warm PBS washes. A second hit of siRNA was transfected as described in section 2.6.2.3. The cells were incubated at 37°C overnight and harvested.

2.8.3. Selection and maintenance of stable cell lines

Stable Flp-In™ T-Rex 293 cell lines were treated with 100 µg/mL Hygromycin B (InvivoGen, 31282-04-9) for 3 weeks until colonies were formed. Single colonies were selected and grown for another 2 weeks. At this stage the cells were harvested and lysed as described in section 2.7.2. The lysates were subjected to SDS-PAGE andwestern blotting (sections 2.7.4 – 2.7.6) with α-TDP1 antibody (Abcam, ab4166) to validate stable expression and knock-down of endogenous TDP1.

2.9. Analysis of proteins from whole cell extracts

2.9.1. Preparation of whole cell extracts from zebrafish embryos

10 – 60 embryos per condition were anaesthetized and de-yolked in ice-cold PBS by pipetting up and down with 200 µL pipette tip (StarLab, S1111-0706). The embryos

were then washed twice in 1 mL PBS, homogenized with a micropestle (Eppendorf, Z317314-1PAK) and lysed in 1 – 1.5 µL/embryo lysis buffer (200 mM Hepes, 40 mM NaCl, 2mM $MgCl_2$, 0.5 % Triton X-100, 1 x protease inhibitor cocktail (Roche, 4693159001), 1 x phosphatase inhibitor cocktail (Roche, 4906837001), 25 U/mL BaseMuncher (Expedeon, BM0025) for 30 minutes on ice. The tissue debris was pelleted at 4°C and 13,300 rpm for 15 minutes and the supernatant containing the protein was collected in a fresh tube. The lysate was stored at -20°C short term and -80°C for long term.

2.9.2. Preparation of lysate from mammalian cells

Cells were washed twice in ice-cold PBS and scraped in 30 – 300 µL lysis buffer (200 mM Hepes, 40 mM NaCl, 2mM $MgCl_2$, 0.5 % Triton X-100, 1 x protease inhibitor cocktail (Roche, 4693159001), 1 x phosphatase inhibitor cocktail (Roche, 4906837001), 25 U/mL BaseMuncher (Expedeon, BM0025)), depending on plate size and confluency. The sample was lysed on ice for 30 minutes, then centrifuged at 4°C and 13,300 rpm for 15 minutes to pellet the cell debris. The supernatant containing the protein was collected in a fresh tube and stored at -20°C short term and -80°C for long term.

2.9.3. Protein quantification

Protein concentration was quantified using the Bradford assay. 2 µL of lysate or lysis buffer as blank was mixed with 998 µL of Coomassie Plus™ Protein Assay Reagent (Thermo Scientific, 23200) and OD_{595} was measured in the Jenway visible spectrophotometer (Genova, 6320D). The concentration of the sample was

determined by using a standard curve of bovine serum albumin optical densities (ODs) at various concentrations.

2.9.4. SDS-polyacrylamide gel electrophoresis

Polyacrylamide gels were cast according to the Sambrook and Russell method (Sambrook and Russell, 2001) in a 1 mm XCell SureLock Mini-Cell cassette (Fisher Scientific, VXNC2010). Occasionally, 4-15 % gradient pre-cast gels were used (Bio-Rad, 456-8094). Protein loading buffer was added to 40 – 100 µg of total protein to a final concentration of 50 mM Tris pH 8.0, 200 mM DTT, 2 % w/v SDS, 10 % glycerol and 0.1 % w/v bromophenol blue. The protein was then denatured at 90°C for 5 minutes and loaded onto the polyacrylamide gel alongside the Precision Plus Protein Dual Colour Standard (Bio-Rad, 1610374) protein marker. XCell SureLock Mini-Cell system or Bio-Rad Mini-PROTEAN Tetra electrophoresis cell (Bio-Rad, 1658004) was used for electrophoresis in 1 x SDS running buffer (25 mM Tris, pH 8.3, 192 mM glycine, 0.1 % w/v SDS) at 150 – 180 V for 1.5 – 2.5 hours.

2.9.5. Protein transfer

Polyacrylamide gels were taken out of the cassette and transferred onto 0.45 µm nitrocellulose membrane (Bio-Rad, 170-4271) using the Trans-Blot Turbo® transfer™ system (Bio-Rad, 17001915), according to manufacturer's instructions.

2.9.6. Immunoblotting

The nitrocellulose membrane (Bio-Rad, 170-4271) was blocked in blocking buffer (5 % w/v milk, 200mM Tris, 140 mM NaCl, 0.1 % Tween-20, pH 7.4) for 30 minutes – 1 hour at room temperature and then incubated at 4°C overnight in an appropriate

dilution of primary antibody in blocking buffer **(table 2.9)**. The membrane was washed three times for 5 minutes in 1 x TBST buffer (200mM Tris, 140 mM NaCl, 0.1% Tween-20, pH 7.4) and incubated for 1 hour with 1:4000 HRP-conjugated secondary antibody **(table 2.10)** in blocking buffer at room temperature. The three washes were repeated before adding the Clarity Western ECL blotting substrate (Bio-Rad, 1705060) onto the membrane and visualizing in the ChemiDoc MP imaging system (Bio-Rad, 1708280).

2.9.7. TDP1 activity assay

Zebrafish lysate was prepared as described in **section 2.5.1**. 10 – 600 ng of total protein were combined with 1 x assay buffer (25 mM HEPES, pH 8.0, 130 mM KCl, 1 mM DTT) and 50 nM of Cy5.5-labelled substrate oligomer containing a 3 ’-phosphotyrosyl group, (5’-(Cy5.5)GATCTAAAAGACT(pY)-3’) (Midland Certified Reagent Company Texas, USA) in a total volume of 10 µL. The reaction was incubated at 37°C for 1 hour and terminated by the addition of 1 x loading buffer (44 % deionized formamide, 2.25 mM Tris-borate, 0.05 mM EDTA, 0.01 % xylene cyanol, 1 % bromophenol blue) and boiling at 90°C for 10 minutes. Oligonucleotides were then loaded onto a pre-run 20 % Urea SequaGel (Fisher, EC-833-1) prepared in a 1 mm XCell SureLock Mini-Cell cassette (Fisher Scientific, VXNC2010) and subjected to 150 V electrophoresis for approximately 1 hour. The bands were imaged using the ChemiDoc MP imaging system (Bio-Rad, 1708280) and quantified in Image Lab v. 4.1 (Bio-Rad).

Primary antibody	Species reactivity	Host species	Supplier (cat. No.)	Concentration	Application
53BP1	human	rabbit	Bethyl Laboratories (A300-272A)	1:1000	IF
DIG-AP	-	sheep	Roche (11093274910)	1:5000	ISH
GFP	-	rabbit	Abcam (ab290)	1:2000	WB
LIG3	human	mouse	Abcam (ab587)	1:250	IP
Myc	-	mouse	Cell Signalling (2276)	1: 2000	WB, IP
PCNA	human, zebrafish	mouse	Novus Biologicals (NB500-106SS)	1:200	IHC-P
PNK	human	rabbit	Abcam (ab181107)	1:1000	WB
PP2Ac	human	rabbit	Cell Signalling (2038)	1:500	WB
TDP1	human	rabbit	Abcam (ab4166)	1:1000	WB
TOP1-cc	human, zebrafish	mouse	Merck, (MABE1084)	1:2000	SB, ChIP
USP-11	human	rabbit	Bethyl Laboratories (A301-613A)	1:1000	WB, IP
β-actin	human, zebrafish	mouse	Sigma (A5316)	1:1000	WB
β-tubulin	human, zebrafish	mouse	Abcam (ab7792)	1:1000	WB
γ-H2AX (ser139)	zebrafish	rabbit	Genetex (GTX127342)	1: 400 – 1:1000	IHC-WM, WB

Table 2.9. Primary antibodies. Species reactivity, host species, supplier, working concentration and application of primary antibodies. WB – western blot, SB – slot blot, IP – co-immunoprecipitation, ChIP – chromatin immunoprecipitation, IHC-P – paraffin immunofluorescence, IHC-WM – whole-mount immunofluorescence, IF – cell culture immunofluorescence, ISH – *in situ* hybridization

Secondary antibody	Species reactivity	Host species	Company (cat. No.)	Concentration
Anti- IgG (H+L)-Alexa Fluor 488	mouse	goat	Molecular Probes (A28175)	1:500
Anti- IgG (H+L)-Alexa Fluor 555	rabbit	goat	Life Technologies (A21428)	1:500 – 1:2500
Anti- IgG (H+L)-Alexa Fluor 568	rabbit	goat	Molecular Probes (A11011)	1:500
Anti-IgG	mouse	goat	Invitrogen (02650712)	1:100
IgG (H + L)-HRP Conjugate	mouse	goat	Bio-Rad (170-6516)	1:4000
IgG (H + L)-HRP Conjugate	rabbit	goat	Bio-Rad (170-6522)	1:4000

Table 2.10. Secondary antibodies. Species reactivity, host species, supplier and working concentration of secondary antibodies used for immunoblotting.

2.9.8. TDP2 activity assay

2.9.8.1. Substrate oligonucleotide preparation

100 pmol of Cy5.5-labelled substrate oligomer (5'-(pY)CATCGTTGCCTACCAT(Cy5)-3') (Midland Certified Reagent Company, Texas, USA) was combined with 100 pmol of a 20 bp complementary oligonucleotide with a 5' overhang (GCATGATGGTAGGCAACGATG) in a total volume of 33.3 µL. The sample was denatured at 95°C for 5 minutes and re-annealed by dropping the temperature by -2°C/second for 5 seconds, then by 0.1°C/second for 600 seconds. Once annealed, 3 µM of a double-stranded substrate oligomer with a 5' overhang was generated. The use of such a substrate in the TDP2 activity assay should prevent ligation of product by zebrafish RNA ligases and thus undesirable full repair.

2.9.8.2. Zebrafish lysate preparation and TDP2 activity assay reaction

Zebrafish lysate was prepared as described in **section 2.5.1**, except no BaseMuncher or phosphatase inhibitor cocktail was added into the lysis buffer. 0.5 µg, 1µg and 5 µg of the lysate were combined with 1 x TDP2 activity assay buffer (5 mM Tris pH 7.5, 5 mM KCl, 0.1 mM DTT, 10 µg/ml BSA, 0.1 mM $MgCl_2$), 60 nM of Cy5.5-labelled substrate oligomer **(section 2.7.8.1)** and 2 µM of competitor oligo. The bands were imaged using the ChemiDoc MP imaging system (Bio-Rad, 1708280) and quantified in Image Lab v. 4.1 (Bio-Rad).

2.9.9. Mass spectrometry

Prior to work commencing, all surfaces and equipment were cleaned with decontamination solution (0.1 % acetic acid, 10 % isopropanol). Protein samples

were loaded onto SDS-PAGE gels **(section 2.5.3)** 1 – 3 wells apart and fractionated until the dye front ran off. The gel was stained with InstantBlue™ stain (Expedeon, ISB1L) and each lane was cut into 6 pieces with a fresh scalpel for in-gel tryptic digestion (Pandey et al., 2000). Approximately 100 µL 50 mM ammonium bicarbonate (ABC) was added to reduce springiness and each piece was further cut into approximately 2 mm^2 cubes. Each cubed ⅙ of the lane was transferred to a new tube. Unless otherwise specified, all incubations were carried out at room temperature. 100 µL of 50 mM ABC were added per sample to submerge all the gel pieces and incubated for 5 minutes. 100 µL of acetonitrile (ACN) were added for 10 minutes to shrink the gel pieces and extract the Coomassie stain. Solvent was discarded and the addition of ABC and ACN was repeated as previously described. 100 µL of freshly prepared reduction reagent (10 mM DTT) were added and incubated at 56°C for 30 minutes, then the samples were briefly centrifuged to collect condensation at the bottom of the tube. 100 µL of ACN were added before discarding all the liquid. Another 100 µL of ACN were added and incubated for 10 minutes, then discarded. 150 µL of freshly prepared alkylation reagent (55 mM iodoacetamide, 50 mM ABC) were added and incubated in the dark for 20 minutes, then discarded. The samples were incubated with 100 µL of 50 mM ABC for 10 minutes before addition of 100 µL ACN for 10 minutes. All the liquid was discarded and the previous step was repeated. 50 µL of ACN were added before discarding the liquid and the gel pieces were dried in a vacuum Concentrator (Eppendorf, 5301) at 40°C for approximately 20 minutes. Digestion solution is prepared by dissolving 20 µg proteomics-grade trypsin in 20 µL of 1 mM HCl and adding ABC and ACN to a final concentration of 50 µg/ml trypsin, 12.5 µM HCl, 47 mM ABC and 0.05 % CAN. The gel

pieces were then rehydrated in 50 µL of this buffer and after 10 minutes more digestion buffer was added as necessary. After another 10 minutes excess buffer was discarded and gel pieces were incubated at 37°C overnight. The samples were briefly centrifuged and the buffer containing digested peptides was transferred to Eppendorf® LoBind tubes (Sigma, Z666505). 50 µL of 25 mM ABC were added to the gel pieces before vortexing the samples on a Fisherbrand™ mini vortex mixer (Thermo Fisher Scientific, 41100000) and incubating for 10 minutes. The liquid was transferred to the corresponding LoBind tubes. 2 estimated volumes of ACN were added to the gel pieces for incubation at 37°C for 15 minutes and vortexing after the first 10 minutes. The samples were briefly centrifuged and the peptide extracts collected in the corresponding tubes. 50 µL of 5 % LC-grade formic acid was added to the gel pieces and incubated at 37°C for 15 minutes with vortexing after the first 10 minutes. The samples were briefly centrifuged and the peptide extracts collected in the corresponding tubes. 2 estimated volumes of ACN were added to the gel pieces for incubation at 37°C for 15 minutes and vortexing after the first 10 minutes. The peptide extract was once again collected at the bottom of the tube by centrifuging and transferred to the LoBind tubes. 50 µL of ACN is added to extract the remainder of the peptides from the gel pieces, which are transferred to the LoBind tubes. The peptide extracts were then dried in the vacuum Concentrator overnight and stored at -20°C.

Peptides were resuspended in 15 µL of 2 % ACN in 0.1% trifluoroacetic acid by vortexing for 1 minute and briefly centrifuged, then sonicated in the Elma Ultrasonic S30H sonicator (Cooksongold, 997 1321) for 5 – 10 minutes. Samples were centrifuged at 13,300 rpm for 10 minutes to pellet any particles. 7 µL were carefully

transferred into a vial and 5 µL were injected into the Q Exactive™ HF Hybrid Quadrupole-Orbitrap™ Mass Spectrometer (Thermo Fisher Scientific, IQLAAEGAAPFALGMBFZ) and analyzed using a 2 hour gradient standard operating procedure. Raw data was processed in MaxQuant v. 1.5.3.3 and Perseus v. 1.5.3.1.

2.9.10. Anti-GFP co-immunoprecipitation

4 x 10^6 Flp-In™ 293T-Rex cells expressing GFP-tagged proteins were plated in 10 cm dishes, induced with 1 µg/mL doxycycline and harvested after 48 hours. Cells were lysed in NP-40 lysis buffer (50 mM Tris pH 8, 150 mM NaCl, 1 % NP-40, 1mM DTT, 1 x protease inhibitor cocktail (Roche, 4693159001) as described in section 2.7.2. 30 µL of GFP-Trap® beads (Chromotek, gtma-100) were prepared by removing the solvent and washing them twice in 0.02 % Tween-20 in PBS. They were resuspended in 200 µL of 0.02 % Tween-20 in PBS. The beads were the equilibrated in NP-40 lysis buffer without DTT or protease inhibitors. Lysis buffer was removed and 300 µL of lysate was added onto the beads. The sample was rotated for 2 hours at 4°C, then lysate was removed. Beads were washed 4 times in NP-40 lysis buffer and resuspended in 30 µL of 1 x protein loading buffer (50 mM Tris pH 8.0, 200 mM DTT, 2 % w/v SDS, 10 % glycerol and 0.1 % w/v bromophenol blue). The sample was boiled for 5 minutes at 95°C and centrifuged at 13,300 rpm for 1 minute, then loaded onto an 8 % SDS-PAGE gel. The gel was subjected to electrophoresis and was used for either mass spectrometry **(section 2.7.10)** or western blotting **(section 2.7.6)**.

2.9.11. Anti-Myc immunoprecipitation with phosphorylation analysis

2.5 x 10^6 HEK293 cells were plated in 10 cm dishes and left to adhere overnight at 37°C. They were transfected with Myc-tagged constructs using calcium phosphate

transfection (section 2.6.2.1). 48 hours post-transfection, dishes were scraped in 400 µL lysis buffer, lysed and protein concentration was quantified, as described in sections 2.7.2 and 2.7.3. 30 µL of lysate was removed for input analysis and resuspended in 30 µL 2 x protein loading buffer to a final concentration of 50 mM Tris pH 8.0, 200 mM DTT, 2 % w/v SDS, 10 % glycerol and 0.1 % w/v bromophenol blue. The input was boiled at 90°C for 5 minutes and stored at -20°C. 2 µL of α-Myc antibody (Cell Signalling, 2276) were added to the remaining lysate and sample was incubated at 4°C for 1 hour with rotation. Solvent was removed from 30 µL of protein G beads (Fisher Scientific, GZ17061801). The beads were washed twice in 20 volumes of wash buffer (20 mM Hepes, 150 mM NaCl) and resuspended in 100 µL of wash buffer. Protein aggregates were removed from lysate by centrifuging at 13,300 rpm for 10 minutes at 4°C and supernatant was transferred to a fresh tube. The beads were added to the lysate and sample was incubated at 4°C for 1 hour. 50 µL of flow-through were collected and prepared for gel loading in the same way as the input and the rest of the supernatant was discarded. The beads were washed 3 times in wash buffer, resuspended in 200 µL of wash buffer and split into two samples. One half was treated with 800 U of λ-phosphatase (New England Biolabs, P0753S), 1 x provided buffer and 1 mM $MnCl_2$. The other half was treated with ddH_20 instead of the enzyme. Both samples were incubated at 60°C for 30 minutes, then the beads were resuspended in 25 µL of 2 x protein loading buffer to a final concentration of 50 mM Tris pH 8.0, 200 mM DTT, 2 % w/v SDS, 10 % glycerol and 0.1 % w/v bromophenol blue. Samples were boiled at 90°C for 15 minutes and 10 µL of supernatant were loaded on a 12 % SDS-PAGE gel. Samples were subjected to

electrophoresis for approximately 2.5 hours at 150 V and subjected to western blotting, as described in **section 2.7.6**.

2.10. DNA damage repair assays

2.10.1. Immunofluorescence for DNA damage markers

2.10.1.1. Adult zebrafish immunofluorescence

4 µm sections were prepared by immersion fixation, decalcification of adult zebrafish and paraffin embedding and sectioning, as described in **sections 2.6.1** and **2.6.2**. Immunofluorescence was carried out according to Ferreira lab protocol (Carneiro et al., 2016). Sections were deparaffinised and hydrated through a series of 5 minute washes: twice in Histo-Clear (National Diagnostics, HS-200), twice in 100 % ethanol, once in 90 % ethanol, once in 70 % ethanol and twice in dH_2O. The slides were microwaved in 0.01 M pH 6 trisodium citrate at 800 W for 4 minutes, followed by 450 W for 10 minutes to achieve a gentle simmer and avoid vigorous boiling. The slides were then cooled on ice until the buffer was lukewarm. The sections were permeabilized with 0.5 % Triton X-100 in PBS for 10 minutes at room temperature and blocked in blocking buffer (3 % w/v BSA, 5 % goat serum, 0.3 % Tween-20 in PBS) for 1 hour at room temperature. The blocking buffer was replaced with 1:200 Mα-PCNA (Novus Biologicals, NB500-106SS) and 1:400 Rα-H2AX (Genetex, GTX127342) antibodies in blocking buffer. The sample was incubated overnight at 4°C in a humid incubating chamber. Excess primary antibody was washed thrice for 10 minutes with PBSTw (0.1 % Tween-20 in PBS) at room temperature with slow shaking. All the following steps are carried out in the dark. The slides were incubated in 1:500 dilution

of anti-mouse Alexa Fluor™ 488 (Invitrogen, A1101) and anti-rabbit Alexa Fluor™ 568 (Fisher Scientific, 10032302) in blocking buffer for 1 hour at room temperature in a humid incubating chamber. Excess secondary antibody was washed off with PBSTw 3 times and once with PBS for 10 minutes with slow shaking. Sections were mounted in VECTASHIELD® mounting medium with DAPI (Vector Laboratories, H-1200) and imaged using a 40x oil objective on the Nikon A1 confocal laser microscope with NIS-elements AR 4.30.02 software in the Wolfson Light Microscopy Facility.

2.10.1.2. Embryonic zebrafish immunofluorescence

24 hpf embryos were dechorionated and treated with varying doses of ionizing radiation in the TORREX TRX2800 X-ray system with or without recovery. The embryos were washed in PBS and fixed in ice-cold 50 % acetone: 50 % methanol at 20°C overnight or longer with tubes lying flat on the side. All timed washes were carried out with slow rocking. The embryos were washed in 50 % methanol in PBS, then in PBS and then 4 times for 10 minutes in PBSTr (1 % Triton X-100 in PBS). The embryos were incubated in blocking buffer (2 % Roche blocking reagent (Roche, 11096176001), 5 % FCS, 1 % DMSO) for 1 hour at room temperature. The blocking buffer was replaced with 1:1000 α-H2AX (Genetex, GTX127342) antibody in blocking buffer. Embryos were incubated in the primary antibody overnight, then washed 4 times for 15 minutes in PBSTw (0.1 % Tween-20 in PBS). A 1:2500 dilution of Goat Anti-Rabbit Alexa Fluor™ 555 (Life Technologies, A21428) was incubated with the embryos for 2 hours at room temperature in the dark. Excess secondary antibody was washed of 4 times for 15 minutes with PBSTw. The embryos were mounted dorsally in VECTASHIELD® mounting medium with DAPI (Vector Laboratories, H-1200)

and imaged using a 40x oil objective on the Nikon A1 confocal laser microscope in the Wolfson Light Microscopy Facility.

2.10.1.3. Mammalian cell immunofluorescence

All mammalian cell immunofluorescence was carried out by Lukas Jasaitis. 10^5 Flp-In™ 293 T-Rex cells were plated on 50 µg/mL poly-D lysine coated 13 mm round coverslips in a 24-well dish, induced with 1 µg/mL doxycycline and left to adhere at 37°C for 48 hours. GFP expression was confirmed using the Nikon Eclipse TE300 inverted microscope and CPT treatments were carried out. Whilst keeping the cells on ice, then media was removed. Coverslips were washed very carefully 3 times with PBS on ice, whilst the plate was being tilted to prevent washing off the cells. All subsequent steps were carried out at room temperature. The cells were fixed in 200 µL 4 % PFA in PBS (Alfa Aesar, J61899.AK) for 10 minutes and washed 3 times in PBS. The cells were permeabilized with 200 µL of 0.5 % Triton-X in PBS for 5 minutes. The triton was washed off at least 3 – 4 times in PBS and the cells were incubated in 200 µL of blocking buffer (3 % w/v BSA in PBS) for 30 minutes. Blocking buffer was removed and a 1:1000 dilution of α53BP1 antibody (Bethyl Laboratories, A300-272A) in blocking buffer was applied. The antibody was incubated for 1 – 2 hours and then washed off 3 times in PBS. All subsequent steps were carried out in the dark. Coverslips were incubated with a 1:500 dilution of Goat Anti-Rabbit Alexa Fluor™ 555 (Life Technologies, A21428) and 1 µg/mL DAPI in blocking buffer for 1 hour and washed in PBS. Excess PBS was removed, coverslips were washed in dH_2O and mounted onto microscope slides in Immu-Mount (Thermo Fisher Scientific, 9990402). The slides were left to set for 1 hour and imaged on a Leica DM5000B microscope.

2.10.2. Detection of topoisomerase 1 cleavage complexes

30 – 40 3dpf zebrafish embryos were lysed in 1.1 mL of lysis buffer (8 M guanidine hydrochloride, 30 mM Tris-HCl pH 7.5, 10 mM EDTA, 1 % sarkosyl, pH 7.5) for 15 minutes at 65°C. 1 mL aliquots of caesium chloride ($CaCl_2$) in range of densities were carefully layered on top of each other to form a gradient (from bottom to top: 1.45 g/ml, 1.5 g/ml, 1.72 g/ml, 1.82 g/mL) in a 5 mL polyallomer centrifuge tube (Beckman, 326819). The lysate was centrifuged at 16,000 x g for 10 minutes, then 1 mL of the supernatant was carefully layered on top of the $CaCl_2$ gradient. The layered sample was centrifuged at 30,000 rpm in a Beckman Ultima LE-80K ultracentrifuge with a swinging rotor for 24 hours at 25°C and stopped gradually without a brake. In the meantime 10 µL of the remaining lysate were made up to 100 µL in 1 x TE buffer (10 mM Tris, 1 mM EDTA, pH 8) and incubated with 0.5 µg/mL RNase A at 37°C overnight. 50 µL of the RNase-digested sample or 1 x TE buffer were mixed with an equal volume of 1 x TE buffer with a 1:200 dilution of PicoGreen® (Invitrogen, P7581). 5 µg/µL of λ DNA standard was also mixed with 1 x TE buffer with PicoGreen® and a serial dilution was carried out to obtain a range of DNA standards (125 ng – 5 µg). DNA concentration was quantified in a FLUOstar® Omega microplate reader (BMG) with fluorescence at EX485-12/EM520. Fractionated lysates were collected by piercing the bottom of the tube with a 19G syringe needle (positioned at 45° with the bevel upwards), connected to a Pharmacia Biotech P-1 peristaltic pump with a silicone tube. Each sample was collected in 10 fractions of 0.5 mL. Fractions with equal dsDNA amounts between samples (200 µL maximum) were subjected to slot-blotting onto a PBS-wetted 0.45 µm nitrocellulose membrane (GE Healthcare, 106000002). The

membrane was air-dried and subjected to immunoblotting with a 1:2000 dilution of the Top1-cc antibody (Merck, MABE1084), as described in **section 2.8.6**.

2.11. Statistical analysis

All data analysis and statistical tests were carried out in Graphpad Prism v. 6 and 7 using a two-tailed t-test, unless otherwise stated. The n number in western blots, slot blots, activity assays, qPCR and cell culture immunofluorescence represents the number of biological repeats of the experiment, whereas in zebrafish whole-animal experiments it represents the number of animals per experiment. *p* values are indicated as follows: not significant (ns) – $p > 0.05$, * – $p < 0.05$, ** – $p < 0.01$, *** – $p < 0.001$ and **** - $p < 0.0001$.

3

Generation and characterization of tdp1$^{-/-}$ zebrafish

3.1. Introduction

Tyrosyl-DNA phosphodiesterase 1 (TDP1) is a single-strand break repair end-processing factor with a role in the repair of several types of damaged 3' termini, including topoisomerase 1 cleavage complexes (TOP1-CCs) (Interthal et al., 2005a; Interthal et al., 2001; Pouliot et al., 1999). Mutation of TDP1 histidine 493 into arginine has been found in patients with spinocerebellar ataxia with axonal neuropathy 1 (SCAN1), a progressive neurodegenerative disease which primarily affects the cerebellum (Takashima et al., 2002).

To be able to fully assess the physiological role of TDP1, an animal model is necessary. In *Drosophila* mutants of glaikit (gkt), an orthologue of TDP1, have been generated in two independent studies, however, the findings are very conflicting (Dunlop et al., 2004; Guo et al., 2014). Dunlop et al. (2004) found that the *tdp1*Δ flies are embryonic lethal due to a severe disruption in CNS architecture, however, the later study by Guo and co-workers (2014) demonstrates that loss of *tdp1* in flies only leads to a shortened life-span in females and hypersensitivity to CPT, the Top1 inhibitor NSC-725776 and bleomycin, a DSB-inducing agent. Although Guo and co-workers were not able to explain such a discrepancy, their study is in agreement with other studies of TDP1 in eukaryotes, such as yeast (Liu et al., 2004), mice (Hawkins et al., 2009; Hirano et al., 2007; Katyal et al., 2007) and chicken (Alagoz et al., 2014; Murai et al., 2012) and human cells (Alagoz et al., 2014), where TDP1 is not essential. *Tdp1*$^{-/-}$ mice show a mild age-related reduction in cerebellar mass, hypoalbuminemia and high sensitivity to the TOP1 poisons, topotecan (TPT) (Katyal et al., 2007) and irinotecan (CPT-11) (Hirano et al., 2007), but are otherwise phenotypically indistinguishable

from their wild-type siblings (Hawkins et al., 2009; Hirano et al., 2007; Katyal et al., 2007). The lack of SCAN1 phenotype can be explained by the specific mutations of TDP1 involved: the H493R mutation confers toxicity by causing the mutant TDP1 to form covalent complexes with the DNA as it attempts to repair TOP1-CCs (Hirano et al., 2007).

To tackle this problem I planned to generate a humanized SCAN1 zebrafish. Fish were until now one of the few organisms, in which Tdp1 function had not been studied. Therefore it was interesting to investigate the effects of Tdp1 loss as well as the effects of human *TDP1*^{H493R} expression in these animals. Zebrafish offer many advantages over traditional models, such as external development, high fecundity and transparent larvae, whilst their genomic sequence is still highly homologous to that of humans. In addition, generating transgenic zebrafish is simpler and less time-consuming than generating transgenic mice. With all of the above in mind, I first generated *tdp1*$^{-/-}$ zebrafish, then used the *tdp1*$^{-/-}$ animals in attempts to integrate a copy of human *TDP1*^{H493R} into their genome. The generation and characterization of *tdp1*$^{-/-}$ zebrafish will be discussed in this chapter and chapter 4, whereas the problems I encountered in the transgenesis process will be discussed in chapter 5.

3.2. Results

3.2.1. Generation of *tdp1*$^{-/-}$ zebrafish

The zebrafish genome contains only one copy of the *tdp1* gene, which is consistent with other species characterized so far. The gene contains 16 exons and 15 introns, which encode a 615 amino acid protein **(figure 3.1A)**. All the catalytic and

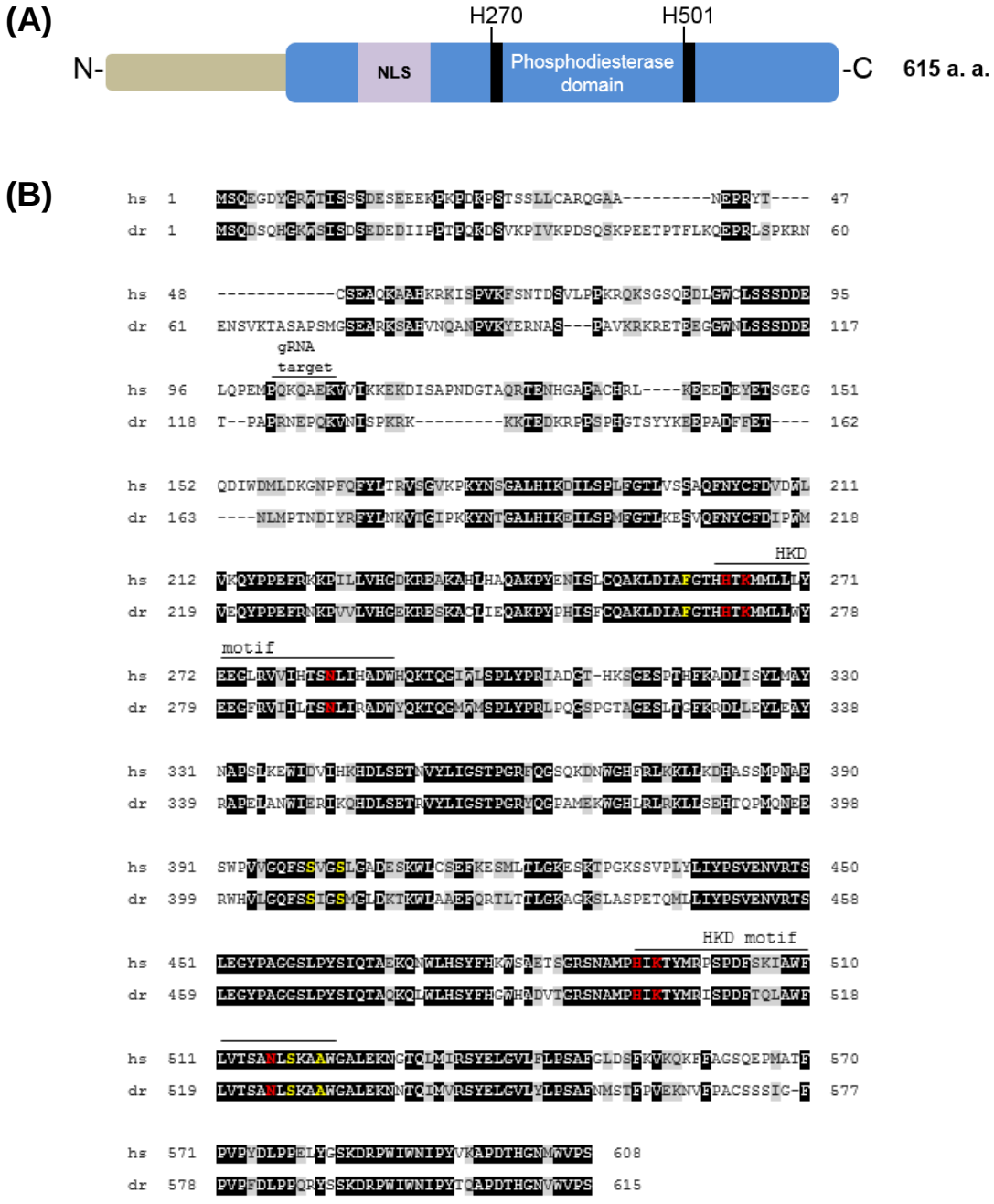

Figure 3.1. Zebrafish Tdp1 protein structure and its sequence alignment with human TDP1. (A) Schematic protein structure of zebrafish tdp1, showing the nuclear localization signal (NLS), phosphodiesterase domain and active site histidines (H270 and H501) (Davies et al. 2002). **(B)** *H. sapiens* (hs) and *D. rerio* (dr) TDP1 protein sequence alignment. Identical sequences are highlighted in black and similar sequences in grey. The area of CRISPR/Cas9 mutation and catalytic HKD motifs ($HxK(x)_4D(x)_6GSxN$) with catalytic sites (in red) are noted (Davies et al. 2002, Pommier et al. 2014). Yellow denotes amino acids, which contact the DNA substrate during repair (Pommier et al. 2014). Accession numbers are as follows: hsTDP1 - ENST00000335725.8 and drTdp1 - ENSDART00000150149.2 Sequences were aligned using the Protein BLAST® website: https://blast.ncbi.nlm.nih.gov/Blast.cgi?PAGE=Proteins

DNA-interacting amino acids are conserved in the zebrafish protein and the catalytic HKD motifs are highly conserved **(figure 3.1B**). Expression of *tdp1* in zebrafish was first examined through whole-mount *in situ* hybridization. Zebrafish *tdp1* mRNA was found ubiquitously in the 24 hpf embryo with an emphasis in the head **(figure 3.2)**, which is a similar expression pattern as previously observed in flies due to its role during neurodevelopment (Guo et al., 2014). In mice, *Tdp1* was shown to be expressed in the brain from embryonic day 9.5 to adulthood, but earlier stages or embryonic expression in other tissues was not studied (Hirano et al., 2007). I then used the CRISPR/Cas9 technology **(section 2.4.1)** to generate deletions in exon 2, i.e. the first coding exon, of the zebrafish *tdp1* **(figure 3.3A, B)**. Deletions are usually targeted early in the gene sequence in the hopes that they will result in an early stop codon, which could lead to nonsense mediated decay, or at least inactivate important domains of the protein. However, alternative splicing and late start codons could lead to the production of a functional protein. There are also some sequence limitations for generating deletions using the CRISPR/Cas9 system, as discussed in **section 2.4.1.1**. Two deletion alleles resulting in a frameshift were isolated in the F_1 generation: $tdp1^{SH475}$ and $tdp1^{SH476}$ **(figure 3.3C)**. $Tdp1^{SH475}$ harboured a deletion of base pairs 1749 – 1753 in the genomic sequence and $tdp1^{SH476}$ was missing base pairs 1749 – 1754. Initially, trans-heterozygotes ($tdp1^{SH475/SH476}$) were generated, harbouring both of these alleles to make sure that any phenotype does not arise from an off-target effect, but further experiments were carried out using the $tdp1^{SH475}$ allele only, either in homozygous or heterozygous form. $Tdp1^{SH475/SH475}$ and $tdp1^{SH475/+}$ genotypes will thus hereafter be referred to as $tdp1^{-/-}$ and $tdp1^{-/+}$, respectively. The protein translated from $tdp1^{-/-}$ mRNA should be 113 a. a. long out

Figure 3.2. *Tdp1* is expressed ubiquitously in the 24 hpf zebrafish embryo. Whole mount *in situ* hybridization (WISH, section 2.5.2) for Tdp1 mRNA in wild-type zebrafish at 24 hpf. *Tdp1* is expressed ubiquitously with an emphasis in the head. Sense probes for *tdp1* mRNA were used as a negative control.

My thanks to our undergraduate student Madeleine Brown, who carried out this experiment.

(A)

5’*AAAGCACCGACTCGGTGCCACTTTTTCAAGTTGATAACGGACTAGCCTT ATTTTAACTTGCTATTTCTAGCTCTAAAAC*TTCCTCAGTTTCTCTCTTCCCTA TAGTGAGTCGTATTACGC 3’

(B)

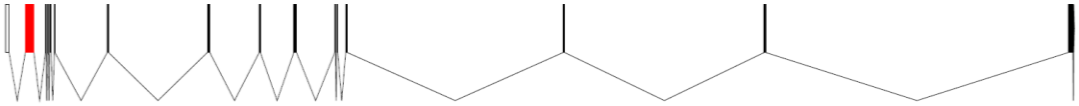

(C)

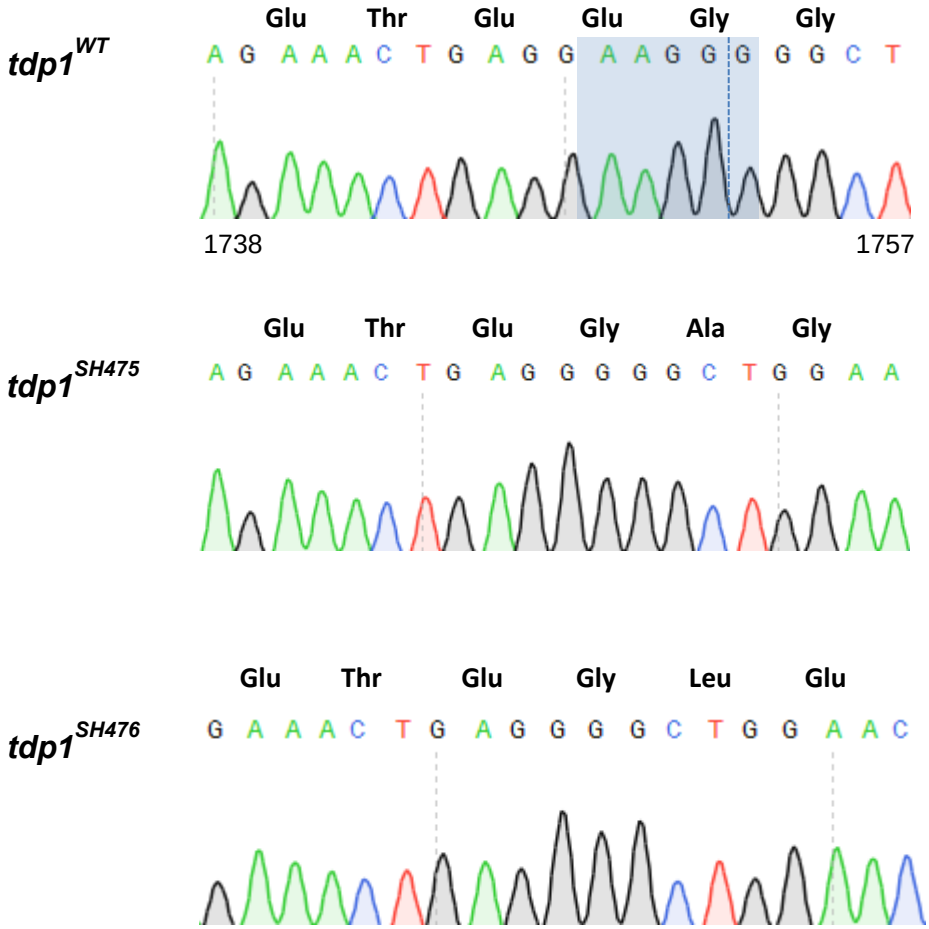

Figure 3.3. Generation of *tdp1*$^{-/-}$ zebrafish using the CRISPR/Cas9 system. (A) Sequence of template ultramer used for *in vitro* synthesis of gRNA (section 2.4.1.2). Scaffolding sequence is indicated in purple, target sequence in green and T7 polymerase promoter in blue. **(B)** Intron-exon structure of the zebrafish Tdp1 gene. Exon 2 (red box), was targeted for Cas9 restriction. **(C)** DNA and amino acid sequences of the target region in *tdp1*^{WT} zebrafish and 2 isolated deletion alleles, *tdp1*^{SH475} and *tdp1*^{SH476}. The 4 bp deletion (SH475), indicated by the light blue box, and the 5 bp deletion (SH476), indicated by the dotted blue line, both result in a frameshift and a stop codon 21 and 6 amino acids downstream of the deletion, respectively. The numbers denote base position in the genomic sequence of Tdp1.

of the full 615 a. a. sequence. It is likely that such a large truncation will be subjected to nonsense mediated decay. However, even if it is not, the product should be missing a part of the N-terminus and all of the C-terminus, which contains the nuclear localization signal and the phosphodiesterase domain with two active site HKD motifs. This should completely abolish the activity of zebrafish Tdp1.

3.2.2. Validation of *tdp1*$^{-/-}$ zebrafish

One of the best ways to validate loss of Tdp1 function in the mutants is to specifically assay its enzymatic activity. Lysates from 4 dpf *tdp1*$^{-/-}$ embryos and adult fish were incubated with labeled oligonucleotides with 3'-phosphotyrosyl (3'-PY) moieties, which mimic Top1-CCs **(figure 3.4A)**. Tdp1 activity processes such moieties into 3'-phosphates, leading to a band shift on the gel. Indeed, no band shift of the oligonucleotide was found after incubation with *tdp1*$^{-/-}$ extracts, suggesting that tdp1 activity was completely abolished both in adults and embryos **(figure 3.4B, C)**. In addition, *tdp1* mRNA localization in the 24 hpf progeny of a *tdp1*$^{-/+}$ incross was observed using whole-mount *in situ* hybridization **(section 2.5.2)**. However, *tdp1* mRNA was found expressed in all of the 20 embryos in the same pattern as that observed in wild-type fish **(figure 3.2)**.

3.2.3. *Tdp1*$^{-/-}$ zebrafish are viable and apparently healthy

TDP1 has been shown to be non-essential for life in mice, yeast and human and chicken cells (Alagoz et al., 2014; Hawkins et al., 2009; Hirano et al., 2007; Katyal et al., 2007; Liu et al., 2004; Murai et al., 2012). It was thus important to test whether Tdp1 was essential for survival in zebrafish and if it is not, whether loss of Tdp1 is

toxic in these animals. A normal Mendelian ratio of all genotypes resulting from a *tdp1*$^{-/+}$ incross was obtained, when the progeny were genotyped at 3 – 5 months of age **(figure 3.5)**. No untimely deaths after that were observed and the zebrafish were apparently indistinguishable from their wild-type siblings until 2 years and 3 months of age, when they were sacrificed.

3.2.4. *Tdp1*$^{-/-}$ embryos are not more sensitized to increased Top1-mediated protein-linked breaks

It was not surprising that *tdp1* was seemingly dispensable in the zebrafish in normal conditions, when even *Tdp1*$^{-/-}$ mice showed no overt phenotype (Hawkins et al., 2009; Hirano et al., 2007; Katyal et al., 2007). However, it was hypothesized that *tdp1*$^{-/-}$ embryos will be hypersensitive to TOP1 inhibitors, like mice (Hirano et al., 2007; Katyal et al., 2007), and human (Alagoz et al., 2014) and avian cells (Murai et al., 2012). Appropriate concentrations were determined empirically. A dose at which wild-type fish were mildly affected, exhibiting mainly mild body curvature, was chosen as the lowest dose, whereas higher doses caused extreme body curvature, brain necrosis and lack of swim bladder. 4 dpf embryos from a *tdp1*$^{-/+}$ incross were challenged overnight with a range of CPT concentrations (350 nM, 500 nM and 750 nM). At 5 dpf the most affected embryos at each concentration were selected. If the hypothesis that *tdp1*$^{-/-}$ embryos will be hypersensitive to CPT was right, the blindly selected embryos should be enriched for the *tdp1*$^{-/-}$ genotype. Strikingly, *tdp1*$^{-/+}$, *tdp1*$^{-/-}$ and *tdp1*^{WT} genotypes were recovered at a normal Mendelian ratio, showing they were all equally sensitive **(figure 3.6A, B)**. To ascertain that the lack of sensitivity to CPT was not due to residual maternal *tdp1* mRNA, maternal-zygotic *tdp1*$^{-/-}$

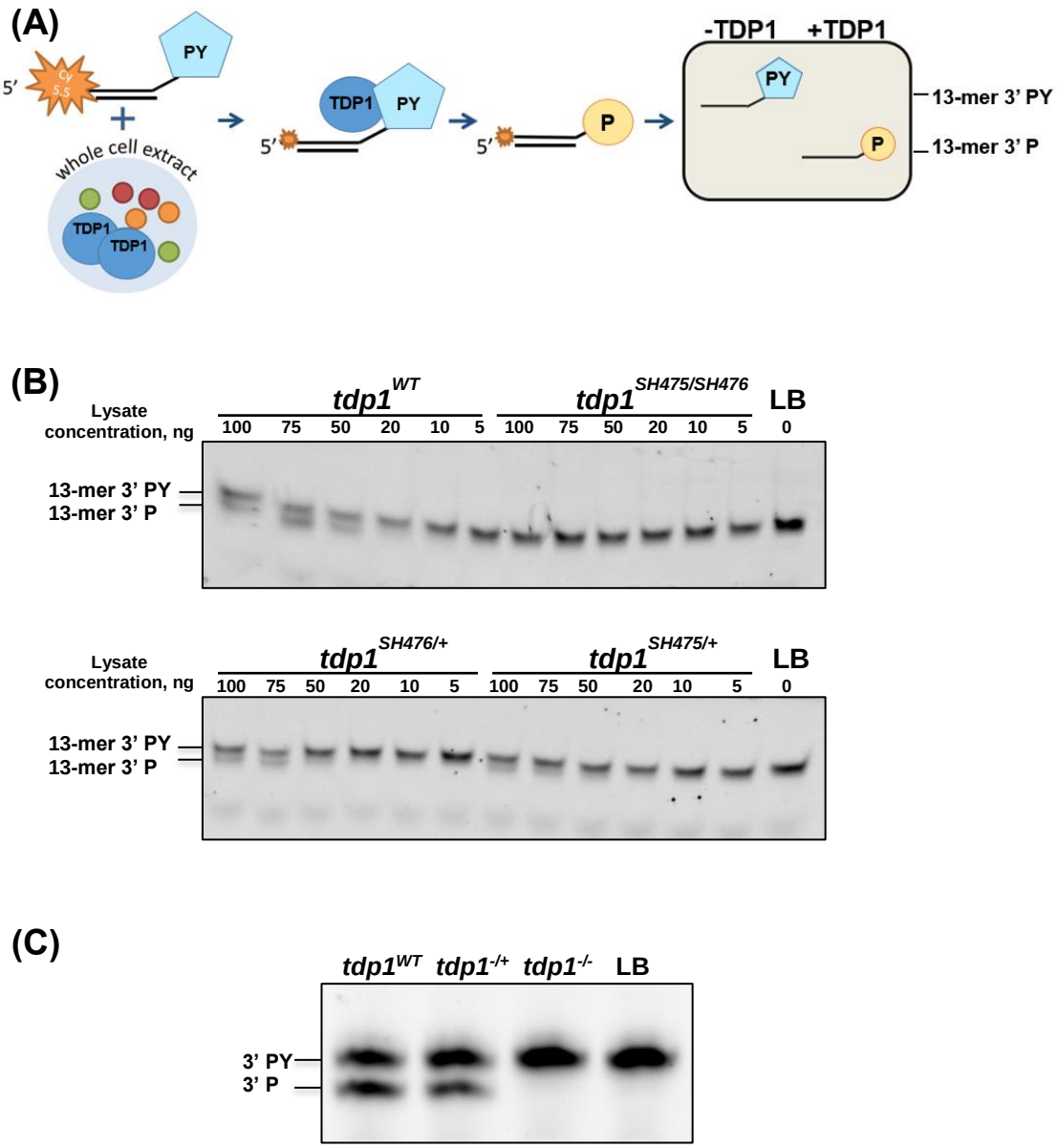

Figure 3.4. Validation of *tdp1*$^{-/-}$ zebrafish. (A) Diagram of TDP1 activity assay (section 2.9.7). A 5' labelled oligonucleotide with a 3'-phosphotyrosyl (PY) moiety is incubated with whole cell extract. If active TDP1 is present in the extract, it processes the phosphotyrosyl moiety into a phosphate group, which results in a band shift on a DNA sequencing gel. After denaturation, the unlabelled strand is dissociated from the labelled strand and is not visible during imaging. **(B)** TDP1 activity assay was carried out on fin clips of adult zebrafish; LB – lysis buffer control. **(C)** TDP1 activity assay was carried out on 600 ng of lysate from 4 dpf embryos; LB – lysis buffer control.

(A)

Genotype (*tdp1*$^{-/+}$	Expected	Observed	No. of adult
tdp1$^{+/+}$	25%	22.5%	23
tdp1$^{-/+}$	50%	45%	46
tdp1$^{-/-}$	25%	32.4%	33
		Total	102

(B)

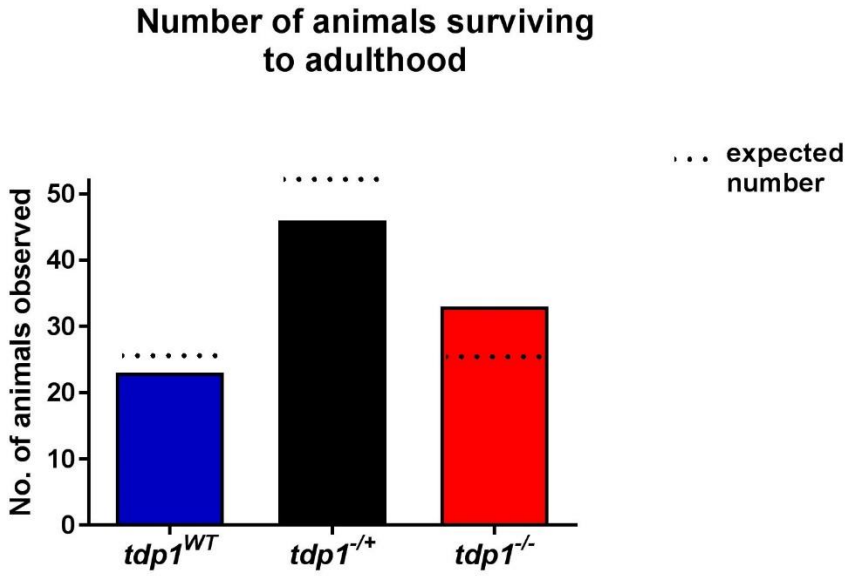

Figure 3.5. *Tdp1*$^{-/-}$ zebrafish are viable. *Tdp1*$^{-/+}$ zebrafish were crossed and genotyped at adulthood, then a chi-squared test was performed. The observed number of the 3 genotypes from a heterozygous incross (n=102) does not differ significantly from the expected ratios; X^2 equals 2.941 with 2 degrees of freedom. The two-tailed P value equals 0.5316.

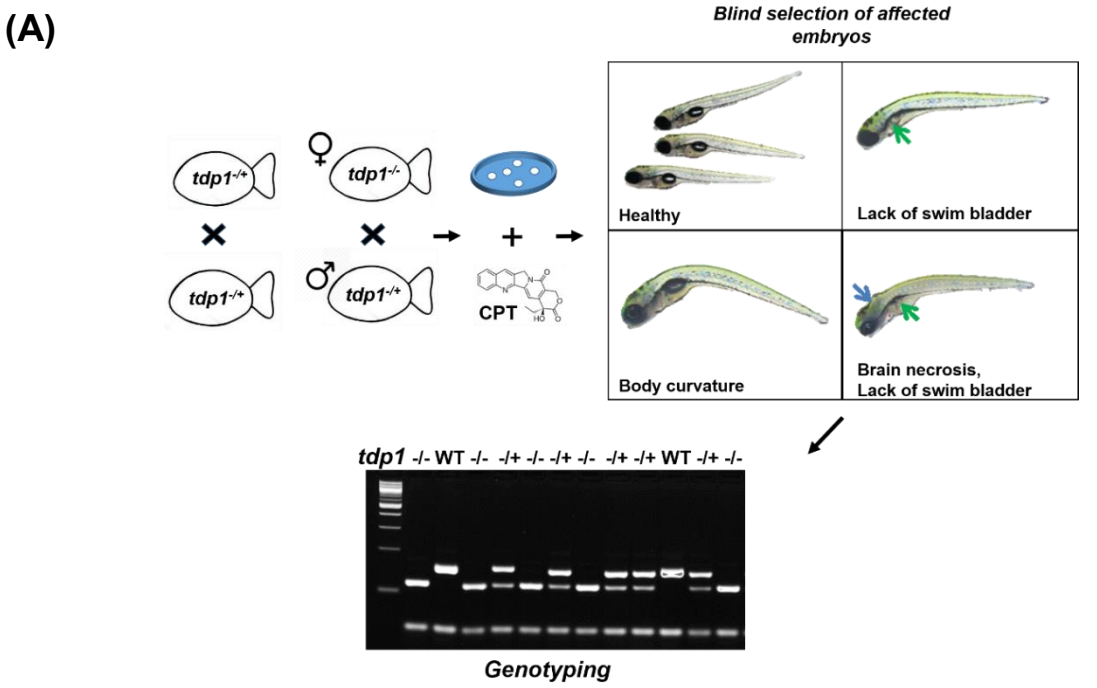

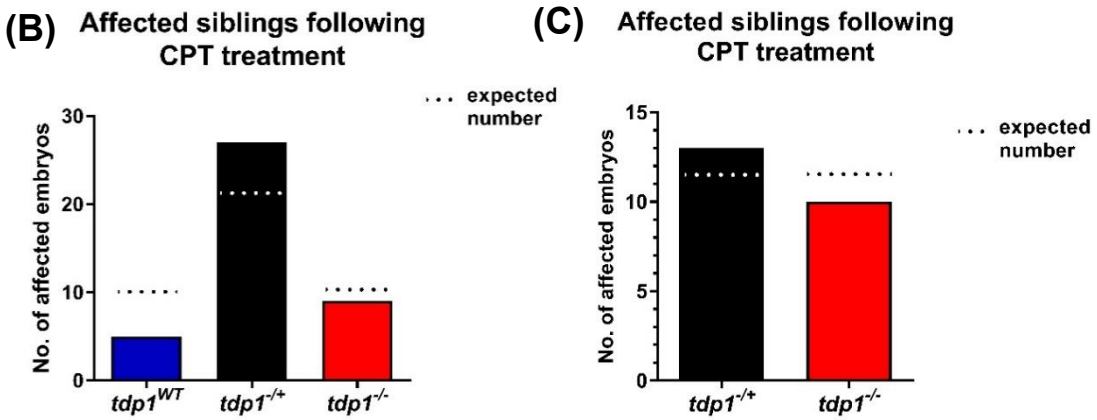

Figure 3.6. ***Tdp1*$^{-/-}$ zebrafish are not more sensitive to CPT than wild-types. (A)** Diagram of blind assay to assess CPT sensitivity. Embryos were collected from zebrafish of required genotypes, then treated at 4 dpf with varying concentrations of CPT. At 5 dpf, embryos most strongly affected by each concentration of CPT, i.e. embryos with severe body curvature, brain necrosis or embryos lacking swim bladders, were selected and genotyped, then a chi-squared test was performed. The null hypothesis assumes that all genotypes are equally affected by CPT and thus normal Mendelian ratios of progeny will be obtained. **(B)** Tdp1$^{-/+}$ fish were crossed and at 4 dpf sibling embryos were treated with a range of CPT concentrations (350 nM, 500 nM and 750 nM) overnight. At 5 dpf, most strongly affected embryos were blindly selected and genotyped. Homozygous mutants were not enriched in a group of 40 strongly affected siblings. X^2 equals 4.902 with 2 degrees of freedom. The two-tailed P value equals 0.0862. **(C)** Female Tdp1$^{-/-}$ fish was crossed with male Tdp1$^{-/+}$ fish, and embryos were collected. At 4 dpf the embryos were treated with 500 nM and 1 µM CPT overnight. At 5 dpf, most strongly affected siblings were blindly selected at each concentration and genotyped. Homozygous mutants were not enriched in a group of 23 strongly affected siblings after CPT treatment of a Tdp1$^{-/+}$ incross. X^2 equals 0.391 with 1 degrees of freedom. The two-tailed P value equals 0.5316.

embryos and their *tdp1*$^{-/+}$ siblings were also subjected to a similar blind assay using 500 nM and 1 µM CPT **(figure 3.6A, C)**. However, both genotypes were found to be equally sensitive to the drug. This data suggests that Tdp1 is not required to cope with elevated Top1 cleavage complexes (Top1-CCs) in zebrafish embryos, which is very surprising in light of previous work in other organisms. It was thus hypothesized that zebrafish have a compensatory DNA repair mechanism to cope with such lesions, at least at embryonic stages. However, first it was tested whether the drug was also inducing comparable levels of Top1-CC and double-strand breaks, which would result from Top1-CCs encountering replication forks.

3.2.5. *Tdp1*$^{-/-}$ embryos do not have increased top1-CCs

To determine if there were any differences at the molecular level, Top1-CC levels were first measured. 3 dpf embryos were treated with a 2 hour pulse of CPT, then lysed. The lysate was fractionated into free DNA, DNA-protein complexes and free protein using a caesium chloride gradient, then loaded onto a membrane and probed for Top1-CC. Top1-CCs were barely detectable in normal conditions, but equally highly enriched after CPT treatment in both *tdp1*$^{-/-}$ and *tdp1*^{WT} embryos **(figure 3.7)**.

3.2.6. *Tdp1*$^{-/-}$ embryos do not have increased γH2AX

Embryonic stages are highly proliferative and thus unrepaired Top1-CCs could be readily turned into DSBs due to collision with replication forks (Avemann et al., 1988; Furuta et al., 2003; Strumberg et al., 2000). To test if that is the case in *tdp1*$^{-/-}$ fish, 4 dpf embryos were treated with CPT overnight, then lysed and subjected to western blotting for γH2ax, a double-strand break marker. ΓH2ax levels were significantly

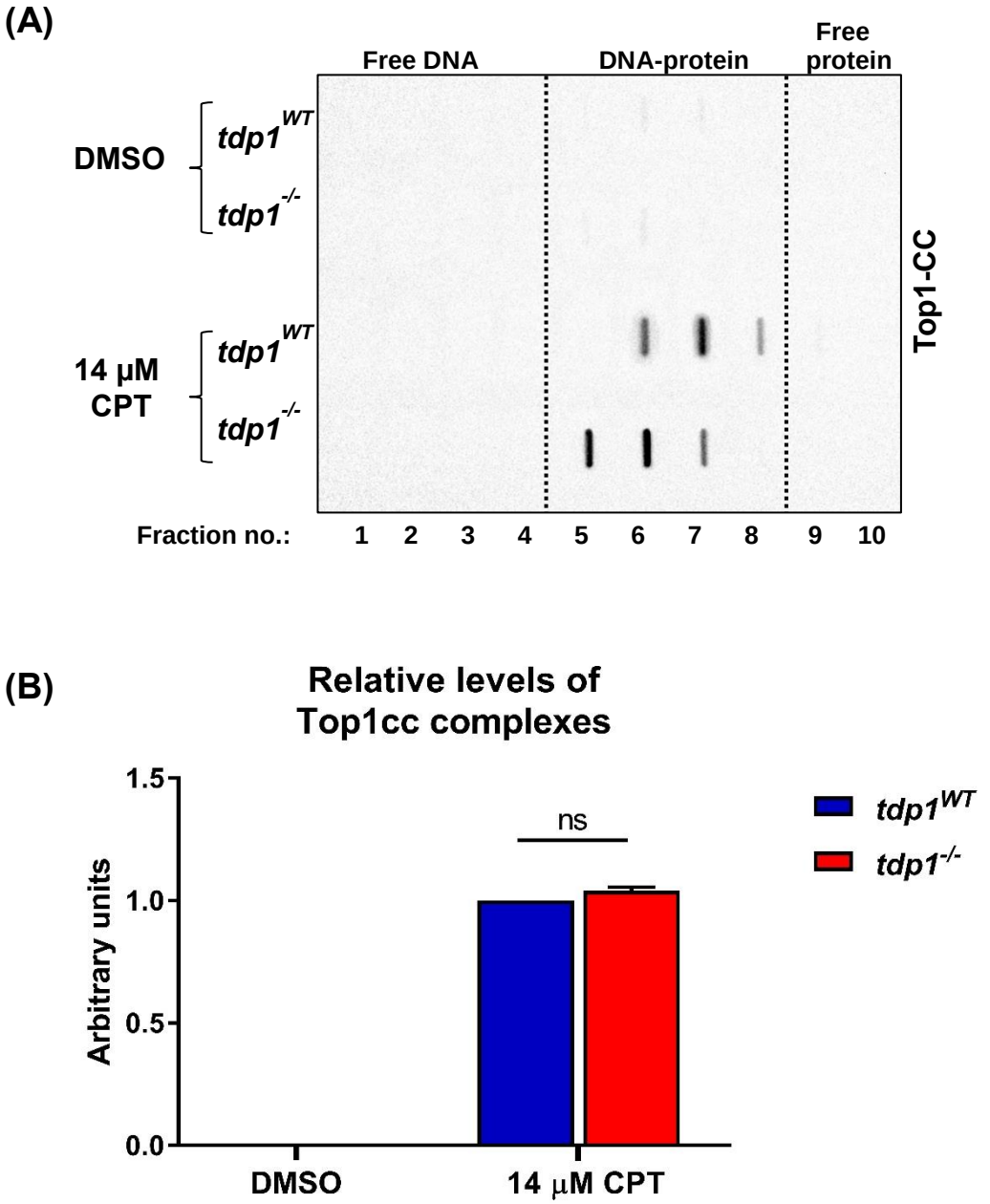

Figure 3.7. *Tdp1*$^{-/-}$ mutants do not have more Top1-CCs than wild-type zebrafish, with or without CPT treatment. (A) 3 dpf embryos were treated with 14 µM CPT for 2 hours, then lysed (section 2.9.1). 1 % of the lysate was used for quantification of gDNA using the pico-green assay after treatment with RNase A. The rest of the lysate was fractionated using 24 hour centrifugation with a caesium chloride gradient (section 2.10.2). The sample was collected in ten equal volume fractions, starting at the bottom of the tube and subjected to slot-blotting onto a nitrocellulose membrane. 200 µL of each fraction from the sample with lowest gDNA concentration was loaded and the equivalent amount of gDNA was loaded for the rest of the samples. Immunoblotting was then performed using anti TOP1-CC antibody (section 2.9.6). **(B)** Quantification of slotblot; 3 independent repeats, ±SEM. *p* values were calculated using a two-tailed Student's T-test.

induced after treatment in both *tdp1*$^{-/-}$ and *tdp1*^{WT} embryos, however no significant differences were found between the genotypes, with or without CPT **(figure 3.8A)**. Additionally, 24 hpf embryos were subjected to γ-irradiation (12 and 20 Gy), which leads to SSBs, DSBs and Top1-trapping base modifications, then lysed and subjected to immunoblotting for γH2AX. However, significant overall induction in γH2AX was not observed after treatment and neither were there any differences between *tdp1*$^{-/-}$ and *tdp1*^{WT} embryos **(figure 3.8B)**. The radiation dose could thus have not been high enough to elicit an obvious increase in overall levels of γH2AX.

As cerebellum is the most impacted by defects in Tdp1 in humans and mice, γH2AX foci formation was measured in the developing cerebellum and optic tectum, as a control, after γ-irradiation. 24 hpf *tdp1*$^{-/-}$ and *tdp1*^{WT} embryos were treated with γ-irradiation, then fixed either immediately or after a 30-minute recovery and stained for γH2AX. A strong induction of focal γH2AX had occurred in both *tdp1*$^{-/-}$ and *tdp1*^{WT} embryos in the cerebellum immediately after treatment, which decreased somewhat after a 30-minute recovery, albeit not significantly **(figure 3.9)**. Significant differences between *tdp1*$^{-/-}$ and *tdp1*^{WT} embryos were not observed in any of the conditions.

This data suggests that Tdp1 is dispensable in the early stages of zebrafish development, even in conditions with elevated Top1-CCs. Although there is no data in embryonic mice, this is contrary to observations in adult mice (Hirano et al., 2007; Katyal et al., 2007; Katyal et al., 2014) and human (Alagoz et al., 2014) and chicken cells (Murai et al., 2012). Top1-CCs thus appear to be repaired as they arise in zebrafish embryos by a compensatory pathway.

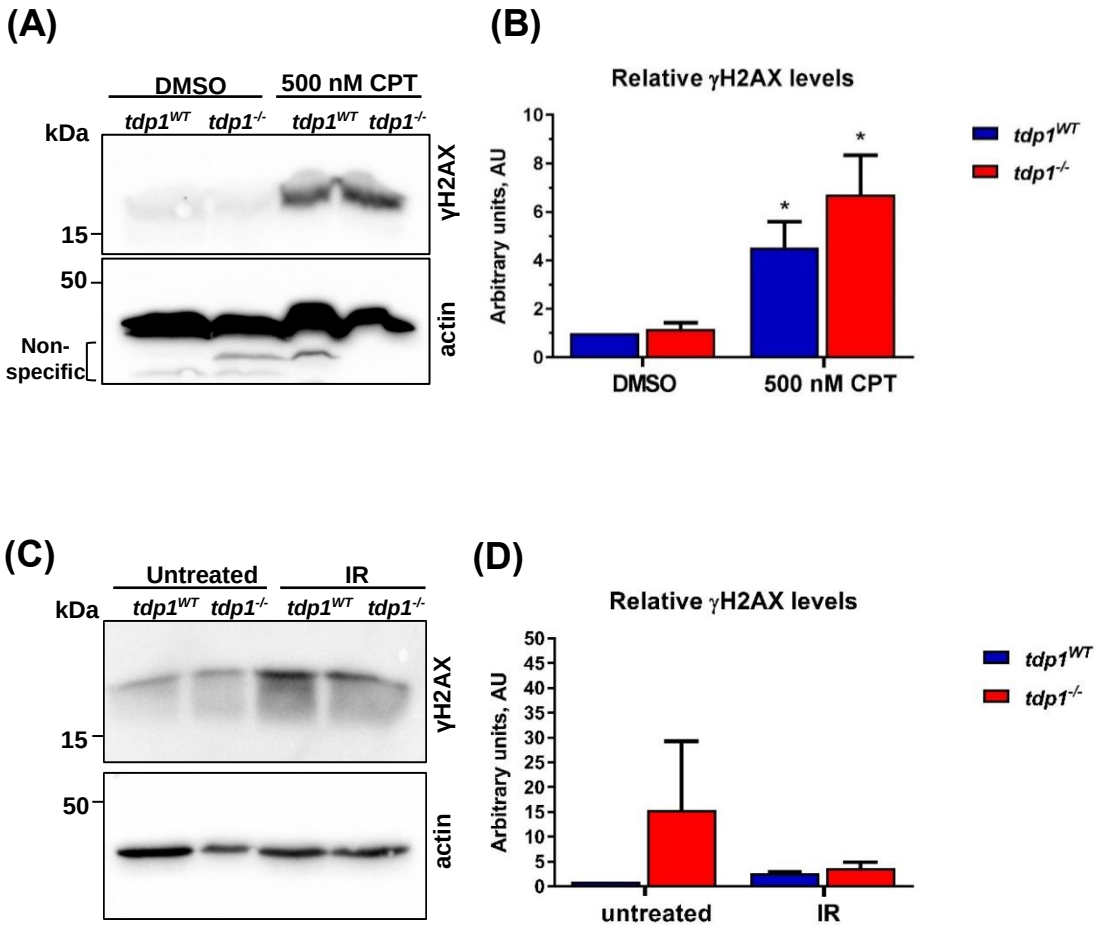

Figure 3.8. *Tdp1*$^{-/-}$ mutants do not have significantly more γH2AX than wild-type zebrafish, with or without DNA damage. (A) 4 dpf embryos were treated with 500 nM CPT overnight, then harvested and subjected to western blotting **(sections 2.9.1, 2.9.3 – 2.9.6)**. **(B)** Quantification of 3.8A; 3 independent repeats, ±SEM. *p* values were calculated using a two-tailed Student's T-test. **(C)** 24 hpf embryos were treated with γ-irradiation of various degrees (12 and 20 Gy), allowed to recover for 1 – 2 hours at 28°C, then harvested and subjected to western blotting **(sections 2.9.1, 2.9.3 – 2.9.6)**. **(D)** Quantification of 3.8C; 2 independent repeats, ±SEM. *p* values were calculated using a two-tailed Student's T-test.

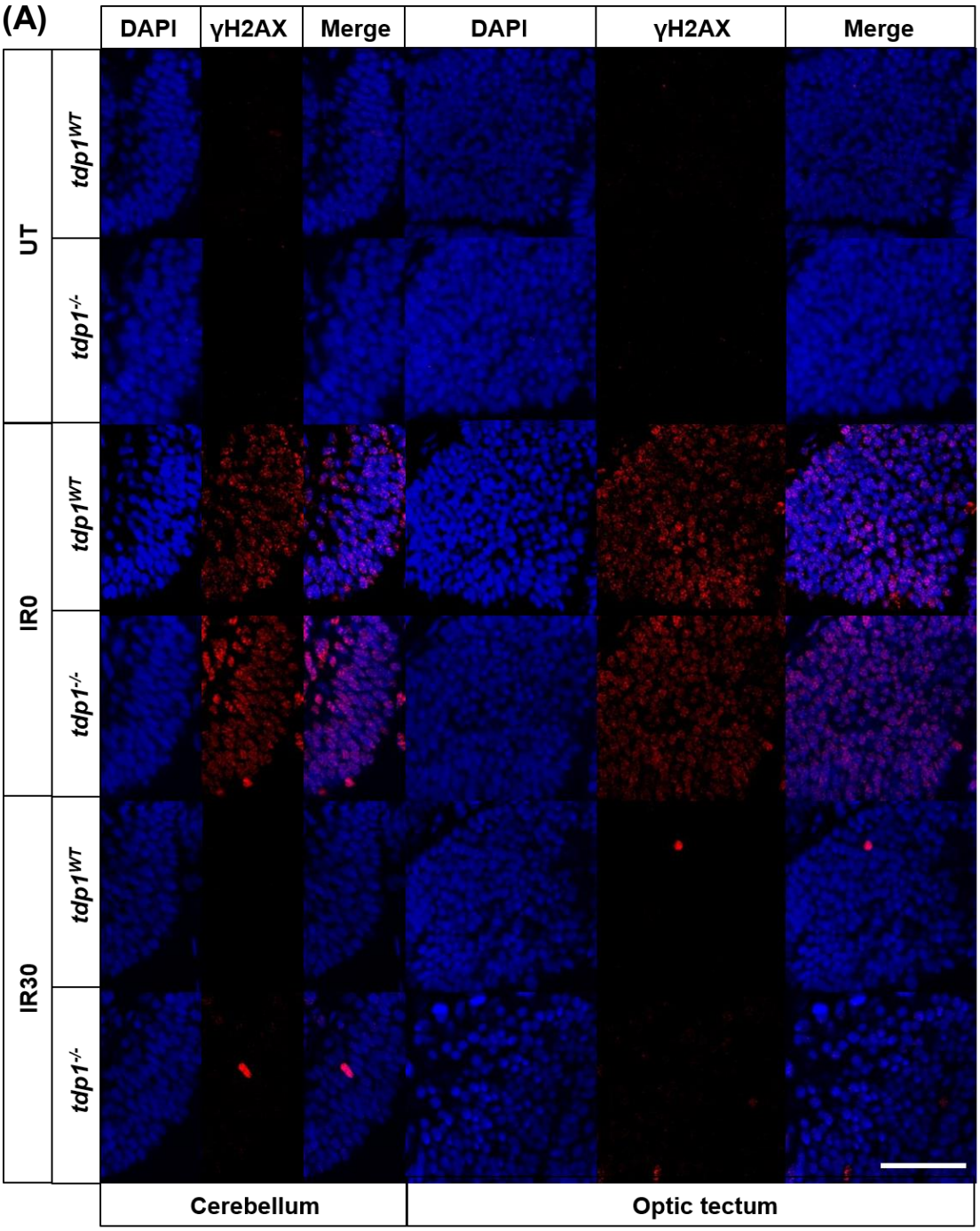

Figure 3.9A. *Tdp1*$^{-/-}$ mutants do not have significantly more γH2AX foci in the cerebellum and optic tectum than wild-type zebrafish, with or without γ-irradiation. 24 hpf embryos were treated with 22 Gy γ-irradiation, fixed in methanol:acetone either straight away (IR0) or after 30 minutes of recovery (IR30) and stained for γH2AX (red) and DAPI (blue), then optic tectum and cerebellum were imaged using confocal microscopy with 40x magnification; scale bar equals 25 µm.

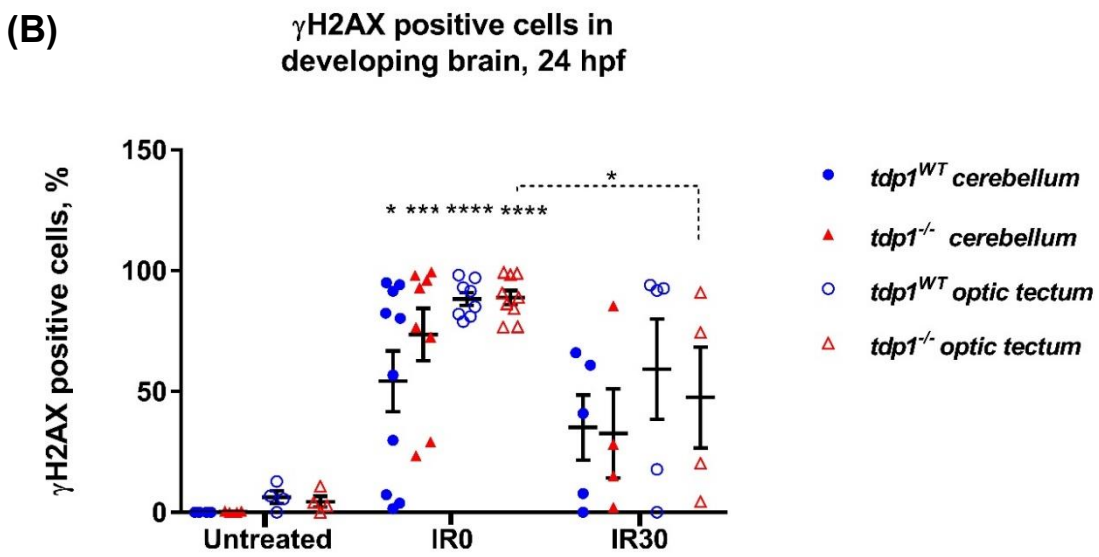

Figure 3.9B. *Tdp1*$^{-/-}$ mutants do not have significantly more γH2AX foci in the cerebellum and optic tectum than wild-type zebrafish, with or without γ-irradiation. Quantification of 3.9A; γH2AX positive cell contains ≥5 foci/nucleus, each data point represents one animal; ±SEM. Unless denoted by the dotted line, *p* values are in relation to the appropriate untreated control. *p* values were calculated using a two-tailed Student's T-test.

3.2.7. Tdp2 or nucleases do not significantly compensate for the loss of Tdp1 in zebrafish

The lack of requirement for Tdp1 could be explained by the availability of compensating factors, such as Mre11, Mus81, Rad1-Rad10 (Hartsuiker et al., 2009; Liu et al., 2002; Vance and Wilson, 2002), CtIP in yeast (Hartsuiker et al., 2009) and avian cells (Nakamura et al., 2010), and Tdp2 in yeast, and avian and murine cells (Liu et al., 2004; Zeng et al., 2012). While TDP1 repairs SSBs with 3'-TOP1-CCs, Tyrosyl-DNA phosphodiesterase 2 (TDP2) normally repairs 5'-topoisomerase 2 cleavage complexes (Ledesma et al., 2009), which create DSBs (Pommier et al., 2016). However, TDP2 has been shown to also process 3'-TOP1-CCs in the absence of TDP1 (Zeng et al., 2012). The structure-specific nucleases may repair these breaks by cleaving the DNA upstream of the TOP1-CC at the replication fork (Ashour et al., 2015).

To test the compensation hypothesis, levels of Tdp2 activity and the expression level of *tdp2* mRNA were first compared between the $tdp1^{-/-}$ and $tdp1^{WT}$ zebrafish embryos. To test Tdp2 activity 4 dpf embryos were treated with CPT overnight, then lysed and incubated with 5'-PY oligonucleotides. In assays with human whole cell extracts, the 5'-PY is processed by TDP2 into a 5'-P moiety, which results in a band shift on a DNA sequencing gel (**figure 3.10A**), allowing TDP2 activity to be easily quantified as product to substrate ratio. When using zebrafish lysates, however, several higher molecular weight bands were obtained, suggesting that further repair

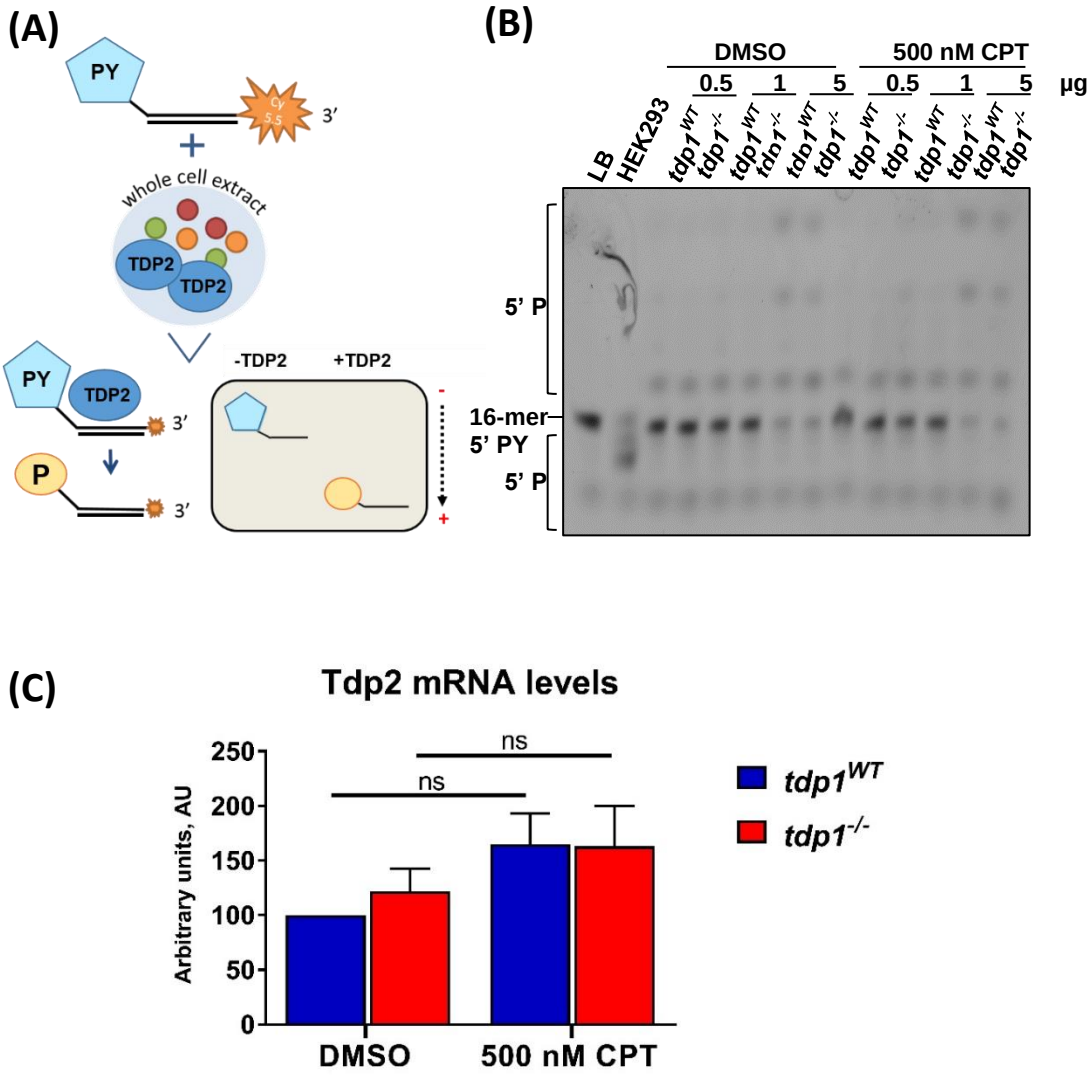

Figure 3.10. TDP2 does not compensate significantly for loss of Tdp1. (A) Diagram of TDP2 activity assay (section 2.9.8). A 3′ labelled oligonucleotide with a 5′-phosphotyrosyl (PY) moiety is incubated with whole cell extract. If active TDP2 is present in the extract, it processes the phosphotyrosyl moiety into a phosphate group, which results in a band shift on a DNA sequencing gel. **(B)** 4 dpf zebrafish were treated with 500 nM CPT overnight, then harvested for the TDP2 activity assay. Lysis buffer (LB) was used as a negative control and HEK293 cell lysate as a positive control. **(C)** 4 dpf zebrafish embryos were treated with 500 nM CPT overnight, then total RNA was harvested (section 2.2.8) for RT-qPCR (section 2.5.1). Quantification for RT-qPCR for the Tdp2 transcript levels normalised to GAPDH is shown; 3 independent repeats, ±SEM. *p* values were calculated using a two-tailed Student's T-test.

My thanks to our undergraduate student Stephen Higgins, who carried out the qPCR and helped in the optimization of the TDP2 activity assay.

of the oligonucleotides was occurring. Even after lengthy optimizations of the TDP2 activity assay with embryonic zebrafish lysates, however, this issue was not averted, and therefore quantification was not performed. The assay was repeated several times and no overt differences were seen in tdp2 reaction products between *tdp1*$^{-/-}$ and *tdp1*^{WT} embryos (oligonucleotides with 5'-phosphate moiety) with or without CPT treatment **(figure 3.10B)**. To quantify *tdp2* mRNA levels, 4 dpf zebrafish embryos were treated with CPT overnight, then their RNA was harvested for quantification by RT-qPCR. *Tdp2* mRNA levels did not show any differences between *tdp1*$^{-/-}$ and *tdp1*^{WT} embryos and they were also not significantly elevated after CPT treatment **(figure 3.10C)**.

Since this data suggested Tdp2 was not compensating for the loss of Tdp1 in zebrafish embryos, the mRNA levels of the nuclease compensation candidates: *mre11*, *mus81*, *ercc1-xpf* (zebrafish orthologue of the yeast *rad1-rad10*) and *ctip*, were next examined using the same method as for quantification of *tdp2* mRNA. Although there appeared to be a trend of increased expression of all the nucleases in the *tdp1*$^{-/-}$ embryos, especially that of *xpf*, it was not statistically significant **(figure 3.11)**.

3.2.8. Aged *tdp1*$^{-/-}$ zebrafish are sensitive to topotecan, but show no overt cerebellar abnormalities

During cellular differentiation the availability of DNA repair pathways is increasingly restricted (Nouspikel and Hanawalt, 2002). In addition, SCAN1 phenotype in humans is progressive and does not fully manifest until early adulthood (Takashima et al., 2002) thus it is most appropriate to study mechanisms of SCAN1 pathology at a comparable stage in animal models. For these reasons, *tdp1*$^{-/-}$ zebrafish and their

wild-type siblings were observed using behaviour analysis tools up to 27 months of age, which will be discussed in more detail in chapter 4. 27 month-old fish were then intraperitoneally injected with topotecan on two consecutive days and sacrificed three days after the second injection for histological analysis. Although *tdp1*$^{-/-}$ fish were more sensitive to topotecan than their wild-type siblings **(section 4.2.4)**, no gross morphological abnormalities were observed in their cerebellum and size and morphology of Purkinje cells appeared similar **(figure 3.12)**. Unfortunately, the sections we obtained were not comparable enough to allow quantification of Purkinje cells, which should be done to ascertain the lack of histological differences. This data suggests that loss of Tdp1 is not toxic to these animals in physiological conditions, but that compensatory pathways, which were active in the embryonic stages, are likely not present anymore, and that Tdp1 is thus now required to cope with elevated Top1-CCs.

3.3. Discussion

In this chapter, I have described a novel protein-linked break repair model. *Tdp1*$^{-/-}$ zebrafish are viable, which is consistent with previous studies in yeast (Liu et al., 2002, 2004), mice (Hawkins et al., 2009; Hirano et al., 2007; Katyal et al., 2007) and one of the studies in flies (Guo et al., 2014). The zebrafish develop normally and, to our surprise, are not hypersensitive to CPT or γ-irradiation at the embryonic stage. Mouse *Tdp1*$^{-/-}$ embryos have not been treated with CPT or its derivatives before, but *Atm*$^{-/-}$ mouse embryos are hypersensitive to TPT (Katyal et al., 2014). As ATM has also been implicated in the repair of TOP1-CCs, this might suggest that a common compensation pathway may be at play in the zebrafish embryo, but not in the mouse

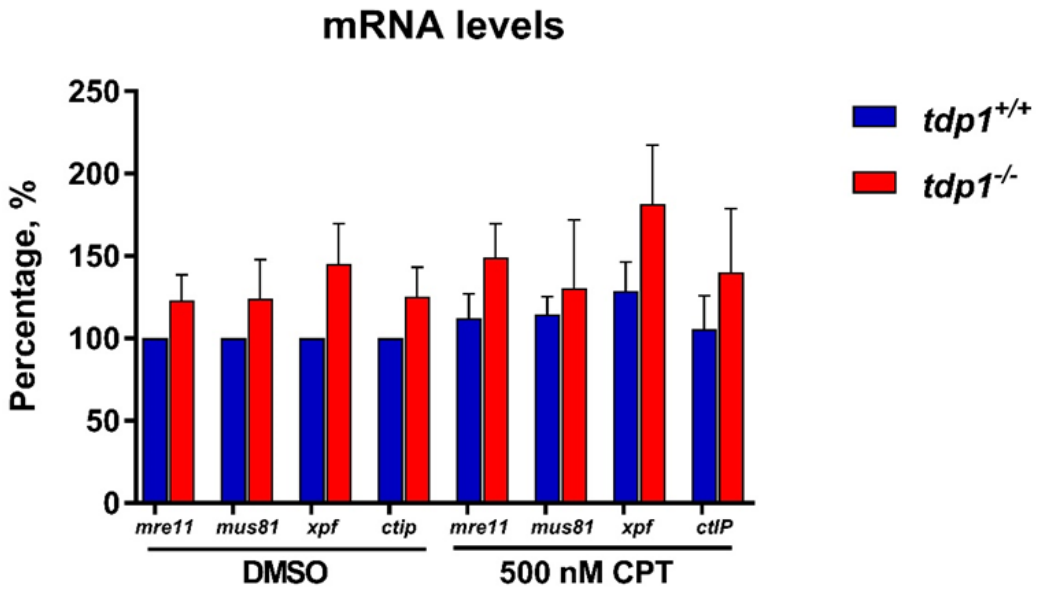

Figure 3.11. Nucleases do not compensate significantly for loss of Tdp1. 4 dpf zebrafish embryos were treated with 500 nM CPT overnight, then total RNA was harvested (section 2.2.8) for RT-qPCR. Quantification for RT-qPCR for transcript levels of candidate nucleases is shown; 4 independent repeats (5 for Xpf), ± SEM. None of the pairs of *tdp1*^{WT}-*tdp1*$^{-/-}$ or DMSO-CPT are statistically significant. *P* values were calculated using a two-tailed Student's T-test.

My thanks to our undergraduate student Ione Smallwood, who carried out this experiment.

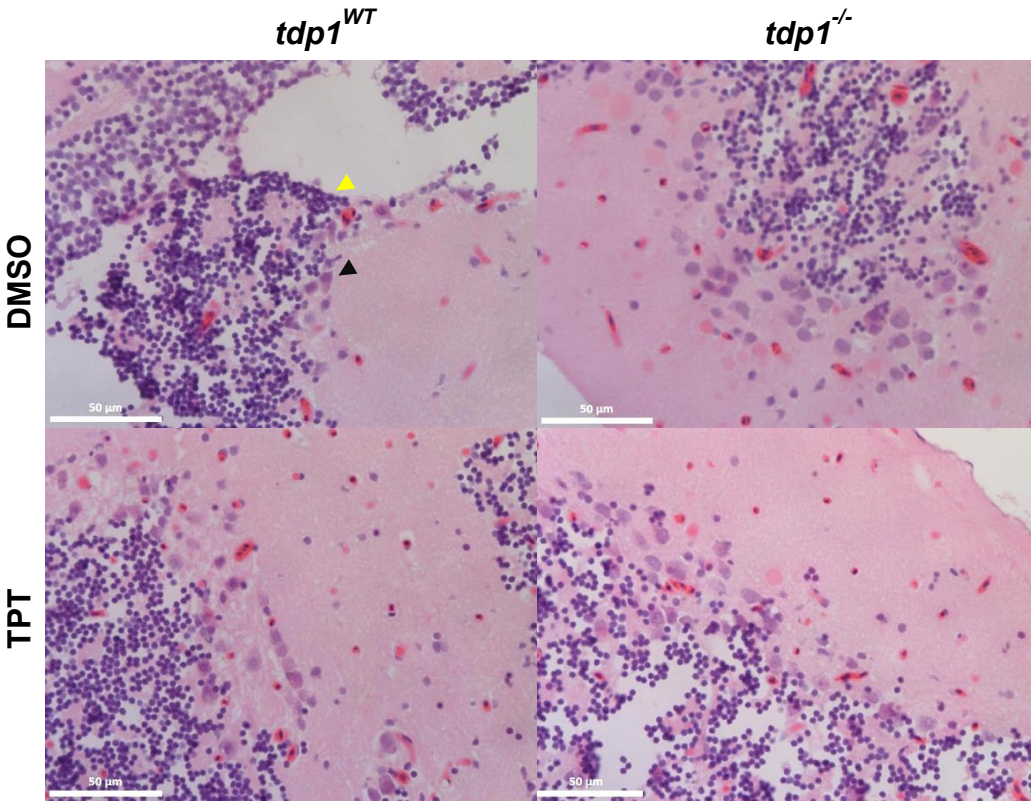

Figure 3.12. No overt abnormalities were observed in the architecture of the cerebellum of aged *tdp1*$^{-/-}$ zebrafish, with or without topotecan treatment. 27-month old fish were intraperitoneally injected (section 2.3.6) with 22.5 mg/kg of topotecan on two consecutive days for a total concentration of 45 mg/kg topotecan, then sacrificed by immersion fixation, paraffin embedded, sectioned transversely and stained with H&E (section 2.7); 4 sections per animal were imaged. Yellow arrow points at a granule cell and black arrow points at a Purkinje cell.

embryo. However, due to the lack of data on the use of topoisomerase poisons in embryonic stages of *Tdp1*$^{-/-}$ mutant mice, it cannot be certain that this is a species-specific phenomenon. This leaves the possibility that it is due to the differences between embryonic and differentiated stages. The lack of hypersensitivity to CPT in *tdp1*$^{-/-}$ zebrafish embryos is further complemented with data showing no increase in overall levels of specific DNA damage, namely Top1-CCs, or DSBs after CPT treatment, and no increase γH2ax foci after irradiation.

It is also worth noting that when whole-mount *in situ* hybridization was carried out on 24 hpf progeny from a *tdp1*$^{-/+}$ incross, *tdp1* mRNA was found in all 20 embryos. Although genotyping of these embryos was not successful, it is highly likely that *tdp1*$^{-/-}$ embryos were among them. The presence of *tdp1* mRNA in *tdp1*$^{-/-}$ embryos would probably be due to maternal contribution, which has previously been observed in *tdp1*Δ *D. melanogaster* embryos (Dunlop et al., 2000; Dunlop et al., 2004). Therefore to circumvent this problem the embryos used for further experiments were either at the later stages of development (4 dpf – 5 dpf), when maternal mRNA should mostly be degraded (Giraldez et al., 2006), or maternal-zygotic mutants.

Regardless of all the data pointing at a compensatory pathway, no single factor stands out in the qPCR and activity assay analysis. It could mean that a factor not yet implicated in this pathway is compensating, which could only be elucidated doing large-scale microarray analysis or inhibitor screens. On the other hand, the trend of increased expression of nucleases in the *tdp1*$^{-/-}$ samples could mean that all candidate nucleases are capable of compensating for the loss of Tdp1 to some

extent. The latter hypothesis would be difficult to confirm, but multiple mutations in combination with inhibitors or morpholinos could be utilized. Slx4 could be an interesting target to inactivate as it has been shown to be required for the function of Slx1 endonuclease and Mus81-Eme1. However, it shares a very low sequence homology with the human gene and protein. In terms of inhibitors, mirin, an MRE11 inhibitor, is available (Dupré et al., 2008), but there is no data about its use in zebrafish. I have tried treating embryos in solution, but found it was highly insoluble at working concentrations. To circumvent this issue, microinjection of mirin in a suitable carrier solution could be considered. Another explanation for the negative results of the compensation analysis could be that compensation is induced at a non-transcriptional level, for example, by modulating protein levels or post-translational modifications, or that Tdp1 is redundant in zebrafish embryos and so the other factors are capable of compensation in endogenous conditions. As it has been demonstrated that in zebrafish genetic compensation may be caused by gene deletions and not knockdowns (Rossi et al., 2015), it would be interesting to observe the effect of α-*tdp1* morpholinos on wild-type embryos. Although we have not directly measured HR levels in these fish, comparable levels of γH2ax **(figures 3.8 and 3.9)** indicate that this repair pathway is not elevated to compensate for increased Top1-CCs, as seen in SCAN1 cells (El-Khamisy et al., 2005). It suggests that in *tdp1*$^{-/-}$ embryos Top1-CCs could be repaired by a compensatory pathway before collision with replication machinery. As Ercc1-Xpf has been shown to cut flapped structures outside of S-phase (Zhang et al., 2011b), it could still be worthwhile further investigating its role in *tdp1*$^{-/-}$ zebrafish embryos. Fen1 and Slx1 have yet to be investigated for compensation capacity due to their gap endonuclease or 3’ flap

processing activity, respectively (Deng et al., 2005; Zheng et al., 2005). Finally, it is not clear whether endonucleases require proteolytic degradation of abortive Top1 by Sprtn and P97, as has been demonstrated for the Tdp1 pathway (Maskey et al., 2017). Sprtn (wws1 in yeast) could be compensating by promoting access to Top1 lesions for the endonucleolytic pathway (Maskey et al., 2017; Stingele et al., 2014; Vaz et al., 2016).

Although the *tdp1*$^{-/-}$ embryos did not exhibit hypersensitization to Top1 inhibition, the adult zebrafish did, in agreement with mice studies (Hirano et al., 2007; Katyal et al., 2007). This is likely due to the fact that as differentiation progresses and growth stalls, the expression profile of the cells becomes more restricted and there is less replication to channel the breaks through HR. This could also partially explain why only the cerebellum is significantly affected in SCAN1 patients, even though we do not see this in *tdp1*$^{-/-}$ zebrafish.

To summarize, I have generated a valuable tool to facilitate further studies of Top1-CC repair at a whole organism level through development. Our results show that strong compensating mechanisms exist that fully overcome a lack of *tdp1* function in embryos. In chapter 4, *tdp1*$^{-/-}$ behavioural characterization will be discussed and in chapter 5 my attempts to generate a SCAN1 zebrafish model using a *tdp1*$^{-/-}$ background. In addition, the *tdp1*$^{-/-}$ zebrafish can be crossed to other zebrafish mutant lines with defects in PDB repair, as it will be discussed in chapter 6.

4

Behavioural analysis of tdp1$^{-/-}$ zebrafish

4.1. Introduction

In chapter 3 I described the generation and partial characterization of *tdp1*$^{-/-}$ zebrafish larvae and adults. My findings demonstrate that *tdp1*$^{-/-}$ zebrafish are viable and not hypersensitive to camptothecin or irradiation at embryonic stages with levels of γH2AX and Top1-CC indistinguishable from those of wild-type fish. Obvious cerebellar defects were not detected. Another way to test for cerebellar defects, which in humans lead to ataxia, is by using behavioural analysis systems. Zebrafish behaviour systems have been widely utilized for phenotyping in developmental, genetics and neuroscience studies (Norton and Bally-Cuif, 2010) and drug discovery (Kokel and Peterson, 2008). Due to the zebrafish size and lower maintenance costs, it is possible to screen much higher numbers of animals in comparison to mouse studies, thus increasing the chances of detecting mild differences in highly variable behavioural phenotypes. Zebrafish also offer the possibility to study behaviour in the embryonic stages, which was not previously possible in other *Tdp1*$^{-/-}$ models. In this chapter, I have utilized a variety of behavioural analysis methods to characterize potential neurological phenotypes of adult and embryonic *tdp1*$^{-/-}$ zebrafish and also harnessed such analysis to determine topotecan sensitivity in adults.

4.2. Results

4.2.1. *Tdp1*$^{-/-}$ embryos do not show significant behavioural abnormalities

To confirm whether zebrafish embryos develop normally without Tdp1 and whether CPT is more toxic to such embryos, 3 dpf and 4 dpf embryos from a female *tdp1*$^{-/-}$ and male *tdp1*$^{-/+}$ cross were treated with CPT overnight and subjected to 5 minute light and dark cycles **(figures 4.1 and 4.2)**. Untreated *tdp1*$^{-/-}$ fish showed a normal

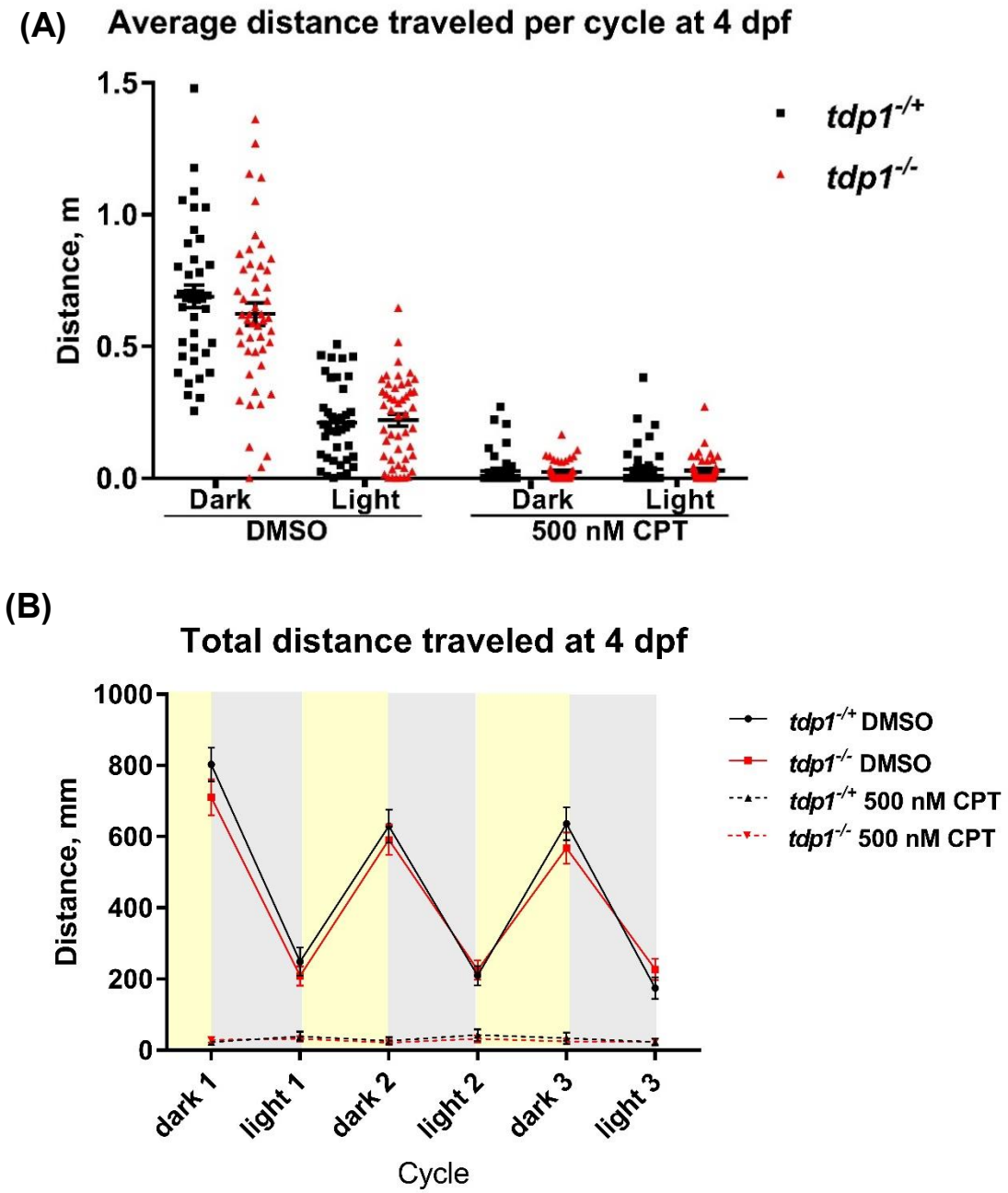

Figure 4.1. *Tdp1*$^{-/-}$ zebrafish do not show any significant abnormal behaviours at 4 dpf. (A, B) 4 dpf embryos from one female *tdp1*$^{-/-}$ and male *tdp1*$^{-/+}$ incross were subjected to 3 cycles of 5 minute darkness and 3 cycles of 5 minute light using the photomotor response assay (section 2.6.1); n=39 for *tdp1*$^{-/+}$ DMSO, n=49 for *tdp1*$^{-/-}$ DMSO, n=43 for *tdp1*$^{-/+}$ CPT and n=45 for *tdp1*$^{-/-}$ CPT. **(A)** Average distance travelled in all light or dark cycles, in metres, was measured. Each data point represents one animal ±SEM. *p* values between *tdp1*$^{-/-}$ and *tdp1*$^{-/+}$ pairs in each condition were calculated using a two-tailed Student's T-test. **(B)** Total distance travelled each cycle, in metres, is plotted in each data point, which represents all animals; ±SEM. *p* values were calculated using a two-tailed Student's T-test.

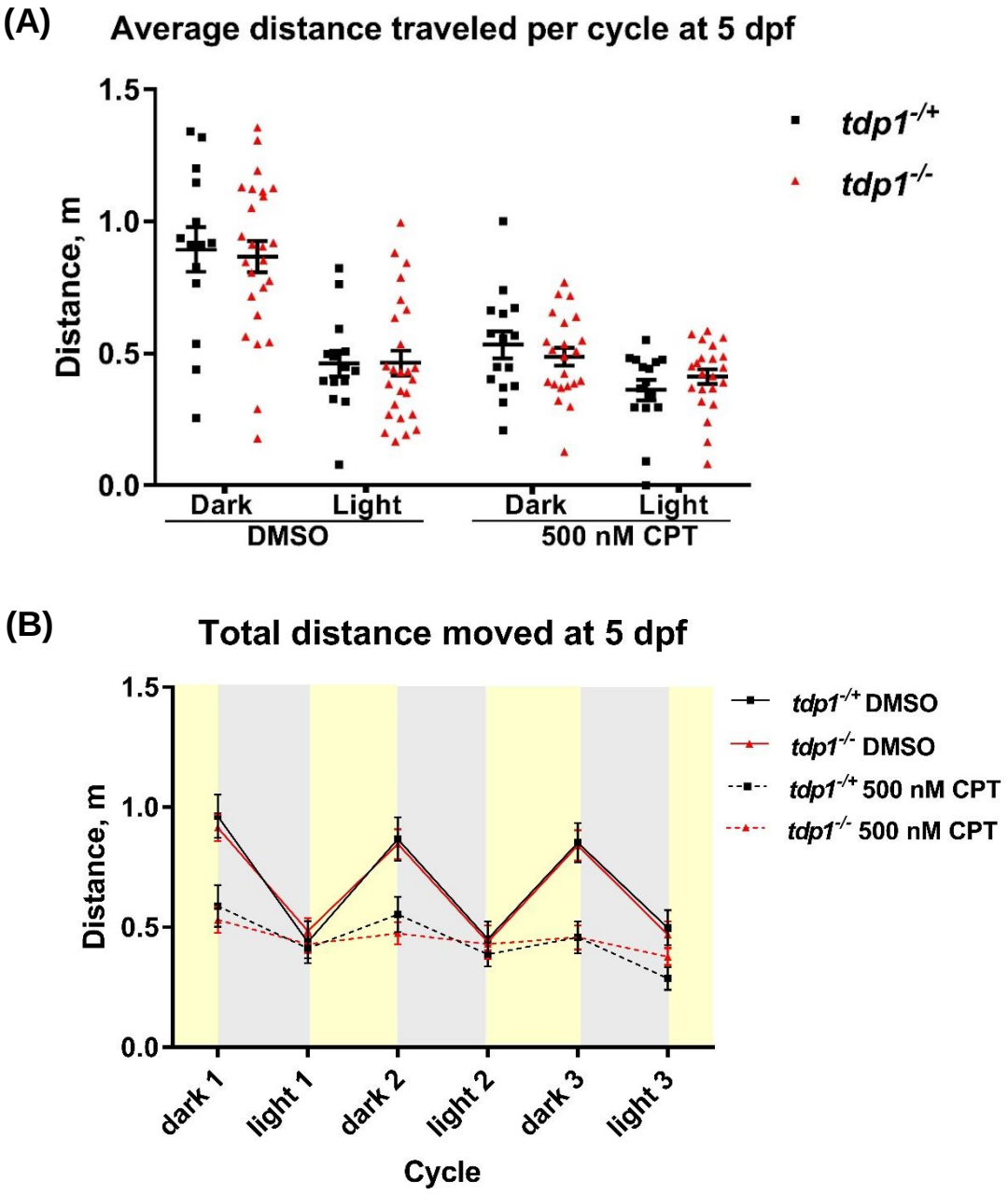

Figure 4.2. *Tdp1*$^{-/-}$ zebrafish do not show any significant abnormal behaviours at 5 dpf. (A, B) 5 dpf embryos from one female *tdp1*$^{-/-}$ and male *tdp1*$^{-/+}$ incross were subjected to 3 cycles of 5 minute darkness and 3 cycles of 5 minute light using the photomotor response assay (section 2.6.1); n=14 for *tdp1*$^{-/+}$ DMSO, n=25 for *tdp1*$^{-/-}$ DMSO, n=15 for *tdp1*$^{-/+}$ CPT and n=22 for *tdp1*$^{-/-}$ CPT. **(A)** Average distance travelled in all light or dark cycles, in metres, was measured. Each data point represents one animal ±SEM. *p* values between *tdp1*$^{-/-}$ and *tdp1*$^{-/+}$ pairs in each condition were calculated using a two-tailed Student's T-test. **(B)** Total distance travelled each cycle, in metres, is plotted in each data point, which represents all animals; ±SEM. *p* values were calculated using a two-tailed Student's T-test.

photomotor response and no significant differences from sibling *tdp1*$^{-/+}$ fish in the distance moved at either light or dark cycles, whereas CPT treatment induced comparable defects in photomotor response of both genotypes.

4.2.2. A time-course analysis of adult *tdp1*$^{-/-}$ zebrafish locomotion

To model progressive neurodegeneration, such as that seen in SCAN1 patients, sibling *tdp1*^{WT} and *tdp1*$^{-/-}$ zebrafish were monitored every 2 months from 14 to 24 months of age using a camera system **(figures 4.3 – 4.6)**. Data was analyzed for parameters such as total distance travelled, average speed, times each of the three speeds (low - <30 mm/s, medium – 30 – 60 mm/s and high >60 mm/s) were initiated, and total time spent traveling at each speed. A trend of decreased movement, i.e. less distance travelled, lower average speed, less time spent in medium and high speed, less times each speed was initiated and more time spent swimming at low speed, was observed in *tdp1*$^{-/-}$ zebrafish across almost every time-point recorded. In 1 – 2 out of the 6 recorded time-points *tdp1*$^{-/-}$ zebrafish showed a significant decrease in low speed count **(figure 4.4B)**, and medium speed duration and count **(figure 4.5)**. The total distance travelled **(figure 4.3A)**, average speed **(figure 4.3B)**, low speed duration **(figure 4.4A)** and high speed duration and count **(figure 4.6)** were not significantly different. This data suggests a mild defect in their locomotion, potentially due to neurological deficiencies caused by loss of Tdp1, however, higher numbers of fish are required to attain statistical significance across more time-points.

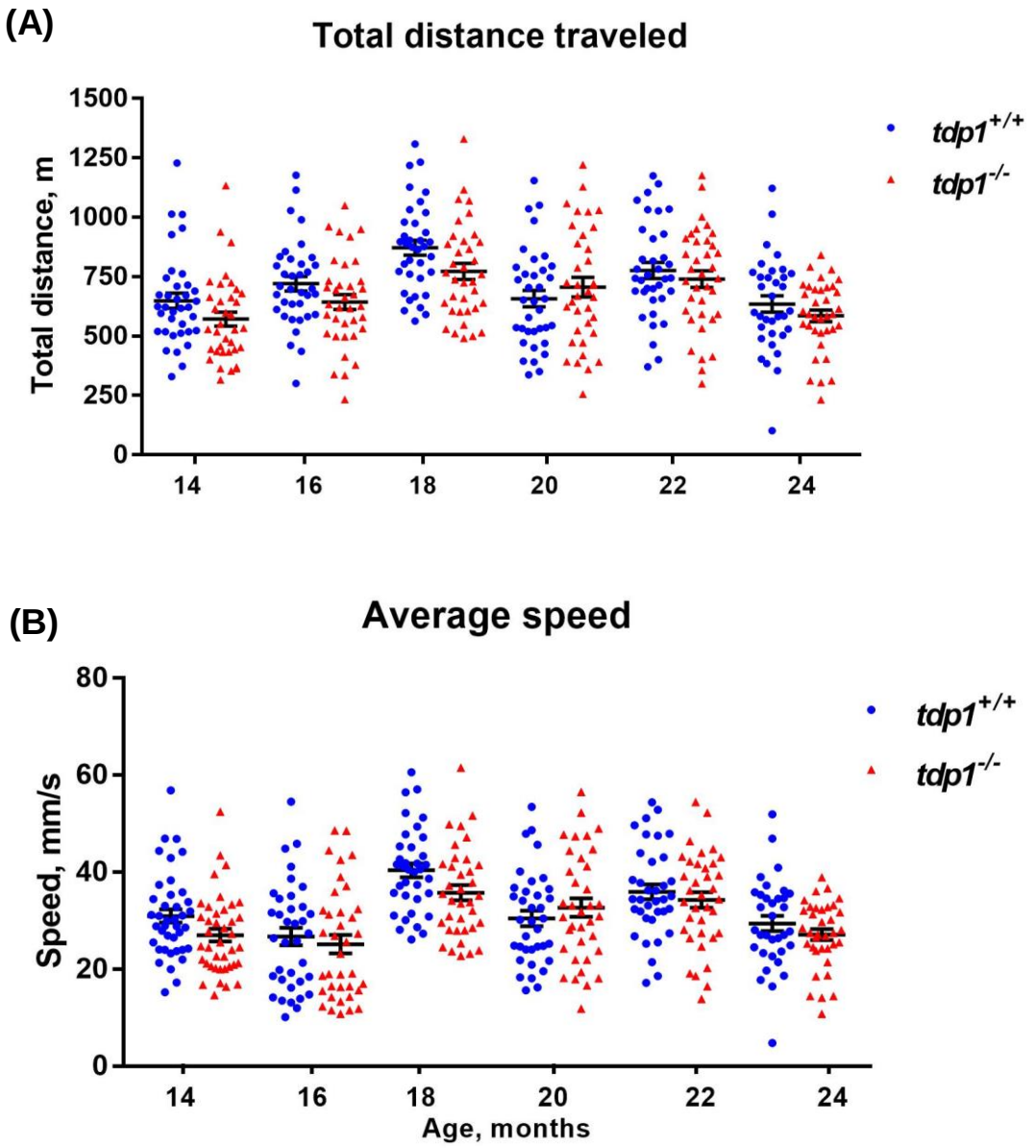

Figure 4.3. Total distance traveled and average speed in *tdp1*$^{-/-}$ fish and their wild-type siblings. Zebrafish were monitored using a camera system for 6 hours (section 2.6.2) and total distance traveled **(A)** and average speed **(B)** were plotted. Analysis was done twice for each of the 18 fish (n=36) from each genotype; ±SEM. *p* values were calculated using a two-tailed Student's T-test with Bonferroni adjustment for multiple comparisons.

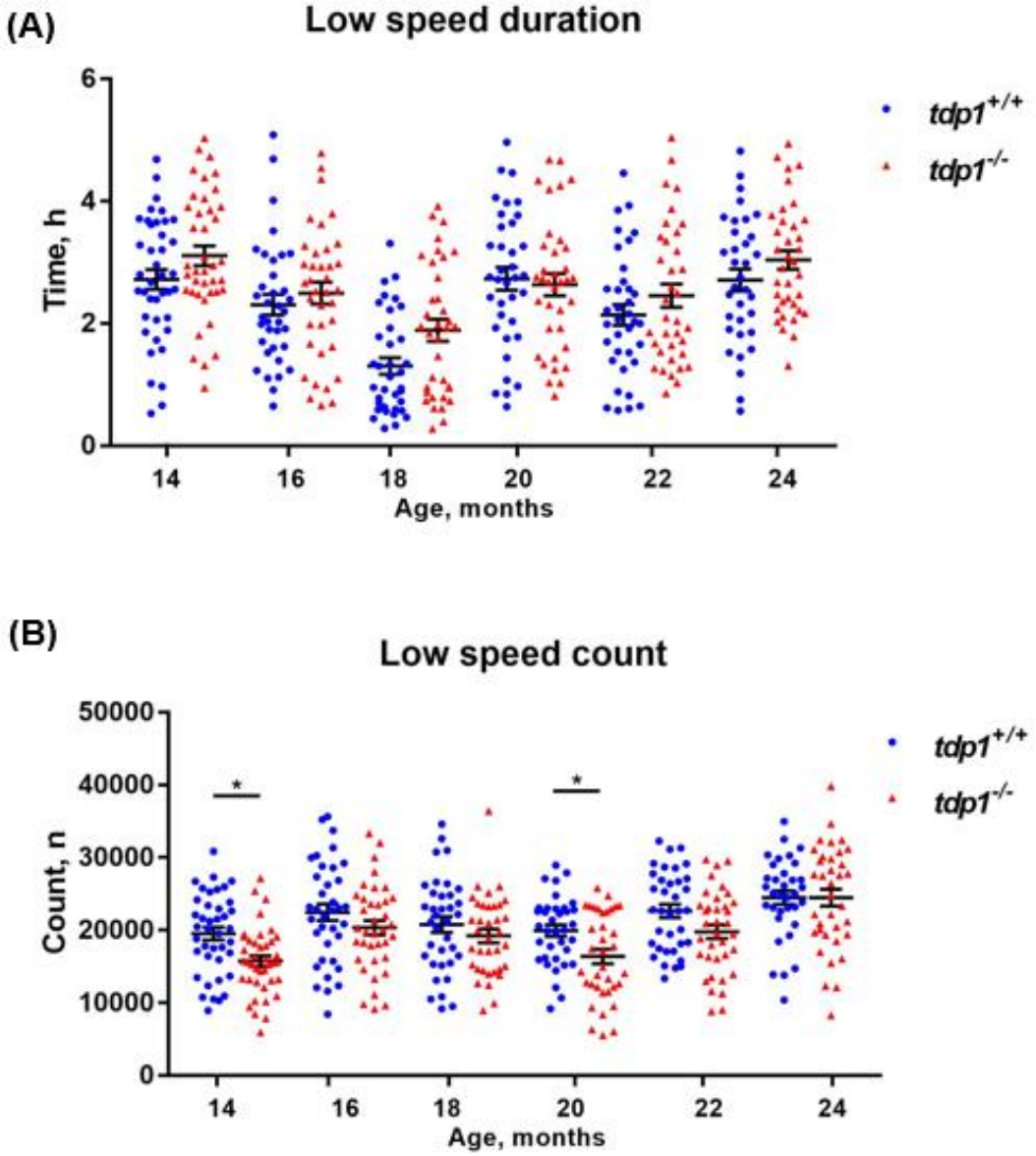

Figure 4.4. Low speed duration and count in *tdp1*$^{-/-}$ fish and their wild-type siblings. Zebrafish were monitored using a camera system for 6 hours (section 2.6.2). Time spent swimming at a low speed (<30 mm/s) **(A)** and count of times low swimming speed was initiated **(B)** were plotted. Analysis was done twice for each of the 18 fish (n=36) from each genotype due to high variation of behavioural phenotypes; ±SEM. *p* values were calculated using a two-tailed Student's T-test with Bonferroni adjustment for multiple comparisons.

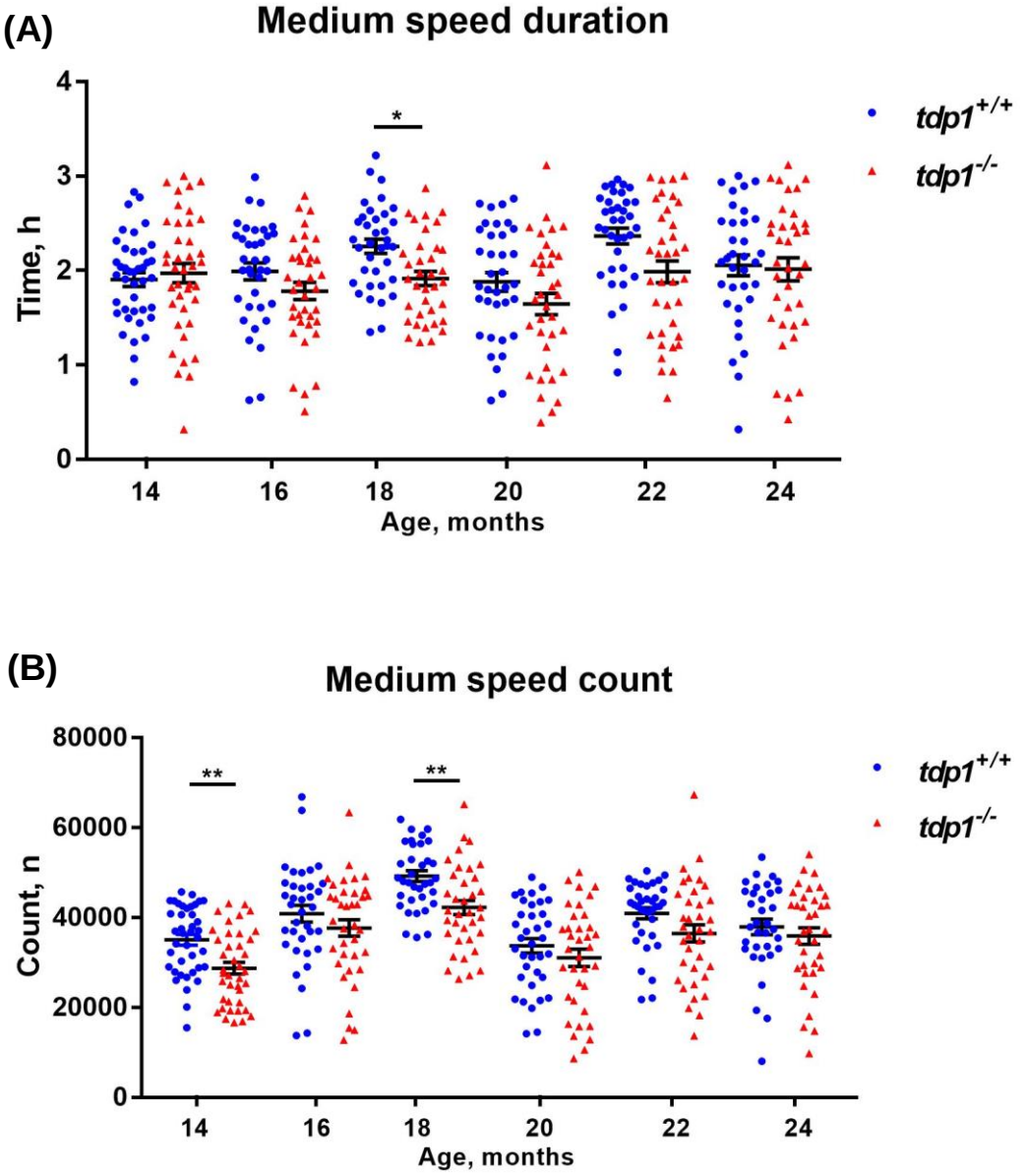

Figure 4.5. Medium speed duration and count in *tdp1*$^{-/-}$ fish and their wild-type siblings. Zebrafish were monitored using a camera system for 6 hours (section 2.6.2). Time spent swimming at medium speed (30 mm/s – 60 mm/s) **(A)** and count of times medium swimming speed was initiated **(B)** were plotted. Analysis was done twice for each of the 18 fish (n=36) from each genotype due to high variation of behavioural phenotypes; ±SEM. *p* values were calculated using a two-tailed Student's T-test with Bonferroni adjustment for multiple comparisons.

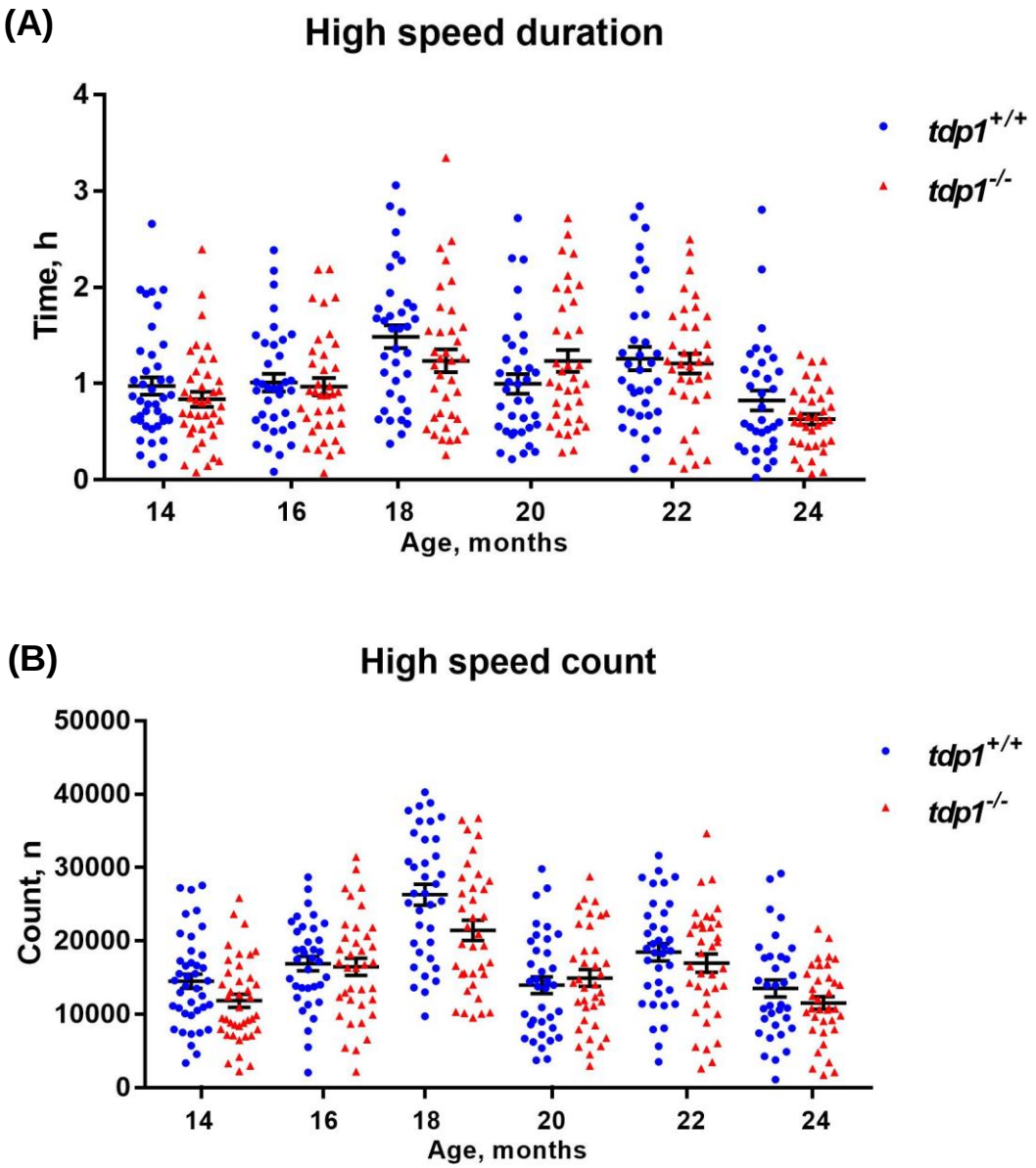

Figure 4.6. High speed duration and count in *tdp1*$^{-/-}$ fish and their wild-type siblings. Zebrafish were monitored using a camera system for 6 hours (section 2.6.2). Time spent swimming at high speed (60 mm/s or above) **(A)** and count of times high swimming speed was initiated **(B)** were plotted. Analysis was done twice for each of the 18 fish (n=36) from each genotype due to high variation of behavioural phenotypes; ±SEM. *p* values were calculated using a two-tailed Student's T-test with Bonferroni adjustment for multiple comparisons.

4.2.3. *Tdp1*$^{-/-}$ zebrafish do not show reduced endurance or balance problems at 19 and 26 months

To test their motor abilities and cerebellar function 9 month-old sibling *tdp1*^{WT} and *tdp1*$^{-/-}$ zebrafish were placed in a water tunnel and water flow was increased every 5 minutes until the fish exhausted (**figure 4.7**). It was hypothesized that straining the fish with an increasing current may exacerbate any mild underlying phenotypes, however *tdp1*^{WT} and *tdp1*$^{-/-}$ zebrafish maintained swimming for similar lengths of time and critical swimming speed was not significantly different (**figure 4.7A, B**). Weight and length of the fish were also recorded, as differences in these parameters can affect performance in a swim tunnel, but no significant differences were found.

26 month-old *tdp1*^{WT} and *tdp1*$^{-/-}$ zebrafish were dropped into deep tanks from a height of ~10 cm and swimming behaviour was recorded using a camera system. Analysis of data revealed no significant differences in time spent at the bottom of the tank (**figure 4.8A**), number of transitions between the top and bottom of the tank (**figure 4.8B**) or freezing duration between *tdp1*^{WT} and *tdp1*$^{-/-}$ zebrafish (**figure 4.8C**).

4.2.4. Adult *tdp1*$^{-/-}$ zebrafish are hypersensitive to topotecan

Although adult *tdp1*$^{-/-}$ zebrafish do not exhibit strong behavioural deficiencies, topoisomerase 1 inhibitors, such as camptothecin (CPT) and topotecan (TPT), may exacerbate the mild phenotype I have observed. Contrary to observations in studies of adult mice (Hirano et al., 2007; Katyal et al., 2007) and human (Alagoz et al., 2014) or avian (Murai et al., 2012) cells, in chapter 3 and figures 4.1 and 4.2, I have shown *tdp1*$^{-/-}$ embryos are not hypersensitive to Top1 inhibition. What remained unclear

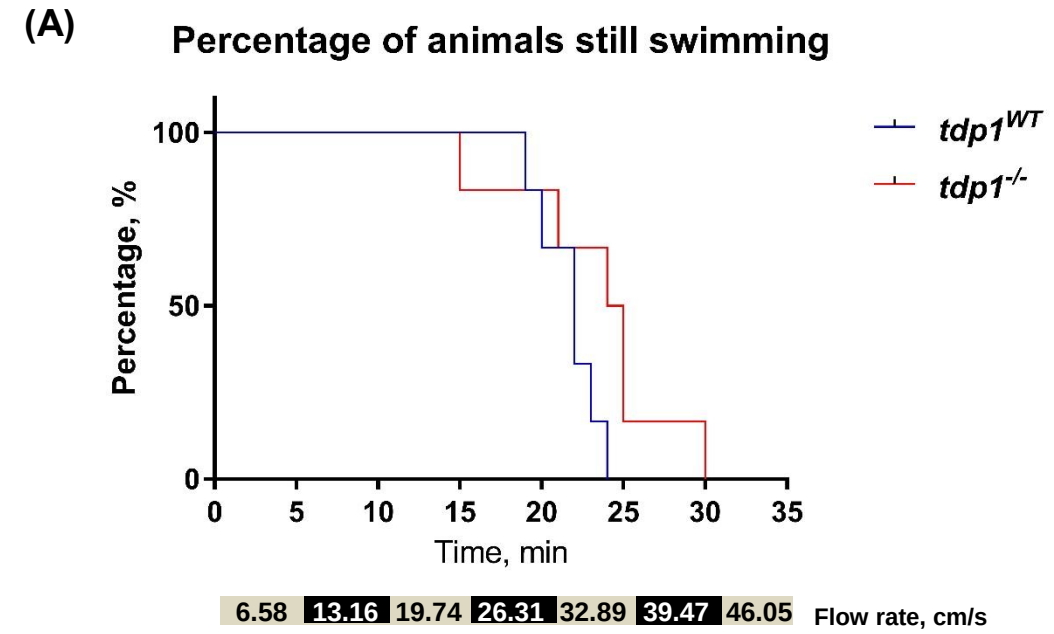

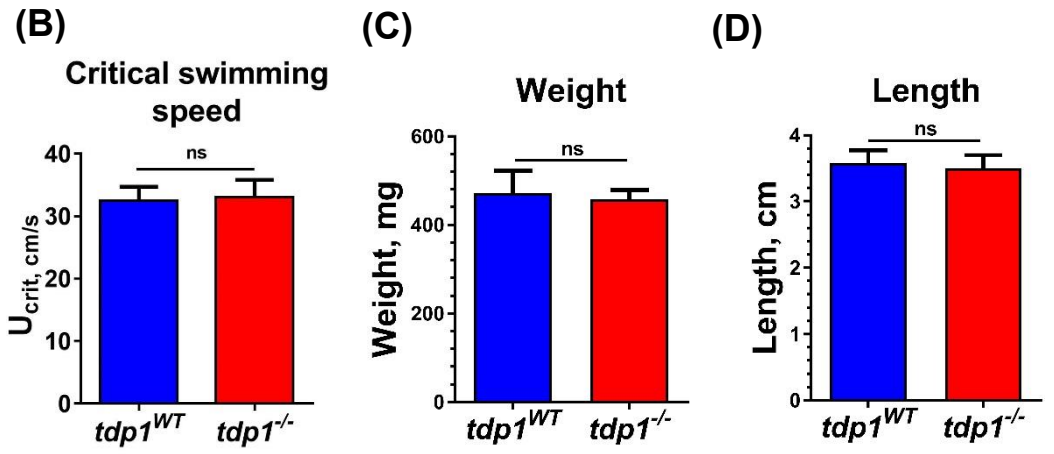

Figure 4.7. *Tdp1*$^{-/-}$ zebrafish do not show reduced endurance or balance problems. 19 month-old sibling zebrafish (n=6) were subjected to the swim tunnel test (section 2.6.3). Fish were placed in a water tunnel and a current was applied, the flow rate of which was increased every 5 minutes. Once the fish exhausted, the current was reduced and then raised again to the highest achieved flow rate to give them a second chance. Once the fish exhausted the second time, the time and the flow rate were recorded. **(A)** Percentage of fish still swimming at each flow rate was plotted. *p* value was calculated using the Mantel-Cox test and showed there were no significant differences between *tdp1*^{WT} and *tdp1*$^{-/-}$. **(B)** Critical swimming speed was calculated as described in section 2.6.3; ±SEM. *p* values were calculated using a two-tailed Student's T-test. **(C)** Fish were weighed and *p* values were calculated using a two-tailed Student's T-test; ±SEM **(D)** The length of the fish was measured and *p* values were calculated using a two-tailed Student's T-test; ±SEM.

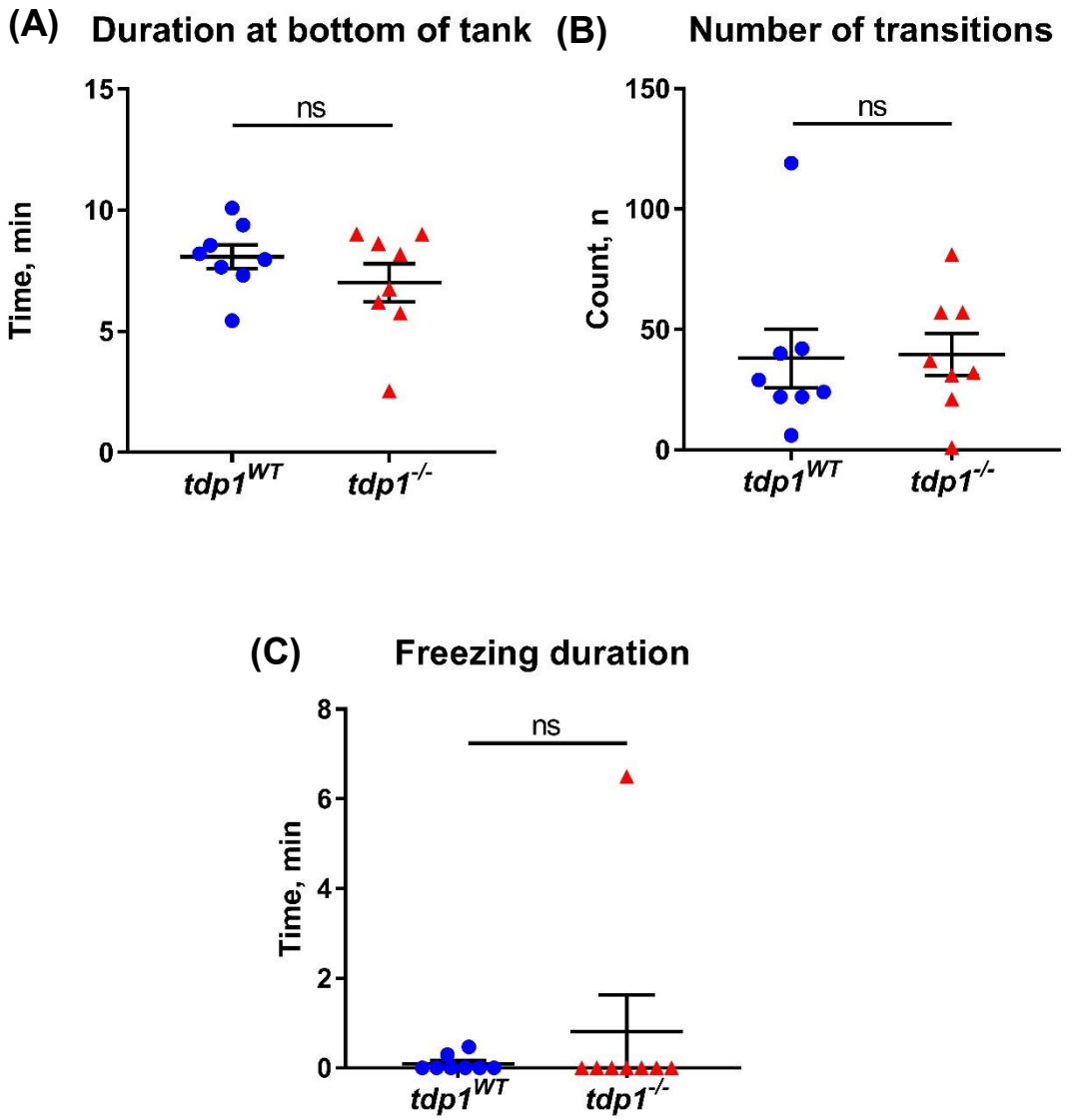

Figure 4.8. *Tdp1*$^{-/-}$ zebrafish recover normally after vestibular disorientation. 26 month-old sibling *tdp1*^{WT} and *tdp1*$^{-/-}$ zebrafish (n=8) were dropped into a deep tank from ~10 cm of height (section 2.6.4) and monitored using a camera system. The tank was divided into two equal horizontal areas, bottom and top, and the duration in the bottom area **(A)**, number of transitions between the two areas **(B)** and overall freezing duration **(C)** were measured. Freezing duration was taken manually by setting a timer each time a fish stopped all fin movements for more than one second. **(A, B, C)** All values ±SEM were plotted. *p* values were calculated using a two-tailed Student's T-test.

was whether the absence of hypersensitivity after loss of Tdp1 is a feature of zebrafish as a species or rather a feature restricted to their larvae. To test this 27 month-old zebrafish were intraperitoneally injected with 22.5 mg/kg topotecan on two consecutive days for a final concentration of 45 mg/kg and monitored using a camera system after each injection and at 24, 48 and 72 hours after administering the final dose (**figures 4.9 – 4.16**). The appropriate dose was determined empirically, starting with concentrations equivalent to those used in *Tdp1*$^{-/-}$ mice (Hirano et al., 2007; Katyal et al., 2007). When zebrafish are sick they tend to spend a lot of time at the bottom of the tank without much movement, therefore sensitivity to the drug should be inversely proportional to total activity of the animals. Two-way ANOVA analysis found that treatment with topotecan significantly reduced total distance travelled **(figure 4.9)**, average speed **(figure 4.10)**, times medium **(figure 4.13)** and high speeds **(figure 4.15)** were initiated (speed count) and the duration of swimming at medium **(figure 4.14)** and high **(figure 4.16)** speeds at 24 and 48 hours after injection, with the 48 hour time-point being the more highly significant. The treatment also significantly reduced low speed count at 48 hours post-injection **(figure 4.11D)** medium **(figure 4.14E)** and high **(figure 4.16E)** speed duration at 72 hours post-injection. This data suggests the topotecan treatment was the most effective at 48 hours after the second injection. Interestingly, two-way ANOVA analysis found significant differences between the genotypes, but not interaction between genotype and treatment, when measuring total distance travelled **(figure 4.9D)**, high speed count **(figure 4.15D)** and duration **(figure 4.6D)** at 48 hours after the 2nd injection and medium speed count at 24 hours post-injection **(figure 4.13C)**. Sidak post-hoc analysis showed a statistically significant reduction in the total

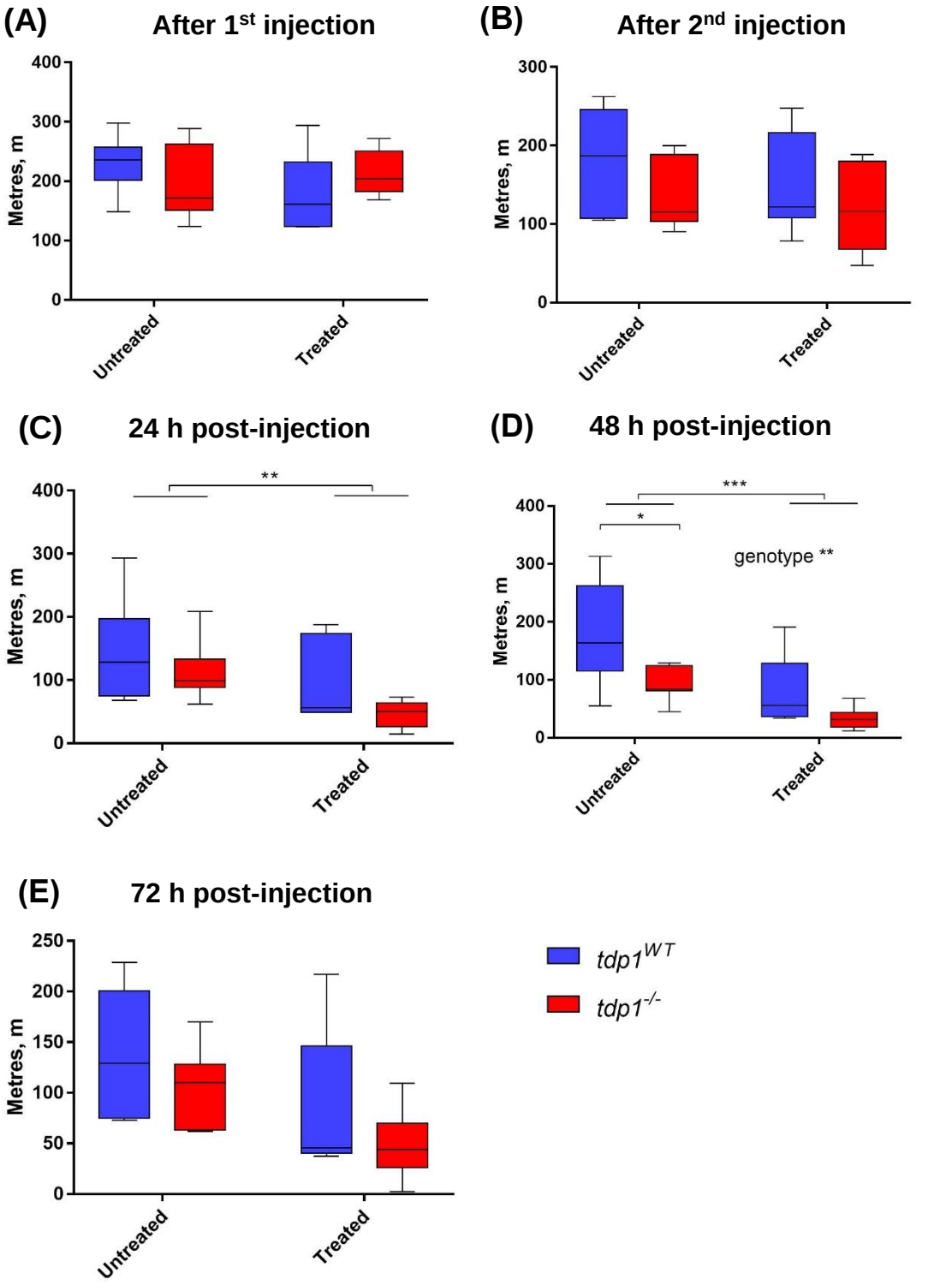

Figure 4.9. Total distance travelled in *tdp1*$^{-/-}$ fish and their wild-type siblings after topotecan treatment. 27-month old zebrafish were intraperitoneally injected with 22.5 mg/kg topotecan on two consecutive days for a final concentration of 45 mg/kg (section 2.3.6), and monitored for 1,5 hours using a camera system (section 2.6.2) after each injection **(A, B)**, then 24 **(C)**, 48 **(D)** and 72 **(E)** hours after the second injection. Total distance travelled was plotted with whiskers representing the minimum and maximum of all data points. N=7 for treated and untreated *tdp1*^{WT}, and untreated *tdp1*$^{-/-}$, n=8 for treated *tdp1*$^{-/-}$ (except for final time-point, where n=6 due to two fish expiring). *p* values were calculated using a two-way ANOVA with Sidak's post-hoc analysis for multiple comparisons.

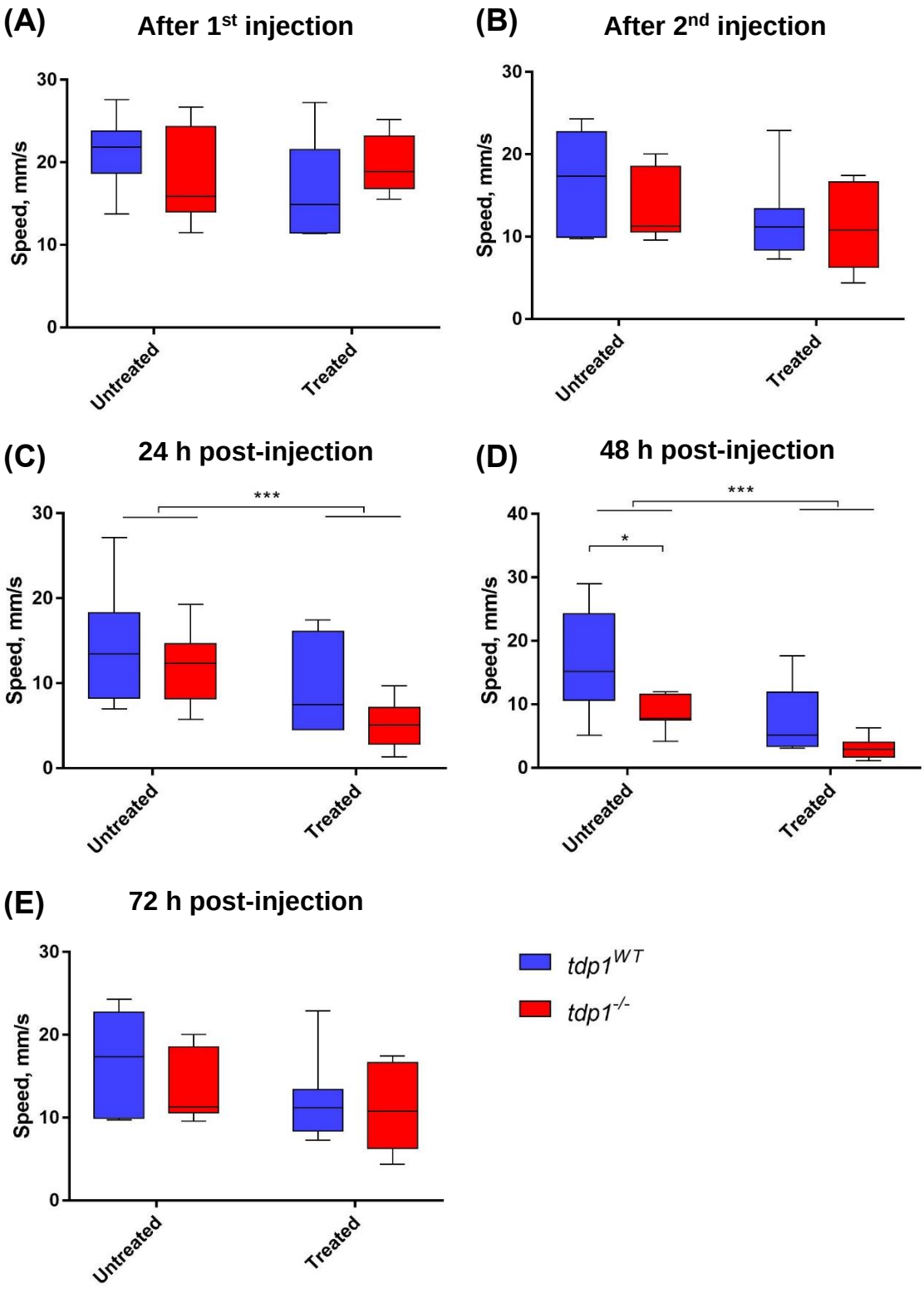

Figure 4.10. Average speed in *tdp1*$^{-/-}$ fish and their wild-type siblings after topotecan treatment. 27-month old zebrafish were intraperitoneally injected with 22.5 mg/kg topotecan on two consecutive days for a final concentration of 45 mg/kg (section 2.3.6), and monitored for 1,5 hours using a camera system (section 2.6.2) after each injection **(A, B)**, then 24 **(C)**, 48 **(D)** and 72 **(E)** hours after the second injection. Average speed was plotted with whiskers representing the minimum and maximum of all data points. N=7 for treated and untreated *tdp1*^{WT}, and untreated *tdp1*$^{-/-}$, n=8 for treated *tdp1*$^{-/-}$ (except for final time-point, where n=6 due to two fish expiring). *p* values were calculated using a two-way ANOVA with Sidak's post-hoc analysis for multiple comparisons.

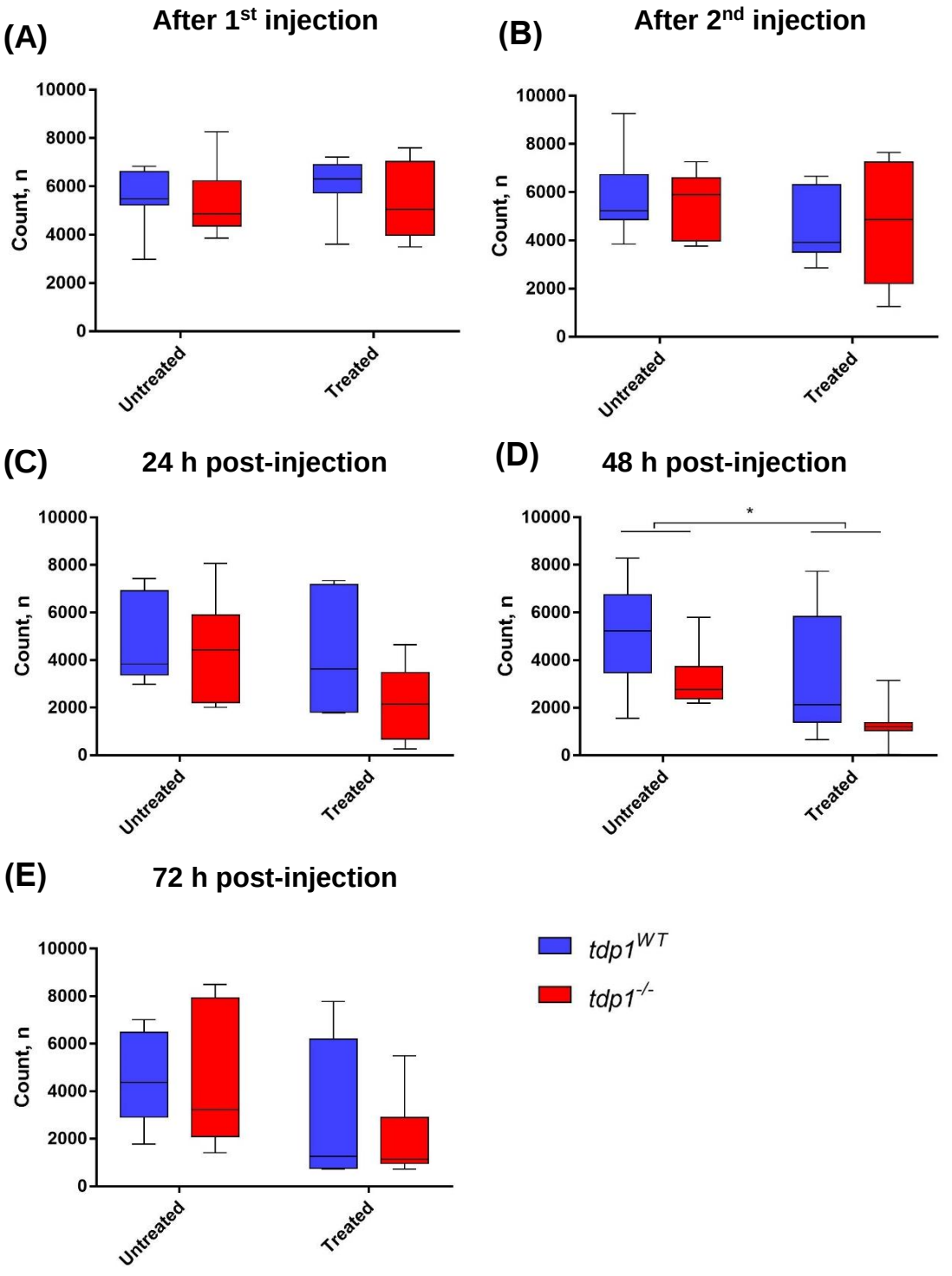

Figure 4.11. Low speed count in *tdp1*$^{-/-}$ fish and their wild-type siblings after topotecan treatment. 27-month old zebrafish were intraperitoneally injected with 22.5 mg/kg topotecan on two consecutive days for a final concentration of 45 mg/kg (section 2.3.6), and monitored for 1,5 hours using a camera system (section 2.6.2) after each injection **(A, B)**, then 24 **(C)**, 48 **(D)** and 72 **(E)** hours after the second injection. Number of times low speed (<30 mm/s) was initiated was plotted with whiskers representing the minimum and maximum of all data points. N=7 for treated and untreated *tdp1*^{WT}, and untreated *tdp1*$^{-/-}$, n=8 for treated *tdp1*$^{-/-}$ (except for final time-point, where n=6 due to two fish expiring). *p* values were calculated using a two-way ANOVA with Sidak's post-hoc analysis for multiple comparisons.

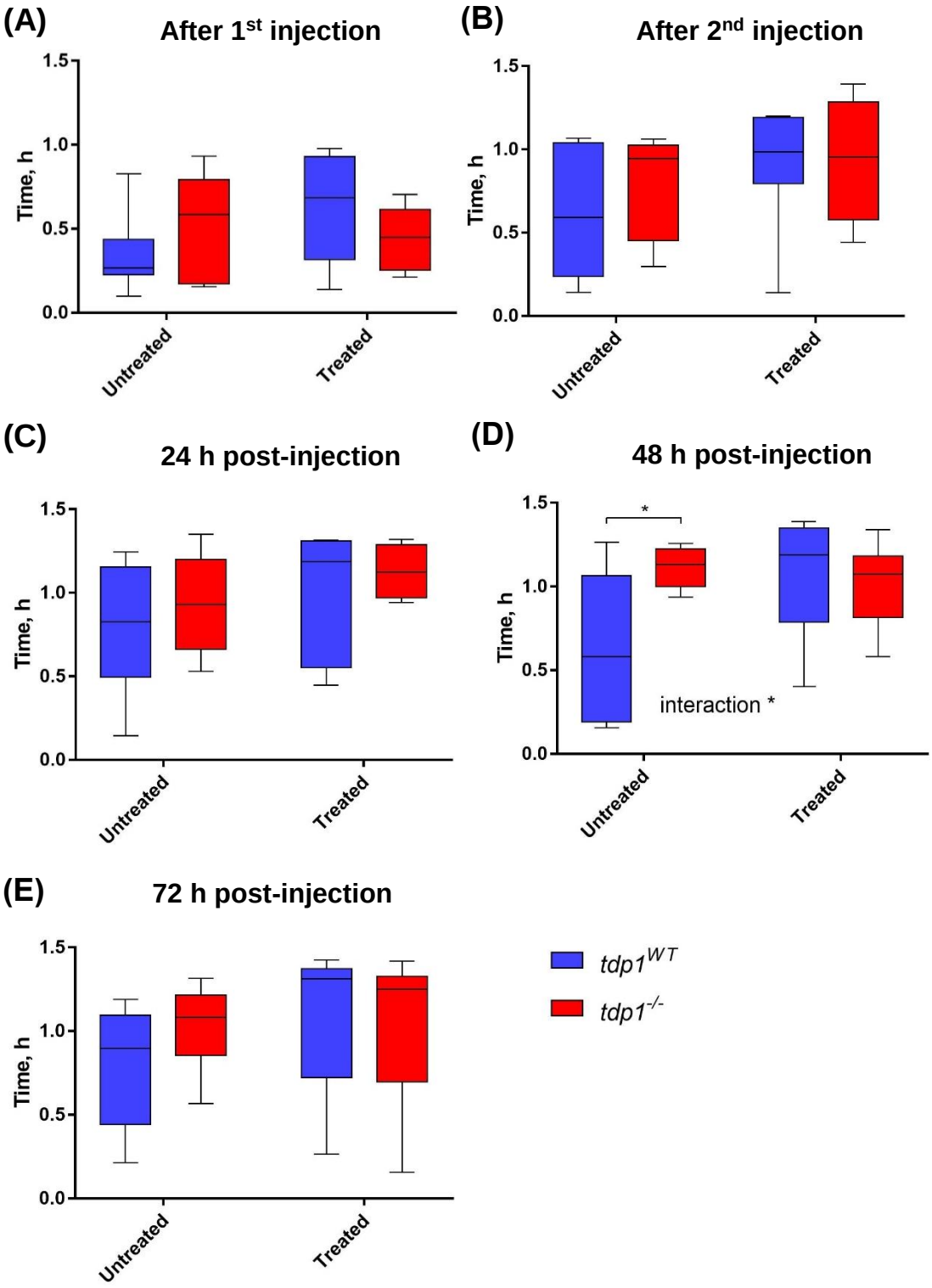

Figure 4.12. Low speed duration in *tdp1*$^{-/-}$ fish and their wild-type siblings after topotecan treatment. 27-month old zebrafish were intraperitoneally injected with 22.5 mg/kg topotecan on two consecutive days for a final concentration of 45 mg/kg (section 2.3.6), and monitored for 1,5 hours using a camera system (section 2.6.2) after each injection **(A, B)**, then 24 **(C)**, 48 **(D)** and 72 **(E)** hours after the second injection. Low speed (<30 mm/s) duration was plotted with whiskers representing the minimum and maximum of all data points. N=7 for treated and untreated *tdp1*^{WT}, and untreated *tdp1*$^{-/-}$, n=8 for treated *tdp1*$^{-/-}$ (except for final time-point, where n=6 due to two fish expiring). *p* values were calculated using a two-way ANOVA with Sidak's post-hoc analysis for multiple comparisons.

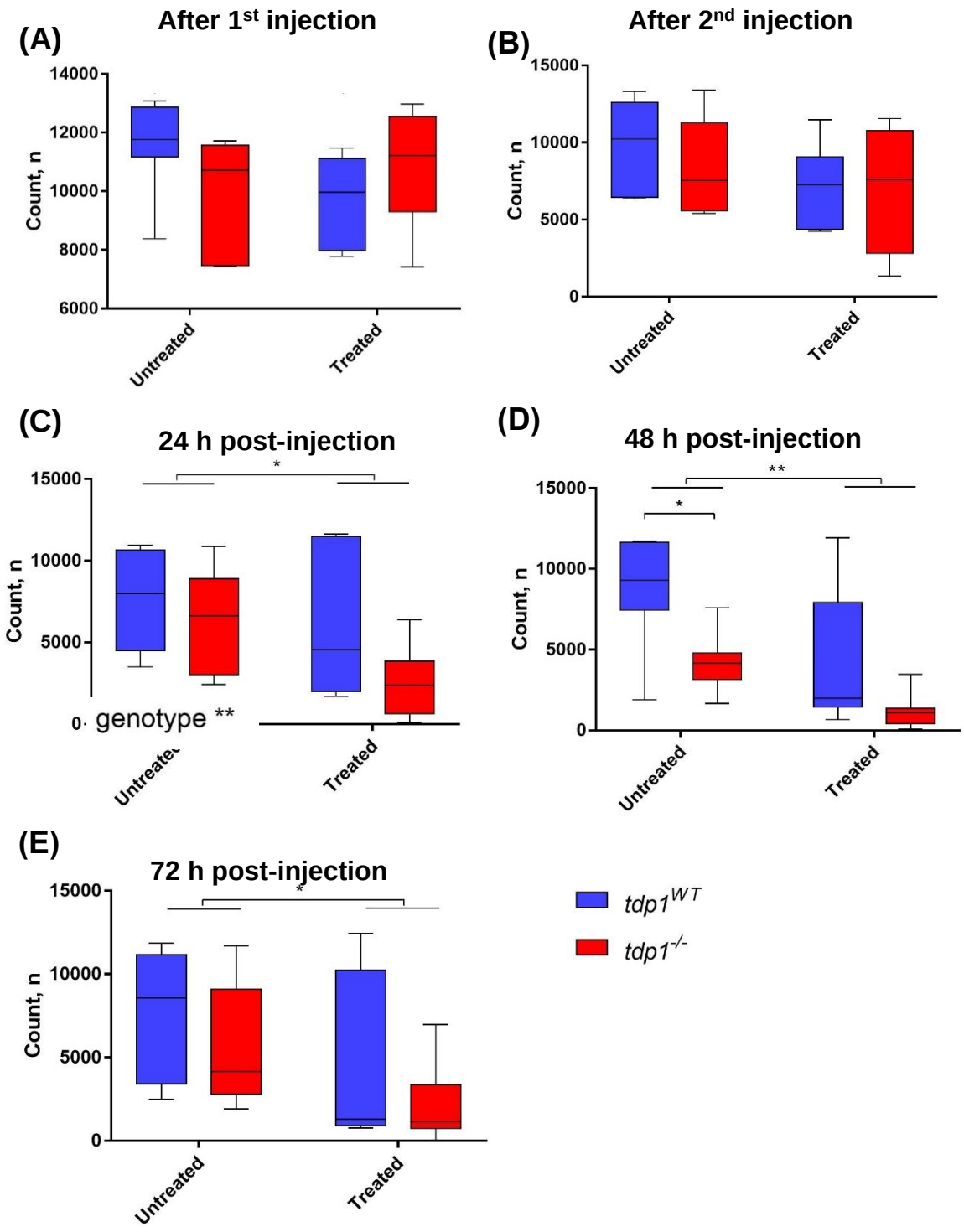

Figure 4.13. Medium speed count in *tdp1*$^{-/-}$ fish and their wild-type siblings after topotecan treatment. 27-month old zebrafish were intraperitoneally injected with 22.5 mg/kg topotecan on two consecutive days for a final concentration of 45 mg/kg (section 2.3.6), and monitored for 1,5 hours using a camera system (section 2.6.2) after each injection **(A, B)**, then 24 **(C)**, 48 **(D)** and 72 **(E)** hours after the second injection. Number of times medium speed (30 – 60 mm/s) was initiated was plotted with whiskers representing the minimum and maximum of all data points and the dot denoting the mean. N=7 for treated and untreated *tdp1*^{WT}, and untreated *tdp1*$^{-/-}$, n=8 for treated *tdp1*$^{-/-}$ (except for final time-point, where n=6 due to two fish expiring). *p* values were calculated using a two-way ANOVA with Sidak's post-hoc analysis for multiple comparisons.

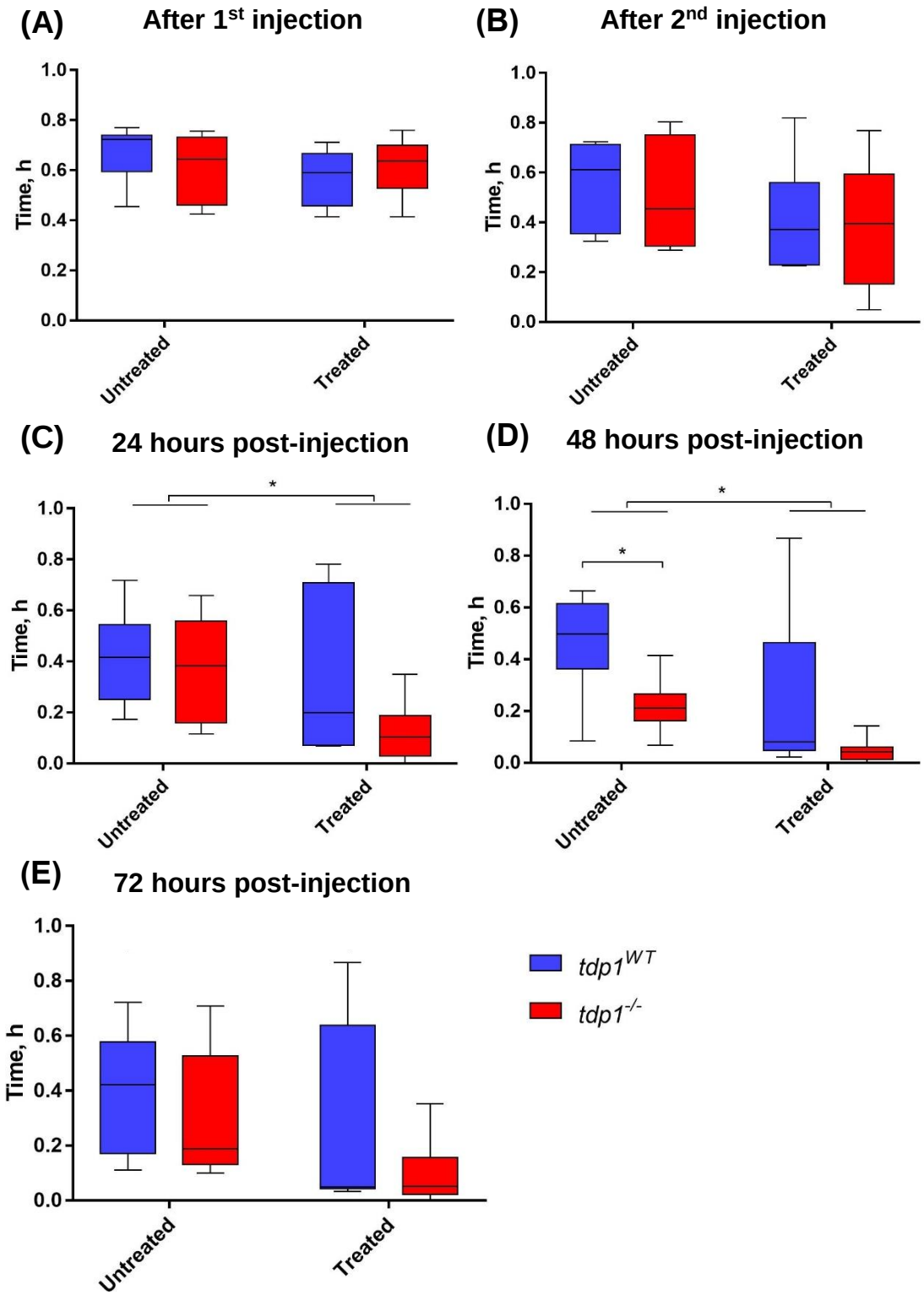

Figure 4.14. Medium speed duration in *tdp1*$^{-/-}$ fish and their wild-type siblings after topotecan treatment. 27-month old zebrafish were intraperitoneally injected with 22.5 mg/kg topotecan on two consecutive days for a final concentration of 45 mg/kg (section 2.3.6), and monitored for 1,5 hours using a camera system (section 2.6.2) after each injection **(A, B)**, then 24 **(C)**, 48 **(D)** and 72 **(E)** hours after the second injection. Medium speed (30 – 60 mm/s) duration was plotted with whiskers representing the minimum and maximum of all data points and the dot denoting the mean. N=7 for treated and untreated *tdp1*^{WT}, and untreated *tdp1*$^{-/-}$, n=8 for treated *tdp1*$^{-/-}$ (except for final time-point, where n=6 due to two fish expiring). *p* values were calculated using a two-way ANOVA with Sidak's post-hoc analysis for multiple comparisons.

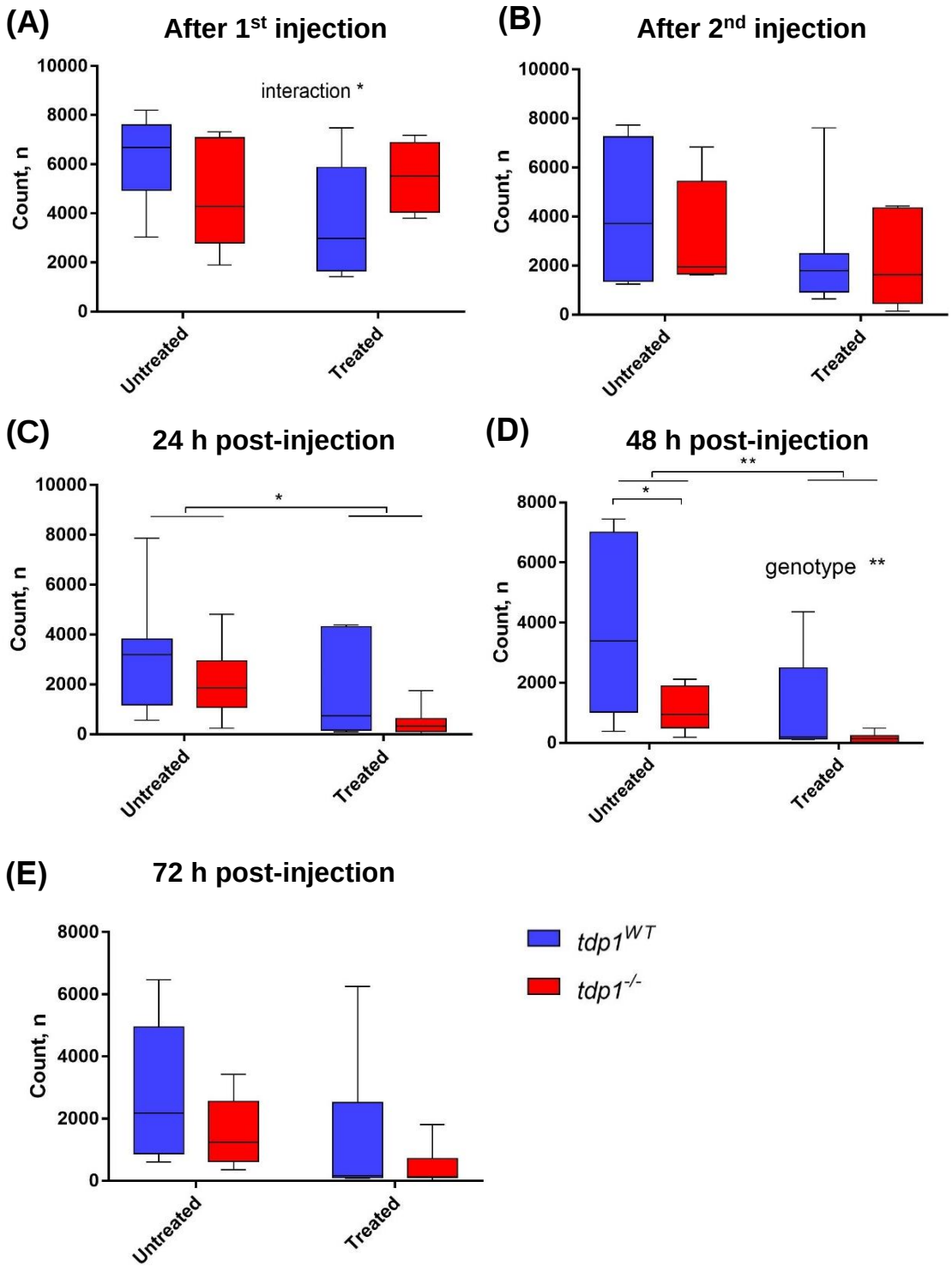

Figure 4.15. High speed count in *tdp1*$^{-/-}$ fish and their wild-type siblings after topotecan treatment. 27-month old zebrafish were intraperitoneally injected with 22.5 mg/kg topotecan on two consecutive days for a final concentration of 45 mg/kg (section 2.3.6), and monitored for 1,5 hours using a camera system (section 2.6.2) after each injection **(A, B)**, then 24 **(C)**, 48 **(D)** and 72 **(E)** hours after the second injection. Total number of times high speed (>60 mm/s) was initiated was plotted with whiskers representing the minimum and maximum of all data points. N=7 for treated and untreated *tdp1*^{WT}, and untreated *tdp1*$^{-/-}$, n=8 for treated *tdp1*$^{-/-}$ (except for final time-point, where n=6 due to two fish expiring). *p* values were calculated using a two-way ANOVA with Sidak's post-hoc analysis for multiple comparisons.

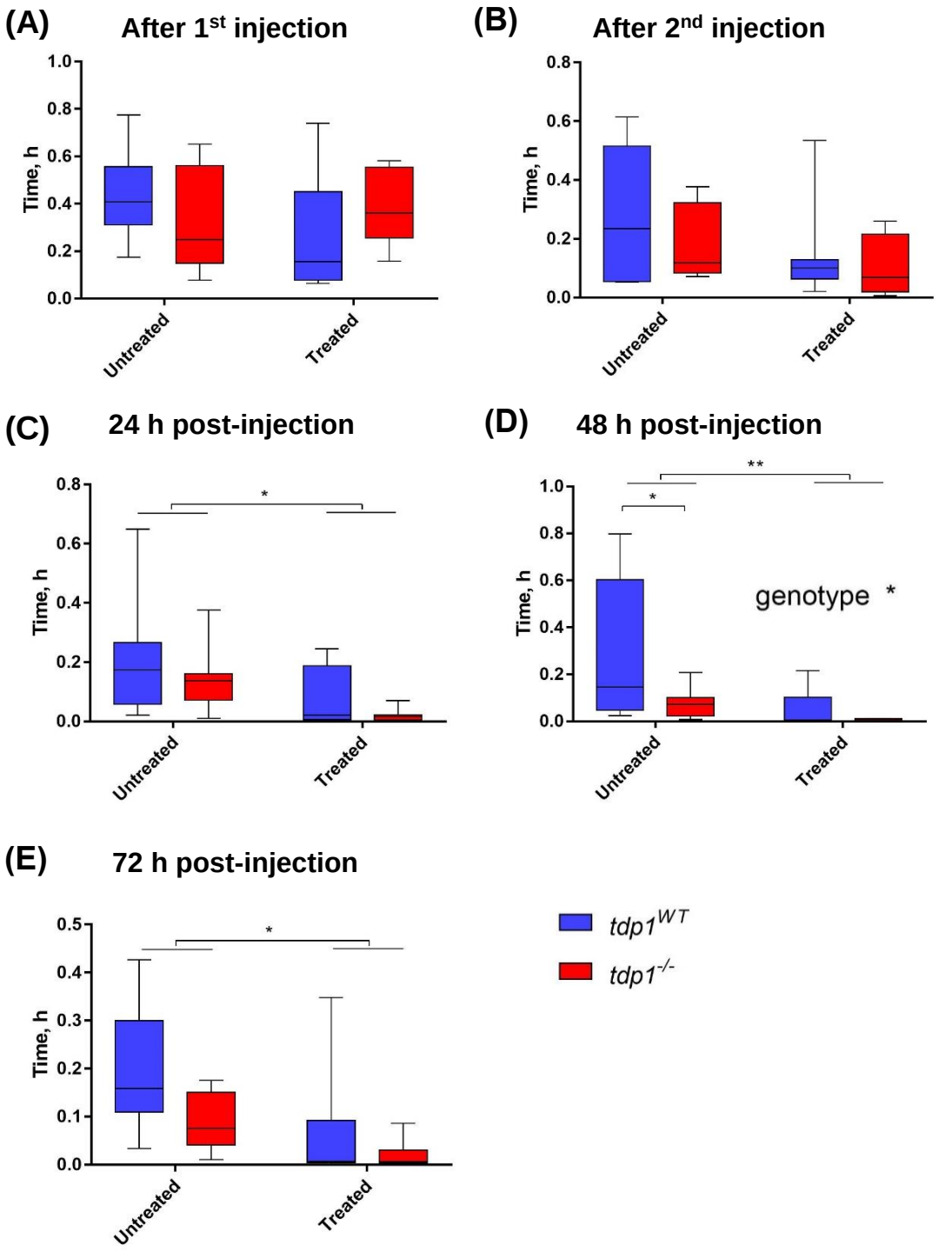

Figure 4.16. High speed duration in *tdp1*$^{-/-}$ fish and their wild-type siblings after topotecan treatment. 27-month old zebrafish were intraperitoneally injected with 22.5 mg/kg topotecan on two consecutive days for a final concentration of 45 mg/kg (section 2.3.6), and monitored for 1,5 hours using a camera system (section 2.6.2) after each injection **(A, B)**, then 24 **(C)**, 48 **(D)** and 72 **(E)** hours after the second injection. Total number of times high speed was initiated (>60 mm/s) was plotted with whiskers representing the minimum and maximum of all data points. N=7 for treated and untreated *tdp1*^{WT}, and untreated *tdp1*$^{-/-}$, n=8 for treated *tdp1*$^{-/-}$ (except for final time-point, where n=6 due to two fish expiring). *p* values were calculated using a two-way ANOVA with Sidak's post-hoc analysis for multiple comparisons.

distance moved **(figure 4.9D)**, average speed **(figure 4.10D)**, medium **(figure 4.13D, 4.14D)** and high **(figure 4.15D, 4.16D)** speed count and duration, and a significant increase in low speed duration in the untreated *tdp1*$^{-/-}$ fish in relation to untreated *tdp1*^{WT} fish at 48 hours post-injection **(figure 4.12D)**. The two-way ANOVA also showed a significant interaction between genotype and topotecan treatment when low speed duration was measured at 48 hours post-injection **(figure 4.12D)** and high speed count **(figure 4.15A)** was measured after the first injection. An overall trend of a reduction in the total distance travelled, average speed, low speed count, medium and high speed duration and count, and an increase in low speed duration was observed in *tdp1*$^{-/-}$ fish in relation to *tdp1*^{wt} fish after treatment. No overall significant differences between treated and untreated animals were observed straight after the first or the second injection.

4.3. Discussion

Following on from the previous chapter, which characterized *tdp1*$^{-/-}$ zebrafish mostly at a molecular level, my results here focus on the phenotype at the level of the entire organism. *Tdp1*$^{-/-}$ larvae did not show any behavioural deficiencies in relation to their *tdp1*$^{-/+}$ siblings when untreated and the effect of CPT was observed in both genotypes equally, consistent with my hypothesis that compensatory pathways are active in the embryonic zebrafish. When adult zebrafish were examined over a time course from 14 to 24 months, however, there appeared to be some differences from their wild-type siblings. An overall trend of mildly decreased locomotion in *tdp1*$^{-/-}$ zebrafish was observed across all tested parameters in most time-points. Statistically significant

differences were also found at some time-points in a few parameters, i.e. low speed count and medium speed duration and count.

These findings indicate a trend of very mild neurological deficiency resulting from loss of Tdp1, which could make it marginally more difficult to swim at speeds and distances comparable to wild-type fish. There did not seem to be a progressive neurodegenerative trend from the obtained results, as in such a case the locomotion gap between *tdp1*^{WT} and *tdp1*$^{-/-}$ animals would have been expected to increase over time and this was not observed. However, for such mild phenotypes the notorious variability of animal behaviour may be masking the effect and thus higher sample sizes are required to confirm the trend at all time-points. Notably, Hawkins *et al.* did not observe any behavioural abnormalities in *Tdp1*$^{-/-}$ mice, but their analysis only extended to 12 months of age and the animal number was very low compared to my experiments (Hawkins et al., 2009).

Physical exertion in the swim tunnel or vestibular disorientation using the drop test, on the other hand, did not exacerbate this phenotype enough to show any significant differences with the lower number of fish tested. In addition, the swim tunnel was performed on relatively young, 19 month-old animals and therefore in the future could be repeated with higher numbers of older fish.

A non-statistically significant trend of reduced locomotion in topotecan-treated *tdp1*$^{-/-}$ fish in comparison with treated *tdp1*^{WT} fish was observed across all three time-points after the final injection. Interestingly, significant reduction in movement across multiple parameters was observed in untreated *tdp1*$^{-/-}$ fish at the 48 hour

time-point and overall significant differences between genotypes were observed at the same time-point in three out of eight parameters, as well as at the 24 hour time-point in one parameter. Unless the additional three months of age have elicited a stronger locomotor phenotype in these fish, the time-course behaviour experiment suggests that it is a coincidence to see a statistically significant phenotype with a much smaller fish number. Moreover, the fact this was only observed in two of the drug treatment time-points at the same age corroborates the idea that these results were observed by chance. Statistically, the addition of treatment does not increase the gap between the locomotion of *tdp1*^{WT} and *tdp1*$^{-/-}$ fish, as expected, and in the one parameter where the interaction between genotype and treatment was revealed, it actually seems to reduce the gap. The interaction observed in the high speed count data after the first injection is also likely an artefact, as it appears that treatment has not started working by this time.

Finally, there was an overall trend of increasingly reduced movement in all DMSO treated animals during the time-course of the procedure. It may be attributed to the amended feeding times due to the injection and behaviour analysis procedure, and is not relevant for the purposes of this experiment (Blanco-Vives and Sánchez-Vázquez, 2009). Although not statistically significant, the apparently greater reduction in locomotor capacity in *tdp1*$^{-/-}$ fish is consistent with the hypersensitivity to topotecan and irinotecan found in adult *Tdp1*$^{-/-}$ mice (Hirano et al., 2007; Katyal et al., 2007). If the trend can be confirmed by using higher numbers of animals it would suggest that, at least in zebrafish, compensatory pathways available in the embryonic stages that can fully cope with a high Top1-CC load are no longer available in

adulthood. Perhaps differentiation of cells restricts the pathway choice in some tissues, making them highly vulnerable to loss of Tdp1 combined with increased Top1-CCs. It would thus be of high interest to uncover the repair pathways responsible, as discussed in the previous chapter.

5

Attempts to Generate a Humanized SCAN1 Zebrafish Model

5.1. Introduction

Spinocerebellar ataxia with axonal neuropathy 1 (SCAN1), as discussed in section 1.5.1, is a progressive neurodegenerative disease, which primarily affects the cerebellum and peripheral nerves (Takashima et al., 2002). SCAN1 is caused by an autosomal recessive *TDP1*$^{H493R/H493R}$ mutation in the active site, which reduces TDP1 activity and traps it on DNA (Hirano et al., 2007; Interthal et al., 2005b). It is thought that both unrepaired TOP1-CCs and TDP1-DNA intermediates lead to the neurological pathology observed in SCAN1.

There are a few theories as to why these lesions predominantly affect the nervous system. Firstly, the human brain consumes approximately 20 % of all inhaled oxygen and has low levels of antioxidant activity, leading to increased oxidative stress (Barzilai et al., 2002; El-Khamisy and Caldecott, 2006). Oxidative stress traps TOP1 on DNA (Alagoz et al., 2013; El-Khamisy, 2011; Katyal et al., 2007; Katyal et al., 2014; Pourquier and Pommier, 2001) and also leads to other lesions that may require TDP1-mediated repair. In addition, post-mitotic neurons require high levels of transcription (Flangas and Bowman, 1970; Sarkander and Dulce, 1978; Sarkander and Uthoff, 1976), which could increase collision between unrepaired PDBs and RNA polymerases and in turn compromise transcription (El-Khamisy and Caldecott, 2006). The lack of cancer predisposition in SCAN1 suggests that other DNA repair pathways, such as homologous recombination (HR), are capable of compensating for aberrant TDP1 activity in cycling cells (Ashour et al., 2015; El-Khamisy and Caldecott, 2006). In non-dividing cells, such as post-mitotic neurons, HR is not accessible due to the lack of a homologous sister chromatid. Finally, neurons have less regenerative capacity

to produce new cells than other terminally differentiated tissues, such as myocytes and adipocytes, which makes CNS tissues more susceptible to degeneration and potential apoptosis (Nouspikel and Hanawalt, 2002; Vierck et al., 2000; Yan, 2017).

To date, there is no appropriate animal model of SCAN1. Three separate groups have generated *Tdp1*$^{-/-}$ mouse models, only one of which displayed mild cerebellar degeneration (Hawkins et al., 2009; Hirano et al., 2007; Katyal et al., 2007). Similarly, the *tdp1*$^{-/-}$ zebrafish which I generated and described in chapter 3 shows no ataxia or cerebellar abnormalities. This is most likely the case due to the unique nature of the *TDP1*$^{H493R/H493R}$ mutation, which does not result in a simple loss of function as seen in *tdp1*$^{-/-}$ animals (Hirano et al., 2007; Interthal et al., 2005b). Therefore, a model, harbouring a *TDP1*^{H493R} transgene in a *tdp1*$^{-/-}$ background is necessary to facilitate the investigation of SCAN1 pathology.

5.2. Results

5.2.1. Generation of SCAN1 transgenic zebrafish

I aimed to generate two transgenic zebrafish lines ubiquitously expressing human TDP1 and TDP1^{H493R}. As the H493R mutation in *TDP1* is toxic (Interthal et al., 2005b; Miao et al., 2006) and its effect in zebrafish cannot be predicted, conditional transgene constructs were generated harbouring a BFP-tagged stop-cassette flanked by loxP sites prior to the transgene (**figure 5.1.**) (for further details on the experimental protocol and materials used please refer to **section 2.4.2.)**. With this construct Cre recombinase could be used to cut the stop-cassette out when required and avoid creating inviable transgenic lines. The ubiquitin promoter was chosen for

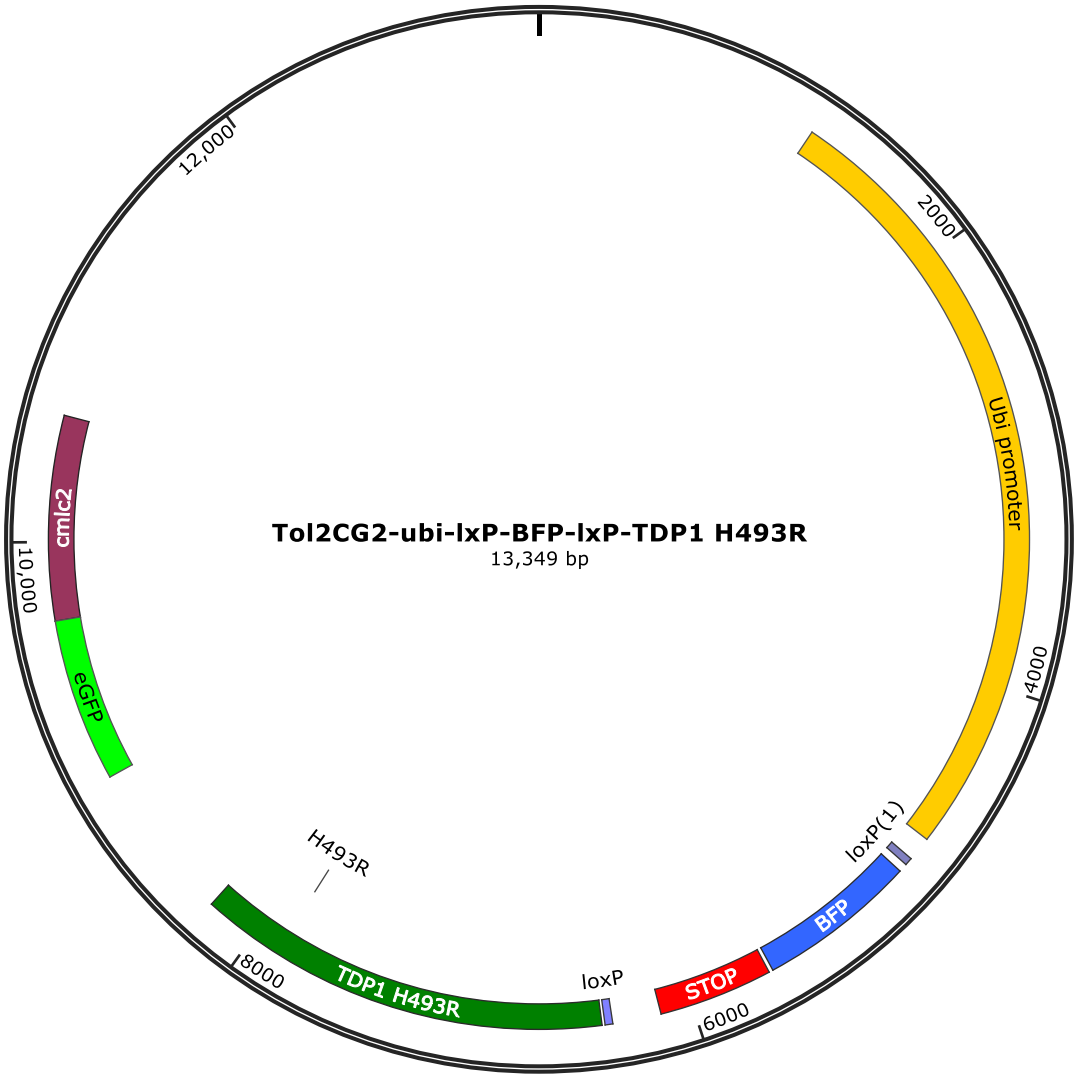

Figure 5.1. Structure of the transgene construct. The final transgene construct contains a ubiquitin promoter, a loxP site-flanked BFP-β-globin terminator cassette, the transgene of interest (in this case, TDP1^{H493R}) and a *cmlc2*:eGFP fusion.

the global expression of genes under its control. The destination vector pDestTol2CG2 was chosen for the early (24 hpf) expression of GFP in the heart as a marker for transgene integration.

First, *TDP1* and *TDP1*^{H493R} were cloned into the multiple cloning site (MCS) of the 3'-entry vector p3E-lxP-*mCherry*pA to replace the *mCherry* and generate p3E-lxP-*TDP1*pA and p3E-lxP-*TDP1*^{H493R}pA constructs. Multi-gateway cloning was then used to integrate the 5'-entry, middle-entry and 3'-entry vectors within the pDestTol2CG2 destination vector to generate: pDestTol2CG2-ubi-lxP-*BFP*-lxP-*TDP1* and pDestTol2CG2-ubi-lxP-BFP-lxP-*TDP1*^{H493R} **(figure 5.2)**.

A range of volumes (0.5 – 2.5 nl) of 50 ng/µL pDestTol2CG2-ubi-lxP-BFP-lxP-transgene construct and 50 ng/µL Tol2 transposase mRNA injection solution were injected into one-cell stage embryos from a *tdp1*$^{SH475/SH476}$ incross for transposase-dependent transgene integration into the genome. At 24 hours post-injection embryos were sorted for GFP expression in the heart (*cmlc2*:EGFP) and at 48 hours post-injection for ubiquitous mosaic BFP expression **(figure 5.3)** The embryos with the highest levels of BFP expression were raised (G_0 generation) and, once mature, outcrossed to *tdp1*$^{-/-}$ fish and selected for green-heart to generate the F_1 generation.

The F_1 fish were then outcrossed to *tdp1*$^{-/+}$ fish and half of the embryos were injected with Cre mRNA to remove the BFP-STOP cassette, allowing expression of *hs*TDP1. *Cre* mRNA was tested separately on embryos from a Ubi-lxP-GFP-STOP-lxP-mCherry line (Roehl lab) and nacre incross, where all injected embryos lost GFP and gained mCherry expression. After Cre mRNA injection the F_1 x *tdp1*$^{-/+}$ cross was selected for green heart at 24 hpf. It was intended to select the fish for loss of BFP at 48 hpf to

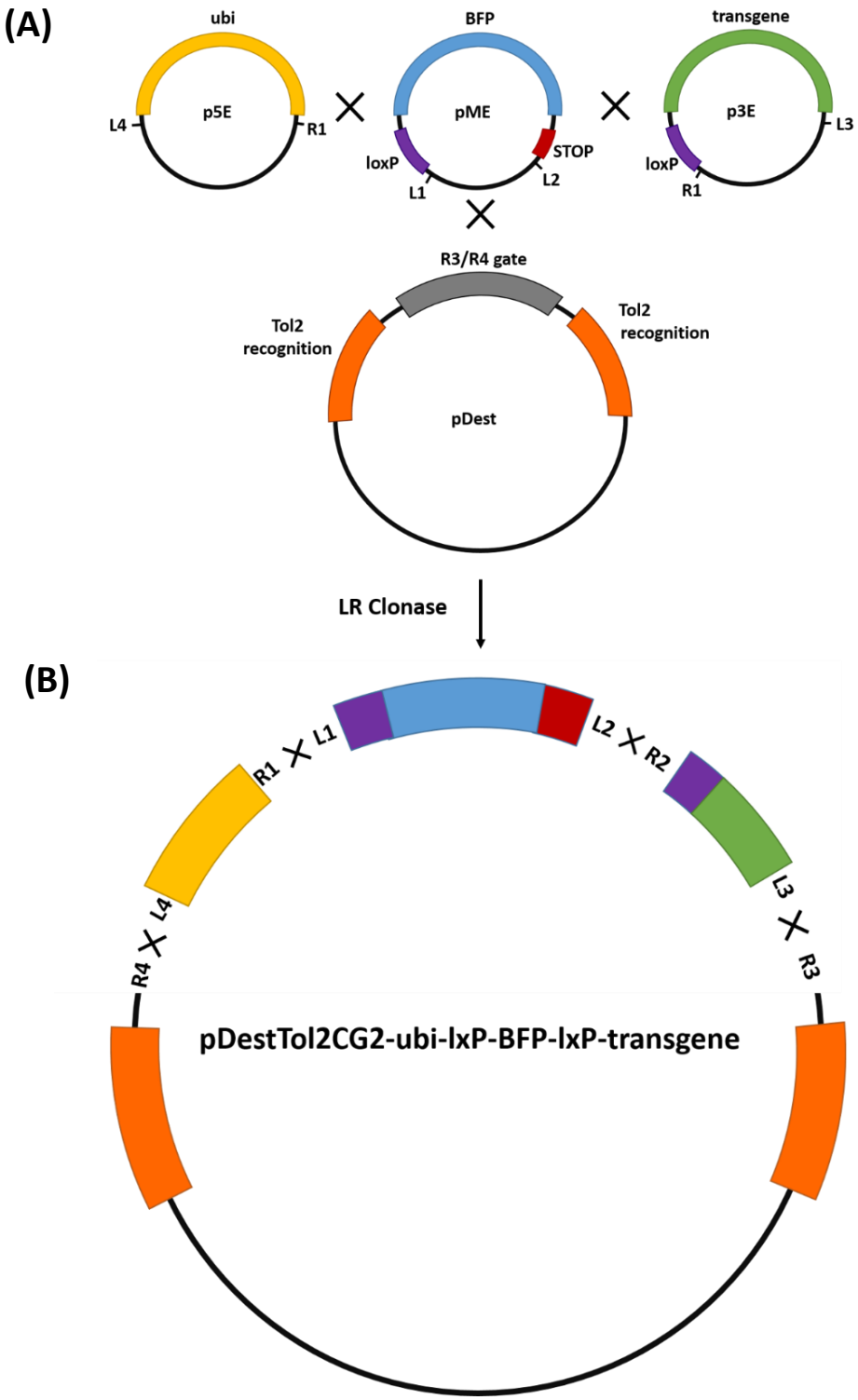

Figure 5.2. Schematic diagram of multi-gateway cloning. Sequence lengths are not to scale. **(A)** Schematic representation of the structure of the 5'-entry (p5E), middle-entry (pME) and 3'-entry (p3E) vectors, and the destination vector (pDest). **(B)** The final product of multi-gateway cloning, showing which attL and attR sites recombine.

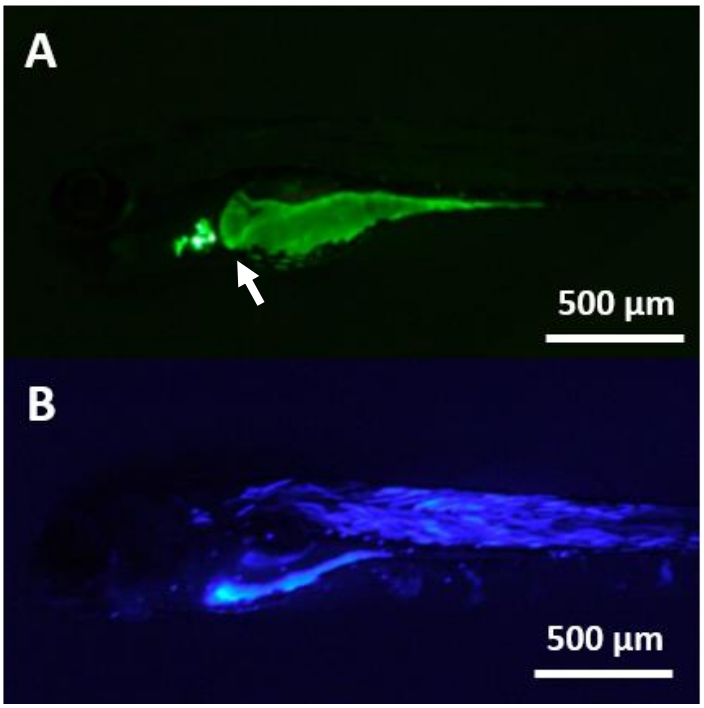

Figure 5.3. Determination of transgene injection efficiency. (A) At 24 hours post-injection embryos were selected for GFP expression in the heart under the *cmlc2* promoter (white arrow). **(B)** At 48 hours post-injection embryos were selected for strong BFP expression under the *ubi* promoter.

determine successful Cre injection, however, the BFP signal was too faint for selection. Instead, the embryos were raised to 5 dpf and subjected to immunoblotting with anti-*hs*TDP1 antibody, which does not recognize zebrafish Tdp1 **(figure 5.4)**. Treatment with Cre mRNA did not induce transgenic *hsTDP1* expression as expected, suggesting problems with expression of the whole transgenic construct, not just BFP. Further G_0 and F_1 fish were then outcrossed to *tdp1*$^{-/-}$ fish to screen for BFP expression, and although many fish were transmitting *cmlc*2:EGFP, only very few of those also expressed BFP at very low levels.

An outcross of one fish from the F_1 did produce many BFP-expressing embryos, however a repeat of this cross did not yield a single BFP-positive embryo. The transmission rate of BFP expression from the F_1 was too low and too sporadic for successful Cre mRNA treatment, therefore the few BFP-positive embryos were raised to adulthood to create the F_2 generation, which should stably express BFP. They were outcrossed to *tdp1*$^{-/-}$ fish again, but BFP expression was lost in the progeny. To test whether the GFP-positive, but BFP-negative embryos had BFP integration in their genomes, genomic DNA was extracted and a 155 bp internal BFP sequence was amplified **(figure 5.5)**. BFP integration was present in both BFP-positive and BFP-negative embryos, suggesting the transgene construct integration was successful, but failed to express.

5.3. Discussion

Unfortunately, my attempts to generate a SCAN1 zebrafish model have so far been unsuccessful due to problems with transgene expression and there was not enough time to repeat the experimental process and then characterize and age the fish, as

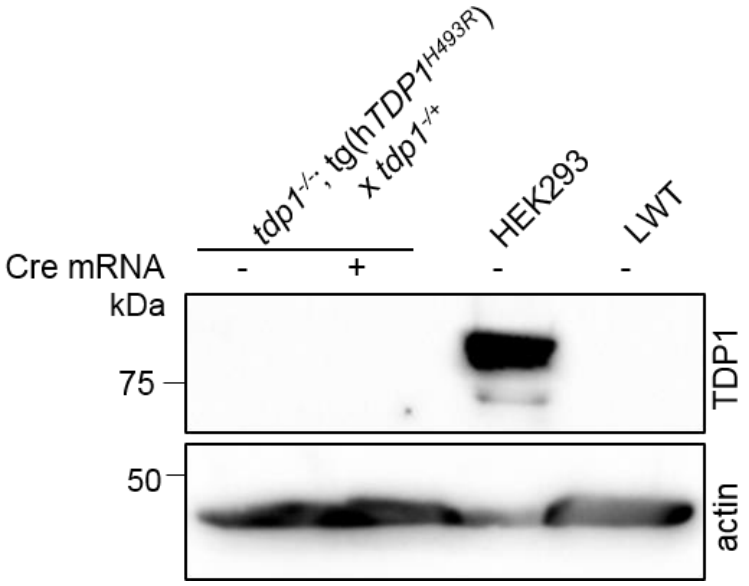

Figure 5.4. Cre-mediated removal of BFP-STOP cassette. Cre mRNA was injected into one-cell stage embryos, as described in section 2.4.2.6, then harvested at 5 dpf for western blotting (sections 2.9.1, 2.9.3 – 2.9.6). HEK293 cell lysate was used as a positive control for anti-TDP1 antibody, and lysate from LWT wild-type embryos was used to show that human TDP1 antibody does not recognize zebrafish tdp1.

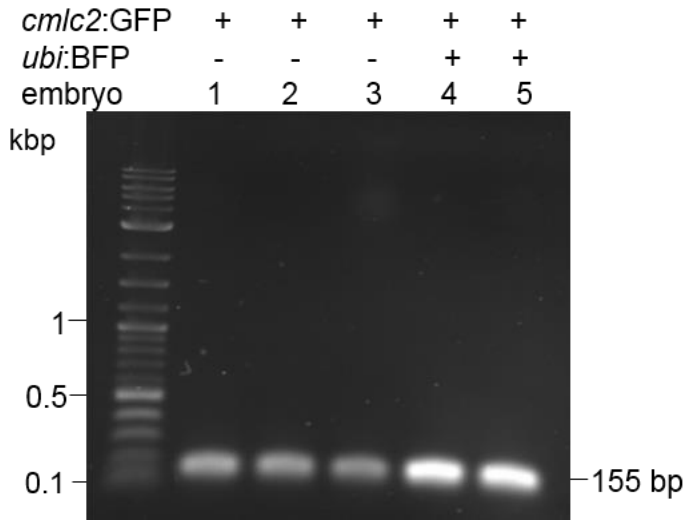

Figure 5.5. Troubleshooting: BFP sequence has been integrated, but not expressed. Genomic DNA was extracted from 48 hpf embryos, expressing GFP in the heart with or without ubiquitous BFP expression, and a 155 bp fragment of the BFP sequence was amplified by PCR (section 2.2.11) and subjected to agarose gel electrophoresis (section 2.2.3).

required to model a progressive disease. The integration of the transgenic construct was successful, as confirmed by GFP expression in the heart and successful amplification of the BFP fragment from genomic DNA, yet BFP expression was not maintained through generations. Even when those few fish that did express were raised and outcrossed, their progeny did not express BFP. Removing the BFP-STOP cassette with Cre also did not promote expression of the transgene and thus it was concluded that the expression of the whole transgenic construct was affected.

The zebrafish ubiquitin promoter chosen to drive expression of the transgenic construct has previously been shown to promote high levels of ubiquitous expression from embryo to adulthood when used with the Tol2 transposase system (Mosimann et al., 2011), and thus it is very likely that the transgene construct was transcriptionally silenced. This phenomenon has been observed using the UAS promoter in the Tol2 system, where methylation of the promoter leads to variegated transgene expression (Akitake et al., 2011). There are several explanations for why silencing could affect the ubi-BFP-STOP-TDP1 transgene. Mechanisms such as small RNAs, histone and DNA methylation, and chromosome organization can repress transcription (Girard and Hannon, 2008; Goll and Bestor, 2005; Heard and Bickmore, 2007; Strahl and Allis, 2000). It is not well understood what causes silencing of specific regions (Campos and Reinberg, 2009; Goll and Bestor, 2005), however, regions containing repetitive DNA, such as the long blocks (>1 kb) of similar sequences found in centromeres, or short tandem repeats (<100 bp) are more susceptible (Gopalakrishnan et al., 2009; Jones, 2012; Koo et al., 2011). If the transposon lands in such a region in the zebrafish genome it may also be repressed.

In this case the strong *cmlc2* promoter (Huang et al., 2003) may resist silencing, whereas the transgene-driving ubiquitin promoter may be more susceptible. On the other hand, Tol2 has been shown to preferentially integrate to open chromatin sites next to transcription start sites in human cells (Grabundzija et al., 2010), so among the 20 founders identified insertions in such regions should have been enriched.

Another possible explanation is that human TDP1 has zebrafish-specific methylation sites, which could result in silencing of normally transcriptionally active DNA. Alternatively, the very strong *cmlc2* promoter may actually repress the weaker transgene-driving ubiquitin promoter. Although the *cmlc2* promoter was placed in the opposite orientation to the main promoter with the aim of reducing such interference and the study published by the Chien group shows no interference between the *cmlc2* and *hsp70* promoter, it may be because the *hsp70* promoter is also very strong (Kwan et al., 2007).

Finally, it is possible that what I have observed is not *bona fide* transposon insertion, but insertion of the naked plasmid. In any transposase-dependent insertion, the *cmlc2*:GFP is in the same stretch of DNA as the main transgene. However, if the plasmid inserts without the help of Tol2, DNA is likely to be rearranged into concatamers, which might not only cause the main transgene to be lost, but are also more prone to methylation due to their repetitive nature (Kawakami, 2005). This explanation seems unlikely due to the relatively high frequency of green-heart founders (~26 %) amongst successfully injected batches in comparison to the rate of founders after plasmid-only injection (~5 – 8 %). Silenced transgenes can be reactivated in fish with hypomethylated genomes and then suppressed again in later

generations (Goll et al., 2009). This could possibly explain why we observed several BFP-positive embryos, the progeny of which did not express BFP anymore.

To circumvent the silencing of the transgene in the future one could try using a different promoter to ubiquitin, such as the ubiquitous beta-actin promoter (Burket et al., 2008) or the neuronal HuC promoter (Park et al., 2000). Zebrafish *tdp1* could be used instead of human *TDP1*, however, as a zebrafish anti-Tdp1 antibody has not been generated, the human version would be more practical for future experiments, unless zebrafish tdp1 was tagged. Finally, either a different transgene reporter to *cmlc2*:GFP could be used, or no such a reporter at all. If no reporter is used, TDP1 would require tagging with a fluorescent marker. To avoid common problems associated with large protein tags like GFP, such as changes in folding, function or localization, self-cleaving fluorescent tags could be exploited (Kim et al., 2011). Alternatively, a different transgenic approach altogether could be used, such as the I-sceI endonuclease method, discussed in section **1.6.3.4.**

To summarize, in this chapter I have described why a SCAN1 animal model would be invaluable and described my attempts to generate a zebrafish SCAN1 model. I have listed the possible reasons for the problems I encountered and suggestions to overcome these problems if this were to be repeated in the future.

6

Generation and characterization of other protein-linked DNA break repair zebrafish models

6.1. Introduction

Although animal models with deficient protein-linked break repair have been generated (Barlow et al., 1996; Quek et al., 2017), including the *Tdp1*$^{-/-}$ mouse (Katyal et al., 2007) and *tdp1*$^{-/-}$ zebrafish, as described in chapter 3, they either do not recapitulate the phenotype sufficiently or are lethal. As the zebrafish is even less closely related to humans than mouse or rat and has a partially duplicated genome (Meyer and Van de Peer, 2005; Taylor et al., 2003; Taylor et al., 2001), knocking out single genes may not be enough to provoke a phenotype equivalent to that seen in humans. Fortunately, zebrafish has only a single *ATM* and *RNaseH2* orthologue. Because working with zebrafish offers many advantages over working with rodents, I have generated two other protein-linked break repair-related mutations and crossed them to the *tdp1*$^{-/-}$ fish to generate double knockouts. In addition, my collaborators and I have crossed the *tdp1*$^{-/-}$ fish with transgenic fish, carrying genes implicated in PDB repair and neurodegeneration.

6.1.1. Other genes implicated in PDB repair and neurodegeneration

6.1.1.1. Ataxia Telangiectasia Mutated

As a master DDR regulator, ATM is also implicated in the repair and prevention of TOP1-CCs (Alagoz et al., 2013; Katyal et al., 2014; Lin et al., 2008; Sordet et al., 2009; Walker et al., 2017). It has been demonstrated that neural *Atm*$^{-/-}$ cells have increased levels of these PDBs primarily due to increased oxidative stress and that these breaks contribute to the neuropathology of ataxia telangiectasia (A-T) by interfering with transcription (Alagoz et al., 2013). ATM also repairs these breaks both in the developing and mature nervous systems (Katyal et al., 2014). Recent evidence also

suggests that ATM promotes the resolution of R-loops, the accumulation of which leads to increased TOP1-CC (Tresini et al., 2015; Walker et al., 2017). It thus comes as no surprise when the most striking neurological manifestation of both A-T and SCAN1 is cerebellar degeneration. These findings identify a role for ATM in both formation and resolution of TOP1-CC, which is independent of TDP1. A mechanism for this role of ATM could be the promotion of proteosomal degradation of TOP1-CCs (Barker et al., 2005; Lin et al., 2008; Maskey et al., 2017; Stingele et al., 2014), quenching of ROS (Bhuller et al., 2017; Ito et al., 2004), R-loop resolution (Tresini et al., 2015; Walker et al., 2017) and/or transcription inhibition (Kruhlak et al., 2007). Indeed, there is evidence for ATM involvement in proteasomal degradation of factors other than TOP1 (McKerlie et al., 2012; Wood et al., 2011b).

Despite the accumulation of TOP1-CCs in their neural cells, *Atm*$^{-/-}$ rodent models show only very subtle neuropathology and no cerebellar degeneration (Barlow et al., 1996; Quek et al., 2017). It has been suggested that a certain DNA damage threshold may need to be passed in order for pathology to appear in neurons (Katyal et al., 2014), which might explain the minor neuronal phenotype in *Atm*$^{-/-}$ and *Tdp1*$^{-/-}$ rodent models as compared to humans. As it has been demonstrated that ATM and TDP1 repair TOP1-CCs in independently of one another (Alagoz et al., 2013; Katyal et al., 2014), depleting cells of both of these factors should result in a compound phenotype. As expected, 90 % of *Atm*$^{-/-}$*; Tdp1*$^{-/-}$ mutant mice are embryonic lethal at stages E13.5 – E16.5, which is due to neuropathology (Katyal et al., 2014). If this was the case in zebrafish, it would have granted us the ability to easily study the stages before embryonic lethality due to its external development. However, if it is not the

case, I would possess a new viable model to interrogate the mechanisms of how these toxic lesions give rise to neurodegeneration.

6.1.1.2. Ribonuclease H2

Ribonuclease H2 (RNase H2) is an RNA/DNA hybrid processing protein complex in the RNase H family. While the rest of the RNase H family can only process R-loops (stretches of RNA/DNA hybrid), RNase H2 can also process single ribonucleotides incorporated into the DNA. This function is essential for the maintenance of mammalian genomic integrity and viability, as accidental incorporation of ribonucleotides into DNA makes it susceptible to hydrolysis (Hiller et al., 2012; Reijns et al., 2012). Coincidentally, mutations in RNase H2 cause neuroinflammatory Aicardi-Goutières Syndrome (AGS), which affects newborns and infants, and is fatal (Rabe, 2013). The molecular mechanisms underlying the syndrome are not really known. However, studies of RNase H2 and other AGS-related genes suggest that the increased presence of ribonucleotides in DNA promotes DNA instability, leading to the accumulation of free intracellular nucleic acids and an inappropriate immune response against them. (Crow and Rehwinkel, 2009; Rice et al., 2014; Stetson et al., 2008).

In eukaryotes, RNase H2 is a protein complex, which contains 3 subunits: the catalytic subunit RNase H2a, and 2 accessory subunits RNase H2b and RNase H2c. The accessory subunits are thought to facilitate the docking of interacting proteins and aid complex assembly (Reijns et al., 2011; Shaban et al., 2010). All of the proteins in the complex are encoded by 3 distinct genes.

Rnaseh2b and *Rnaseh2c* knockout mice are not viable: *Rnaseh2b* null mice have a terminal phenotype at E11.5 stage (Reijns et al., 2012) and *Rnaseh2*c mice die approximately at E9.5 stage (Hiller et al., 2012). This data demonstrates that ribonucleotide removal is essential in mammalian development. In fact to this date, it was thought to only be non-essential in unicellular organisms, such as *S. cerevisiae* (Huang et al., 2017; Nick McElhinny et al., 2010).

The reason Rnase H2 was targeted in the zebrafish, is because it has been demonstrated that TOP1 repairs single genomic ribonucleotides in the absence of RNase H2 (Huang et al., 2017), thus generating more TOP1-CC. The role of TDP1 in DNA repair involves processing TOP1-CC and other 3' lesions, such as 3'-phosphoglycolate and 3'-dRP termini (Davies et al., 2002; Interthal et al., 2005a; Lebedeva et al., 2011; Murai et al., 2012; Zhou et al., 2009). However, it is difficult to dissect away these roles, therefore modulating RNase H2 offers a worthy approach to physiologically increase Top1-CC and then examine the need for Tdp1.

To determine the contribution of TDP1 in the repair of non TOP1-mediated lesions, I attempted to generate a zebrafish model in which *top1* is deleted, so that additional deletion of *tdp1* would reveal the function of Tdp1 in the repair of non Top1-mediated lesions. Unfortunately, generating a full *top1* knockout zebrafish would have been very difficult due to the zebrafish harbouring 4 copies of the *top1* gene (*top1*, *top1*l, *zgc:173742* and *top1mt*). An alternative approach is to increase the demand for Top1-CC repair by generating an *rnaseh2* knockout, an organism with increased Top1-CCs and genomic instability (Huang et al., 2016).

6.1.1.3. Genetic factors in Amyotrophic Lateral Sclerosis

Amyotrophic lateral sclerosis is a fatal neurodegenerative disease, which results in the death of motor neurons and, consequently, paralysis of the muscles they innervate (Bruijn et al., 2004). Protein aggregates have been found in the neurons of familial ALS (fALS) patients and they have also been implicated in the pathogenicity of other neurodegenerative diseases, such as Parkinson's, Huntington's and Alzheimer's (Steffan et al., 2001; Taylor et al., 2002). However it is thought that it is a secondary characteristic of the disease, and the actual cause is poorly understood. Although primarily a sporadic disease, with only 10 % of familial cases, studying the genetic causes has been crucial in unravelling its mechanisms (Bruijn et al., 2004). As mutations in SOD1 and hexanucleotide repeat expansions in the C9orf72 are the most common cause of fALS, these two genes have been studied extensively. In the process of studying the pathology of ALS, increasing evidence is being gathered to implicate mutant SOD1 and C9orf72 alleles in inducing DNA damage (Carroll et al., 2015; Lopez-Gonzalez et al., 2016), including TOP1-CC formation (Chiang et al., 2017; Walker et al., 2017).

6.1.1.4. Superoxide Dismutase 1

SOD1 is a eukaryotic copper/zinc superoxide dismutase, which protects the DNA by destroying superoxide radicals (Bruijn et al., 2004). It is mainly expressed in the cytosol, but can also be found in the nucleus, peroxisomes and mitochondrial intermembrane space (Okado-Matsumoto and Fridovich, 2001; Sturtz et al., 2001; Weisiger and Fridovich, 1973). SOD1 converts superoxide into hydrogen peroxide, which is then processed by catalase and glutathione peroxidase into water and

oxygen (Fridovich, 1986). Over 150 different point mutations throughout SOD1 have been implicated in fALS (http://alsod.iop.kcl.ac.uk/), which account for approximately 20 % of fALS cases. SOD1 knockout does not lead to a phenotype, which suggested that a toxic gain of function is responsible for the pathogenicity (Bruijn et al., 2004). Therefore $SOD1^{G93A}$ mutation has been studied extensively. The mutation destabilizes the structure of SOD1, leading it to misfold and aggregate in neurons (Chattopadhyay et al., 2008; Furukawa et al., 2008). SOD1 catalytic activity remains unaffected by the mutation (Cleveland, 1999). The exact mechanism of the mutant SOD1 pathogenicity is, however, unknown and the protein aggregates are deemed to be a secondary event. Transgenic mice, overexpressing human $SOD1^{G93A}$ showed ALS phenotypes, increased oxidative stress and ROS-induced DNA damage (Gurney et al., 1994; Robberecht, 2000; Tu et al., 1996). More recently a zebrafish $SOD1^{G93R}$ model was generated, which overexpresses the zebrafish $SOD1^{G93R}$ gene (Ramesh et al., 2010). This mutation is also often found in fALS patients as it affects the conserved glycine 93 (Elshafey et al., 1994). The overexpressing fish manifested the major phenotypes of ALS, including changes at the neuromuscular junction and increased fatigue in a swim tunnel test. At the end stage of the disease, fish showed motor neuron loss, consequent muscle atrophy, paralysis and premature death (Ramesh et al., 2010).

It has been demonstrated that oxidative stress in postmitotic neurons can lead to lesions that trap TOP1 (El-Khamisy, 2011; Katyal et al., 2007; Katyal et al., 2014; Pourquier and Pommier, 2001). This can impair transcription, lead to DSBs and promote apoptosis and senescence. Although it is known that TDP1 can protect cells against oxidative damage, it was unclear whether it was due to the repair of 3'-

oxidized DNA breaks or oxidative-damage induced TOP1-CCs. Recently, TDP1 was directly implicated in the repair of TOP1 lesions, caused by oxidative damage (Chiang et al., 2017).

6.1.1.5. C9orf72

Chromosome 9 open reading frame 72 (C9orf72) function is not yet fully characterized, but there is evidence to suggest it is a member of the DENN-like protein superfamily, and thus regulates membrane trafficking (Levine et al., 2013; Zhang et al., 2012). Recently this gene has gained a lot of attention due to its clinical significance. The C9orf72 gene noncoding region usually has 2 – 25 x GGGGCC repeats, which are non-pathogenic (Rutherford et al., 2012). However, C9orf72 nucleotide repeat expansions (NERs) larger than that are the most common genetic cause of ALS and frontotemporal dementia, and have also been implicated in other neurodegenerative diseases, such as Alzheimer's, multiple sclerosis, Huntington's and cerebellar ataxias (Schottlaender et al., 2015). Three potential mechanisms have been proposed to explain the pathogenicity of the NERs in C9orf72: loss of C9orf72 function, accumulation and aggregation of dipeptide repeat proteins and RNA repeat-expansion foci (Haeusler et al., 2016). Recently it was also demonstrated that the NERs in C9orf72 lead to increased TOP1-CCs, R-loops, DSBs and impair ATM-mediated DDR, thus elevating genomic instability (Walker et al., 2017).

6.2. Results

6.2.1. Generation and validation of *atm*$^{-/+}$ zebrafish

Atm deletion in the zebrafish was generated using the CRISPR/Cas9 system, as described in section 2.4.1. Guide RNA was *in vitro* transcribed from a DNA template

containing a target sequence for exon 6 of the zebrafish *atm* gene (**figure 6.1A, B**). In the G_0 generation, a founder transmitting multiple indels, including a 5 bp deletion (SH477, **figure 6.1C**) was detected. It results in a stop codon 18 amino acids downstream of the deletion and a predicted truncated protein of 273 a. a. (full length Atm - 3091 a. a., **figure 6.2D**). Such a large truncation is very likely to lead to nonsense mediated decay. However if it does not, it would still result in loss of all of the residues conserved across the phosphatidylinositol 3-kinase-like kinase (PIKK) family, namely FRAP/ATM/TRRAP (FAT), catalytic phosphatidylinositol 3-kinase-like (PI3K-like) and C-terminal FAT (FATC) domains (Guleria and Chandna, 2016; Jiang et al., 2006). In addition, the N-terminal leucine zipper and proline rich domains, which may be involved in correct cellular localization of ATM or protein-protein interactions, would also be lost (Chen et al., 2003a; Imamura and Kishi, 2005; Khalil et al., 2012; Morgan et al., 1997).

The founder was therefore outcrossed to a nacre fish to create the F_1 generation. The F_1 fish were finclipped and genomic DNA was extracted. Genomic DNA was sequenced, then one of the 5 bp deletion baring fish was outcrossed to LWT to create the F_2 of generation. The F_2 were genotyped for *atm*, and only $atm^{-/+}$ fish were kept.

6.2.2. Generation *of* $atm^{-/-}$ and $atm^{-/-}; tdp1^{-/-}$ zebrafish

$Atm^{-/+}$ F_2 zebrafish were crossed with $tdp1^{-/-}$ zebrafish to generate an F_3 generation of $atm^{-/+}; tdp1^{-/+}$. The F_3 fish were in turn incrossed to give rise to $atm^{-/-}$ and $atm^{-/-}; tdp1^{-/-}$ F_4 fish.

6.2.3. *Atm*$^{-/-}$ and *atm*$^{-/-}$; *tdp1*$^{-/-}$ zebrafish are viable

Progeny from *atm*$^{-/+}$; *tdp1*$^{-/+}$ incross were observed and genotyped at 5 dpf and 4 months of age. Genotyping revealed that the ratios of observed progeny genotypes did not differ significantly from the expected, both at 5 dpf and 4 months of age (**figure 6.2**). Nothing abnormal was noted in the embryonic stages. Because of time constraints, further characterization of *atm*$^{-/-}$ and *atm*$^{-/-}$; *tdp1*$^{-/-}$ fish has been carried out by Mirinda Tattan.

6.2.4. *Atm*$^{-/-}$ zebrafish are all males and may be infertile

Once the fish from an *atm*$^{-/+}$; *tdp1*$^{-/+}$ incross were sexually mature, it came to light that all 26 *atm*$^{-/-}$ fish were males (**figure 6.3**). Although sex determination in zebrafish is not dependent on a single chromosome like in most mammals and is not fully understood, it seems it can be influenced both genetically and environmentally (Nagabhushana and Mishra, 2016). Thus, if we assumed that this variability is comparable between sibling zebrafish raised in the same tank under the same conditions, a chi-squared test may be performed. As the rest of the genotypes from the *atm*$^{-/+}$; *tdp1*$^{-/+}$ incross had a 1.13:1 ratio of females to males (34 females and 30 males), it is possible to work out the expected number of females and males in the *atm*$^{-/-}$ mutants. The chi-squared test was performed and showed a significant difference between the expected and observed sexes.

In addition, 8 *atm*$^{-/-}$ and 7 *atm*$^{-/-}$; *tdp1*$^{-/-}$ male fish were pair-mated with nacre females, however not a single cross laid. On the other hand, their *atm*$^{-/+}$ and *tdp1*$^{-/-}$; *atm*$^{-/+}$ siblings were mated successfully multiple times, which suggests the *atm*$^{-/-}$ fish may be infertile. Further repeats of the experiment are required in parallel with

(A)

5'*AAAGCACCGACTCGGTGCCACTTTTTCAAGTTGATAACGGACTAGCCTTATTTTAAC TTGCTATTTCTAGCTCTAAAAC*GGTGTGTGGTCTGGGTGAGGCTATAGTGAGTCGTA TTACGC 3'

(B)

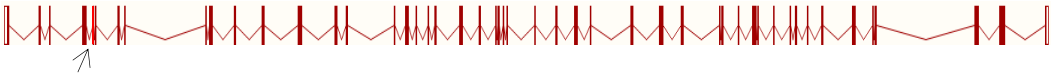

(C)

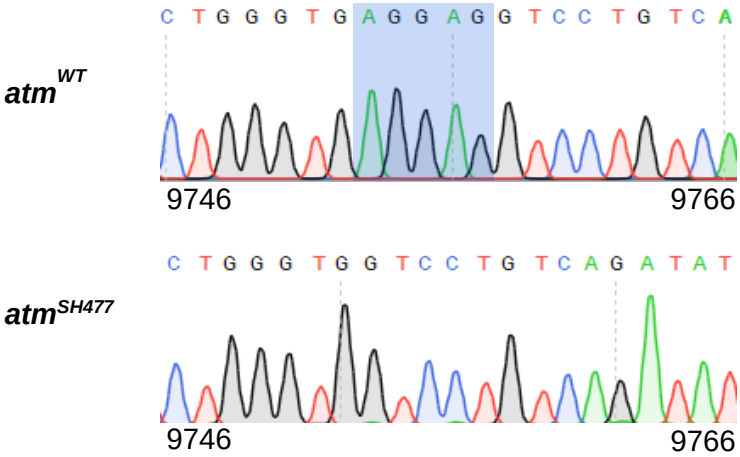

(D)

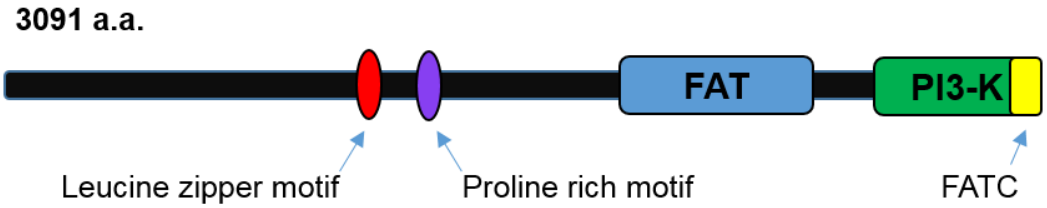

Figure 6.1. Generation and validation of *atm*$^{-/-}$ zebrafish with the CRISPR/Cas9 system. (A) Sequence of template ultramer used for *in vitro* synthesis of gRNA. Scaffolding sequence is indicated in purple, target sequence in green and T7 polymerase promoter in blue. **(B)** Intron-exon structure of the zebrafish *atm* gene (www.ensembl.org). Exon 6, indicated by the arrow, was targeted for Cas9 restriction. **(C)** Sequences of the target region in *atm*^{WT} and *atm*$^{-/-}$ zebrafish; numbers mark base position in *atm* genomic sequence. The 5 bp deletion, indicated by the light blue box, results in a frameshift and a stop codon 18 amino acids downstream of the deletion. The numbers denote base position in the genomic sequence of *atm*. **(D)** Protein sequence of zebrafish Atm; FAT – FRAP/ATM/TRRAP superfamily domain, PI3K-like – phosphatidylinositol 3-kinase-like domain, FATC – C-terminal FAT domain. Adapted from Imamura and Kishi (2005).

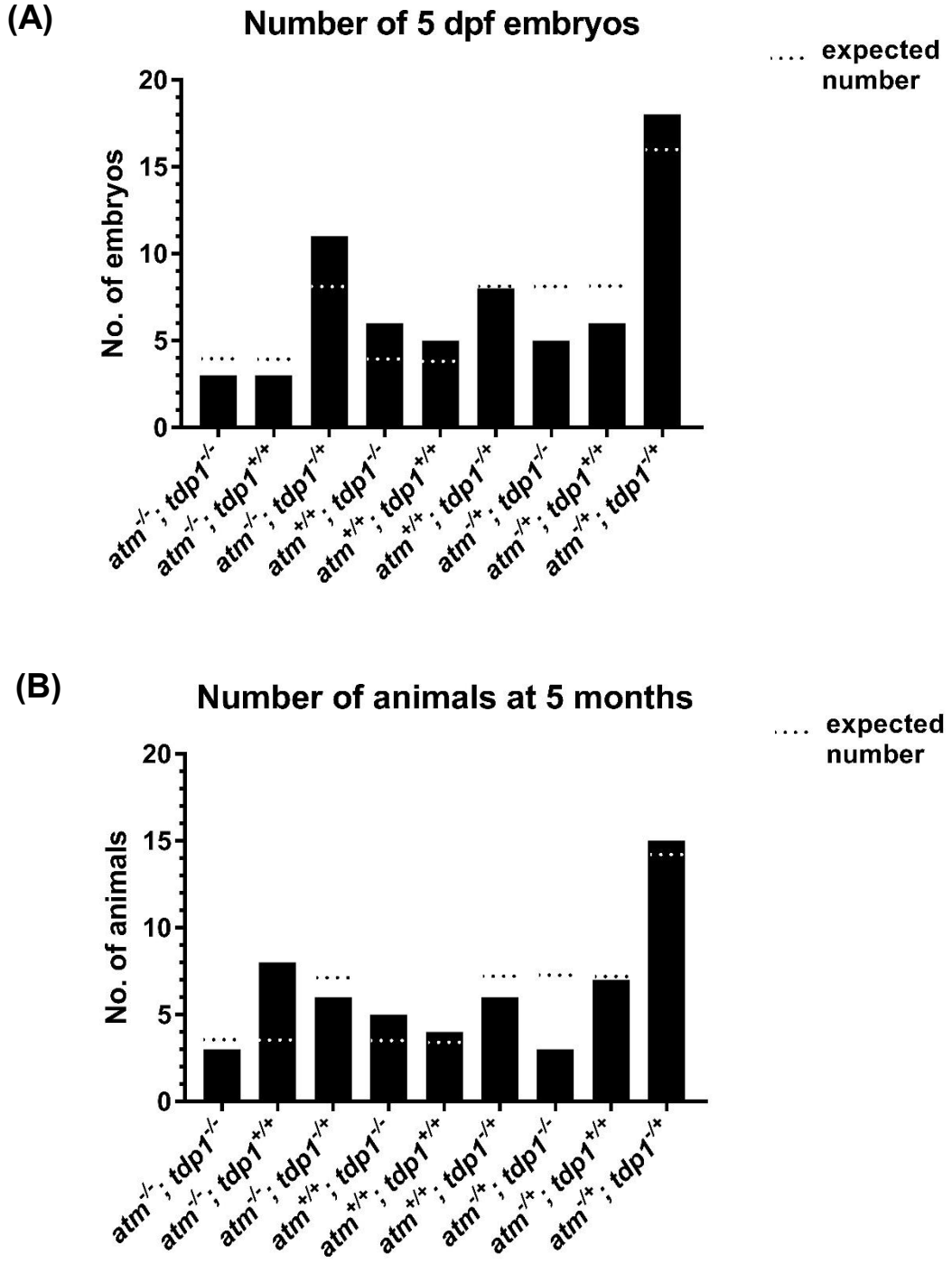

Figure 6.2. ***Atm*$^{-/-}$*; tdp1*$^{-/-}$ zebrafish are viable. (A)** *Atm*$^{-/+}$*; tdp1*$^{-/+}$ zebrafish were incrossed and genotyped at 5 dpf (n=65), then a chi-squared test was performed. Chi squared equals 0.25 with 2 degrees of freedom. The two-tailed P value equals 0.883. **(B)** *Atm*$^{-/+}$*; tdp1*$^{-/+}$ zebrafish were incrossed and genotyped at 5 months of age (n=57), then a chi-squared test was performed. Chi squared equals 9.035 with 8 degrees of freedom. The two-tailed P value equals 0.339.

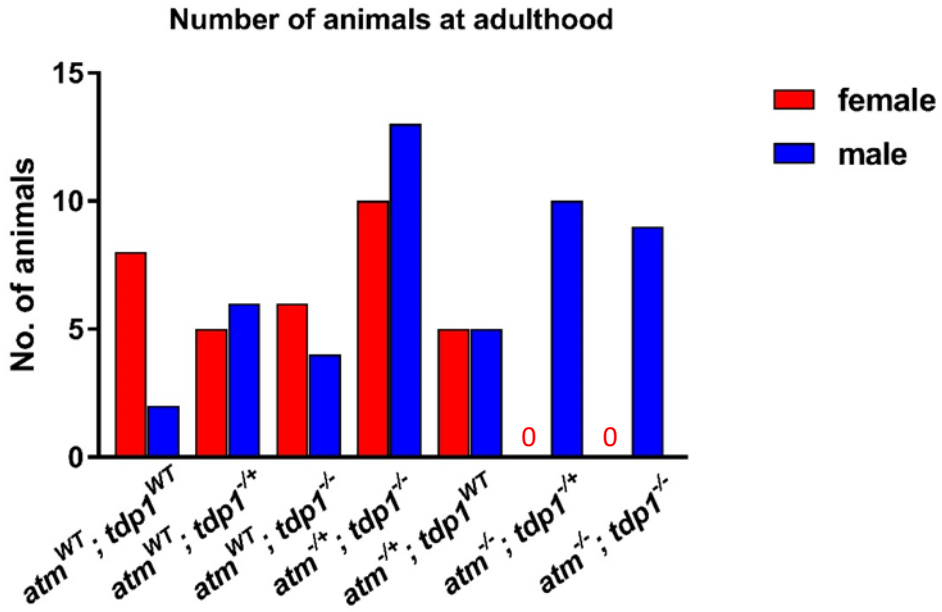

Figure 6.3. All observed *atm*$^{-/-}$ zebrafish are male. Zebrafish were raised from an *atm*$^{-/+}$; *tdp1*$^{-/+}$ incross, genotyped and sexed at adulthood. Sex ratio data not available for *atm*$^{-/+}$; *tdp1*$^{-/+}$ fish as they were not kept after genotyping. In *atm*^{WT} and *atm*$^{-/+}$ fish, the ratio of females to males was, on average, 1:0.89. In *atm*$^{-/-}$ zebrafish the observed number of females equals 0 and observed number of males equals 23. Applying the ratio observed in other genotypes, the expected number of females would equal 14 and expected number of males would equal 12. A chi-squared test was performed using these numbers. Chi squared equals 30.333 with 1 degrees of freedom. The two-tailed P value is less than 0.0001.

My thanks to Mirinda Tattan, a PhD student, who made these observations.

atm^{WT} and *atm*$^{-/+}$ siblings. However, if the results are confirmed, they would complement the existing data from *Atm*$^{-/-}$ mice and rats (Barlow et al., 1996; Quek et al., 2017).

6.2.5. *Atm*$^{-/+}$ and *atm*$^{-/-}$ embryos appear to be hypoactive in the dark

Photomotor response (PMR) analysis was performed in the ViewPoint Zebrabox behaviour analysis system **(section 2.6.1)** on 5 dpf progeny from two independent *atm*$^{-/+}$ incrosses **(figure 6.4)**. Consistent with the well-documented phenomenon, all fish had increased movement in the dark cycles and reduced movement in the light cycles (Rihel and Schier, 2012; Sun et al., 2016; Truong et al., 2012). However, *atm*$^{-/+}$ and *atm*$^{-/-}$ embryos appeared to be mildly, but significantly hypoactive in the dark stages in comparison to their wild-type siblings. This may suggest that losing even one copy of *atm* results in a delay in the development of the central nervous system (CNS) or neuromuscular system (Rihel and Schier, 2012; Sun et al., 2016; Truong et al., 2012).

6.2.6. *Atm*$^{-/-}$*; tdp1*$^{-/-}$ embryos have a normal photomotor response (PMR)

PMR analysis was performed on 5 dpf progeny from an *atm*$^{-/+}$*; tdp1*$^{-/-}$ incross and the expected reaction to light and dark cycles was seen in all resulting genotypes (**figure 6.5**). However, no significant differences were observed between them. This is very interesting given the findings with *atm*$^{-/-}$ single mutants, suggesting that *tdp1* knockout may be counteracting the effect of atm loss. This is opposite to what would be expected from a compounded phenotype of elevated PDBs, unless the loss of functions of atm other than its PDBR role was causing an opposite PMR. However, as the difference in PMR observed between atm embryos and their wild-type siblings is

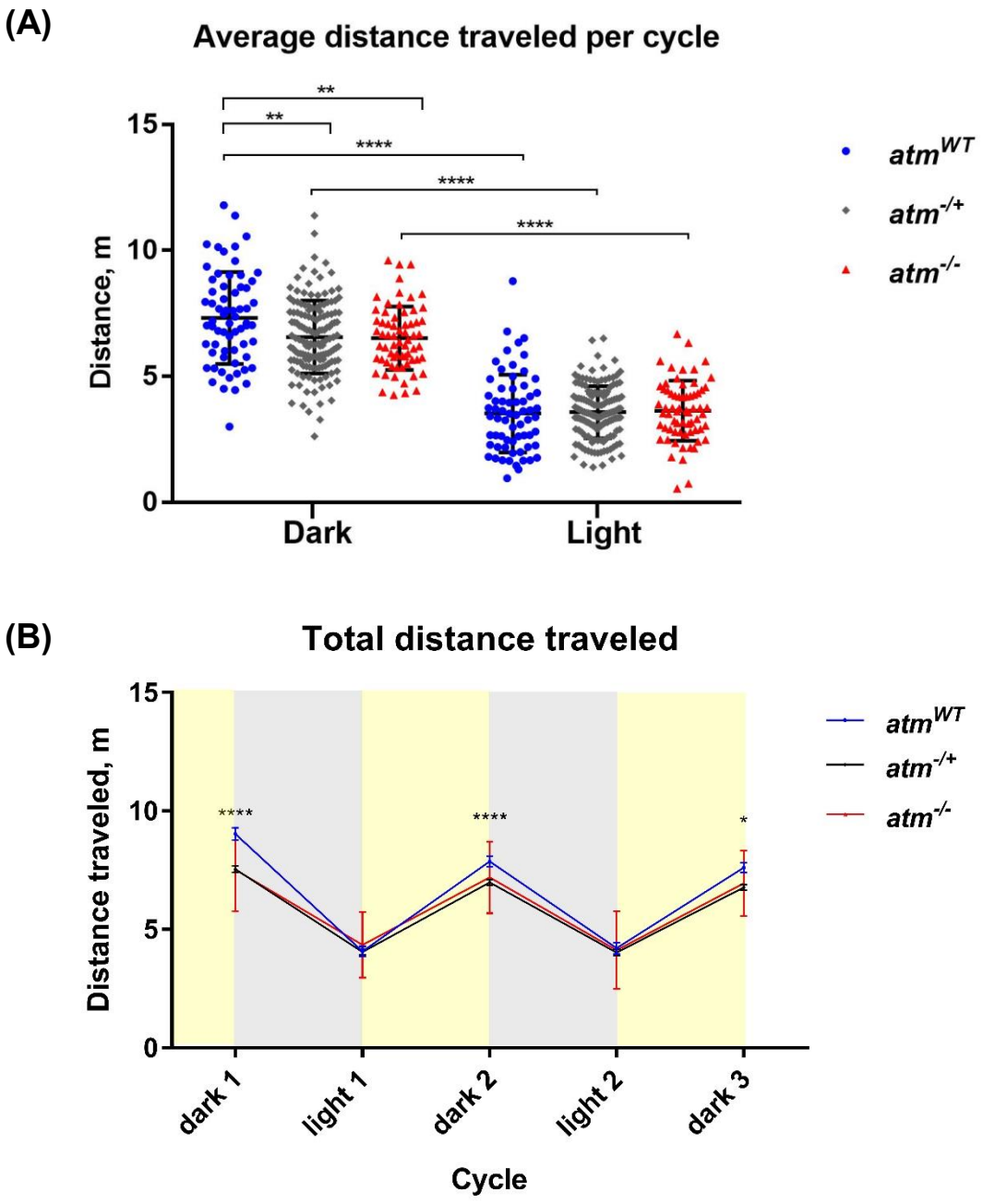

Figure 6.4. *Atm*$^{-/-}$ and *atm*$^{-/+}$ zebrafish appear to show hypoactivity in the dark. (A, B) 5 dpf embryos from an *atm*$^{-/+}$ incross were subjected 3 cycles of 5 minute darkness and 2 cycles of 5 minute light using the photomotor response assay (section 2.6.1); n=65 for *atm*^{WT}, n=147 for *atm*$^{-/+}$, n=66 for *atm*$^{-/-}$; data was obtained from two independent repeats from two separate incrosses. **(A)** Average distance traveled in all light or dark cycles, in metres, was measured. Each data point represents one animal; ±SD. *p* values were calculated using two-way ANOVA. **(B)** Total distance traveled each cycle, in metres, is plotted in each data point, which represents all animals; ±SEM. Significance values are denoted for *atm*$^{-/-}$ in comparison to their wild-type siblings. *p* values were calculated using one-way ANOVA**.**

My thanks to Mirinda Tattan, a PhD student, who carried out this experiment.

very mild, it may only be a matter of repeating the experiment with more animals before the difference becomes clear.

6.2.7. *Atm*$^{-/-}$ and *atm*$^{-/-}$*; tdp1*$^{-/-}$ adults show no stamina defect

In addition, 10 month-old sibling *atm*$^{+/+}$*; tdp1*$^{-/-}$*, atm*$^{-/+}$*; tdp1*$^{+/+}$*, atm*$^{-/-}$*; tdp1*$^{+/+}$ *atm*$^{+/+}$*; tdp1*$^{+/+}$ and *atm*$^{-/-}$*; tdp1*$^{-/-}$ fish were subjected to swim tunnel analysis (**section 2.6.3**). Fish of all the genotypes had a similar critical swimming speed, suggesting the mutations do not affect their stamina **(figure 6.6)**.

6.2.8. Generation and validation of *rnaseh2α*$^{-/+}$ zebrafish

Ribonuclease H2, subunit A (*rnaseH2a*) gene deletion in the zebrafish was generated using the CRISPR/Cas9 system, as described in **section 2.4.1**. Guide RNA was *in vitro* transcribed from a DNA template containing a target sequence for exon 6 of the zebrafish *rnaseh2a* gene **(figure 6.7A, B)**. In the G_0 generation, a founder transmitting multiple indels, including a 49 bp deletion (SH478, figure 6.7C) was detected. It results in a stop codon 52 amino acids downstream of the deletion and thus a truncated protein of 206 a. a. (full-length Rnaseh2a – 307 a. a.). The deleted protein sequence harbours four conserved residues, which are mutated in AGS in humans (N212, R235, T240 and R291), and one residue with highly similar properties (T240 in humans, Y241 in zebrafish) (Coffin et al., 2011). This suggests that such a truncation will be deleterious. The founder was therefore outcrossed to a nacre fish to create *rnaseh2a*$^{-/+}$ F_1 generation. The F_1 fish were finclipped and sequenced, and several fish, carrying the 49 bp deletion were identified.

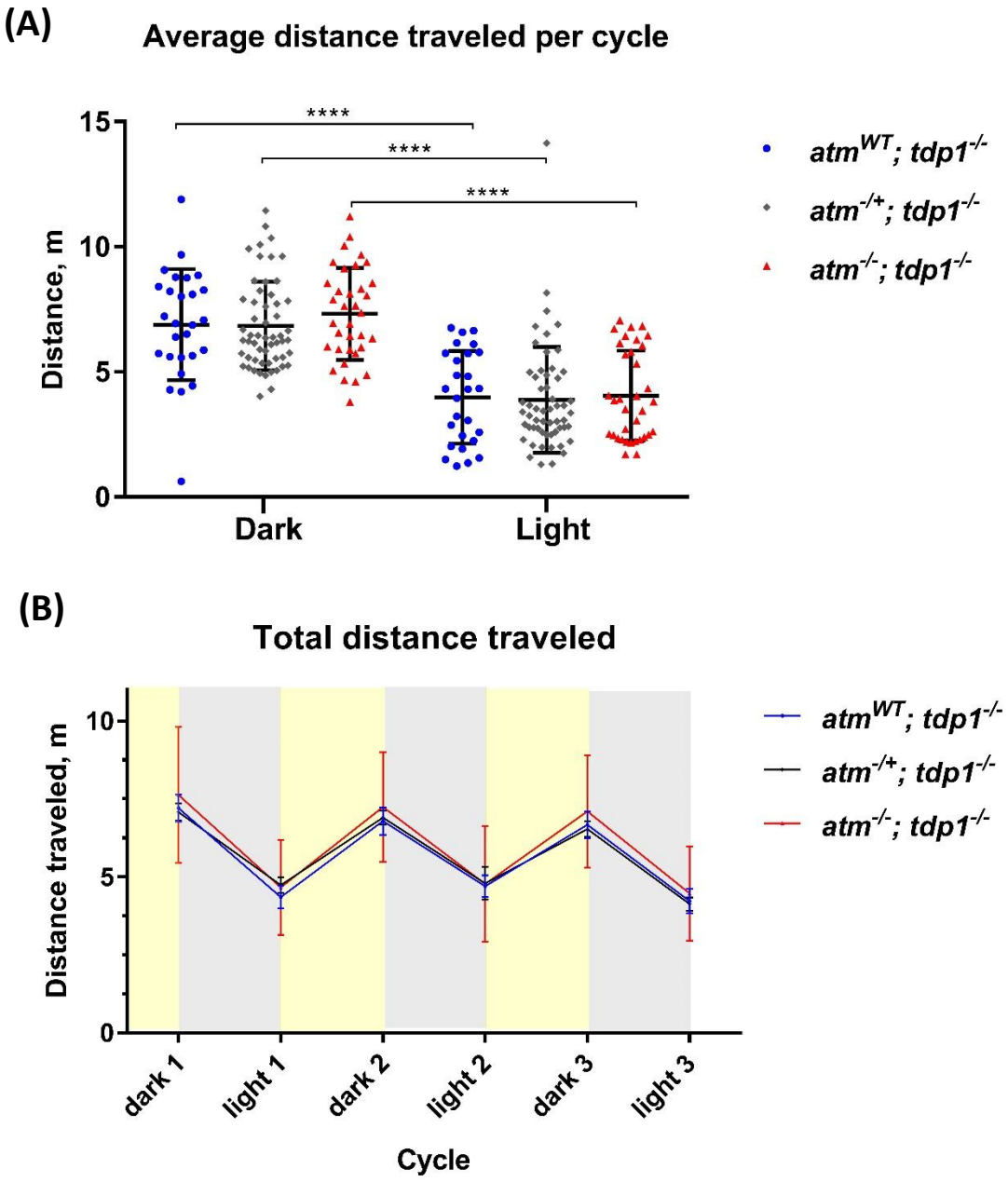

Figure 6.5. *Atm*$^{-/-}$*; tdp1*$^{-/-}$ zebrafish do not show any significant abnormal behaviours. (A, B) 5 dpf embryos from an *atm*$^{-/+}$*; tdp1*$^{-/-}$ incross were subjected to 3 cycles of 5 minute darkness and 3 cycles of 5 minute light using the photomotor response assay (section 2.6.1); n=27 for *atm*^{WT} *tdp1*$^{-/-}$, n=56 for *atm*$^{-/+}$*; tdp1*$^{-/-}$, n=35 for *atm*$^{-/-}$*; tdp1*$^{-/-}$*;* data was obtained from two independent repeats from two separate incrosses. **(A)** Average distance traveled in all light or dark cycles, in metres, was measured. Each data point represents one animal ±SD. *p* values were calculated using two-way ANOVA. **(B)** Total distance traveled each cycle, in metres, is plotted in each data point, which represents all animals; ±SEM. *p* values were calculated using one-way ANOVA.

My thanks to Mirinda Tattan, a PhD student, who carried out this experiment.

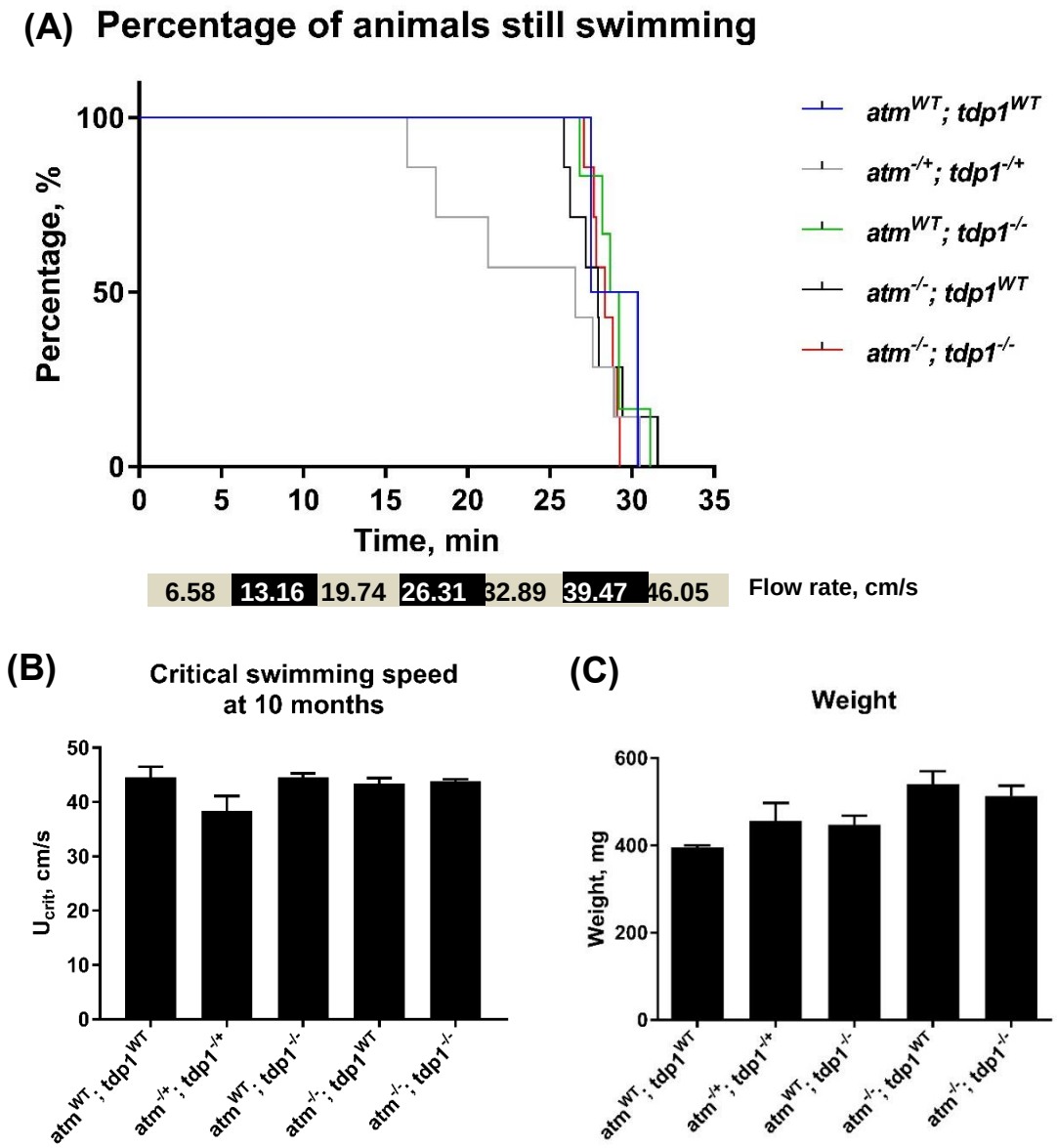

Figure 6.6. A*tm*$^{-/-}$, *tdp1*$^{-/-}$ and *atm*$^{-/-}$; *tdp1*$^{-/-}$ zebrafish do not show reduced endurance. 10 month-old sibling zebrafish were subjected to the swim tunnel test (section 2.6.3). **(A)** Percentage of fish still swimming at each flow rate was plotted. Each genotype was compared in a pairwise manner against the *atm*$^{-/+}$; *tdp1*$^{-/+}$ fish using the Mantel-Cox test and the *p* value was adjusted for multiple comparisons using the Bonferroni corrected threshold to ≤0.017. **(B)** Critical swimming speed was calculated as described in section 2.6.3; ±SEM. *p* values were calculated using one-way ANOVA. **(C)** Fish were weighed and *p* values were calculated using one-way ANOVA; ±SEM.

My thanks to Mirinda Tattan, a PhD student, who carried out this experiment.

(A)

5’*AAAGCACCGACTCGGTGCCACTTTTTCAAGTTGATAACGGACTAGCCTTATTTTA ACTTGCTATTTCTAGCTCTAAAAC*CGGTGTGGAGGTCACAGTCCCTATAGTGAGTC GTATTACGC 3’

(B)

(C)

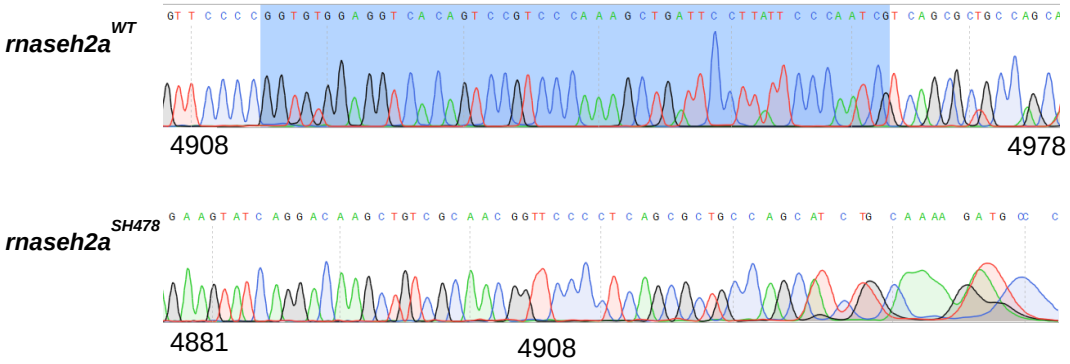

Figure 6.7. Generation and validation of *rnaseh2a*$^{-/-}$ zebrafish with the CRISPR/Cas9 system. **(A)** Sequence of template ultramer used for *in vitro* synthesis of gRNA. Scaffolding sequence is indicated in purple, target sequence in green and T7 polymerase promoter in blue. **(B)** Intron-exon structure of the zebrafish *atm* gene (www.ensembl.org). Exon 6, indicated by a red box, was targeted for Cas9 restriction. **(C)** Sequence of *rnaseh2a*^{WT} and *rnaseh2a*$^{-/-}$ zebrafish; the 49bp deletion in the light blue box results in a frameshift and a stop codon 52 amino acids downstream of the deletion. The numbers denote base position in the genomic sequence of RNase H2a.

6.2.9. Generation of *rnaseh2$^{-/-}$; tdp1$^{-/-}$* zebrafish

Rnaseh2a$^{-/-}$ F_1 and *tdp1$^{-/-}$* zebrafish were crossed to create the F_2 generation of *rnaseh2a$^{-/+}$; tdp1$^{-/+}$* zebrafish. The F_2 fish were in turn incrossed to give rise to *rnaseh2a$^{-/-}$* and *rnaseh2a$^{-/-}$; tdp1$^{-/-}$* F_3 fish.

6.2.10. *Rnaseh2$^{-/-}$; tdp1$^{-/-}$* zebrafish are viable with no obvious defects

Progeny from *rnaseh2$^{-/+}$; tdp1$^{-/+}$* incross were observed and genotyped at 5 dpf and 4 months of age. Genotyping revealed that the ratios of observed progeny genotypes did not differ significantly from the expected, both at 5 dpf and 4 months of age (**figure 6.8**). No morphological abnormalities were detected in the embryonic stages or adulthood.

6.2.11. Generation of *tdp1$^{-/-}$*; tg(sod1^{G93R})$^{-/+}$ and tdp1$^{-/-}$; tg(sod1^{WT})$^{-/+}$ zebrafish

To study the effects of the absence of Tdp1 in an increased oxidative stress environment, sod1^{G93R} os10 and Sod1^{WT} os4 fish with a dsRED marker driven by the heat shock protein 70 (hsp70) promoter (Ramesh et al., 2010) were crossed with *tdp1$^{-/-}$* fish. The transgenes were selected by looking at dsRED expression at adulthood. The adult *tdp1$^{-/+}$; tg(sod1^{G93R})$^{-/+}$* were then crossed with *tdp1$^{-/+}$* and *tdp1$^{-/+}$; tg(sod1^{WT})$^{-/+}$* were crossed with *tdp1$^{-/-}$* fish.

6.2.12. Tdp1$^{-/-}$; tg(sod1^{G93R})$^{-/+}$ zebrafish are viable

The progeny of the *tdp1$^{-/+}$; tg(sod1^{G93R})$^{-/+}$* and *tdp1$^{-/+}$* cross, were selected for dsRED expression at embryonic stage and genotyped at 5 months of age. Genotyping revealed that the ratios of observed progeny genotypes did not differ significantly

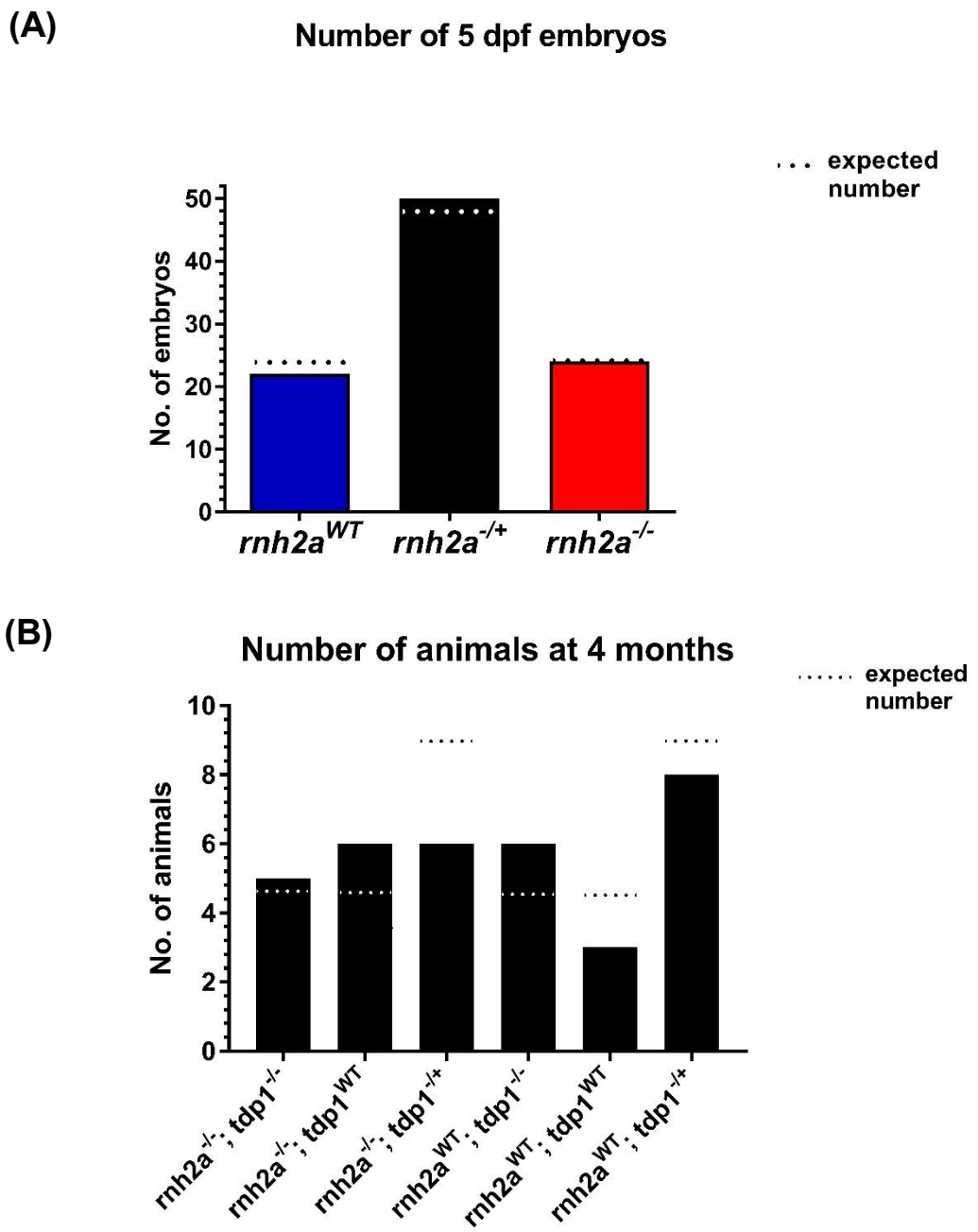

Figure 6.8. R*naseh2a*$^{-/-}$*; tdp1*$^{-/-}$ zebrafish are viable. (A) *rnaseh2a*$^{-/-}$*; tdp1*$^{-/-}$ zebrafish were incrossed and genotyped at 5 dpf for *rnaseh2a* (n=96). The two-tailed P value equals 0.8825. Chi squared equals 0.25 with 2 degrees of freedom. The two-tailed P value equals 0.883. **(B)** Only *rnaseh2a*$^{-/-}$ (n=24) and *rnaseh2a*$^{+/+}$ (n=22) embryos were raised to adulthood and genotyped at 4 months (n=34), then a chi-squared test was performed. Chi squared equals 2.706 with 5 degrees of freedom. The two-tailed P value equals 0.745.

from the expected **(figure 6.9)**. An initial cross was set up between *tdp1*$^{-/+}$*; tg(sod1G93R)*$^{-/+}$ and *Tdp1*$^{-/-}$ by Dr. Tennore Ramesh, but an increase in dsRED expression was not seen in half of dsRED-positive embryos, and therefore further experiments were not performed. The fish were observed by eye until 1 year and 6 months of age, but nothing abnormal was noted.

6.2.13. Generation of tdp1$^{-/-}$; tg(c9orf72)$^{-/+}$ zebrafish

To study the effects of the absence of tdp1 in an elevated genomic instability environment with increased TOP1-CCs, Matthew Shaw has carried out the following crosses. *Tdp1*$^{-/-}$ fish were crossed with c9orf72$^{+/+}$ transgenic fish, carrying a GFP-tagged C9orf72 gene with 102 X GGGGCC repeats and expressed under the zebrafish ubiquitin promoter. The resulting *tdp1*$^{-/+}$*; tg(c9orf72)*$^{-/+}$ fish were crossed with *tdp1*$^{-/+}$ fish to generate *tdp1*$^{-/-}$*; tg(c9orf72)*$^{-/+}$ zebrafish, and only GFP-positive embryos were raised. From observations by eye, there does not appear to be an obvious phenotype in the progeny of this cross thus far (up to 1 year and 5 months of age).

6.3. Discussion

We have generated several potential models for PDB repair, where the increased Top1-CC phenotype should be compounded. The single *atm*$^{-/-}$ mutants are viable, which goes in line with published rodent data (Barlow et al., 1996; Quek et al., 2017).

In addition, lack of atm appears to be affecting zebrafish sex determination and fertility, as all the *atm*$^{-/-}$ fish raised so far are males, which appear to be infertile. This needs further confirmation by raising and sexing higher numbers of fish from an

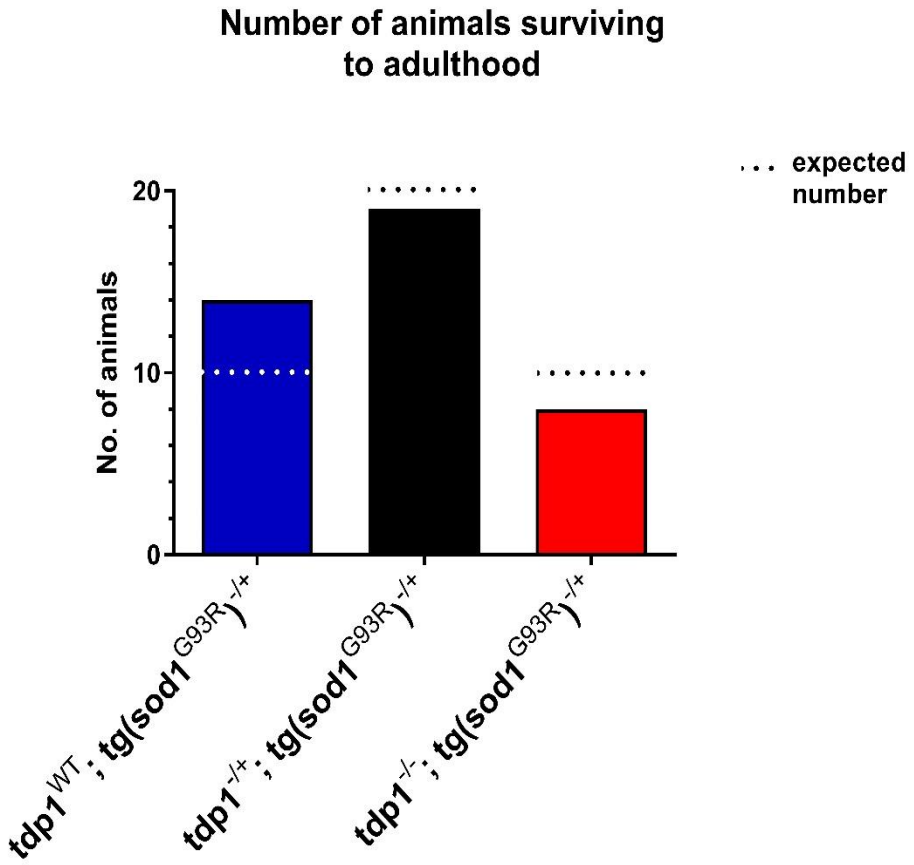

Figure 6.9. *tdp1$^{-/-}$; tg(sod1^{G93R})$^{-/+}$* zebrafish are viable. *tdp1$^{-/+}$; tg(sod1^{G93R})$^{-/+}$* zebrafish were crossed with *tdp1$^{-/+}$* fish. *Tg(sod1^{G93R})$^{-/+}$* embryos were selected by sorting for dsRED, raised and genotyped (n=41), then a chi-squared test was performed. Chi squared equals 1.976 with 2 degrees of freedom. The two-tailed P value equals 0.3724.

atm$^{-/+}$ incross and setting up more *atm*$^{-/-}$ males with wild-type females in tanks with dividers to gain statistical power. If these results are confirmed, they would also overlap with phenotypes previously observed in rodent models (Barlow et al., 1996; Quek et al., 2017). Some sex differences have also been seen in the *Atm*$^{-/-}$ rats, as the lifespan of female *Atm*$^{-/-}$ rats was significantly shorter than the lifespan of their male siblings (Quek et al., 2017). In addition, both the mouse and rat are infertile due to the lack of mature gametes (Barlow et al., 1996; Quek et al., 2017). Furthermore zebrafish *brca2* mutants have defects in homologous recombination, resulting in strong meiotic defects and the development of homozygous fish as sterile males (Rodriguez-Mari et al., 2011; van Eeden, unpublished). *Atm* mutants are expected to have similar defects to *brca2*, therefore our findings were not unexpected. Although we have not been able to show loss of atm protein due to lack of a zebrafish antibody, the above findings strongly suggest that atm is indeed lost.

Strikingly, the double *atm*$^{-/-}$*; tdp1*$^{-/-}$ knockout zebrafish are also viable to adulthood, as opposed to the *Atm*$^{-/-}$*; Tdp1*$^{-/-}$ mice, which die *in utero* (Katyal et al., 2014). This is likely due to the either a functional shift of Atm and/or Tdp1 during evolution from fish to mice, leading to the gain of novel functions in the mouse proteins, or compensation by a different pathway, which is not available in mice. Pathway choice between endonuclease repair and the TDP1 pathway is not very well understood, but PARP1 has been implicated in channelling TOP1-CCs to the TDP1 pathway (Ashour et al., 2015). This pathway has been shown to require proteolytic degradation of TOP1 by wss1 (SPRTN orthologue in humans and zebrafish) in yeast, whereas studies in Spo11-CC repair indicate the endonucleolytic pathway might not require this. The

reason embryonic lethality did not occur could perhaps be due to the endonucleolytic pathway compensating for increased Top1-CCs and, although its requirement is not clear, sprtn could be compensating by promoting access to these lesions (Stingele et al., 2014).

We also observed a significant reduction in movement of 5 dpf *atm*$^{-/+}$ and *atm*$^{-/-}$ embryos in the dark, however, we think this is a coincidence due to several reasons. Both *atm*$^{-/+}$ and *atm*$^{-/-}$ embryos showed the same level of reduction in movement. It seems unlikely that losing only one copy of atm would be as deleterious as losing both. For example, in mice the loss of each copy has an additive effect for increasing radiation sensitivity (Worgul et al., 2002). Secondly, we observed a normal induction of photomotor response in *atm*$^{-/+}$ and *atm*$^{-/-}$ embryos in a *tdp1*$^{-/-}$ background and no differences from *atm*^{WT}*; tdp1*$^{-/-}$ fish. As both ATM and TDP1 contribute to the repair of TOP1-CCs in a non-epistatic manner (Alagoz et al., 2013; Katyal et al., 2014), the phenotype of losing both should be compounded and not improved. The reason a significant reduction was observed could be a segregating dominant off-target mutation or perhaps the difficulties with setting optimal thresholds for zebrafish movement to avoid reflections and shadows being recorded. In addition, the standard deviation of samples between different genotypes was also significantly different, which means a more careful interpretation is required. Future repeats with higher numbers of animals are thus crucial to confirm that our reasoning is correct.

Increased fatigue was not detected in 10 month-old *atm*$^{-/-}$*, tdp1*$^{-/-}$ and *atm*$^{-/-}$*; tdp1*$^{-/-}$ zebrafish in the swim tunnel test. However, it is likely too early for such neuropathology to occur at an early time point, due to the slow progressive nature

of Top1-CC-induced degeneration. Thus further time points should be taken over time, especially at end-stages.

The *rnaseh2a*$^{-/-}$ and *rnaseh2a*$^{-/-}$*; tdp1*$^{-/-}$ zebrafish were also viable, in striking contrast to *Rnaseh2b*$^{-/-}$ and *Rnaseh2c*$^{-/-}$ mice (Hiller et al., 2012; Reijns et al., 2012) *Rnaseh2a* knockout mice have not been reported. This is the first multicellular organism found to not require RNase H2 activity, which can be explained in the same way as the viability of *atm*$^{-/-}$*; tdp1*$^{-/-}$ mutants. The fact that the catalytic subunit A was knocked out, rather than the accessory subunits B or C, should make no difference as it has been shown in vitro that all 3 subunits of yeast and human RNase H2 are required for catalytic activity of the enzyme (Cerritelli and Crouch, 2009). In addition, AGS is caused by mutations in any of the 3 subunits. Therefore, we have generated a viable *rnaseh2a*$^{-/-}$*; tdp1*$^{-/-}$ zebrafish, which should not only have increased levels of Top1-CCs, but also ribonucleotide contamination and the consequent genomic instability. *Tdp1*$^{-/-}$*; tg(sod1*^{G93R}*)*$^{-/+}$ zebrafish are viable as expected. Although no increase in dsRED was seen in the *tdp1*$^{-/-}$ background at embryonic stages and no abnormalities were observed by eye until adulthood, further experiments need to be carried out. Quantification of dsRED, γh2ax and Top1-CCs with or without various DNA damaging drugs would reveal endogenous levels of cellular stress, DSBs and protein-linked breaks in these fish and their capacity to sustain genotoxic challenges. Swim tunnel analysis is also crucial to determine whether loss of tdp1 exacerbates the Sod1^{G93R} phenotype. As both the *tdp1*$^{-/-}$ and *sod1*$^{G93R-/+}$ phenotypes are progressive, it would be more prudent to characterize older fish, even if a compound phenotype is expected.

Tdp1$^{-/-}$*; tg(c9orf72)*$^{-/+}$ fish appear to be viable and healthy by eye, but more data is required to confirm this observation. Similar experiments to the ones suggested for the *Tdp1*$^{-/-}$*; tg(sod1*^{G93R}*)*$^{-/+}$ fish could also be carried out for characterization.

Albeit further evolutionarily from humans than rodent models, zebrafish allow interrogation of PDBs with knockouts and techniques unavailable in other model systems. Unfortunately, due to time restraints further experiments were not carried out. As well as confirming and expanding the experiments carried out in this chapter, there are many more ways our new models can be utilized in the future. By interrogating the mechanism which allows the *atm*$^{-/-}$*; tdp1*$^{-/-}$ and *rnaseh2a*$^{-/-}$*; tdp1*$^{-/-}$ zebrafish to evade embryonic lethality, it might be possible to unravel the tissue-specific vulnerability question. Using the *atm*$^{-/-}$*; tdp1*$^{-/-}$ fish, it may also be possible to pinpoint the mechanism by which ATM promotes the repair of TOP1-CCs. Additionally, drug screens can be utilized to identify compounds that specifically sensitize the double mutant, but not wild-type fish, thus elucidating the potential backup repair pathway. All of the described models will facilitate learning about the pathological mechanisms underlying neurodegenerative disease. And finally, they can be used as a tool for large scale drug screening to find targets for the treatment of neurological disease and cancer by utilizing synthetic lethality and phenotype alleviation.

7

Analysis of TDP1 post-translational regulation

7.1. Introduction

The human TDP1 protein is 68.2 kDa in size and contains a highly conserved catalytic C-terminal domain (Interthal et al., 2001). In contrast, the short (150 a.a.) N-terminus domain is only present in higher eukaryotes. This may suggest a function only necessary with a more complex tissue architecture and larger genome size. Indeed, post-translational modifications (PTMs) in the N-terminus of TDP1 have been shown to tightly control its function. In response to TOP1-CCs, kinases ATM and DNA-PK phosphorylate serine 81 of TDP1, which stabilizes the protein, promotes its interaction with DNA Ligase 3 and XRCC1, promotes TDP1 recruitment to DNA damage sites and facilitates cell survival after genotoxic stress (Chiang et al., 2010; Das et al., 2009). This was elucidated by using a phosphomutant version of serine 81 (S>A). PARP1 binds TDP1 N-terminus and PARylates it, channeling TOP1-CC repair to TDP1, instead of the endonucleolytic pathway which removes TOP1-CC by cleaving the DNA several nucleotides upstream of the lesion (Das et al., 2014). PARylation also stabilizes TDP1 and promotes its recruitment at sites of DNA damage (Das et al., 2014), much like its SUMOylation at lysine 111, which promotes the repair of partly transcription-dependent DNA lesions (Hudson et al., 2012). However, it is not clear how these post-translational modifications interact with each other and whether there are further layers of regulation. Phenomena such as phosphorylation-dependent SUMOylation (Hietakangas et al., 2003; Hietakangas et al., 2006) and phosphorylation-dependent loss of SUMO (Yang et al., 2003) have previously been described and thus phosphorylation sites near the lysine 111 SUMOylation site are an interesting target to investigate. Such interactions can provide an extra layer of

control for the target protein and allow rapid changes between SUMOylation and other post-translational modifications, which target lysine, such as acetylation and ubiquitination. Indeed, data in our lab shows that the N-terminus of TDP1 most likely has additional phosphorylation sites to serine 81, which are constitutive and could be the result of a cluster of phosphorylation events (Wells, 2014). As TDP1 phosphorylation by ATR was ruled out (Das et al., 2009), other kinases that are capable of constitutive phosphorylation and that modify TDP1 interacting partners were considered. CK2 is a good candidate; it is a protein kinase that can phosphorylate constitutively (Grankowski et al., 1991), has previously been implicated in DNA repair (Kang et al., 2009; Keller et al., 2001; Loizou et al., 2004) and phosphorylates XRCC1 (Loizou et al., 2004), a binding partner of TDP1. In addition, data in our lab demonstrates that TDP1 is phosphorylated by CK2 *in vitro* (Wells, 2014). Therefore it was hypothesized that SUMOylation at K111 may be regulated by phosphorylation of nearby serines by CK2.

7.1.1. The SUMOylation pathway

Like other post-translational modifications, SUMOylation can modulate enzymatic activity (Yang et al., 2007), protein stability (Wang et al., 2005), transcription (Martin et al., 2009), intracellular localization (Takahashi et al., 2005a) and protein-protein interactions (Gareau and Lima, 2010; Ouyang et al., 2009). The small ubiquitin-like modifier (SUMO) is widely utilized in DNA damage response and repair processes (Dou et al., 2011; Galanty et al., 2009; Martin et al., 2009; Messner et al., 2009; Morris et al., 2009; Ouyang et al., 2009; Takahashi et al., 2005a; Wang et al., 2005; Yang et al., 2007). Similarly to the ubiquitin pathway, the SUMO pathway comprises

an E1 activating enzyme, the UBA2/AOS1 heterodimer, an E2 conjugating enzyme, called UBC9, and several E3 ligases (Dohmen, 2004). First, SUMO is processed into its mature form, then activated by UBA2/AOS1 and conjugated to the consensus sequence Ψ-K-x-[D/E] (Ψ -hydrophobic a. a.) of the target protein by UBC9, with or without an E3 ligase **(figure 7.1)** (Dohmen, 2004; Hoeller et al., 2007). The C-terminal glycine residue of SUMO then becomes covalently linked to the ε-amino group of its target's lysine (Johnson, 2004). There are 4 SUMO paralogues in humans: SUMO1, SUMO2, SUMO3 and SUMO4 (Dou et al., 2011). SUMO2 and SUMO3 can form chains *in vitro* and *ex vivo* (Fu et al., 2005; Tatham et al., 2001), whereas SUMO1 has only been shown to polymerize *in vitro* (Ulrich, 2008; Yang et al., 2006). However, SUMO1 may terminate a chain formed by SUMO2 and/or SUMO3 (Knipscheer et al., 2007; Tatham et al., 2001). The physiological role of SUMO4 is not clear. To maintain an equilibrium between bound and free SUMO, sentrin specific proteases (SENPS) remove it from target proteins (Mukhopadhyay and Dasso, 2007).

7.1.2. Protein kinase CK2

Protein kinase CK2, previously known as casein kinase II, is a 130 kDa heterotetramer, consisting of two catalytic subunits (αα, α'α' or αα') and two regulatory β subunits (Pinna, 1990). The regulatory subunit stabilizes the structure (Meggio et al., 1992), promotes enzymatic activity (Grankowski et al., 1991) and determines substrate specificity (Bidwai et al., 1992; Meggio et al., 1992). CK2 is highly conserved, expressed ubiquitously and can be found in most sub-cellular compartments (Faust and Montenarh, 2000). It is constitutively active and highly pleiotropic with more than 300 substrates, usually phosphorylating them at the consensus sequence

(A)

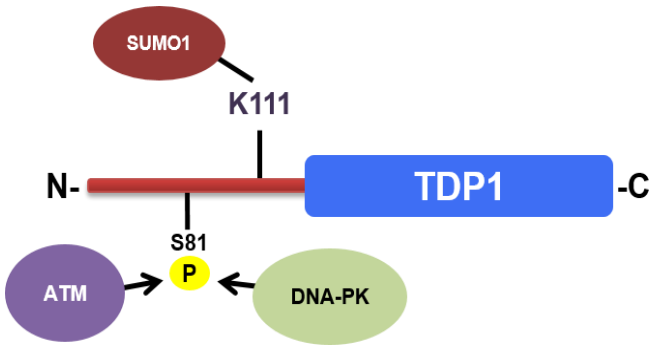

(B)

Site	S2	S2	S2	Y7	S13	S14	S15	S18	S18	S29	S32	Y46
Kinase	CK1	DNAPK	ATM	EGFR	CK2	CK2	CK2	CK2	CK1	PKA	PKC	SRC
Score	0.53	0.64	0.57	0.57	0.55	0.69	0.68	0.68	0.54	0.71	0.51	0.56
Site	S61	S61	S61	S61	S79	S79	S79	S81	S81	S90	S91	S92
Kinase	RSK	PKA	PKG	CDK5	RSK	PKA	PKG	DNAPK	ATM	CK2	CK2	CK2
Score	0.64	0.60	0.51	0.55	0.55	0.83	0.58	0.64	0.63	0.54	0.59	0.66

(C)

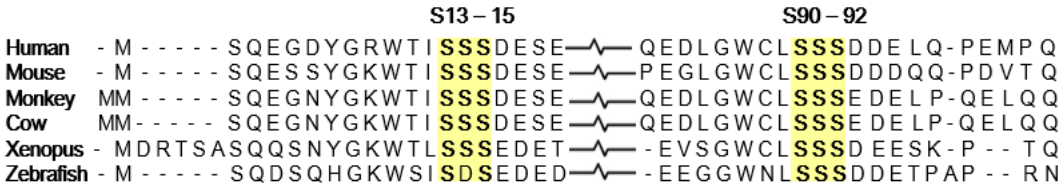

Figure 7.2. Established and putative post-translational TDP1 modifications. (A) Schematic representation of established TDP1 post-translational modifications (Chiang et al., 2010; Das et al., 2009; Hudson et al., 2012). (B) Kinase-specific phosphorylation site prediction was carried out using the NetPhosK 1.0 server (http://www.cbs.dtu.dk/services/NetPhosK/) (Blom et al., 2004). Predicted CK2 phosphorylation clusters are highlighted in yellow. The score represents a value from 0 to 1; the threshold for phosphorylation is 0.5, however the closer the value is to 1 the higher the confidence that the site is phosphorylated. (C) Alignment of serine clusters S13 – 15 and S90 – 92 in higher eukaryotes: mouse (*M. musculus*, ENSMUST00000153627.7), monkey (*M. mulatta*, ENSMMUT00000006316.3), cow (*B. taurus*, ENSBTAT00000017463.5), xenopus (*X. tropicalis*, ENSXETT00000034227.3) and zebrafish (*D. rerio*, ENSDART00000150149.2).

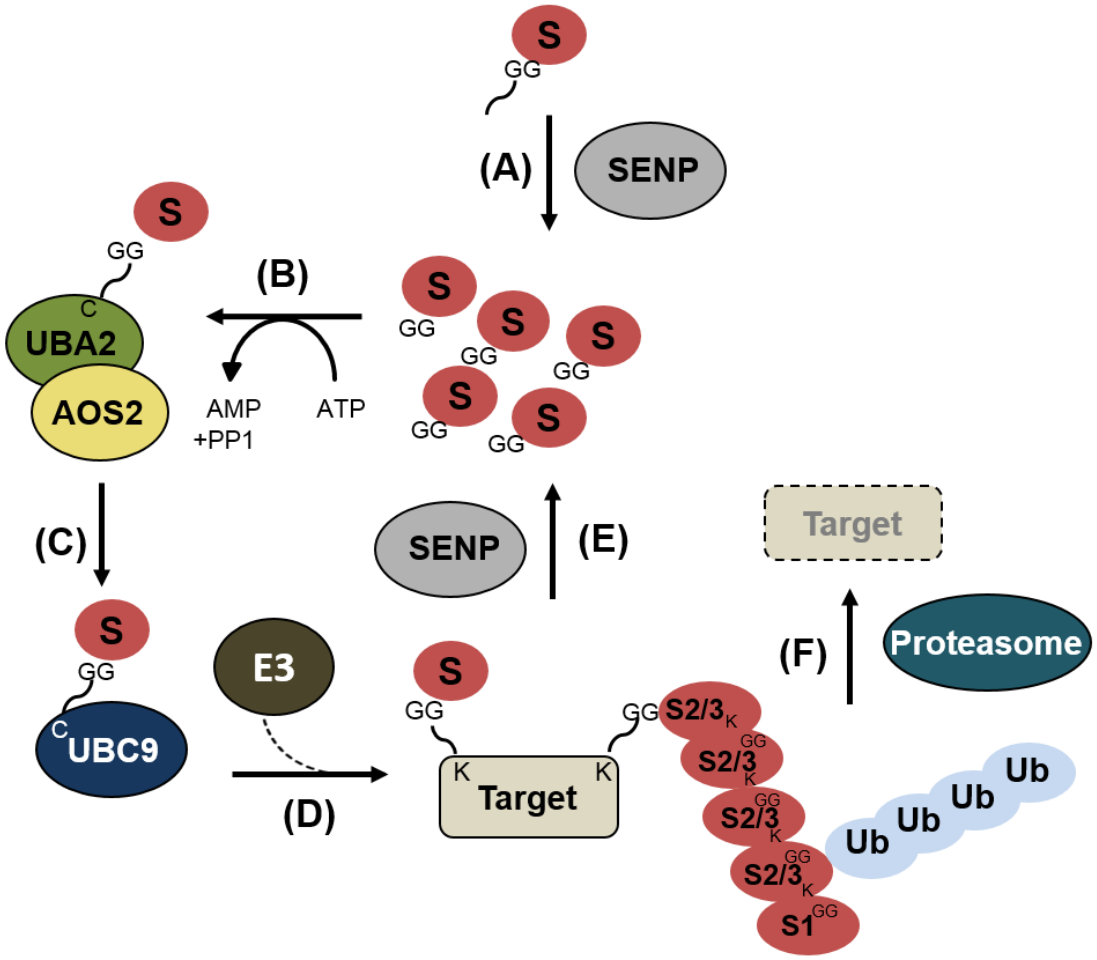

Figure 7.1. The SUMO pathway. Schematic representation of the SUMO pathway. (A) Sentrin specific proteases (SENPs) activate the SUMO precursor by cleaving its short C-terminal extension and exposing a di-glycine residue. (B) The E1 enzyme heterodimer UBA2/AOS1 activates the mature SUMO in an ATP-dependent reaction, where SUMO1 becomes covalently bound to a cysteine residue in UBA2 via a thioester bond. (C) Activated SUMO is transferred onto the E2 conjugating enzyme UBC9 via a transesterification reaction. (D) In vitro SUMO is conjugated to the consensus site Ψ-K-x-[D/E] of the target protein directly by UBC9, whereas in vivo this process is facilitated by a target-specific E3 ligase. (E) SENPs deSUMOylate the target, replenishing the free SUMO pool. (F) SUMO-targeted ubiquitin ligases can recognize and ubiquitinate SUMO chains, directing the target to proteasomal degradation. Adapted from Dohmen, 2004 and Gareau and Lima, 2010.

SXXE/D/pS/pY (Litchfield, 2003; Songyang et al., 1996). The consensus sequence, however, may vary and does not guarantee phosphorylation by CK2.

The CK2 kinase was first discovered in 1954 and has been studied extensively due to its involvement in many cellular processes, such as signalling, development, DNA damage repair, cell cycle regulation, RNA synthesis and ubiquitination (Faust and Montenarh, 2000; Litchfield, 2003; Pinna, 2002). Although our lab has shown that SUMOylation of TDP1 promotes its accumulation at DNA damage sites (Hudson et al., 2012), it is not clear whether phosphorylation by kinases, such as CK2, could be further regulating the cellular function of TDP1.

7.2. Results

7.2.1. TDP1 is phosphorylated at S13-15 and S90-92 *ex vivo*

In addition to the well-established post-translational modifications of TDP1, such as phosphorylation at serine 81 and SUMOylation at lysine 111 (**figure 7.2A**) (Chiang et al., 2010; Das et al., 2009; Hudson et al., 2012), it has been shown that TDP1 N-terminus is hyperphosphorylated *ex vivo* (Wells, 2014). Recombinant TDP1 was phosphorylated by CK2 *in vitro* and by whole-cell extracts, unless they were pre-incubated with TBB, a CK2 inhibitor (Wells, 2014). To determine which sites were phosphorylated, kinase-specific phosphorylation site prediction was performed *in silico* (figure 7.2B). It showed possible CK2 phosphorylation sites at serines 13 – 15, 18 and 90 – 92, in line with studies showing CK2 phosphorylation clusters (Loizou et al., 2004; Sarno et al., 1996; Torres and Pulido, 2001). These sites were aligned among several higher eukaryotes to reveal that serine clusters 13 – 15 and 90 – 92 are highly conserved from human to xenopus, with the only exception being the

substitution of serine 14 to the chemically similar aspartic acid in zebrafish. All of the serines in one of the clusters (S13 – 15 = 3S>A), or both (S13 – 15, S90 – 92 = 6S>A) were changed to alanine in myc-tagged *TDP1*$^{1\text{-}150}$ using site-directed mutagenesis. Only N-terminus of *TDP1* was used to better visualize any differences in molecular weight during western blotting. These phosphomutant TDP1$^{1\text{-}150}$ variants were then expressed in HEK293 cells alongside wild-type TDP1$^{1\text{-}150}$, pulled-down and subjected to SDS-PAGE and western blotting **(figure 7.3)**. TDP1$^{1\text{-}150;\ 3S>A}$ ran at a lower molecular weight than the wild-type TDP1$^{1\text{-}150}$ (>25 kDa), and TDP1$^{1\text{-}150;\ 6S>A}$ ran even lower than the one-cluster mutant, TDP1$^{1\text{-}150;\ 3S>A}$. λ-phosphatase treatment of samples to remove potential serine phosphorylation caused a large band shift in the wild-type TDP1$^{1\text{-}150}$ lane, a smaller one in TDP1$^{1\text{-}150;\ 3S>A}$, and no band shift in the TDP1$^{1\text{-}150;\ 6S>A}$ lane. These data together suggest that the observed molecular weight differences (from the predicted 17kDa) of the wild-type TDP1 N-terminus account for *ex vivo* phosphorylation of TDP1 serines 13 – 15 and 90 – 92.

7.2.2. TDP1 phosphorylation at S13 – 15 and S90 – 92 inhibits SUMOylation at K111

To test whether phosphorylation at serines 13 – 15 and 90 – 92 affected SUMOylation at lysine 111, levels of SUMO1-TDP1 conjugates should be compared between cells expressing wild-type and phosphomutant TDP1. However, repeated immunoblotting consistently showed higher levels of the phosphomutant TDP1 than wild-type TDP1 (figure 7.4A, B). Although the increase in phosphomutant protein was not significant, it complicated accurate quantification of SUMO1-TDP1 conjugates. To circumvent this problem a phosphomimetic version of *TDP1* was generated via site directed

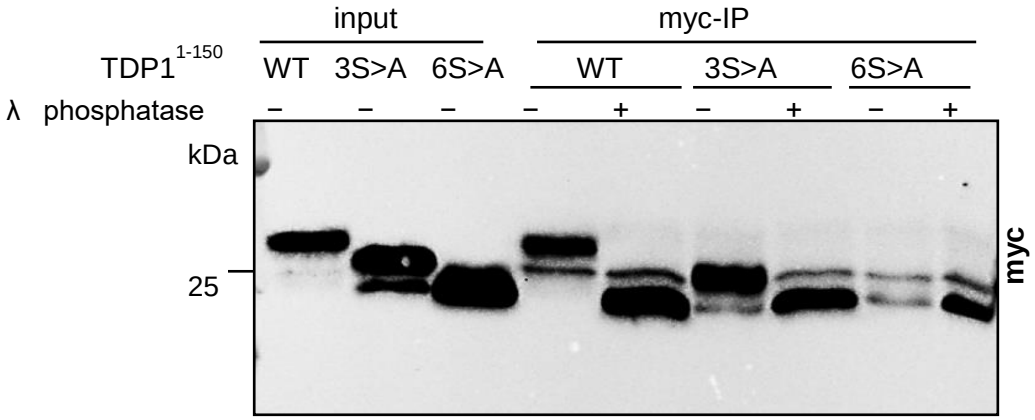

Figure 7.3. TDP1 is phosphorylated at S13, S14, S15, S90, S91 and S92 in human cells. Site-directed mutagenesis (section 2.2.13) was carried out on serine clusters 90 – 92 and then 13 – 15 in $TDP1^{1-150}$ to turn them into alanines. TDP1 with phosphomutant mutations in cluster 90 – 92 is hereafter called 3S>A, and 6S>A in both 90 – 92 and 13 – 15 clusters. HEK293 cells were transfected with wild-type or mutagenized myc-tagged N-terminus of TDP1 (1 – 150 aa.), then harvested 48 hours later and subjected to myc-IP with λ-phosphatase assay (section 2.9.12), SDS-PAGE and western blotting (sections 2.9.4 – 2.9.6) with anti-myc antibody.

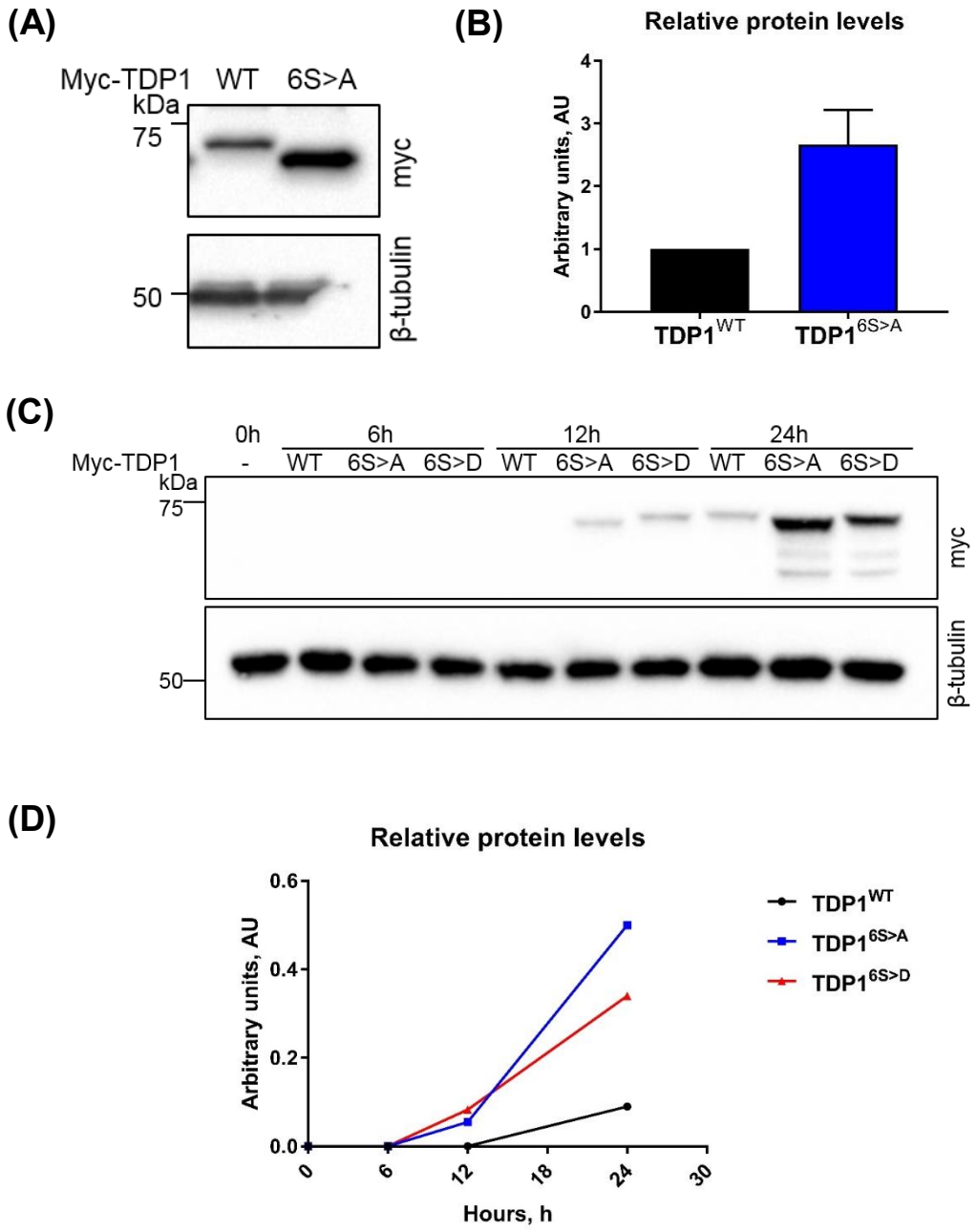

Figure 7.4. Phosphorylation mutants of TDP1 serine clusters S13 – S15 and S90 – S92 are expressed at higher levels than TDP1^{WT}. (A) HEK293 cells were transfected with full-length myc-tagged TDP1, then harvested 48 hours later and subjected to SDS-PAGE and western blotting (sections 2.9.4 – 2.9.6). **(B)** Quantification of 7.6A; 2 independent repeats ±SEM. *p* value was calculated using a two-tailed Student's T-test. **(C)** HEK293 cells were transfected with full-length myc-tagged TDP1, harvested straight away and 6, 12 and 24 hours later, then subjected to SDS-PAGE and western blotting (sections 2.9.4 – 2.9.6). **(D)** Quantification of 7.6C. The quantity of β-tubulin in 6S>A 12 hour time-point was set to 1 AU and all other values were quantified relative to it. Relative TDP1 signal normalized against β-tubulin was plotted.

mutagenesis, by changing serines 13 – 15 and 90 – 92 into aspartic acid (6S>D). As the increased protein levels of TDP1$^{6S>A}$ could be due to either increased protein stability as a result of the mutations or lack of phosphorylation, or increased expression due to the mutations, the expression levels of all the TDP1 variants were first compared. *TDP1^{WT}*, *TDP1$^{6S>A}$* and *TDP1$^{6S>D}$* vectors were transfected into HEK293 cells and expression of proteins was monitored via immunoblotting over a 24 hour time-course **(figure 7.4C, D)**. The experiment revealed an increase and an earlier start of expression in both phosphorylation variants, concluding that phosphorylation itself did not play a part in modulating stability and rather that the chemical change in the residues was responsible for increased expression. Due to this observation only TDP1$^{6S>A}$ and TDP1$^{6S>D}$ were compared for SUMO1-TDP1 levels. SUMO1 and TDP1$^{6S>A}$ or TDP1$^{6S>D}$ were expressed in HEK293 cells and levels of SUMO1-TDP1 conjugates were quantified **(figure 7.5)**. Quantification revealed that SUMOylation was significantly reduced when TDP1$^{6S>D}$ was expressed, suggesting that phosphorylation at serines 13 – 15 and 90 – 92 suppresses SUMOylation at lysine 111.

7.2.3. Loss of CK2 kinase function or its inhibition does not abolish TDP1 phosphorylation

Having demonstrated that serines 13 – 15 and 90 – 92 of TDP1 are phosphorylated, it was important to confirm whether CK2 was the responsible kinase *ex vivo*, as well as *in vitro* (Wells, 2014). To test this two approaches were used: transfection of *CK2α^{KD}*, a kinase-dead variant, and inhibition of CK2 using its specific inhibitor TBB. First, *myc-TDP1$^{1-150}$* **(figure 7.6A, B)** or full-length *myc-TDP1* **(figure 7.6C)** were co-transfected into HEK293 cells together with *CK2α^{KD}*

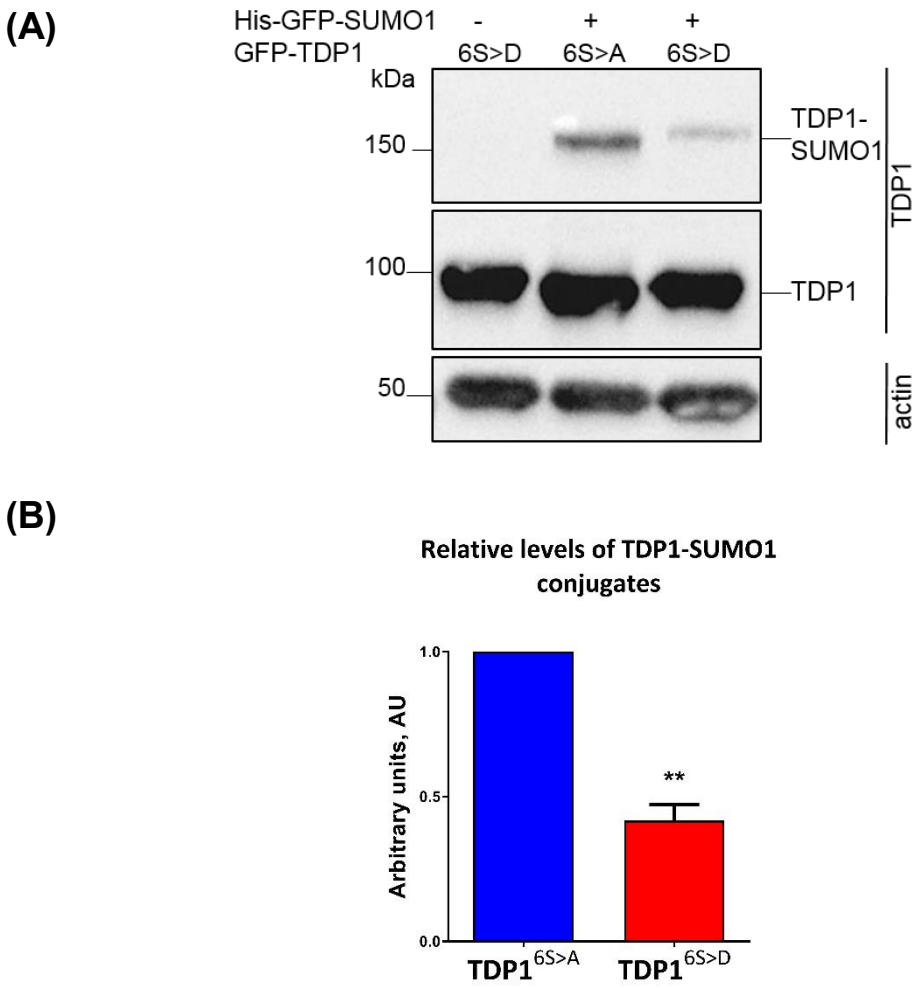

Figure 7.5. Phosphorylation of serine clusters S13 – S15 and S90 – S92 suppresses SUMOylation at K111. (A) HEK293 cells were co-transfected with full-length GFP-tagged TDP1 and GFP-SUMO1 or empty vector, harvested 48 hours later and subjected to SDS-PAGE and western blotting (sections 2.9.4 – 2.9.6). **(B)** Quantification of 7.7A. Relative levels of TDP1-SUMO1 conjugates in $TDP1^{6S>D}$ were quantified in relation to TDP1-SUMO1 conjugates in $TDP1^{6S>D}$, the value of which was set to 1. n=3, ±SEM. 3 independent repeats, ±SEM. *p* values were calculated using a two-tailed Student's T-test.

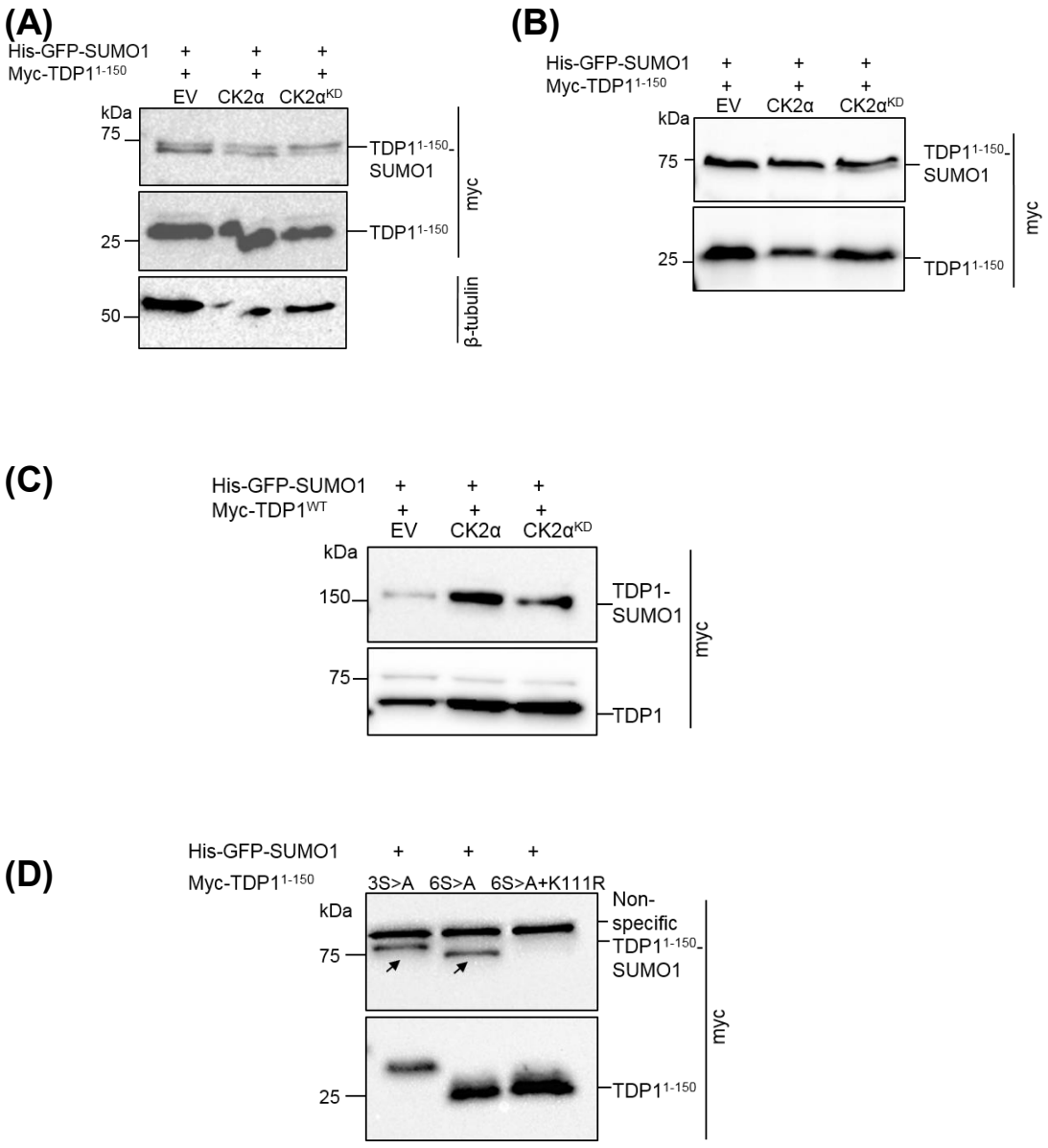

Figure 7.6. Loss of CK2 kinase activity does not result in loss of TDP1 phosphorylation. (A, B, C) HEK293 cells were co-transfected with TDP1$^{1-150}$ **(A, B)** or full-length **(C)** myc-tagged TDP1, his-GFP-SUMO1 and CK2, CK2^{KD} (kinase-dead) or empty (EV) vectors, then harvested 48 hours later and subjected to SDS-PAGE and western blotting (sections 2.9.4 – 2.9.6). **(D)** HEK293 cells were co-transfected with myc-tagged TDP1 n-terminus and his-GFP-SUMO1, then harvested 48 hours later and subjected to SDS-PAGE and western blotting (sections 2.9.4 – 2.9.6).

(Turowec et al., 2010; Vilk et al., 1999) and *His-GFP-SUMO1*, as it was hypothesized that phosphorylation by CK2 may affect SUMOylation at lysine 111. Immunoblotting of lysates from these cells, however, showed that expression of *CK2α*^{KD} does not cause a band-shift of TDP1 and thus does not seem to affect its phosphorylation. SUMOylation at lysine 111, as confirmed by immunoblotting of TDP1-SUMO1 conjugates in TDP1$^{1\text{-}150}$ and TDP1$^{1\text{-}150;\ K111R}$ **(figure 7.6D)**, was also not affected. Next, *myc-TDP1* and *His-GFP-SUMO1* were expressed in HEK293 cells, which were then treated with TBB. Immunoblotting of lysates from these cells showed no changes in TDP1 phosphorylation and no overt changes in its SUMOylation at K111 **(figure 7.7)**. From this data it was suggested that protein kinase CK2 is not the primary kinase of TDP1 in human cells.

7.2.4. Generation of stable Flp-In T-Rex 293 cell lines

To facilitate further experiments in attempts to elucidate the physiological role of hyperphosphorylation in TDP1 N-terminus, cell lines stably expressing TDP1^{WT}, TDP1$^{6S>A}$ and TDP1$^{6S>D}$ were generated **(figure 7.8)**. First, the pcDNA5-FRT-TDP1$_{TR}$-miTDP1 plasmid, harbouring two miRNA targeting sequences for nucleotides 28 – 48 (a.a. 10 - 16) and 259 – 279 (a.a. 87 - 93) in the human TDP1 mRNA, and targeting resistant TDP1 cDNA (Chiang et al., 2017), was mutagenized to generate pcDNA5-FRT-TDP1$_{TR}^{S13\text{-}15A,S90\text{-}92A}$-miTDP1 (6S>A) and pcDNA5-FRT-TDP1$_{TR}^{S13\text{-}15D,S90\text{-}92D}$-miTDP1 (6S>D) vectors, whilst maintaining the targeting-resistant nucleotides of TDP1. The plasmid harbours specific sequences required for miRNA processing *in vivo* and an EmGFP-tagged TDP1 together with the miRNA precursor, both under the control of CMV/TetO$_2$ promoter. The generated vectors were then co-transfected into Flp-In T-

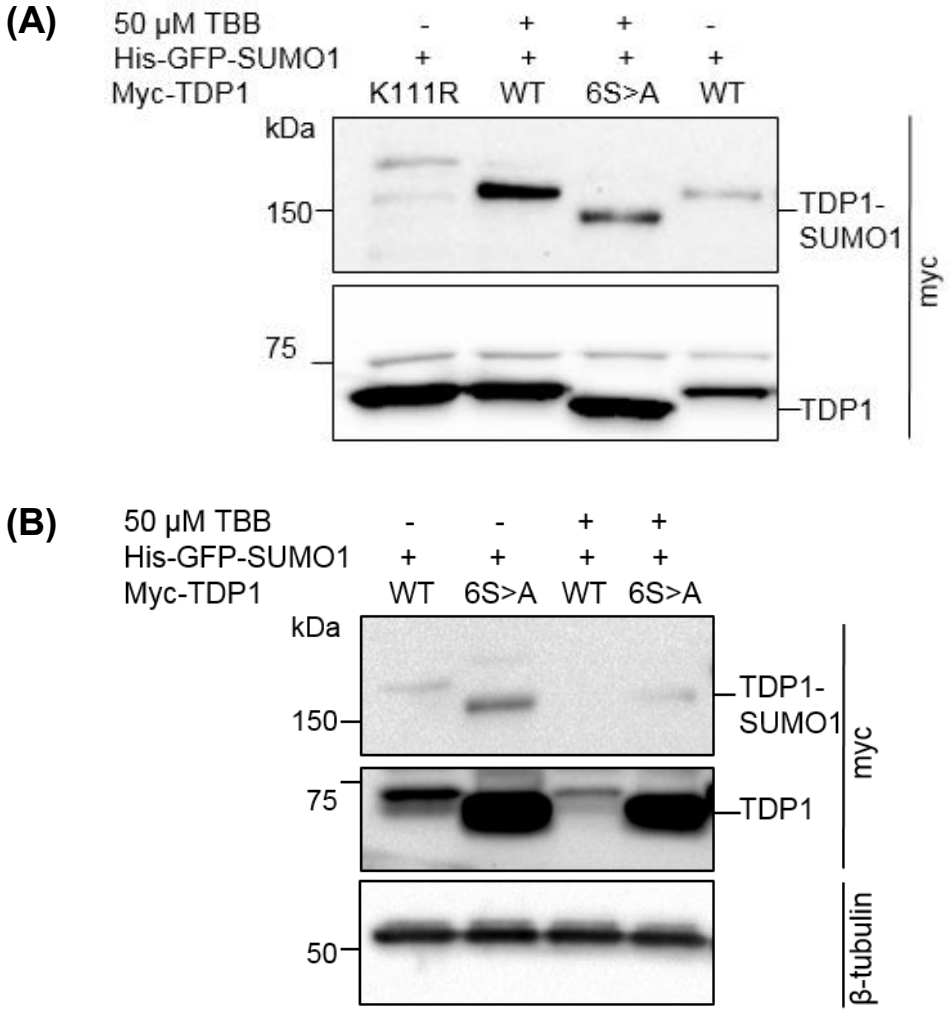

Figure 7.7. Inhibition of CK2 kinase does not result in loss of TDP1 phosphorylation. (A) HEK293 cells were transfected with full-length myc-tagged TDP1 and his-GFP-SUMO1, treated with TBB 24 hours post-transfection, then harvested 24 hours later and subjected to SDS-PAGE and western blotting (sections 2.9.4 – 2.9.6). **(B)** HEK293 cells were transfected with full-length myc-tagged TDP1 and his-GFP-SUMO1, and treated with TBB, then harvested 24 hours later and subjected to SDS-PAGE and western blotting (sections 2.9.4 – 2.9.6).

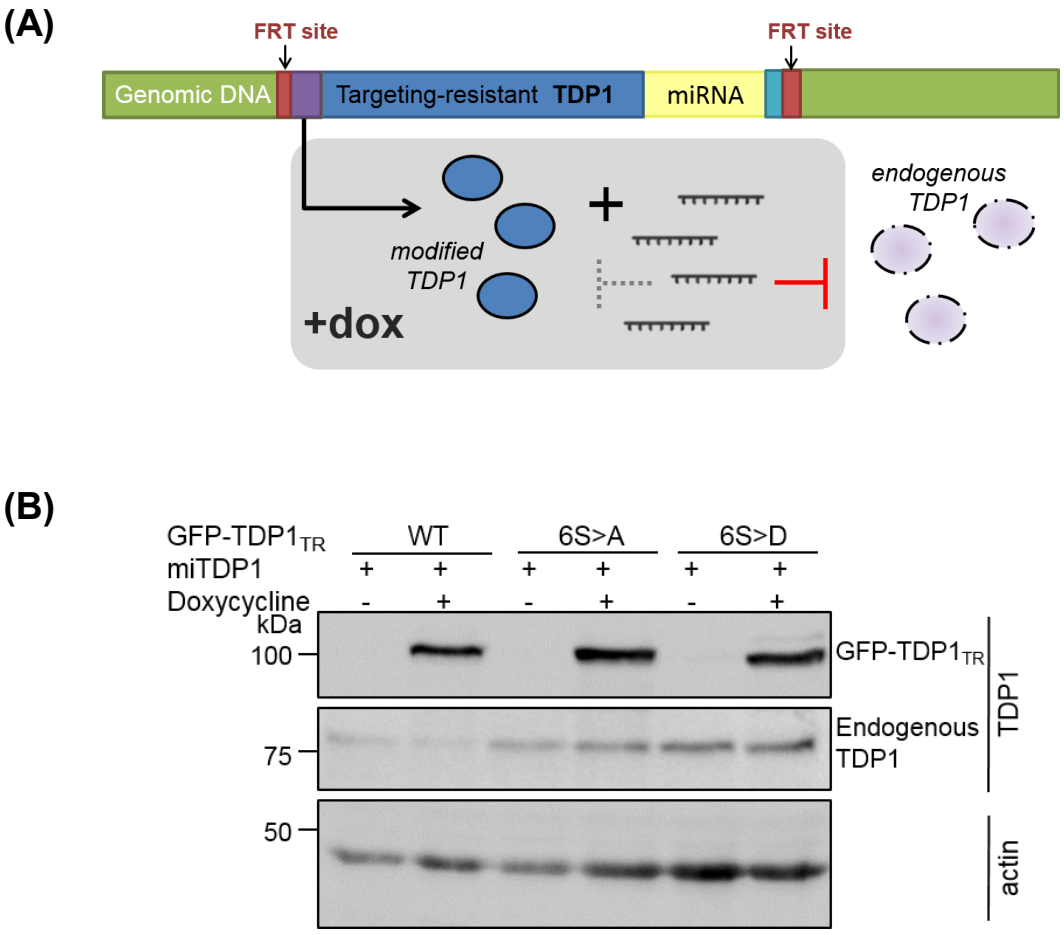

Figure 7.8. Generation and validation of stable cell lines, expressing TDP1 phosphorylation mutants. (A) Schematic representation of the Flp-In system. A targeting-resistant gene of interest (for example, TDP1) along with short hairpin RNA (shRNA) is inserted into an FRT site in the genomic DNA of T-REx 293 cells. Upon induction with doxycycline, the gene and shRNA are expressed. The shRNA knocks-down endogenous TDP1, but not the targeting-resistant TDP1. **(B)** Flp-In T-Rex 293 cells were induced with doxycycline and harvested 48 hours later, then subjected to SDS-PAGE and western blotting (sections 2.9.4 – 2.9.6).

Rex 293 cells with pPGKFLP, a Flp recombinase expression construct, and stable clones were selected by hygromycin treatment for three weeks. The resulting clones were validated by induction with doxycycline and immunoblotting for TDP1 **(figure 7.8B)**. In all three clones, expressing $TDP1_{TR}^{WT}$, $TDP1_{TR}^{6S>A}$ and $TDP1_{TR}^{6S>D}$, GFP-$TDP1_{TR}$ expression was induced upon doxycycline addition, however a knockdown of endogenous TDP1 was only observed in the original $TDP1_{TR}^{WT}$-expressing clone. It is possible that site-directed mutagenesis introduced off-target mutations in the miRNA precursor or processing sequences, abrogating TDP1 knockdown. However, the high overexpression of GFP-$TDP1_{TR}$ in relation to endogenous TDP1 should mean that it is out-competing the endogenous TDP1.

7.2.5. TDP1 phosphorylation at S13-15 and S90-92 does not affect DNA damage levels

As phosphorylation at serines 13 – 15 and 90 – 92 was shown to suppress SUMOylation at lysine 111, it was hypothesized that it should also reduce the rate of TDP1 accumulation at DNA damage sites, thus leading to a lag in DNA damage repair. Since a lag in DNA damage repair would also result in higher overall DNA damage levels, the foci formation of 53BP1, a double-strand break marker, was first measured (**figure 7.9**). Stable cell lines, overexpressing $TDP1_{TR}^{WT}$ along with miTDP1, $TDP1_{TR}^{6S>A}$ and $TDP1_{TR}^{6S>D}$ were treated with CPT, fixed and stained for 53BP1. 53BP1 foci quantification revealed no significant differences between wild-type TDP1 and its phosphorylation variants before or after CPT treatment. This data suggests that phosphorylation of serine clusters 13 – 15 and 90 – 92 does not affect DNA damage

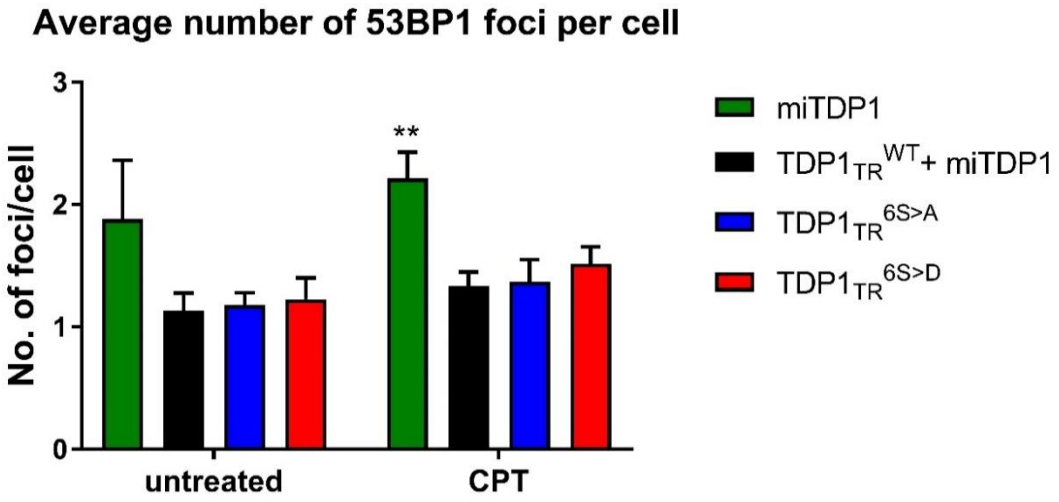

Figure 7.9. TDP1 S13-15 and S90-92 phosphorylation mutants do not have altered levels of 53BP1 foci. Flp-In Trex 293 cells were plated, induced, treated with 1 µM CPT for one hour, fixed and subjected to anti-53BP1 immunofluorescence as described in section 2.10.1.3. Average number of foci per cell was plotted from 3 independent repeats ±SEM. *p* values were calculated using two-way ANOVA (not repeated measures) and are plotted in relation to $TDP1^{TR\text{-}WT}$ + mi-TDP1.

My thanks to our undergraduate student Lukas Jasaitis, who carried out this experiment.

levels, which is very surprising considering its negative effects on SUMOylation at lysine 111.

7.2.6. Mass spectrometry analysis in search of binding partner differences between phosphomutant and phosphomimetic TDP1

It is currently unknown, which kinase phosphorylates TDP1 serine clusters 13 – 15 and 90 – 92, which phosphatase dephosphorylates them, if any, and which E3 SUMO ligase facilitates the conjugation of SUMO1 to lysine 111. $TDP1_{TR}^{6S>A}$ and $TDP1_{TR}^{6S>D}$ were utilized to identify generic TDP1 binding partners by mass spectrometry and also look for potential differences between the two variants. Stable cell lines, expressing $TDP1_{TR}^{6S>A}$ and $TDP1_{TR}^{6S>D}$, were lysed, then TDP1 was pulled-down and subjected to SDS-PAGE, tryptic in-gel digestion and mass spectrometry (figure 7.10). Data analysis did not reveal any overt differences in the binding partner repertoire of $TDP1_{TR}^{6S>A}$ and $TDP1_{TR}^{6S>D}$, but several hits for different subunits and isoforms of protein phosphatase 2A (PP2a) were identified in both samples. In addition, ubiquitin carboxyl-terminal hydrolase 11 (USP11), was pulled down in three of the four repeats and initially it was thought that $TDP1_{TR}^{6S>A}$ had a reduced or abrogated binding of PNK and LIG3. Three different isoforms of casein kinase 1 (CK1), a pleiotropic serine threonine kinase (Knippschild et al., 2005), were also identified as potential binding partners of TDP1, whereas CK2 was not found in either of the samples.

7.2.7. Validation of mass spectrometry hits

7.2.7.1. USP11 interacts with TDP1, but PP2A does not

USP11 is a deubiquitinase, which has been widely implicated in inflammation (Al-Salihi et al., 2012; Liu et al., 2016) and DNA damage repair processes

Figure 7.10. Mass spectrometry after pull-down of $TDP1_{TR}^{6S>A}$ and $TDP1_{TR}^{6S>D}$. Flp-In T-Rex 293 cells were induced with doxycycline and harvested 48 hours later, then subjected to GFP pull-down, SDS-PAGE, in-gel tryptic digestion and mass spectrometry (sections 2.9.2 – 2.9.4, 2.9.10 and 2.9.11). Proteins were ranked by intensity and only the top 50 hits were considered. Out of these hits, candidates of potential interest have been listed in this table. The data is from 4 independent repeats (R): I, II, III and IV. Column 'R' denotes which repeats the protein was found in and column 'P' indicates the peptide number in each repeat. Hits only found in $TDP1_{TR}^{6S>A}$ or $TDP1_{TR}^{6S>D}$ in a particular repeat are listed in the appropriate column. **Continued on the next page.**

TDP1$_{TR}^{6S>A}$ and TDP1$_{TR}^{6S>D}$			Only in TDP1$_{TR}^{6S>A}$			Only in TDP1$_{TR}^{6S>D}$		
ID	**R**	**P (6S>A; 6S>D)**	**ID**	**R**	**P**	**ID**	**R**	**P**
TDP1	I, II, II, IV	41, 45, 41, 62; 43, 49, 44, 54	SIAH1	II, III	1, 3	LIG3	I, II	17,33
PARP1	I, II, III, IV	38, 15, 24, 27; 27, 33, 21, 20	PP2Aaα	I	2	CK1δ	II	12
UBA1	I, IV	24, 2; 8, 3	PP2Ac	II	3	CK1ε	II	9
XRCC1	I	2; 8	PP2Abα	II, IV	1, 1	CK1δ; ε	I	11
XRCC6	I, III, IV	25, 10, 7; 8, 6, 10	XRCC1	IV	2	XRCC1	II	7
XRCC5	I, IV	20, 5; 5, 5	PNK	III, IV	4, 4	XRCC5	II	4
SUMO2; SUMO4; SUMO3	III	2; 1	SUMO2; SUMO4; SUMO3	III	3	SUMO2; SUMO4; SUMO3	II	1
PP2Abα; δ	I	5; 2	XRCC5	III,IV	5, 7	XRCC6	II	4
PP2Aaα	I, IV	14, 3; 3, 5	LIG3	IV	1	SUMO2	I	2
PP2Abα	I, II, III	2, 3, 1, 2	CK1ε	III, IV	21, 16	SIAH1; SIAH2	II	2
CK1δ	III	11, 3	CK1δ	III, IV	11, 17	USP11	II, III	3, 3
SHMT	III	4; 4	CK1α;α-like	IV	25	PP2Ac	II	1
SIAH1	IV	5; 3	TRIM32	IV	8	PNK	I, II	4, 2
PGAM5, mito.	IV	2; 2				UBAP2l	I, II, III	1, 1, 3
USP11	IV	1; 4				UBA1	II, III	2, 4
E2N	IV	1; 2				PP2Aaα	III	4
						PGAM5, mito.	III	2
						TRIM32	III, IV	1, 2
						E2N	IV	1

TDP1 and its interacting partners
Kinases
Phosphatases
Ubiquitin ligases
Ubiquitin-associated proteins

(Deng et al., 2017; Ke et al., 2014; Schoenfeld et al., 2004; Wiltshire et al., 2010; Yu et al., 2016). It can specifically deubiquitylate hybrid ubiquitin-SUMO chains (Hendriks et al., 2015). The interaction between TDP1 and USP11 was confirmed by GFP co-immunoprecipitation of lysate from stable cell lines, expressing GFP-$TDP1_{TR}$ or free GFP (figure 7.11A), and immunoblotting. USP11 co-immunoprecipitated with $TDP1_{TR}$, but not free GFP, making TDP1 a potential target for USP11 deubiquitylation.

PP2A is one of 4 major phosphatases, which dephosphorylate virtually all phosphoproteins (Ingebritsen and Cohen, 1983). Mammalian PP2A consists of 3 subunits: scaffold subunit A (α or β isoform), structural subunit B (α, β or γ isoform), B' (α, β, γ, δ or ε isoforms) or B'', and catalytic subunit C (α and β isoforms) (Millward et al., 1999). Subunits A and C form a constitutive heterodimeric core, which can be further supplemented by one of the three B subunits. To test for TDP1 interaction with PP2A catalytic subunit (PP2Ac) stable cell lines, expressing $TDP1_{TR}^{WT}$, $TDP1_{TR}^{6S>A}$ and $TDP1_{TR}^{6S>D}$, were lysed and TDP1 was pulled-down (**figure 7.11B**). PP2Ac did not co-immunoprecipitate with any of the TDP1 variants.

7.2.7.2. Knockdown of PP2Ac does not alter TDP1 SUMOylation at K111

Phosphorylation is a very important post-translational modification, which serves as an intracellular signal between proteins and is crucial for homeostasis (Cordeiro et al., 2017). A constant equilibrium is thus normally kept by kinases and phosphatases, which add or remove a phosphoryl moiety, often in response to cellular ques. However, dysregulation of phosphorylation can lead to various diseases, such as cancer (Creixell et al., 2015) and immunodeficiency (Alsadeq et al., 2014).

TDP1 appears to be constitutively phosphorylated (Wells, 2014). As phosphorylation suppresses SUMOylation, a small proportion of TDP1 might get dephosphorylated in

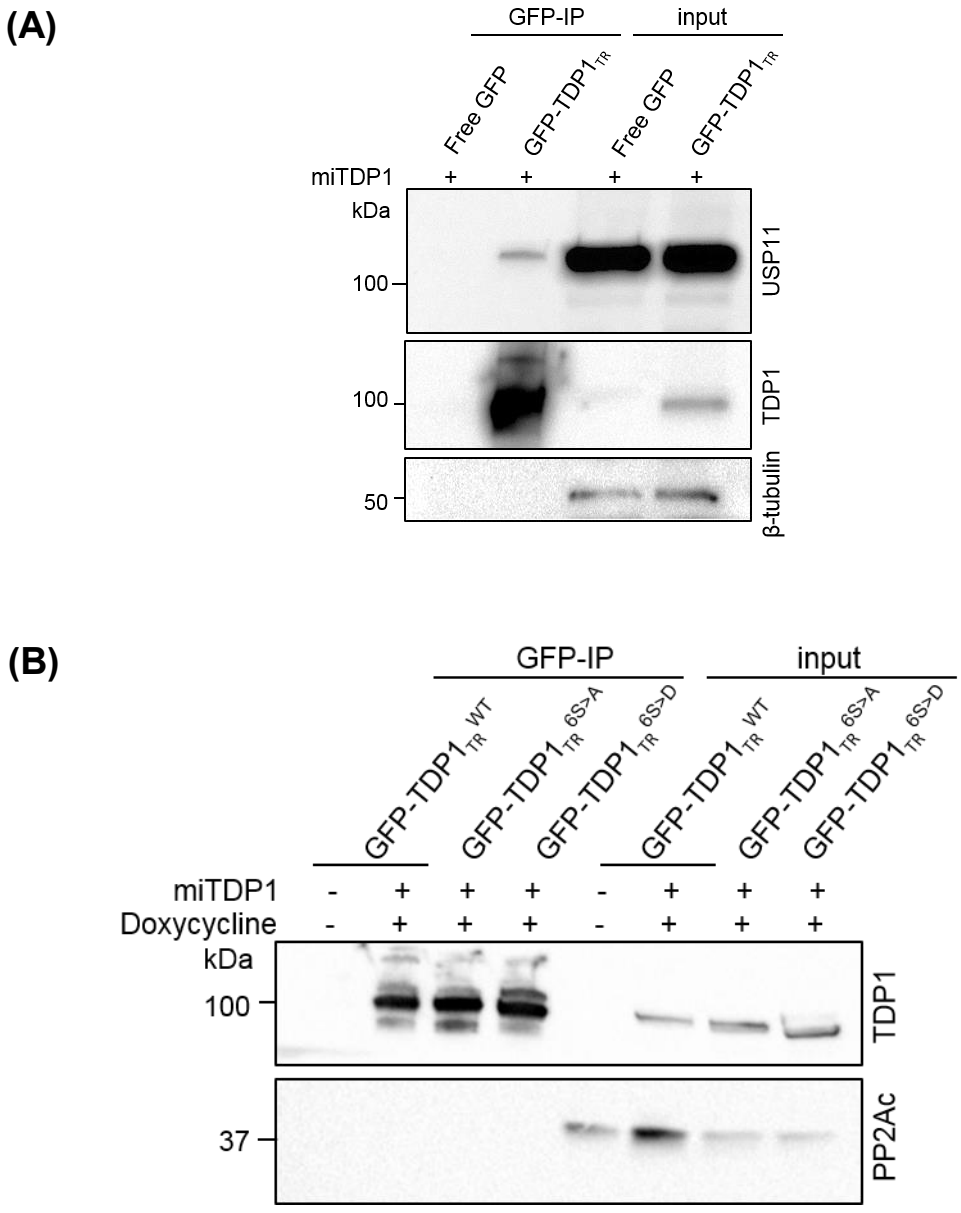

Figure 7.11. Validating mass spectrometry hits: USP11 interacts with TDP1, but PP2Ac does not. (A, B) Flp-In T-Rex 293 cells were induced with doxycycline and harvested 48 hours later, then subjected to GFP pull-down, SDS-PAGE and western blotting (sections 2.9.4 – 2.9.6 and 2.9.11). 40 – 50 µg of lysate were saved prior to the pull-down to be loaded as input.

response to DNA damage to allow SUMOylation, which promotes its accummulation at DNA damage sites (Hudson et al., 2012). A lack of interaction between PP2Ac and TDP1 by co-immunoprecipitation does not exclude the possibility that PP2A dephosphorylates TDP1. The interaction could be so transient that it is not picked up by Co-IP, or only happen under specific conditions, such as genotoxic stress. Therefore it was important to also confirm this by PP2A knockdown. If PP2A is dephosphorylating TDP1 at phosphoserines 13 – 15 and 90 – 92, then knockdown of PP2A should result in more phosphorylation and therefore less SUMOylation at K111. Immunoblotting of TDP1 and SUMO1-TDP1 complexes from HEK293 cells, transfected with TDP1, SUMO1 and αPP2Ac siRNA, however, showed no differences in SUMOylation levels, suggesting that PP2A is not regulating SUMOylation, at least under unstressed conditions **(figure 7.12)**.

7.2.7.3. Constitutive phosphorylation of TDP1 at serine 13 – 15 and 90 – 92 suppresses its interaction with LIG3α and PNK

DNA Ligase 3α (LIG3α) and Polynucleotide Kinase (PNK) form a complex with TDP1 and XRCC1 during TDP1-mediated SSBR, through a direct interaction between LIG3α and TDP1 N-terminus (Caldecott, 2008; El-Khamisy et al., 2005). This complex is crucial for successful TDP1-mediated TOP1-cc repair (El-Khamisy et al., 2005), as TDP1 cleaves the phosphotyrosyl bond, PNK processes the 3'-phosphate (Rasouli-Nia et al., 2004) and subsequent ligation of DNA ends is carried out by LIG3, all with the aid of XRCC1 scaffolding (Caldecott, 2003; Caldecott, 2008; Loizou et al., 2004; Whitehouse et al., 2001). Initial two repeats of mass spectrometry **(figure 7.10)** suggested a difference in binding of TDP1 to LIG3 and PNK between $TDP1_{TR}^{6S>A}$ and $TDP1_{TR}^{6S>D}$, and thus co-IP studies were carried out to confirm this observation **(figure**

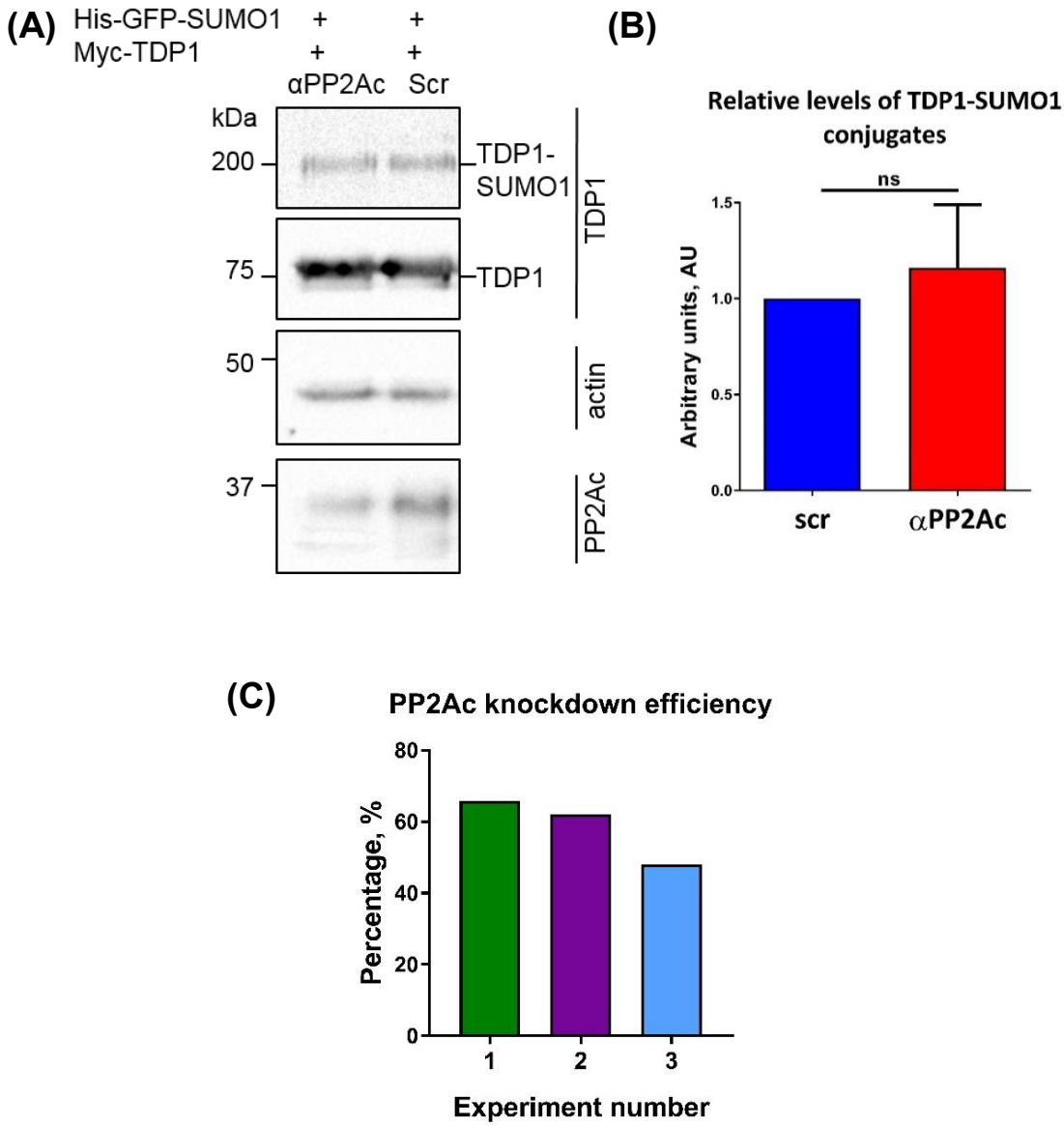

Figure 7.12. Validating mass spectrometry hits: PP2Ac knockdown does not alter TDP1-SUMO1 conjugate levels. (A) HEK293 cells were plated, co-transfected with myc-TDP1, his-GFP-SUMO1 and 50 nM αPP2Ac siRNA 24 hours later, then given a second hit of 100 nM siRNA after another 24 hours. The cells were harvested after a total of 48 hours from the first transfection, then subjected to SDS-PAGE and western blotting (sections 2.9.4 – 2.9.9); scr – scrambled siRNA control. **(B)** Quantification of 7.13A and two other similar PP2Ac knockdown experiments (2 and 3), all with ~50 – 70 % knockdown efficiency. In experiment number 2, HEK293 cells were plated, co-transfected with myc-TDP1 and his-GFP-SUMO1 after 24 hours, then 6 hours later transfected with 50 nM αPP2Ac siRNA and given a second hit of 100 nM siRNA after another 14 hours. The cells were harvested after a total of 48 hours from the first transfection, then subjected to SDS-PAGE and western blotting (sections 2.9.4 – 2.9.9). In experiment number 3, HEK293 cells were plated, transfected with 50 nM siRNA 24 hours later, then co-transfected with myc-TDP1 and his-GFP-SUMO1 another 24 hours later, then given a second hit of 50 nM siRNA after another 24 hours. The cells were harvested after a total of 72 hours after the first transfection, then subjected to SDS-PAGE and western blotting (sections 2.9.4 – 2.9.9). Relative levels of TDP1-SUMO1 conjugates were quantified in relation to TDP1-SUMO1 conjugates in the scrambled (scr) siRNA-treated controls, the intensity of which was arbitrarily set to 1. n=3, ±SEM. *p* values were calculated using a two-tailed Student's T-test. **(C)** Knockdown efficiencies in experiments 1-3 were plotted as a percentage of PP2Ac knockdown in relation to scrambled siRNA (scr) treated control.

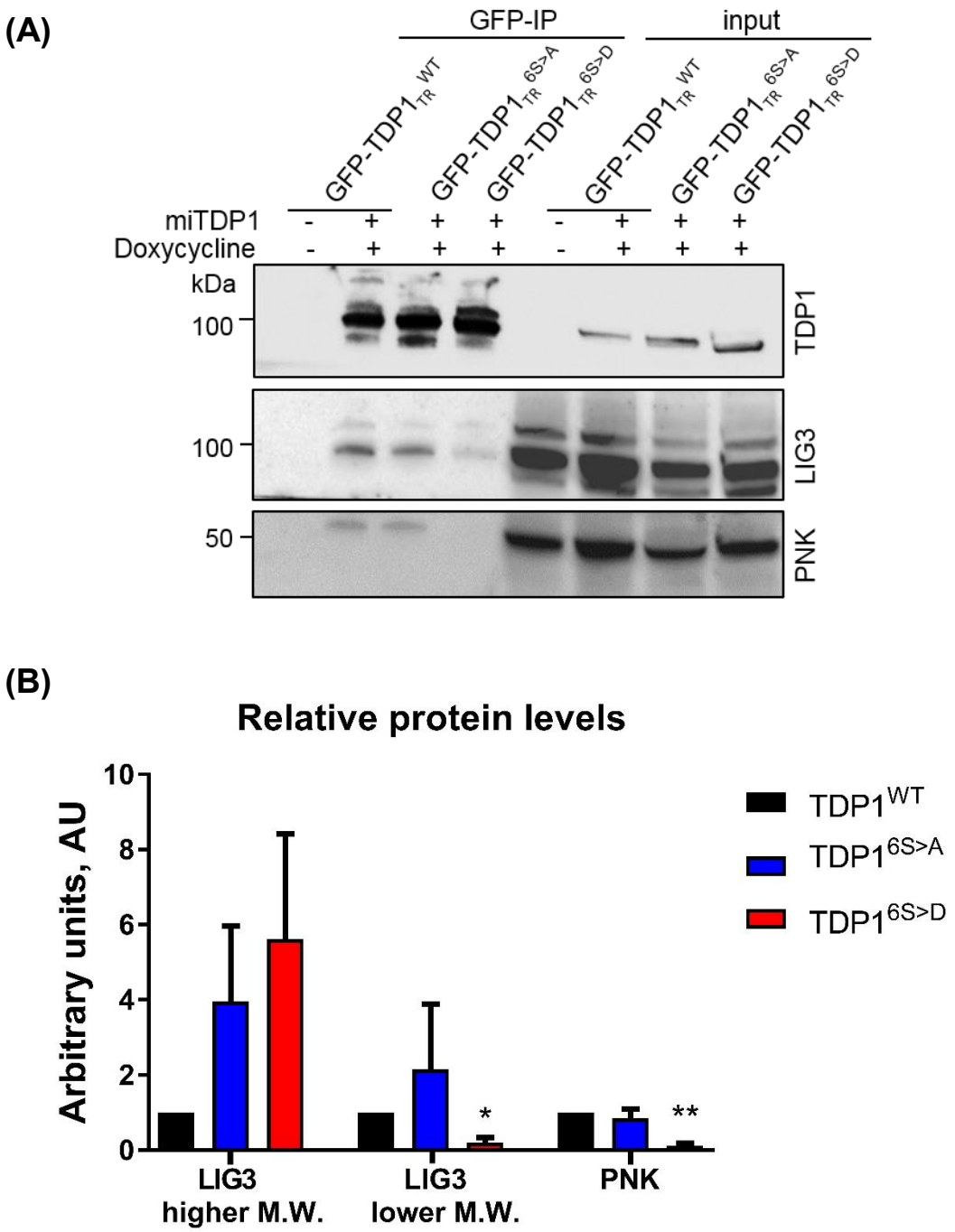

Figure 7.13. Validating mass spectrometry hits: constitutive phosphorylation of TDP1 at serines 13 – 15 and 90-92 suppresses its interaction with LIG3 and PNK. (A) Flp-In T-Rex 293 cells were induced with doxycycline and harvested 48 hours later, then subjected to GFP pull-down, SDS-PAGE and western blotting (sections 2.9.4 – 2.9.6 and 2.9.11). 40 – 50 µg of lysate were saved prior to the pull-down to be loaded as input. **(B)** Quantification of 7.14A. Levels of each protein in $TDP1^{WT}$ lane were given a value of 1 and the protein levels in the mutant lanes were quantified relative to $TDP1^{WT}$. Values were then normalized to the appropriate TDP1 IP; M.W. – molecular weight. Data is the mean of three independent repeats (4 for PNK) ±SEM. *p* values were calculated using a repeated measures one-way ANOVA.

7.13). Stable cell lines, expressing $TDP1_{TR}^{WT}$, $TDP1_{TR}^{6S>A}$ and $TDP1_{TR}^{6S>D}$, were lysed and TDP1 was pulled-down with GFP beads, then immunoblotting was performed for PNK, LIG3 and TDP1. Strikingly, interaction with the lower molecular weight LIG3 was significantly impaired in the presence of $TDP1_{TR}^{6S>D}$, and subsequently the interaction with PNK. An increase in co-immunoprecipitation of the higher molecular weight LIG3 was also noted in both $TDP1_{TR}^{6S>A}$ and $TDP1_{TR}^{6S>D}$ in comparison to $TDP1_{TR}^{WT}$ but was not significant. These results suggest that phosphorylation at serines 13 – 15 and 90 – 92 suppresses TDP1 interaction with SSBR machinery.

7.3. Discussion

This chapter describes the identification and characterization of phosphorylation sites S13 – 15 and S90 – 92 in TDP1 N-terminus by utilizing their phosphomimetic and phosphomutant variants. I have demonstrated that phosphorylation at these sites suppresses SUMOylation at lysine 111, a PTM that promotes TDP1 accumulation at sites of DNA damage. This could be due to a conformational change of TDP1 caused by the phosphorylation, which prevents the access of the E2 conjugating enzyme UBC9 and/or an E3 SUMO ligase. It was expected that such suppression of SUMOylation would result in increased DNA damage due to its role in TDP1-mediated DNA damage repair. However, quantification of 53BP1 foci before and after CPT treatment reveals no increase in DSB levels. In the future alkaline comet assays, which primarily measure SSBs, could be used for this purpose, as data in our lab suggests they are more sensitive for detecting SSBs in T-REx 293 cells. However, I will need to generate a homogenous population of cells to perform comet assays, which is not required for readouts using IF.

Two LIG3 bands were recovered after $TDP1_{TR}^{6S>A}$ and $TDP1_{TR}^{6S>D}$ pull-down. They may be nuclear and mitochondrial LIG3α isoforms or reflect a post-translational modification of any of the isoforms (Lakshmipathy and Campbell, 1999; Mackey et al., 1997; Nash et al., 1997). It is unlikely to be LIG3β, which is normally only found in germ cells and has not been shown to interact with TDP1, as opposed to LIG3α (El-Khamisy et al., 2005). Phosphomimetic TDP1 appears to have a significant defect in interacting with the lower molecular weight LIG3 and thus also pulls down less PNK, which is normally found in a complex with LIG3/XRCC1 heterodimer, than wild-type TDP1. This data may thus suggest that phosphorylation at S13 – 15 and S90 – 92 suppresses TDP1 interaction with SSBR machinery. It seems unlikely, however that this is a result of impaired SUMOylation as the $TDP1^{K111R}$ mutant did not show any differences in binding of LIG3α (Hudson et al., 2012). In addition, experiments with kinase-dead CK2 and TBB suggest that CK2 is not the primary kinase phosphorylating these sites, as previously predicted by *in vitro* (Wells, 2014) and *in silico* studies.

Mass spectrometry analysis picked up potential novel binding partners of TDP1, two of which, USP11 and PP2A, were tested for interaction with TDP1. Nitrocellulose membranes from previous experiments did not show an interaction between TDP1 and PP2Ac when reprobed for PP2Ac, nor did PP2Ac knockdown affect TDP1 SUMOylation at lysine 111, suggesting that in physiological conditions PP2A is not the phosphatase responsible for regulating SUMOylation. In the future the effects of PP2A knockdown should be carried out in different conditions, for example after CPT challenge, and antibodies for different subunits of PP2A could be used for immunoblotting after TDP1 co-IP. However, if no effects or interactions are observed a different phosphatase may need to be considered. USP11 was found to interact

with TDP1 and, although it does not appear to be related to the SUMO1 site and phosphorylation sites of interest, the possibility of TDP1 deubiquitylation by USP11 should further be investigated due to the involvement of USP11 in DNA damage repair (Deng et al., 2017; Ke et al., 2014; Schoenfeld et al., 2004; Wiltshire et al., 2010; Yu et al., 2016). CK1 was the only kinase identified by mass spectrometry analysis, and although there is evidence it phosphorylates certain non-canonical sequences (Marin et al., 2003) or that phosphorylation may depend on the tertiary structure of the protein substrate rather than sequence specificity (Cegielska et al., 1998), serines 13 – 15 and 90 – 92 score low or below threshold for CK1 phosphorylation in *in silico* phosphorylation analysis. However, phosphorylation of these serine clusters by CK1 cannot be fully ruled out due to possible non-canonical sequence phosphorylation and its presence in the mass spectrometry hits may indicate a role for CK1 in phosphorylation of other serine or threonine residues in TDP1. Involvement of CK1 could be tested in a similar manner to experiments carried out in this chapter for CK2 by using kinase-dead mutations and selective CK1 inhibitors.

In summary, phosphorylation sites S13 – 15 and S90 – 92 were identified in TDP1. Their phosphorylation suppresses SUMOylation at K111 and interaction with LIG3, which suggests a currently unidentified phosphatase is required to facilitate TDP1-mediated DNA repair. If the phosphatase or kinase is identified, they may present a valuable target for cancer therapy.

8

Discussion

8.1. Overview

TDP1 is an important single-strand break repair factor, involved in the repair of 3' lesions. The most notable of such lesions are TOP1 cleavage complexes (TOP1-CCs). The persistence of TOP1-CCs can interfere with replication and transcription, a quality that has been widely utilized in chemotherapy (Ashour et al., 2015). However, a lot is yet unclear about the exact role of TDP1 and other factors, such as ATM, spartan (SPRTN) and endonucleases, in the repair of TOP1-CCs. To further improve available treatments, these questions need to be addressed first.

The phenotype of SCAN1, which results from a recessive hypomorphic *TDP1*^{H493R} mutation, has provided as many answers as it has questions (Takashima et al., 2002). It is known that the cerebellum and peripheral nerves are selectively vulnerable to this mutation, but it is not known why. It is also known that such neurodegeneration progresses slowly over time. It is known how the mutation affects TDP1 activity and that it creates TDP1-DNA intermediates, however, it is not known how exactly this leads to the SCAN1 phenotype and what is the underlying reason of selective vulnerability of specific neuronal tissues (El-Khamisy et al., 2005; Interthal et al., 2005b; Miao et al., 2006).

The aim of this thesis was to generate and characterize a humanized SCAN1 zebrafish model to help answer these questions. Another aim was to generate a *tdp1*$^{-/-}$ zebrafish to allow a more extensive interrogation of the expected mild phenotype of loss of Tdp1 in a more tractable animal model than mice, offering the option to carry out behaviour analysis with high animal numbers. In order to exacerbate this phenotype, it was also aimed to cross the *tdp1*$^{-/-}$ zebrafish to mutants of other genes,

known to be involved in the regulation of Top1-CCs or maintaining genomic stability, such as *atm*. The final goal was to increase understanding of post-translational modifications that evolved in higher eukaryotes with the acquisition of the N-terminus, allowing for more complex regulation of TDP1.

8.2. Lessons from *tdp1*$^{-/-}$ zebrafish

In chapters 3 and 4 I discuss the finding that *tdp1*$^{-/-}$ zebrafish are viable, but express a trend of mild behavioural deficiencies and a trend of hypersensitivity to topotecan at adulthood. Overall, my findings agree with the *Tdp1*$^{-/-}$ mouse studies by Katyal *et al*. (2007), Hirano *et al.* (2007) and Hawkins *et al. (2009)*, who all found that *Tdp1*$^{-/-}$ mice are viable. In addition, Katyal *et al*. and Hirano *et al.* observed hypersensitivity to TOP1 poisons, similarly to the trend observed in adult fish. However, only Katyal *et al.*, observed pathologies, namely a mild age-related reduction in cerebellar mass and hypoalbuminemia in *Tdp1*$^{-/-}$ mice, neither of which were measured in this thesis or in the other two studies. Although behavioural analysis of *Tdp1*$^{-/-}$ mice by Hawkins and co-workers showed no significant abnormalities, I did observe statistically significant differences in behaviour of *tdp1*$^{-/-}$ zebrafish in a few of the recorded time-points in two of the analysed six locomotion parameters. This is likely because I used a lot more animals in the experiment. However, it is difficult to make a clear conclusion from my data and thus in the future even more animals need to be analysed.

Had I been successful in generating a humanized SCAN1 zebrafish model, it would have added some invaluable insights into the question of whether loss of Tdp1 is

deleterious, or if the SCAN1 phenotype is caused by the specific neomorphic mutation. In chapter 5, I have outlined the issues I encountered and have made several suggestions to evade those issues for future follow-up studies, such as the use of a different promoter or transgene reporter. It should facilitate the generation of a SCAN1 transgenic zebrafish, if it is attempted again in the future. Without the availability of this model, I can only speculate that perhaps the phenotypes exhibited by animal models do not sufficiently recapitulate the human phenotype due to differences in life span or the species. However, I cannot rule out the hypothesis that the TDP1-DNA complexes in SCAN1 are more toxic to neurons than TOP1-CCs alone.

Another striking observation that I have made in regards to the *tdp1*$^{-/-}$ zebrafish is the lack of hypersensitivity to CPT in *tdp1*$^{-/-}$ embryos. Although no attempt has been made to test for this in embryonic stages of other models, hypersensitivity to TOP1 poisons and other SSB-inducing agents, such as IR and H_2O_2, has always been observed in TDP1-deficient cells and organisms (Alagoz et al., 2014; El-Khamisy et al., 2009; Guo et al., 2014; Katyal et al., 2014). This strongly suggests the presence of alternative pathways in the zebrafish embryo, which are fully capable of Top1-CC repair, even in conditions with elevated Top1-CCs. Although I have been unable to pinpoint one pathway, which compensated for loss of Tdp1 significantly, this phenomenon should be investigated in the future. If the trend of topotecan hypersensitivity in adults can be confirmed with higher animal numbers, this would suggest that compensatory mechanisms are compromised or overwhelmed in the adult animals. Identifying the compensation mechanism may thus be key to

explaining selective vulnerability of the cerebellum to accumulation of protein-linked breaks (PDBs).

On the other hand, cancerous cells are known to be able to switch on the expression of genes which are normally only active throughout development (Emons et al., 2017; Reya and Clevers, 2005; Suzuki et al., 2004; Wu et al., 2017). If such a pathway is available to human cancers, it would negate the effects of TOP1 poisons in chemotherapy. Therefore, elucidating the pathway in zebrafish embryos could provide invaluable insight for the development of adjuvants in cancer therapy. Identification of the compensatory pathway could be done by large scale microarray analysis or using specific inhibitors and morpholinos for potential compensation candidates. Furthermore, large-scale chemical screens would allow the detection of potential factors not previously implicated in PDB repair mechanisms. Attempts were made to develop a ChIP-MS assay, where Top1-CCs would be pulled down after chromatin immunoprecipitation (ChIP) together with all the proteins surrounding the lesion, and such proteins would then be identified by mass spectrometry (MS). However, it is unclear whether the antibody is suitable for ChIP experiments and more optimization is required in the future.

8.3. Findings in other PDB models and their potential

The other generated zebrafish PDB models, discussed in chapter 6, may also prove a useful resource for studying compensatory pathways, particularly the *atm*$^{-/-}$ and *atm*$^{-/-}$; *tdp1*$^{-/-}$ zebrafish models. ATM is a master kinase in DDR, which phosphorylates TDP1, but has also been implicated in TOP1-CC repair in a TDP1-independent manner

(Chiang et al., 2010; Das et al., 2009). A*tm*$^{-/-}$ zebrafish were viable, which agrees with studies of mice and rats (Barlow et al., 1996; Quek et al., 2017). Strikingly, the double mutant was also viable in contrast to the *Atm*$^{-/-}$*; Tdp1*$^{-/-}$ mice, which die *in utero* (Katyal et al., 2014). This model would therefore allow the interrogation of Top1-CC repair in the absence of two important repair factors, which contribute to the repair of Top1-CCs independently of one another. Once again, a drug screen could be used to find a compound, which would selectively sensitize the double mutant, without affecting wild-type fish.

In addition, preliminary work by my colleague has suggested that *atm*$^{-/-}$ fish may have sex-related problems, such as female-to-male sex reversal and infertility, although embryonic behaviour analysis and adult swim tunnel showed normal results in both *atm*$^{-/-}$ and *atm*$^{-/-}$; *tdp1*$^{-/-}$ zebrafish. Such sex reversal has also been observed in zebrafish mutants of another HR factor, *brca2*, corroborating my colleague's results (Rodriguez-Mari et al., 2011; van Eeden, unpublished). Any effects observed from loss of Tdp1 should be compounded in the double mutants. Thus the *atm*$^{-/-}$ model, particularly in conjunction with the *atm*$^{-/-}$; *tdp1*$^{-/-}$ zebrafish, can be used to learn more about the mechanism by which atm regulates Top1-CCs.

The *rnaseh2a*$^{-/-}$*; tdp1*$^{-/-}$, *tdp1*$^{-/-}$*; tg(sod1*^{G93R}*)*$^{-/+}$, *tdp1*$^{-/-}$*; tg(c9orf72)*$^{-/+}$ fish were all viable and normal by visual inspection. They are expected to exhibit additional genomic instability in relation to *tdp1* single mutants and thus have exacerbated phenotypes. This would hopefully facilitate future experiments by promoting any neurodegeneration that may be happening in the *tdp1*$^{-/-}$ fish and thus reducing the requirement for high numbers of animals. These models can also be utilized in

compensation studies in the future, as discussed in regards to the other models. Unfortunately, due to time constraints no further work was carried out.

The fact that *rnaseh2a*$^{-/-}$and *rnaseh2a*$^{-/-}$*; tdp1*$^{-/-}$ fish were viable was very surprising, as mouse knockouts of the other two Rnaseh2 subunits, b and c, were embryonic lethal (Hiller et al., 2012; Reijns et al., 2012). In addition, only hypomorphic mutations of *RNaseH2* are found in humans with Aicardi-Goutières Syndrome, suggesting that complete loss of RNase H2 function is incompatible with life (Crow et al., 2015; Perrino et al., 2009). Hence, the zebrafish once again provides a system to study loss of Tdp1 function in a background which is unachievable in mouse models.

8.4. Post-translational regulation of TDP1

I identified phosphorylation sites at serines 13 – 15 and 90 – 92 in human TDP1. Phosphorylation at these sites suppresses SUMOylation at lysine 111 and interaction with the SSBR factors LIG3 and PNK. I suggest these effects of phosphorylation may be imposed by the induction of conformational changes in the structure of TDP1, which could prevent access of the E2 conjugating enzyme UBC9 and/or an E3 SUMO ligase to lysine 111 and reduce TDP1 affinity for LIG3. This would in turn lead to less PNK being pulled down through LIG3 interaction with XRCC1 (Caldecott et al., 1994; Caldecott et al., 1995). The impaired interactions are likely not a result of SUMOylation itself, as it has been shown that TDP1^{K111R} SUMOylation mutant interacts with LIG3 at normal levels (Hudson et al., 2012). Although I have been unable to identify the kinase or phosphatase responsible, my experiments suggest that CK2 is not the primary kinase and PP2A is not the primary phosphatase which

regulates TDP1 SUMOylation. Nevertheless, mass spectrometry studies have identified CK1 as a potential binding partner for TDP1. This could be first tested using selective CK1 kinase inhibitors, such as D4476 (Rena et al., 2004), or kinase-dead CK1 in cells transfected with TDP1 N-terminus, similarly to my experiments with CK2. Interaction between CK1 and TDP1 could be confirmed by co-immunoprecipitation and/or yeast two-hybrid assays.

8.5. Summary

In short, the original contribution of this thesis is the generation and characterization of the novel *tdp1*$^{-/-}$ zebrafish model, the generation and part characterization of *atm*$^{-/-}$, *atm*$^{-/-}$; *tdp1*$^{-/-}$, *rnaseh2*$^{-/-}$, *rnaseh2*$^{-/-}$; *tdp1*$^{-/-}$, *tdp1*$^{-/-}$; *tg(sod1*^{G93R}*)*$^{-/+}$ and *tdp1*$^{-/-}$; *tg(c9orf72)*$^{-/+}$ zebrafish and the finding of SUMOylation and LIG3 and PNK interaction-suppressing novel phosphorylation sites in the N-terminus of human TDP1. These findings and zebrafish models can be utilized in further interrogating the selective vulnerability question of SCAN1 and for identification of potential adjuvants to be used in conjunction with TOP1 poisons in cancer therapy.

References

Adolf, B., Chapouton, P., Lam, C.S., Topp, S., Tannhauser, B., Strahle, U., Gotz, M., and Bally-Cuif, L. (2006). Conserved and acquired features of adult neurogenesis in the zebrafish telencephalon. Dev Biol *295*, 278-293.

Aguilera, A., and Garcia-Muse, T. (2012). R Loops: From Transcription Byproducts to Threats to Genome Stability. Molecular Cell *46*, 115-124.

Ahel, I., Rass, U., El-Khamisy, S.F., Katyal, S., Clements, P.M., McKinnon, P.J., Caldecott, K.W., and West, S.C. (2006). The neurodegenerative disease protein aprataxin resolves abortive DNA ligation intermediates. Nature *443*, 713-716.

Ahmad, M., Xue, Y., Lee, S.K., Martindale, J.L., Shen, W., Li, W., Zou, S., Ciaramella, M., Debat, H., Nadal, M*., et al.* (2016). RNA topoisomerase is prevalent in all domains of life and associates with polyribosomes in animals. Nucleic Acids Res *44*, 6335-6349.

Akitake, C.M., Macurak, M., Halpern, M.E., and Goll, M.G. (2011). Transgenerational analysis of transcriptional silencing in zebrafish. Developmental Biology *352*, 191-201.

Al-Salihi, M.A., Herhaus, L., Macartney, T., and Sapkota, G.P. (2012). USP11 augments TGFβ signalling by deubiquitylating ALK5.

Alagoz, M., Chiang, S.-C., Sharma, A., and El-Khamisy, S.F. (2013). ATM Deficiency Results in Accumulation of DNA-Topoisomerase I Covalent Intermediates in Neural Cells. PloS one *8*, e58239.

Alagoz, M., Wells, O.S., and El-Khamisy, S.F. (2014). TDP1 deficiency sensitizes human cells to base damage via distinct topoisomerase I and PARP mechanisms with potential applications for cancer therapy. Nucleic Acids Research *42*, 3089-3103.

Alsadeq, A., Hobeika, E., Medgyesi, D., Klasener, K., and Reth, M. (2014). The role of the Syk/Shp-1 kinase-phosphatase equilibrium in B cell development and signaling. J Immunol *193*, 268-276.

Amores, A., Force, A., Yan, Y.L., Joly, L., Amemiya, C., Fritz, A., Ho, R.K., Langeland, J., Prince, V., Wang, Y.L*., et al.* (1998). Zebrafish hox clusters and vertebrate genome evolution. Science *282*, 1711-1714.

Amsterdam, A., Nissen, R.M., Sun, Z., Swindell, E.C., Farrington, S., and Hopkins, N. (2004). Identification of 315 genes essential for early zebrafish development.

Arvidsson, A., Collin, T., Kirik, D., Kokaia, Z., and Lindvall, O. (2002). Neuronal replacement from endogenous precursors in the adult brain after stroke. Nat Med *8*, 963-970.

Ashour, M.E., Atteya, R., and El-Khamisy, S.F. (2015). Topoisomerase-mediated chromosomal break repair: an emerging player in many games. Nature Reviews Cancer *15*, 137-151.

Ata, H., Clark, K.J., and Ekker, S.C. (2016). The zebrafish genome editing toolkit. Zebrafish: Genetics, Genomics, and Transcriptomics, 4th Edition *135*, 149-170.

Avemann, K., R, K., T, K., JM, S., Fakultät für Biologie, U.K., Federal Republic of Germany., Avemann, K., Knippers, R., Koller, T., and Sogo, J.M. (1988). Camptothecin, a specific inhibitor of type I DNA topoisomerase, induces DNA breakage at replication forks.

Bae, Y.-K., Kani, S., Shimizu, T., Tanabe, K., Nojima, H., Kimura, Y., Higashijima, S.-i., and Hibi, M. (2009). Anatomy of zebrafish cerebellum and screen for mutations affecting its development. Developmental Biology *330*, 406-426.

Bai, Q., Wei, X.Y., and Burton, E.A. (2009). Expression of a 12-kb promoter element derived from the zebrafish enolase-2 gene in the zebrafish visual system. Neuroscience Letters *449*, 252-257.

Bandmann, O., and Burton, E.A. (2010). Genetic zebrafish models of neurodegenerative diseases. Neurobiology of Disease *40*, 58-65.

Barker, S., Weinfeld, M., and Murray, D. (2005). DNA-protein crosslinks: their induction, repair, and biological consequences. Mutation Research-Reviews in Mutation Research *589*, 111-135.

Barlow, C., Hirotsune, S., Paylor, R., Liyanage, M., Eckhaus, M., Collins, F., Shiloh, Y., Crawley, J.N., Ried, T., Tagle, D.*, et al.* (1996). Atm-deficient mice: A paradigm of ataxia telangiectasia. Cell *86*, 159-171.

Barrangou, R., Fremaux, C., Deveau, H., Richards, M., Boyaval, P., Moineau, S., Romero, D.A., and Horvath, P. (2007). CRISPR provides acquired resistance against viruses in prokaryotes. Science *315*, 1709-1712.

Barzilai, A., Rotman, G., and Shiloh, Y. (2002). ATM deficiency and oxidative stress: a new dimension of defective response to DNA damage. DNA Repair *1*, 3-25.

Baxendale, S., Holdsworth, C.J., Meza Santoscoy, P.L., Harrison, M.R., Fox, J., Parkin, C.A., Ingham, P.W., and Cunliffe, V.T. (2012). Identification of compounds with anti-convulsant properties in a zebrafish model of epileptic seizures. Dis Model Mech *5*, 773-784.

Beck, C., Robert, I., Reina-San-Martin, B., Schreiber, V., and Dantzer, F. (2014). Poly(ADP-ribose) polymerases in double-strand break repair: Focus on PARP1, PARP2 and PARP3. Experimental Cell Research *329*, 18-25.

Bhuller, Y., Jeng, W., and Wells, P.G. (2017). Variable In Vivo Embryoprotective Role for Ataxia-Telangiectasia–Mutated against Constitutive and Phenytoin-Enhanced Oxidative Stress in Atm Knockout Mice. Toxicological Sciences *93*, 146-155.

Bibikova, M., Beumer, K., Trautman, J.K., and Carroll, D. (2003). Enhancing gene targeting with designed zinc finger nucleases. Science *300*, 764.

Bibikova, M., Carroll, D., Segal, D.J., Trautman, J.K., Smith, J., Kim, Y.G., and Chandrasegaran, S. (2001). Stimulation of homologous recombination through targeted cleavage by chimeric nucleases. Mol Cell Biol *21*, 289-297.

Bibikova, M., Golic, M., Golic, K.G., and Carroll, D. (2002). Targeted chromosomal cleavage and mutagenesis in Drosophila using zinc-finger nucleases. Genetics *161*, 1169-1175.

Bidwai, A.P., Hanna, D.E., and Glover, C.V.C. (1992). PURIFICATION AND CHARACTERIZATION OF CASEIN KINASE-II (CKII) FROM DELTA-CKA1 DELTA-CKA2 SACCHAROMYCES-CEREVISIAE RESCUED BY DROSOPHILA CKII SUBUNITS - THE FREE CATALYTIC SUBUNIT OF CASEIN KINASE-II IS NOT TOXIC INVIVO. Journal of Biological Chemistry *267*, 18790-18796.

Bladen, C.L., Lam, W.K., Dynan, W.S., and Kozlowski, D.J. (2005). DNA damage response and Ku80 function in the vertebrate embryo. Nucleic Acids Research *33*, 3002-3010.

Bladen, C.L., Navarre, S., Dynan, W.S., and Kozlowski, D.J. (2007). Expression of the Ku70 subunit (XRCC6) and protection from low dose ionizing radiation during zebrafish embryogenesis. Neuroscience Letters *422*, 97-102.

Blanco-Vives, B., and Sánchez-Vázquez, F.J. (2009). Synchronisation to light and feeding time of circadian rhythms of spawning and locomotor activity in zebrafish. Physiology & Behavior *98*, 268-275.

Blom, N., Sicheritz-Ponten, T., Gupta, R., Gammeltoft, S., and Brunak, S. (2004). Prediction of post-translational glycosylation and phosphorylation of proteins from the amino acid sequence. Proteomics *4*, 1633-1649.

Boch, J., Scholze, H., Schornack, S., Landgraf, A., Hahn, S., Kay, S., Lahaye, T., Nickstadt, A., and Bonas, U. (2009). Breaking the code of DNA binding specificity of TAL-type III effectors. Science *326*, 1509-1512.

Boehler, C., Gauthier, L.R., Mortusewicz, O., Biard, D.S., Saliou, J.M., Bresson, A., Sanglier-Cianferani, S., Smith, S., Schreiber, V., Boussin, F.*, et al.* (2011). Poly(ADP-ribose) polymerase 3 (PARP3), a newcomer in cellular response to DNA damage and mitotic progression. Proceedings of the National Academy of Sciences of the United States of America *108*, 2783-2788.

Bras, J., Alonso, I., Barbot, C., Costa, M.M., Darwent, L., Orme, T., Sequeiros, J., Hardy, J., Coutinho, P., and Guerreiro, R. (2015). Mutations in PNKP Cause Recessive Ataxia with Oculomotor Apraxia Type 4. American Journal of Human Genetics *96*, 474-479.

Brett, J.R. (1964). THE RESPIRATORY METABOLISM AND SWIMMING PERFORMANCE OF YOUNG SOCKEYE SALMON. Journal of the Fisheries Research Board of Canada *21*, 1183-1226.
Bruijn, L.I., Miller, T.M., and Cleveland, D.W. (2004). Unraveling the mechanisms involved in motor neuron degeneration in ALS. Annual Review of Neuroscience *27*, 723-749.

Bryson-Richardson, R.J., Berger, S., Schilling, T.F., Hall, T.E., Cole, N.J., Gibson, A.J., Sharpe, J., and Currie, P.D. (2007). FishNet: an online database of zebrafish anatomy. Bmc Biology *5*.

Burket, C.T., Montgomery, J.E., Thummel, R., Kassen, S.C., LaFave, M.C., Langenau, D.M., Zon, L.I., and Hyde, D.R. (2008). Generation and characterization of transgenic zebrafish lines using different ubiquitous promoters. Transgenic Res *17*, 265-279.

Caldecott, K.W. (2003). XRCC1 and DNA strand break repair. DNA Repair *2*, 955-969.

Caldecott, K.W. (2008). Single-strand break repair and genetic disease. Nature Reviews Genetics *9*, 619-631.

Caldecott, K.W., McKeown, C.K., Tucker, J.D., Ljungquist, S., and Thompson, L.H. (1994). AN INTERACTION BETWEEN THE MAMMALIAN DNA-REPAIR PROTEIN XRCC1 AND DNA LIGASE-III. Molecular and Cellular Biology *14*, 68-76.

Caldecott, K.W., Tucker, J.D., Stanker, L.H., and Thompson, L.H. (1995). Characterization of the XRCC1-DNA ligase III complex in vitro and its absence from mutant hamster cells. Nucleic Acids Research *23*, 4836-4843.

Campos, E.I., and Reinberg, D. (2009). Histones: Annotating Chromatin. Annual Review of Genetics *43*, 559-599.

Candy, J., and Collet, C. (2005). Two tyrosine hydroxylase genes in teleosts. Biochimica et Biophysica Acta (BBA) - Gene Structure and Expression *1727*, 35-44.

Carneiro, M.C., Henriques, C.M., Nabais, J., Ferreira, T., Carvalho, T., and Ferreira, M.G. (2016). Short Telomeres in Key Tissues Initiate Local and Systemic Aging in Zebrafish. PLoS Genet *12*, e1005798.

Carroll, J., Page, T.K., Chiang, S.C., Kalmar, B., Bode, D., Greensmith, L., McKinnon, P.J., Thorpe, J.R., Hafezparast, M., and El-Khamisy, S.F. (2015). Expression of a pathogenic mutation of SOD1 sensitizes aprataxin-deficient cells and mice to oxidative stress and triggers hallmarks of premature ageing. In Hum Mol Genet, pp. 828-840.

Cegielska, A., Gietzen, K.F., Rivers, A., and Virshup, D.M. (1998). Autoinhibition of casein kinase I epsilon (CHI epsilon) is relieved by protein phosphatases and limited proteolysis. Journal of Biological Chemistry *273*, 1357-1364.

Cerritelli, S.M., and Crouch, R.J. (2009). Ribonuclease H: the enzymes in Eukaryotes. FEBS J *276*, 1494-1505.

Champoux, J.J. (2001). DNA topoisomerases: Structure, function, and mechanism. In Annual Review of Biochemistry, C.C. Richardson, J.N. Abelson, C.R.H. Raetz, and J.W. Thorner, eds., pp. 369-413.

Chattopadhyay, M., Durazo, A., Sohn, S.H., Strong, C.D., Gralla, E.B., Whitelegge, J.P., and Valentine, J.S. (2008). Initiation and elongation in fibrillation of ALS-linked superoxide dismutase. Proceedings of the National Academy of Sciences of the United States of America *105*, 18663-18668.

Chen, S., Oikonomou, G., Chiu, C.N., Niles, B.J., Liu, J., Lee, D.A., Antoshechkin, I., and Prober, D.A. (2013). A large-scale in vivo analysis reveals that TALENs are significantly more mutagenic than ZFNs generated using context-dependent assembly. In Nucleic Acids Res, pp. 2769-2778.

Chen, S., Paul, P., and Price, B.D. (2003a). ATM's leucine-rich domain and adjacent sequences are essential for ATM to regulate the DNA damage response. Oncogene *22*, 6332-6339.

Chen, S.K., Hsieh, W.A., Tsai, M.H., Chen, C.C., Hong, A.I., Wei, Y.H., and Chang, W.P. (2003b). Age-associated decrease of oxidative repair enzymes, human 8-oxoguanine DNA glycosylases (hOgg1), in human aging. J Radiat Res *44*, 31-35.

Chiang, S.-C., Carroll, J., and El-Khamisy, S.F. (2010). TDP1 serine 81 promotes interaction with DNA ligase III alpha and facilitates cell survival following DNA damage. Cell Cycle *9*, 588-595.

Chiang, S.C., Meagher, M., Kassouf, N., Hafezparast, M., McKinnon, P.J., Haywood, R., and El-Khamisy, S.F. (2017). Mitochondrial protein-linked DNA breaks perturb mitochondrial gene transcription and trigger free radical-induced DNA damage. Science Advances *3*.

Chiruvella, K.K., Liang, Z.B., and Wilson, T.E. (2013). Repair of Double-Strand Breaks by End Joining. Cold Spring Harbor Perspectives in Biology *5*.

Christoffels, A., Koh, E.G.L., Chia, J.-m., Brenner, S., Aparicio, S., and Venkatesh, B. (2018). Fugu Genome Analysis Provides Evidence for a Whole-Genome Duplication Early During the Evolution of Ray-Finned Fishes. Molecular Biology and Evolution *21*, 1146-1151.

Ciccia, A., and Elledge, S.J. (2010). The DNA Damage Response: Making It Safe to Play with Knives. Molecular Cell *40*, 179-204.

Cleveland, D.W. (1999). From Charcot to SOD1: Mechanisms of selective motor neuron death in ALS. Neuron *24*, 515-520.

Coffin, S.R., Hollis, T., and Perrino, F.W. (2011). Functional Consequences of the RNase H2A Subunit Mutations That Cause Aicardi-Goutières Syndrome*. In J Biol Chem, pp. 16984-16991.

Colon-Cruz, L., Kristofco, L., Crooke-Rosado, J., Acevedo, A., Torrado, A., Brooks, B.W., Sosa, M.A., and Behra, M. (2017). Alterations of larval photo-dependent swimming responses (PDR): New endpoints for rapid and diagnostic screening of aquatic contamination. Ecotoxicol Environ Saf *147*, 670-680.

Cooke, M.S., Evans, M.D., Dizdaroglu, M., and Lunec, J. (2003). Oxidative DNA damage: mechanisms, mutation, and disease. Faseb Journal *17*, 1195-1214.

Cordeiro, M.H., Smith, R.J., and Saurin, A.T. (2017). A fine balancing act: A delicate kinase-phosphatase equilibrium that protects against chromosomal instability and cancer. The International Journal of Biochemistry & Cell Biology.

Creixell, P., Schoof, E.M., Simpson, C.D., Longden, J., Miller, C.J., Lou, H.J., Perryman, L., Cox, T.R., Zivanovic, N., Palmeri, A.*, et al.* (2015). Kinome-wide Decoding of Network-Attacking Mutations Rewiring Cancer Signaling. Cell *163*, 202-217.

Crow, Y.J., Chase, D.S., Schmidt, J.L., Szynkiewicz, M., Forte, G.M.A., Gornall, H.L., Oojageer, A., Anderson, B., Pizzino, A., Helman, G.*, et al.* (2015). Characterization of Human Disease Phenotypes Associated with Mutations in TREX1, RNASEH2A, RNASEH2B, RNASEH2C, SAMHD1, ADAR, and IFIH1. American Journal of Medical Genetics Part A *167*, 296-312.

Crow, Y.J., and Rehwinkel, J. (2009). Aicardi-Goutières syndrome and related phenotypes: linking nucleic acid metabolism with autoimmunity. In Hum Mol Genet, pp. R130-136.

Culp, P., Nussleinvolhard, C., and Hopkins, N. (1991). HIGH-FREQUENCY GERM-LINE TRANSMISSION OF PLASMID DNA-SEQUENCES INJECTED INTO FERTILIZED ZEBRAFISH EGGS. Proceedings of the National Academy of Sciences of the United States of America *88*, 7953-7957.

Dai, J., Cui, X.J., Zhu, Z.Y., and Hu, W. (2010). Non-Homologous End Joining Plays a Key Role in Transgene Concatemer Formation in Transgenic Zebrafish Embryos. International Journal of Biological Sciences *6*, 756-768.

Dang, M., Henderson, R.E., Garraway, L.A., and Zon, L.I. (2016). Long-term drug administration in the adult zebrafish using oral gavage for cancer preclinical studies. In Dis Model Mech, pp. 811-820.

Dantuma, N.P., and van Attikum, H. (2016). Spatiotemporal regulation of posttranslational modifications in the DNA damage response. Embo j *35*, 6-23.

Das, B.B., Antony, S., Gupta, S., Dexheimer, T.S., Redon, C.E., Garfield, S., Shiloh, Y., and Pommier, Y. (2009). Optimal function of the DNA repair enzyme TDP1 requires its phosphorylation by ATM and/or DNA-PK. Embo Journal *28*, 3667-3680.

Das, B.B., Huang, S.-y.N., Murai, J., Rehman, I., Ame, J.-C., Sengupta, S., Das, S.K., Majumdar, P., Zhang, H., Biard, D*., et al.* (2014). PARP1-TDP1 coupling for the repair of topoisomerase I-induced DNA damage. Nucleic Acids Research *42*, 4435-4449.

Date, H., Onodera, O., Tanaka, H., Iwabuchi, K., Uekawa, K., Igarashi, S., Koike, R., Hiroi, T., Yuasa, T., Awaya, Y*., et al.* (2001). Early-onset ataxia with ocular motor apraxia and hypoalbuminemia is caused by mutations in a new HIT superfamily gene. Nature Genetics *29*, 184-188.

Davies, D.R., Interthal, H., Champoux, J.J., and Hol, W.G.J. (2002). Insights into substrate binding and catalytic mechanism of human tyrosyl-DNA phosphodiesterase (Tdp1) from vanadate and tungstate-inhibited structures. Journal of Molecular Biology *324*, 917-932.

Davies, D.R., Interthal, H., Champoux, J.J., and Hol, W.G.J. (2003). Crystal structure of a transition state mimic for Tdp1 assembled from vanadate, DNA, and a topoisomerase I-derived peptide. Chemistry & Biology *10*, 139-147.

de Boer, J., and Hoeijmakers, J.H.J. (2000). Nucleotide excision repair and human syndromes. Carcinogenesis *21*, 453-460.

Delia, D., Piane, M., Buscemi, G., Savio, C., Palmeri, S., Lulli, P., Carlessi, L., Fontanella, E., and Chessa, L. (2004). MRE11 mutations and impaired ATM-dependent responses in an Italian family with ataxia-telangiectasia-like disorder. Hum Mol Genet *13*, 2155-2163.

Deng, C.C., Brown, J.A., You, D.Q., and Brown, J.M. (2005). Multiple endonucleases function to repair covalent topoisomerase I complexes in Saccharomyces cerevisiae. Genetics *170*, 591-600.

Deng, T., Yan, G., Zhou, Y., Hu, X., Li, J., Hu, J., Zhang, H., Feng, P., Sheng, X., Chen, J.*, et al.* (2017). Deubiquitylation and stabilization of p21 by USP11 is critical for cell cycle progression and DNA damage responses.

Detrich, H.W., III, Westerfield, M., and Zon, L.I. (2016). Mammalian Base Excision Repair: the Forgotten Archangel. Nucleic Acids Research *41*, 3483-3490.

Dohmen, R.J. (2004). SUMO protein modification. Biochimica Et Biophysica Acta-Molecular Cell Research *1695*, 113-131.

Dong, Q., Svoboda, K., Tiersch, T.R., and Monroe, W.T. (2007). Photobiological effects of UVA and UVB light in zebrafish embryos: Evidence for a competent photorepair system. J Photochem Photobiol B *88*, 137-146.

Dou, H., Huang, C., Nguyen, T.V., Lu, L.S., and Yeh, E.T.H. (2011). SUMOylation and de-SUMOylation in response to DNA damage. Febs Letters *585*, 2891-2896.

Doyon, Y., McCammon, J.M., Miller, J.C., Faraji, F., Ngo, C., Katibah, G.E., Amora, R., Hocking, T.D., Zhang, L., Rebar, E.J.*, et al.* (2008). Heritable targeted gene disruption in zebrafish using designed zinc-finger nucleases. Nat Biotechnol *26*, 702-708.

Draper, B.W., McCallum, C.M., Stout, J.L., Slade, A.J., and Moens, C.B. (2004). A high-throughput method for identifying N-ethyl-N-nitrosourea (ENU)-induced point mutations in zebrafish. Methods Cell Biol *77*, 91-112.

Draper, B.W., Morcos, P.A., and Kimmel, C.B. (2001). Inhibition of zebrafish fgf8 pre-mRNA splicing with morpholino oligos: a quantifiable method for gene knockdown. Genesis *30*, 154-156.

Dudley, D.D., Chaudhuri, J., Bassing, C.H., and Alt, F.W. (2005). Mechanism and control of V(D)J recombination versus class switch recombination: similarities and differences. Adv Immunol *86*, 43-112.

Dumitrache, L.C., and McKinnon, P.J. (2017). Polynucleotide kinase-phosphatase (PNKP) mutations and neurologic disease. Mechanisms of Ageing and Development *161*, 121-129.

Dunlop, J., Corominas, M., and Serras, F. (2000). The novel gene glaikit, is expressed during neurogenesis in the Drosophila melanogaster embryo. Mechanisms of Development *96*, 133-136.

Dunlop, J., Morin, X., Corominas, M., Serras, F., and Tear, G. (2004). glaikit is essential for the formation of epithelial polarity and neuronal development. Current Biology *14*, 2039-2045.
Dupré, A., Boyer-Chatenet, L., Sattler, R.M., Modi, A.P., Lee, J.H., Nicolette, M.L., Kopelovich, L., Jasin, M., Baer, R., Paull, T.T.*, et al.* (2008). A forward chemical genetic screen reveals an inhibitor of the Mre11–Rad50–Nbs1 complex. Nat Chem Biol *4*, 119-125.

Ekker, S.C. (2008). Zinc finger-based knockout punches for zebrafish genes. Zebrafish *5*, 121-123.

El Hage, A., French, S.L., Beyer, A.L., and Tollervey, D. (2010). Loss of Topoisomerase I leads to R-loop-mediated transcriptional blocks during ribosomal RNA synthesis. Genes & Development *24*, 1546-1558.

El-Khamisy, S.F. (2011). To live or to die: a matter of processing damaged DNA termini in neurons. Embo Molecular Medicine *3*, 78-88.

El-Khamisy, S.F., and Caldecott, K.W. (2006). TDP1-dependent DNA single-strand break repair and neurodegeneration. Mutagenesis *21*, 219-224.

El-Khamisy, S.F., Katyal, S., Patel, P., Ju, L., McKinnon, P.J., and Caldecott, K.W. (2009). Synergistic decrease of DNA single-strand break repair rates in mouse neural cells lacking both Tdp1 and aprataxin. DNA Repair *8*, 760-766.

El-Khamisy, S.F., Saifi, G.M., Weinfeld, M., Johansson, F., Helleday, T., Lupski, J.R., and Caldecott, K.W. (2005). Defective DNA single-strand break repair in spinocerebellar ataxia with axonal neuropathy-1. Nature *434*, 108-113.

Elshafey, A., Lanyon, W.G., and Connor, J.M. (1994). IDENTIFICATION OF A NEW MISSENSE POINT MUTATION IN EXON-4 OF THE CU/ZN SUPEROXIDE-DISMUTASE (SOD-1) GENE IN A FAMILY WITH AMYOTROPHIC-LATERAL-SCLEROSIS. Human Molecular Genetics *3*, 363-364.

Emons, G., Spitzner, M., Reineke, S., Moller, J., Auslander, N., Kramer, F., Hu, Y., Beissbarth, T., Wolff, H.A., Rave-Frank, M*., et al.* (2017). Chemoradiotherapy Resistance in Colorectal Cancer Cells is Mediated by Wnt/beta-catenin Signaling. Molecular Cancer Research *15*, 1481-1490.

Fan, L.C., Moon, J., Crodian, J., and Collodi, P. (2006). Homologous recombination in zebrafish ES cells. Transgenic Research *15*, 21-30.

Faust, M., and Montenarh, M. (2000). Subcellular localization of protein kinase CK2 - A key to its function? Cell and Tissue Research *301*, 329-340.

Feitsma, H., de Bruijn, E., van de Belt, J., Nijman, I.J., and Cuppen, E. (2008a). Mismatch repair deficiency does not enhance ENU mutagenesis in the zebrafish germ line. Mutagenesis *23*, 325-329.

Feitsma, H., Akay, A., Cuppen, E. (2008). Alkylation damage causes MMR-dependent chromosomal instability in vertebrate embryos. Nucleic Acids Research *36*, 4047-4056.

Feitsma, H., Kuiper, R.V., Korving, J., Nijman, I.J., and Cuppen, E. (2008b). Zebrafish with mutations in mismatch repair genes develop neurofibromas and other tumors. Cancer Research *68*, 5059-5066.

Feitsma, H., Leal, M.C., Moens, P.B., Cuppen, E., and Schulz, R.W. (2007). Mlh1 Deficiency in Zebrafish Results in Male Sterility and Aneuploid as Well as Triploid Progeny in Females.

Finley, K.R., Davidson, A.E., and Ekker, S.C. (2001). Three-color imaging using fluorescent proteins in living zebrafish embryos. Biotechniques *31*, 66-70, 72.

Flangas, A.L., and Bowman, R.E. (1970). DIFFERENTIAL METABOLISM OF RNA IN NEURONAL-ENRICHED AND GLIAL-ENRICHED FRACTIONS OF RAT CEREBRUM. Journal of Neurochemistry *17*, 1237-&.

Fleming, A., Diekmann, H., and Goldsmith, P. (2013). Functional Characterisation of the Maturation of the Blood-Brain Barrier in Larval Zebrafish. Plos One *8*.

Foley, J.E., Yeh, J.R., Maeder, M.L., Reyon, D., Sander, J.D., Peterson, R.T., and Joung, J.K. (2009). Rapid mutation of endogenous zebrafish genes using zinc finger nucleases made by Oligomerized Pool ENgineering (OPEN). PLoS One *4*, e4348.

Forterre, P., Gribaldo, S., Gadelle, D., and Serre, M.C. (2007). Origin and evolution of DNA topoisomerases. Biochimie *89*, 427-446.

Fortier, S., Yang, X., Bennett, R.A.O., Wang, Y., and Strauss, P.R. (2009). Base Excision Repair in Early Zebrafish Development: Evidence for DNA Polymerase Switching and Standby AP endonuclease Activity. Biochemistry *48*, 5396-5404.

French, S.L., Sikes, M.L., Hontz, R.D., Osheim, Y.N., Lambert, T.E., El Hage, A., Smith, M.M., Tollervey, D., Smith, J.S., and Beyer, A.L. (2011). Distinguishing the Roles of Topoisomerases I and II in Relief of Transcription-Induced Torsional Stress in Yeast rRNA Genes. Molecular and Cellular Biology *31*, 482-494.

Fridovich, I. (1986). SUPEROXIDE DISMUTASES. Advances in Enzymology and Related Areas of Molecular Biology *58*, 61-97.

Fu, C., Ahmed, K., Ding, H., Ding, X., Lan, J., Yang, Z., Miao, Y., Zhu, Y., Shi, Y., Zhu, J.*, et al.* (2005). Stabilization of PML nuclear localization by conjugation and oligomerization of SUMO-3. Oncogene *24*, 5401-5413.

Furukawa, Y., Kaneko, K., Yamanaka, K., O'Halloran, T.V., and Nukina, N. (2008). Complete loss of post-translational modifications triggers fibrillar aggregation of SOD1 in the familial form of amyotrophic lateral sclerosis. Journal of Biological Chemistry *283*, 24167-24176.

Furuta, T., Takemura, H., Liao, Z.Y., Aune, G.J., Redon, C., Sedelnikova, O.A., Pilch, D.R., Rogakou, E.P., Celeste, A., Chen, H.T.*, et al.* (2003). Phosphorylation of histone H2AX and activation of Mre11, Rad50, and Nbs1 in response to replication-dependent DNA double-strand breaks induced by mammalian DNA topoisomerase I cleavage complexes. Journal of Biological Chemistry *278*, 20303-20312.

Galanty, Y., Belotserkovskaya, R., Coates, J., Polo, S., Miller, K.M., and Jackson, S.P. (2009). Mammalian SUMO E3-ligases PIAS1 and PIAS4 promote responses to DNA double-strand breaks. Nature *462*, 935-U132.

Gareau, J.R., and Lima, C.D. (2010). The SUMO pathway: emerging mechanisms that shape specificity, conjugation and recognition. Nat Rev Mol Cell Biol *11*, 861-871.

Garg, L.C., Diangelo, S., and Jacob, S.T. (1987). ROLE OF DNA TOPOISOMERASE-I IN THE TRANSCRIPTION OF SUPERCOILED RIBOSOMAL-RNA GENE. Proceedings of the National Academy of Sciences of the United States of America *84*, 3185-3188.

Gasiunas, G., Barrangou, R., Horvath, P., and Siksnys, V. (2012). Cas9-crRNA ribonucleoprotein complex mediates specific DNA cleavage for adaptive immunity in bacteria. Proc Natl Acad Sci U S A *109*, E2579-2586.

Gaspar, P., and Lillesaar, C. (2012). Probing the diversity of serotonin neurons. Philosophical Transactions of the Royal Society B-Biological Sciences *367*, 2382-2394.

Genschel, J., Bazemore, L.R., and Modrich, P. (2002). Human exonuclease I is required for 5 ' and 3 ' mismatch repair. Journal of Biological Chemistry *277*, 13302-13311.

Gilbert, M.J., Zerulla, T.C., and Tierney, K.B. (2014). Zebrafish (Danio rerio) as a model for the study of aging and exercise: physical ability and trainability decrease with age. Exp Gerontol *50*, 106-113.

Giraldez, A.J., Mishima, Y., Rihel, J., Grocock, R.J., Dongen, S.V., Inoue, K., Enright, A.J., and Schier, A.F. (2006). Zebrafish MiR-430 Promotes Deadenylation and Clearance of Maternal mRNAs.

Girard, A., and Hannon, G.J. (2008). Conserved themes in small-RNA-mediated transposon control. Trends Cell Biol *18*, 136-148.

Goll, M.G., Anderson, R., Stainier, D.Y.R., Spradling, A.C., and Halpern, M.E. (2009). Transcriptional Silencing and Reactivation in Transgenic Zebrafish. In Genetics, pp. 747-755.
Goll, M.G., and Bestor, T.H. (2005). Eukaryotic cytosine methyltransferases. Annu Rev Biochem *74*, 481-514.

Gopalakrishnan, S., Sullivan, B.A., Trazzi, S., Della Valle, G., and Robertson, K.D. (2009). DNMT3B interacts with constitutive centromere protein CENP-C to modulate DNA methylation and the histone code at centromeric regions. In Hum Mol Genet, pp. 3178-3193.
Grabundzija, I., Irgang, M., Mátés, L., Belay, E., Matrai, J., Gogol-Döring, A., Kawakami, K., Chen, W., Ruiz, P., Chuah, M.K.L*., et al.* (2010). Comparative Analysis of Transposable Element Vector Systems in Human Cells. In Mol Ther, pp. 1200-1209.

Grandel, H., Kaslin, J., Ganz, J., Wenzel, I., and Brand, M. (2006). Neural stem cells and neurogenesis in the adult zebrafish brain: origin, proliferation dynamics, migration and cell fate. Dev Biol *295*, 263-277.

Grankowski, N., Boldyreff, B., and Issinger, O.G. (1991). ISOLATION AND CHARACTERIZATION OF RECOMBINANT HUMAN CASEIN KINASE-II SUBUNITS ALPHA AND BETA FROM BACTERIA. European Journal of Biochemistry *198*, 25-30.

Guillet, M., and Boiteux, S. (2002). Endogenous DNA abasic sites cause cell death in the absence of Apn1, Apn2 and Rad1/Rad10 in Saccharomyces cerevisiae. Embo Journal *21*, 2833-2841.

Guleria, A., and Chandna, S. (2016). ATM kinase: Much more than a DNA damage responsive protein. DNA Repair *39*, 1-20.

Guo, D., Dexheimer, T.S., Pommier, Y., and Nash, H.A. (2014). Neuroprotection and repair of 3 '-blocking DNA ends by glaikit (gkt) encoding Drosophila tyrosyl-DNA phosphodiesterase 1

(TDP1). Proceedings of the National Academy of Sciences of the United States of America *111*, 15816-15820.

Guo, S., Presnell, S.R., Gu, L., and Li, G.-M. (2004). Differential requirements for PCNA in 3 '- and 5 '-nick-directed mismatch repair in HeLa nuclear extracts. Proceedings of the American Association for Cancer Research Annual Meeting *45*, 612-612.

Gurney, M.E., Pu, H.F., Chiu, A.Y., Dalcanto, M.C., Polchow, C.Y., Alexander, D.D., Caliendo, J., Hentati, A., Kwon, Y.W., Deng, H.X., *et al.* (1994). MOTOR-NEURON DEGENERATION IN MICE THAT EXPRESS A HUMAN CU,ZN SUPEROXIDE-DISMUTASE MUTATION. Science *264*, 1772-1775.

Habraken, Y., and Verly, W.G. (1988). FURTHER PURIFICATION AND CHARACTERIZATION OF THE DNA 3'-PHOSPHATASE FROM RAT-LIVER CHROMATIN WHICH IS ALSO A POLYNUCLOTIDE 5'-HYDROXYL KINASE. European Journal of Biochemistry *171*, 59-66.

Haeusler, A.R., Donnelly, C.J., and Rothstein, J.D. (2016). The expanding biology of the C9orf72 nucleotide repeat expansion in neurodegenerative disease. Nature Reviews Neuroscience *17*, 383-U379.

Hagmann, M., Bruggmann, R., Xue, L., Georgiev, O., Schaffner, W., Rungger, D., Spaniol, P., and Gerster, T. (1998). Homologous recombination and DNA-end joining reactions in zygotes and early embryos of zebrafish (Danio rerio) and Drosophila melanogaster. Biological Chemistry *379*, 673-681.

Hakem, R. (2008). DNA-damage repair; the good, the bad, and the ugly. In EMBO J, pp. 589-605.

Hanai, R., Yazu, M., and Hieda, K. (1998). On the experimental distinction between ssbs and dsbs in circular DNA. Int J Radiat Biol *73*, 475-479.

Harper, J.W., and Elledge, S.J. (2007). The DNA damage response: Ten years after. Molecular Cell *28*, 739-745.

Hartsuiker, E., Neale, M.J., and Carr, A.M. (2009). Distinct requirements for the Rad32(Mre11) nuclease and Ctp1(CtIP) in the removal of covalently bound topoisomerase I and II from DNA. Mol Cell *33*, 117-123.

Hawkins, A.J., Subler, M.A., Akopiants, K., Wiley, J.L., Taylor, S.M., Rice, A.C., Windle, J.J., Valerie, K., and Povirk, L.F. (2009). In vitro complementation of Tdp1 deficiency indicates a stabilized enzyme-DNA adduct from tyrosyl but not glycolate lesions as a consequence of the SCAN1 mutation. DNA Repair *8*, 654-663.

Heard, E., and Bickmore, W. (2007). The ins and outs of gene regulation and chromosome territory organisation. Curr Opin Cell Biol *19*, 311-316.

Hendriks, I.A., Schimmel, J., Eifler, K., Olsen, J.V., and Vertegaal, A.C.O. (2015). Ubiquitin-specific Protease 11 (USP11) Deubiquitinates Hybrid Small Ubiquitin-like Modifier (SUMO)-Ubiquitin Chains to Counteract RING Finger Protein 4 (RNF4)*. In J Biol Chem, pp. 15526-15537.

Hewamadduma, C.A.A., Grierson, A.J., Ma, T.P., Pan, L., Moens, C.B., Ingham, P.W., Ramesh T., Shaw, P. (2013). Tardbpl splicing rescues motor neuron and axonal development in a mutant tardbp zebrafish. Human Molecular Genetics *22*, 2376-2386.

Heyer, W.-D., Ehmsen, K.T., and Liu, J. (2010). Regulation of Homologous Recombination in Eukaryotes. Annual Review of Genetics, Vol 44 *44*, 113-139.

Hietakangas, V., Ahlskog, J.K., Jakobsson, A.M., Hellesuo, M., Sahlberg, N.M., Holmberg, C.I., Mikhailov, A., Palvimo, J.J., Pirkkala, L., and Sistonen, L. (2003). Phosphorylation of serine 303 is a prerequisite for the stress-inducible SUMO modification of heat shock factor 1. Molecular and Cellular Biology *23*, 2953-2968.

Hietakangas, V., Anckar, J., Blomster, H.A., Fujimoto, M., Palvimo, J.J., Nakai, A., and Sistonen, L. (2006). PDSM, a motif for phosphorylation-dependent SUMO modification. Proceedings of the National Academy of Sciences of the United States of America *103*, 45-50.

Hiller, B., Achleitner, M., Glage, S., Naumann, R., Behrendt, R., and Roers, A. (2012). Mammalian RNase H2 removes ribonucleotides from DNA to maintain genome integrity. In J Exp Med, pp. 1419-1426.

Hirano, R., Interthal, H., Huang, C., Nakamura, T., Deguchi, K., Choi, K., Bhattacharjee, M.B., Arimura, K., Umehara, F., Izumo, S*., et al.* (2007). Spinocerebellar ataxia with axonal neuropathy: consequence of a Tdp1 recessive neomorphic mutation? Embo Journal *26*, 4732-4743.

Hirayama, J., Miyamura, N., Uchida, Y., Asaoka, Y., Honda, R., Sawanobori, K., Todo, T., Yamamoto, T., Sassone-Corsi, P., and Nishina, H. (2009). Common light signaling pathways controlling DNA repair and circadian clock entrainment in zebrafish. Cell Cycle *8*, 2794-2801.
Hoeijmakers, J.H.J. (2001). Genome maintenance mechanisms for preventing cancer. Nature *411*, 366-374.

Hoeller, D., Hecker, C.M., Wagner, S., Rogov, V., Dotsch, V., and Dikic, I. (2007). E3-independent monoubiquitination of ubiquitin-binding proteins. Mol Cell *26*, 891-898.

Howe, D.G., Bradford, Y.M., Eagle, A., Fashena, D., Frazer, K., Kalita, P., Mani, P., Martin, R., Moxon, S.T., Paddock, H*., et al.* (2018). The Zebrafish Model Organism Database: new support for human disease models, mutation details, gene expression phenotypes and searching. Nucleic Acids Research *45*.

Howe, K., Clark, M.D., Torroja, C.F., Torrance, J., Berthelot, C., Muffato, M., Collins, J.E., Humphray, S., McLaren, K., Matthews, L*., et al.* (2013). The zebrafish reference genome sequence and its relationship to the human genome. Nature *496*, 498-503.

Hruscha, A., Krawitz, P., Rechenberg, A., Heinrich, V., Hecht, J., Haass, C., and Schmid, B. (2013). Efficient CRISPR/Cas9 genome editing with low off-target effects in zebrafish. Development *140*, 4982-4987.

Hsu, P.D., Scott, D.A., Weinstein, J.A., Ran, F.A., Konermann, S., Agarwala, V., Li, Y., Fine, E.J., Wu, X., Shalem, O*., et al.* (2013). DNA targeting specificity of RNA-guided Cas9 nucleases. Nat Biotechnol *31*, 827-832.

Huang, C.J., Tu, C.T., Hsiao, C.D., Hsieh, F.J., and Tsai, H.J. (2003). Germ-line transmission of a myocardium-specific GFP transgene reveals critical regulatory elements in the cardiac myosin light chain 2 promoter of zebrafish. Dev Dyn *228*, 30-40.

Huang, P., Xiao, A., Zhou, M., Zhu, Z., Lin, S., and Zhang, B. (2011a). Heritable gene targeting in zebrafish using customized TALENs. In Nat Biotechnol (United States), pp. 699-700.

Huang, S.N., Pommier, Y., and Marchand, C. (2011b). Tyrosyl-DNA Phosphodiesterase 1 (Tdp1) inhibitors. Expert Opin Ther Pat *21*, 1285-1292.

Huang, S.Y.N., Williams, J.S., Arana, M.E., Kunkel, T.A., and Pommier, Y. (2016). Topoisomerase I-mediated cleavage at unrepaired ribonucleotides generates DNA double-strand breaks. Embo Journal *36*, 361-373.

Huang, S.Y.N., Williams, J.S., Arana, M.E., Kunkel, T.A., and Pommier, Y. (2017). Topoisomerase I-mediated cleavage at ribonucleotides generates DNA double-strand breaks. Embo Journal *36*, 361-373.

Hudson, J.J.R., Chiang, S.-C., Wells, O.S., Rookyard, C., and El-Khamisy, S.F. (2012). SUMO modification of the neuroprotective protein TDP1 facilitates chromosomal single-strand break repair. Nature Communications *3*.

Hudziak, R.M., Barofsky, E., Barofsky, D.F., Weller, D.L., Huang, S.B., and Weller, D.D. (1996). Resistance of morpholino phosphorodiamidate oligomers to enzymatic degradation. Antisense & Nucleic Acid Drug Development *6*, 267-272.

Hwang, W.Y., Fu, Y., Reyon, D., Maeder, M.L., Tsai, S.Q., Sander, J.D., Peterson, R.T., Yeh, J.R., and Joung, J.K. (2013). Efficient genome editing in zebrafish using a CRISPR-Cas system. Nat Biotechnol *31*, 227-229.

Hwang, W.Y., Peterson, R.T., and Yeh, J.R. (2014). Methods for targeted mutagenesis in zebrafish using TALENs. Methods *69*, 76-84.

Ikehata, H., and Ono, T. (2011). The Mechanisms of UV Mutagenesis. Journal of Radiation Research *52*, 115-125.

Imamura, S., and Kishi, S. (2005). Molecular cloning and functional characterization of zebrafish ATM. International Journal of Biochemistry & Cell Biology *37*, 1105-1116.

Inamdar, K.V., Pouliot, J.J., Zhou, T., Lees-Miller, S.P., Rasouli-Nia, A., and Povirk, L.F. (2002). Conversion of phosphoglycolate to phosphate termini on 3 ' overhangs of DNA double strand breaks by the human tyrosyl-DNA phosphodiesterase hTdp1. Journal of Biological Chemistry *277*, 27162-27168.

Ingebritsen, T.S., and Cohen, P. (1983). PROTEIN PHOSPHATASES - PROPERTIES AND ROLE IN CELLULAR-REGULATION. Science *221*, 331-338.

Inohara, N., and Nunez, G. (2000). Genes with homology to mammalian apoptosis regulators identified in zebrafish. Cell Death and Differentiation *7*, 509-510.

Interthal, H., Chen, H.J., and Champoux, J.J. (2005a). Human Tdp1 cleaves a broad spectrum of substrates, including phosphoamide linkages. Journal of Biological Chemistry *280*, 36518-36528.

Interthal, H., Chen, H.J., Kehl-Fie, T.E., Zotzmann, J., Leppard, J.B., and Champoux, J.J. (2005b). SCAN1 mutant Tdp1 accumulates the enzyme-DNA intermediate and causes camptothecin hypersensitivity. Embo Journal *24*, 2224-2233.

Interthal, H., Pouliott, J.J., and Champoux, J.J. (2001). The tyrosyl-DNA phosphodiesterase Tdp1 is a member of the phospholipase D superfamily. Proceedings of the National Academy of Sciences of the United States of America *98*, 12009-12014.

Isalan, M., Choo, Y., and Klug, A. (1997). Synergy between adjacent zinc fingers in sequence-specific DNA recognition. Proc Natl Acad Sci U S A *94*, 5617-5621.

Ishido, T., Yamazaki, N., Ishikawa, M., and Hirano, K. (2011). Characterization of DNA polymerase beta from Danio rerio by overexpression in E-coli using the in vivo/in vitro compatible pIVEX plasmid. Microbial Cell Factories *10*.

Ito, K., Hirao, A., Arai, F., Matsuoka, S., Takubo, K., Hamaguchi, I., Nomiyama, K., Hosokawa, K., Sakurada, K., Nakagata, N*., et al.* (2004). Regulation of oxidative stress by ATM is required for self-renewal of haematopoietic stem cells. Nature *431*, 997-1002.

Izumi, T., Hazra, T.K., Boldogh, I., Tomkinson, A.E., Park, M.S., Ikeda, S., and Mitra, S. (2000). Requirement for human AP endonuclease 1 for repair of 3 '-blocking damage at DNA single-strand breaks induced by reactive oxygen species. Carcinogenesis *21*, 1329-1334.

Jackson, S.P. (2002). Sensing and repairing DNA double-strand breaks. Carcinogenesis *23*, 687-696.

Jackson, S.P., and Bartek, J. (2009). The DNA-damage response in human biology and disease. Nature *461*, 1071-1078.

Jacob, K.D., Noren Hooten, N., Tadokoro, T., Lohani, A., Barnes, J., and Evans, M.K. (2013). Alzheimer's disease-associated polymorphisms in human OGG1 alter catalytic activity and sensitize cells to DNA damage. Free Radic Biol Med *63*, 115-125.

Jacquier, A., and Dujon, B. (1985). An intron-encoded protein is active in a gene conversion process that spreads an intron into a mitochondrial gene. Cell *41*, 383-394.

Jakobsen, A.K., Lauridsen, K.L., Samuel, E.B., Proszek, J., Knudsen, B.R., Hager, H., and Stougaard, M. (2015). Correlation between topoisomerase I and tyrosyl-DNA phosphodiesterase 1 activities in non-small cell lung cancer tissue. Experimental and Molecular Pathology *99*, 56-64.

Jeong, J.Y., Kwon, H.B., Ahn, J.C., Kang, D., Kwon, S.H., Park, J.A., and Kim, K.W. (2008). Functional and developmental analysis of the blood-brain barrier in zebrafish. Brain Res Bull *75*, 619-628.

Jiang, X.F., Sun, Y.L., Chen, S.J., Roy, K., and Price, B.D. (2006). The FATC domains of PIKK proteins are functionally equivalent and participate in the Tip60-dependent activation of DNA-PKcs and ATM. Journal of Biological Chemistry *281*, 15741-15746.

Jilani, A., Ramotar, D., Slack, C., Ong, C., Yang, X.M., Scherer, S.W., and Lasko, D.D. (1999). Molecular cloning of the human gene, PNKP, encoding a polynucleotide kinase 3 '-phosphatase and evidence for its role in repair of DNA strand breaks caused by oxidative damage. Journal of Biological Chemistry *274*, 24176-24186.

Jim, K.K., Engelen-Lee, J., van der Sar, A.M., Bitter, W., Brouwer, M.C., van der Ende, A., Veening, J.W., van de Beek, D., and Vandenbroucke-Grauls, C. (2016). Infection of zebrafish embryos with live fluorescent Streptococcus pneumoniae as a real-time pneumococcal meningitis model. In J Neuroinflammation.

Jinek, M., Chylinski, K., Fonfara, I., Hauer, M., Doudna, J.A., and Charpentier, E. (2012). A programmable dual-RNA-guided DNA endonuclease in adaptive bacterial immunity. Science *337*, 816-821.

Jiricny, J. (2006). The multifaceted mismatch-repair system. Nature Reviews Molecular Cell Biology *7*, 335-346.

Johnson, E.S. (2004). Protein modification by SUMO. Annual Review of Biochemistry *73*, 355-382.

Johnson, W.G. (2000). Late-onset neurodegenerative diseases--the role of protein insolubility. J Anat *196 (Pt 4)*, 609-616.

Jones, P.A. (2012). Functions of DNA methylation: islands, start sites, gene bodies and beyond. Nature Reviews Genetics *13*, 484-492.

Kakarougkas, A., and Jeggo, P.A. (2014). DNA DSB repair pathway choice: an orchestrated handover mechanism. Br J Radiol *87*, 20130685.

Kalueff, A.V., Stewart, A.M., and Gerlai, R. (2014). Zebrafish as an emerging model for studying complex brain disorders. Trends Pharmacol Sci *35*, 63-75.

Kang, H., Jung, J.W., Kim, M.K., and Chung, J.H. (2009). CK2 Is the Regulator of SIRT1 Substrate-Binding Affinity, Deacetylase Activity and Cellular Response to DNA-Damage. Plos One *4*.
Kari, G., Rodeck, U., and Dicker, A.P. (2007). Zebrafish: An emerging model system for human disease and drug discovery. Clinical Pharmacology & Therapeutics *82*, 70-80.

Kasparek, T.R., and Humphrey, T.C. (2011). DNA double-strand break repair pathways, chromosomal rearrangements and cancer. Seminars in Cell & Developmental Biology *22*, 886-897.

Katyal, S., El-Khamisy, S.F., Russell, H.R., Li, Y., Ju, L., Caldecott, K.W., and McKinnon, P.J. (2007). TDP1 facilitates chromosomal single-strand break repair in neurons and is neuroprotective in vivo. Embo Journal *26*, 4720-4731.

Katyal, S., Lee, Y., Nitiss, K.C., Downing, S.M., Li, Y., Shimada, M., Zhao, J., Russell, H.R., Petrini, J.H.J., Nitiss, J.L*., et al.* (2014). Aberrant topoisomerase-1 DNA lesions are pathogenic in neurodegenerative genome instability syndromes. Nature Neuroscience *17*, 813-821.

Kawahara, G., and Hayashi, Y.K. (2016). Characterization of Zebrafish Models of Marinesco-Sjogren Syndrome. Plos One *11*.

Kawakami, K. (2005). Transposon tools and methods in zebrafish. Developmental Dynamics *234*, 244-254.

Kawakami, K., Shima, A., and Kawakami, N. (2000). Identification of a functional transposase of the Tol2 element, an Ac-like element from the Japanese medaka fish, and its transposition in the zebrafish germ lineage. Proceedings of the National Academy of Sciences of the United States of America *97*, 11403-11408.

Ke, J.Y., Dai, C.J., Wu, W.L., Gao, J.H., Xia, A.J., Liu, G.P., Lv, K.S., and Wu, C.L. (2014). USP11 regulates p53 stability by deubiquitinating p53. Journal of Zhejiang University-Science B *15*, 1032-1038.

Keeney, S., and Neale, M.J. (2006). Initiation of meiotic recombination by formation of DNA double-strand breaks: mechanism and regulation. Biochemical Society Transactions *34*, 523-525.

Keller, D.M., Zeng, X.Y., Wang, Y., Zhang, Q.H., Kapoor, M., Shu, H.J., Goodman, R., Lozano, G., Zhao, Y.M., and Lu, H. (2001). A DNA damage-induced p53 serine 392 kinase complex contains CK2, hSpt16, and SSRP1. Molecular Cell *7*, 283-292.

Kelner, A. (1949). Effect of Visible Light on the Recovery of Streptomyces Griseus Conidia from Ultra-violet Irradiation Injury. Proc Natl Acad Sci U S A *35*, 73-79.

Khalil, H.S., Science, Tummala, H., Drink, F.a., Zhelev, N., N510529@abertay.ac.uk, and Science (2012). ATM in focus: a damage sensor and cancer target. BioDiscovery *5*.

Khanna, K.K., Lavin, M.F., Jackson, S.P., and Mulhern, T.D. (2001). ATM, a central controller of cellular responses to DNA damage. Cell Death and Differentiation *8*, 1052-1065.

Kiernan, M.C., Vucic, S., Cheah, B.C., Turner, M.R., Eisen, A., Hardiman, O., Burrell, J.R., and Zoing, M.C. (2011). Amyotrophic lateral sclerosis. The Lancet *377*, 942-955.

Kim, J.H., Lee, S.R., Li, L.H., Park, H.J., Park, J.H., Lee, K.Y., Kim, M.K., Shin, B.A., and Choi, S.Y. (2011). High Cleavage Efficiency of a 2A Peptide Derived from Porcine Teschovirus-1 in Human Cell Lines, Zebrafish and Mice. Plos One *6*.

Kim, Y.G., Cha, J., and Chandrasegaran, S. (1996). Hybrid restriction enzymes: zinc finger fusions to Fok I cleavage domain. Proc Natl Acad Sci U S A *93*, 1156-1160.

Kishimoto, N., Shimizu, K., and Sawamoto, K. (2012). Neuronal regeneration in a zebrafish model of adult brain injury. In Dis Model Mech, pp. 200-209.

Kithcart, A., and MacRae, C.A. (2017). Using Zebrafish for High-Throughput Screening of Novel Cardiovascular Drugs. JACC: Basic to Translational Science *2*, 1-12.

Knippschild, U., Gocht, A., Wolff, S., Huber, N., Löhler, J., and Stöter, M. (2005). The casein kinase 1 family: participation in multiple cellular processes in eukaryotes. Cellular Signalling *17*, 675-689.

Knipscheer, P., Dijk, W.J.v., Olsen, J.V., Mann, M., and Sixma, T.K. (2007). Noncovalent interaction between Ubc9 and SUMO promotes SUMO chain formation.

Kobayashi, Y., Ishikawa, T., Hirayama, J., Daiyasu, H., Kanai, S., Toh, H., Fukuda, I., Tsujimura, T., Terada, N., Kamei, Y.*, et al.* (2000). Molecular analysis of zebrafish photolyase/cryptochrome family: two types of cryptochromes present in zebrafish. Genes Cells *5*, 725-738.

Kokel, D., Bryan, J., Laggner, C., White, R., Cheung, C.Y.J., Mateus, R., Healey, D., Kim, S., Werdich, A.A., Haggarty, S.J.*, et al.* (2010). Rapid behavior-based identification of neuroactive small molecules in the zebrafish. Nature Chemical Biology *6*, 231-237.

Kokel, D., and Peterson, R.T. (2008). Chemobehavioural phenomics and behaviour-based psychiatric drug discovery in the zebrafish. In Brief Funct Genomic Proteomic, pp. 483-490.

Koo, D.H., Han, F., Birchler, J.A., and Jiang, J. (2011). Distinct DNA methylation patterns associated with active and inactive centromeres of the maize B chromosome. Genome Res *21*, 908-914.

Kristofco, L.A., Cruz, L.C., Haddad, S.P., Behra, M.L., Chambliss, C.K., and Brooks, B.W. (2016). Age matters: Developmental stage of Danio rerio larvae influences photomotor response thresholds to diazinion or diphenhydramine. Aquatic Toxicology *170*, 344-354.

Kruhlak, M., Crouch, E.E., Orlov, M., Montano, C., Gorski, S.A., Nussenzweig, A., Misteli, T., Phair, R.D., and Casellas, R. (2007). The ATM repair pathway inhibits RNA polymerase I transcription in response to chromosome breaks. Nature *447*, 730-U716.

Ku-Centurion, M., Gonzalez-Marin, B., Calderon-Ezquerro, M.C., Martinez-Valenzuela, M.C., Maldonado, E., and Calderon-Segura, M.E. (2016). DNA Damage Assessment in Zebrafish Embryos Exposed to Monceren((R)) 250 SC Fungicide Using the Alkaline Comet Assay. Zebrafish *13*, 442-448.

Kunkel, T.A. (1993). NUCLEOTIDE REPEATS - SLIPPERY DNA AND DISEASES. Nature *365*, 207-208.

Kunkel, T.A., and Erie, D.A. (2005). DNA mismatch repair. Annual Review of Biochemistry *74*, 681-710.

Kuzminov, A. (2001). Single-strand interruptions in replicating chromosomes cause double-strand breaks. Proceedings of the National Academy of Sciences of the United States of America *98*, 8241-8246.

Kwan, K.M., Fujimoto, E., Grabher, C., Mangum, B.D., Hardy, M.E., Campbell, D.S., Parant, J.M., Yost, H.J., Kanki, J.P., and Chien, C.B. (2007). The Tol2kit: A multisite Gateway-based construction kit for Tol2 transposon transgenesis constructs. Developmental Dynamics *236*, 3088-3099.

Lakshmipathy, U., and Campbell, C. (1999). The human DNA ligase III gene encodes nuclear and mitochondrial proteins. Mol Cell Biol *19*, 3869-3876.

Langenau, D.M., Feng, H., Berghmans, S., Kanki, J.P., Kutok, J.L., and Look, A.T. (2005). Cre/lox-regulated transgenic zebrafish model with conditional myc-induced T cell acute lymphoblastic leukemia. Proceedings of the National Academy of Sciences of the United States of America *102*, 6068-6073.

Lau, P.J., and Kolodner, R.D. (2003). Transfer of the MSH2 center dot MSH6 complex from proliferating cell nuclear antigen to mispaired bases in DNA. Journal of Biological Chemistry *278*, 14-17.

Leal, M.C., Feitsma, H., Cuppen, E., Franca, L.R., and Schulz, R.W. (2008). Completion of meiosis in male zebrafish (Danio rerio) despite lack of DNA mismatch repair gene mlh1. Cell and Tissue Research *332*, 133-139.

Lebedeva, N.A., Rechkunova, N.I., and Lavrik, O.I. (2011). AP-site cleavage activity of tyrosyl-DNA phosphodiesterase 1. Febs Letters *585*, 683-686.

Ledesma, F.C., El Khamisy, S.F., Zuma, M.C., Osborn, K., and Caldecott, K.W. (2009). A human 5 '-tyrosyl DNA phosphodiesterase that repairs topoisomerase-mediated DNA damage. Nature *461*, 674-U125.

Lee, K.C., Goh, W.L.P., Xu, M., Kua, N., Lunny, D., Wong, J.S., Coomber, D., Vojtesek, B., Lane, E.B., and Lane, D.P. (2008). Detection of the p53 response in zebrafish embryos using new monoclonal antibodies. Oncogene *27*, 629-640.

Lees-Miller, S.P., and Meek, K. (2003). Repair of DNA double strand breaks by non-homologous end joining. Biochimie *85*, 1161-1173.

Levine, T.P., Daniels, R.D., Gatta, A.T., Wong, L.H., and Hayes, M.J. (2013). The product of C9orf72, a gene strongly implicated in neurodegeneration, is structurally related to DENN Rab-GEFs. Bioinformatics *29*, 499-503.

Liao, H.K., and Essner, J.J. (2011). Use of RecA fusion proteins to induce genomic modifications in zebrafish. Nucleic Acids Research *39*, 4166-4179.

Lin, C.P., Ban, Y., Lyu, Y.L., Desai, S.D., and Liu, L.F. (2008). A ubiquitin-proteasome pathway for the repair of topoisomerase I-DNA covalent complexes. Journal of Biological Chemistry *283*, 21074-21083.

Lindahl, T. (1993). INSTABILITY AND DECAY OF THE PRIMARY STRUCTURE OF DNA. Nature *362*, 709-715.

Lindahl, T., and Karlstrom, O. (1973). HEAT-INDUCED DEPYRIMIDINATION OF DEOXYRIBONUCLEIC ACID IN NEUTRAL SOLUTION. Biochemistry *12*, 5151-5154.

Litchfield, D.W. (2003). Protein kinase CK2: structure, regulation and role in cellular decisions of life and death. Biochemical Journal *369*, 1-15.

Liu, C.Y., Pouliot, J.J., and Nash, H.A. (2002). Repair of topoisomerase I covalent complexes in the absence of the tyrosyl-DNA phosphodiesterase Tdp1. Proceedings of the National Academy of Sciences of the United States of America *99*, 14970-14975.

Liu, C.Y., Pouliot, J.J., and Nash, H.A. (2004). The role of TDP1 from budding yeast in the repair of DNA damage. DNA Repair *3*, 593-601.

Liu, C.Y., Zhou, S.Y., Begum, S., Sidransky, D., Westra, W.H., Brock, M., and Califano, J.A. (2007). Increased expression and activity of repair genes TDP1 and XPF in non-small cell lung cancer. Lung Cancer *55*, 303-311.

Liu, J.G., Gong, L., Chang, C.Q., Liu, C., Peng, J.R., and Chen, J. (2012). Development of Novel Visual-Plus Quantitative Analysis Systems for Studying DNA Double-Strand Break Repairs in Zebrafish. Journal of Genetics and Genomics *39*, 489-502.

Liu, S.J., de Boeck, M., van Dam, H., and ten Dijke, P. (2016). Regulation of the TGF-beta pathway by deubiquitinases in cancer. International Journal of Biochemistry & Cell Biology *76*, 135-145.

Liu, T., and Huang, J. (2016). DNA End Resection: Facts and Mechanisms. In Genomics Proteomics Bioinformatics, pp. 126-130.

Liu, Y., Ma, P., Cassidy, P.A., Carmer, R., Zhang, G., Venkatraman, P., Brown, S.A., Pang, C.P., Zhong, W., Zhang, M.*, et al.* (2017). Statistical Analysis of Zebrafish Locomotor Behaviour by Generalized Linear Mixed Models. In Sci Rep.

Loeb, L.A., and Preston, B.D. (1986). MUTAGENESIS BY APURINIC APYRIMIDINIC SITES. Annual Review of Genetics *20*, 201-230.

Loizou, J.I., El-Khamisy, S.F., Zlatanou, A., Moore, D.J., Chan, D.W., Qin, J., Sarno, S., Meggio, F., Pinna, L.A., and Caldecott, K.W. (2004). The protein kinase CK2 facilitates repair of chromosomal DNA single-strand breaks. Cell *117*, 17-28.

Lopez-Gonzalez, R., Lu, Y.B., Gendron, T.F., Karydas, A., Tran, H., Yang, D.J., Petrucelli, L., Miller, B.L., Almeida, S., and Gao, F.B. (2016). Poly(GR) in C9ORF72-Related ALS/FTD Compromises Mitochondrial Function and Increases Oxidative Stress and DNA Damage in iPSC-Derived Motor Neurons. Neuron *92*, 383-391.

Lu, Z., and DeSmidt, A.A. (2013). Early Development of Hearing in Zebrafish. In J Assoc Res Otolaryngol, pp. 509-521.

Lucas-Lledó, J.I., Lynch, M. (2018). Evolution of Mutation Rates: Phylogenomic Analysis of the Photolyase/Cryptochrome Family. Molecular Biology and Evolution *26*, 1143-1153.

Lynch, M., Sung, W., Morris, K., Coffey, N., Landry, C.R., Dopman, E.B., Dickinson, W.J., Okamoto, K., Kulkarni, S., Hartl, D.L.*, et al.* (2008). A genome-wide view of the spectrum of spontaneous mutations in yeast. Proceedings of the National Academy of Sciences of the United States of America *105*, 9272-9277.

Mackey, Z.B., Ramos, W., Levin, D.S., Walter, C.A., McCarrey, J.R., and Tomkinson, A.E. (1997). An alternative splicing event which occurs in mouse pachytene spermatocytes

generates a form of DNA ligase III with distinct biochemical properties that may function in meiotic recombination. Molecular and Cellular Biology *17*, 989-998.

Mahmood, F., Fu, S., Cooke, J., Wilson, S.W., Cooper, J.D., and Russell, C. (2013). A zebrafish model of CLN2 disease is deficient in tripeptidyl peptidase 1 and displays progressive neurodegeneration accompanied by a reduction in proliferation. Brain *136*, 1488-1507.

Mali, P., Aach, J., Stranges, P.B., Esvelt, K.M., Moosburner, M., Kosuri, S., Yang, L., and Church, G.M. (2013a). CAS9 transcriptional activators for target specificity screening and paired nickases for cooperative genome engineering. Nat Biotechnol *31*, 833-838.

Mali, P., Yang, L., Esvelt, K.M., Aach, J., Guell, M., DiCarlo, J.E., Norville, J.E., and Church, G.M. (2013b). RNA-Guided Human Genome Engineering via Cas9. Science *339*, 823-826.

Marin, O., Bustos, V.H., Cesaro, L., Meggio, F., Pagano, M.A., Antonelli, M., Allende, C.C., Pinna, L.A., and Allende, J.E. (2003). A noncanonical sequence phosphorylated by casein kinase 1 in β-catenin may play a role in casein kinase 1 targeting of important signaling proteins.

Marteijn, J.A., Lans, H., Vermeulen, W., and Hoeijmakers, J.H.J. (2014). Understanding nucleotide excision repair and its roles in cancer and ageing. Nature Reviews Molecular Cell Biology *15*, 465-481.

Martin, N., Schwamborn, K., Schreiber, V., Werner, A., Guillier, C., Zhang, X.D., Bischof, O., Seeler, J.S., and Dejean, A. (2009). PARP-1 transcriptional activity is regulated by sumoylation upon heat shock. Embo Journal *28*, 3534-3548.

Maskey, R.S., Flatten, K.S., Sieben, C.J., Peterson, K.L., Baker, D.J., Nam, H.J., Kim, M.S., Smyrk, T.C., Kojima, Y., Machida, Y.*, et al.* (2017). Spartan deficiency causes accumulation of Topoisomerase 1 cleavage complexes and tumorigenesis. In Nucleic Acids Res, pp. 4564-4576.

Mayden, R.L., Tang, K.L., Conway, K.W., Freyhof, J., Chamberlain, S., Haskins, M., Schneider, L., Sudkamp, M., Wood, R.M., Agnew, M.*, et al.* (2007). Phylogenetic relationships of Danio within the order cypriniformes: A framework for comparative and evolutionary studies of a model species. Journal of Experimental Zoology Part B-Molecular and Developmental Evolution *308B*, 642-654.

McCallum, C.M., Comai, L., Greene, E.A., and Henikoff, S. (2000). Targeting Induced Local Lesions IN Genomes (TILLING) for Plant Functional Genomics. Plant Physiol *123*, 439-442.

McCormick, J.P., Fischer, J.R., Pachlatko, J.P., and Eisenstark, A. (1976). Characterization of a cell-lethal product from the photooxidation of tryptophan: hydrogen peroxide. Science *191*, 468-469.

McCulloch, S.D., and Kunkel, T.A. (2008). The fidelity of DNA synthesis by eukaryotic replicative and translesion synthesis polymerases. Cell Research *18*, 148-161.

McKerlie, M., Lin, S.C., and Zhu, X.D. (2012). ATM regulates proteasome-dependent subnuclear localization of TRF1, which is important for telomere maintenance. Nucleic Acids Research *40*, 3975-3989.

Meek, K., Dang, V., and Lees-Miller, S.P. (2008). DNA-PK: The Means to Justify the Ends? Advances in Immunology, Vol 99 *99*, 33-58.

Meggio, F., Boldyreff, B., Marin, O., Pinna, L.A., and Issinger, O.G. (1992). ROLE OF THE BETA SUBUNIT OF CASEIN KINASE-2 ON THE STABILITY AND SPECIFICITY OF THE RECOMBINANT RECONSTITUTED HOLOENZYME. European Journal of Biochemistry *204*, 293-297.

Meng, X., Noyes, M.B., Zhu, L.J., Lawson, N.D., and Wolfe, S.A. (2008). Targeted gene inactivation in zebrafish using engineered zinc-finger nucleases. Nat Biotechnol *26*, 695-701.
Messner, S., Schuermann, D., Altmeyer, M., Kassner, I., Schmidt, D., Schar, P., Muller, S., and Hottiger, M.O. (2009). Sumoylation of poly(ADP-ribose) polymerase 1 inhibits its acetylation and restrains transcriptional coactivator function. Faseb Journal *23*, 3978-3989.

Meyer, A., and Van de Peer, Y. (2005). From 2R to 3R: evidence for a fish-specific genome duplication (FSGD). Bioessays *27*, 937-945.

Miao, Z.H., Agama, K., Sordet, O., Povirk, L., Kohn, K.W., and Pommier, Y. (2006). Hereditary ataxia SCAN1 cells are defective for the repair of transcription-dependent topoisomerase I cleavage complexes. DNA Repair *5*, 1489-1494.

Miller, J.C., Holmes, M.C., Wang, J., Guschin, D.Y., Lee, Y.L., Rupniewski, I., Beausejour, C.M., Waite, A.J., Wang, N.S., Kim, K.A*., et al.* (2007). An improved zinc-finger nuclease architecture for highly specific genome editing. Nat Biotechnol *25*, 778-785.

Miller, J.C., Tan, S., Qiao, G., Barlow, K.A., Wang, J., Xia, D.F., Meng, X., Paschon, D.E., Leung, E., Hinkley, S.J*., et al.* (2011). A TALE nuclease architecture for efficient genome editing. Nat Biotechnol *29*, 143-148.

Millward, T.A., Zolnierowicz, S., and Hemmings, B.A. (1999). Regulation of protein kinase cascades by protein phosphatase 2A. Trends in Biochemical Sciences *24*, 186-191.

Mitchell, D.L., and Nairn, R.S. (1989). THE BIOLOGY OF THE (6–4) PHOTOPRODUCT. Photochemistry and Photobiology *49*, 805-819.

Mjelle, R., Hegre, S.A., Aas, P.A., Slupphaug, G., Drablos, F., Saetrom, P., and Krokan, H.E. (2015). Cell cycle regulation of human DNA repair and chromatin remodeling genes. DNA Repair (Amst) *30*, 53-67.

Moens, P.B. (2006). Zebrafish: chiasmata and interference. Genome *49*, 205-208.

Moore, L.D., Le, T., and Fan, G. (2013). DNA Methylation and Its Basic Function. In Neuropsychopharmacology, pp. 23-38.

Moreira, M.D., Barbot, C., Tachi, N., Kozuka, N., Mendonca, P., Barros, J., Coutinho, P., Sequeiros, J., and Koenig, M. (2001). Homozygosity mapping of portuguese and Japanese forms of ataxia-oculomotor apraxia to 9p13, and evidence for genetic heterogeneity. American Journal of Human Genetics *68*, 501-508.

Morgan, S.E., Lovly, C., Pandita, T.K., Shiloh, Y., and Kastan, M.B. (1997). Fragments of ATM which have dominant-negative or complementing activity. Mol Cell Biol *17*, 2020-2029.

Morris, J.R., Boutell, C., Keppler, M., Densham, R., Weekes, D., Alamshah, A., Butler, L., Galanty, Y., Pangon, L., Kiuchi, T.*, et al.* (2009). The SUMO modification pathway is involved in the BRCA1 response to genotoxic stress. Nature *462*, 886-U877.

Morton, S.M., and Bastian, A.J. (2004). Cerebellar control of balance and locomotion. Neuroscientist *10*, 247-259.

Mosimann, C., Kaufman, C.K., Li, P., Pugach, E.K., Tamplin, O.J., and Zon, L.I. (2011). Ubiquitous transgene expression and Cre-based recombination driven by the ubiquitin promoter in zebrafish. Development *138*, 169-177.

Mukhopadhyay, D., and Dasso, M. (2007). Modification in reverse: the SUMO proteases. Trends in Biochemical Sciences *32*, 286-295.

Murai, J., Huang Sy, N., Das, B.B., Dexheimer, T.S., Takeda, S., and Pommier, Y. (2012). Tyrosyl-DNA Phosphodiesterase 1 (TDP1) Repairs DNA Damage Induced by Topoisomerases I and II and Base Alkylation in Vertebrate Cells*. In J Biol Chem, pp. 12848-12857.

Nagabhushana, A., and Mishra, R.K. (2016). Finding clues to the riddle of sex determination in zebrafish. J Biosci *41*, 145-155.

Nakamura, K., Kogame, T., Oshiumi, H., Shinohara, A., Sumitomo, Y., Agama, K., Pommier, Y., Tsutsui, K.M., Tsutsui, K., Hartsuiker, E.*, et al.* (2010). Collaborative action of Brca1 and CtIP in elimination of covalent modifications from double-strand breaks to facilitate subsequent break repair. PLoS Genet *6*, e1000828.

Nasevicius, A., and Ekker, S.C. (2000). Effective targeted gene 'knockdown' in zebrafish. Nature Genetics *26*, 216-220.

Nash, R.A., Caldecott, K.W., Barnes, D.E., and Lindahl, T. (1997). XRCC1 protein interacts with one of two distinct forms of DNA ligase III. Biochemistry *36*, 5207-5211.

Nick McElhinny, S.A., Kumar, D., Clark, A.B., Watt, D.L., Watts, B.E., Lundström, E.B., Johansson, E., Chabes, A., and Kunkel, T.A. (2010). Genome instability due to ribonucleotide incorporation into DNA. Nat Chem Biol *6*, 774-781.

Nitiss, J.L. (2009). Targeting DNA topoisomerase II in cancer chemotherapy. Nature Reviews Cancer *9*, 338-350.

Norton, W., and Bally-Cuif, L. (2010). Adult zebrafish as a model organism for behavioural genetics. Bmc Neuroscience *11*.

Notch, E.G., and Mayer, G.D. (2009). 17α-Ethinylestradiol hinders nucleotide excision repair in zebrafish liver cells. Aquatic Toxicology *95*, 273-278.

Notch, E.G., Miniutti, D.M., and Mayer, G.D. (2007). 17α-Ethinylestradiol decreases expression of multiple hepatic nucleotide excision repair genes in zebrafish (Danio rerio). Aquatic Toxicology *84*, 301-309.

Nouspikel, T., and Hanawalt, P.C. (2002). DNA repair in terminally differentiated cells. DNA Repair *1*, 59-75.

O'Reilly-Pol, T., and Johnson, S.L. (2008). Neocuproine Ablates Melanocytes in Adult Zebrafish. Zebrafish *5*, 257-264.

Okado-Matsumoto, A., and Fridovich, I. (2001). Subcellular distribution of superoxide dismutases (SOD) in rat liver - Cu,Zn-SOD in mitochondria. Journal of Biological Chemistry *276*, 38388-38393.

Olsson, M., and Lindahl, T. (1980). REPAIR OF ALKYLATED DNA IN ESCHERICHIA-COLI - METHYL-GROUP TRANSFER FROM O-6-METHYLGUANINE TO A PROTEIN CYSTEINE RESIDUE. Journal of Biological Chemistry *255*, 569-571.

Ordas, A., Raterink, R.J., Cunningham, F., Jansen, H.J., Wiweger, M.I., Jong-Raadsen, S., Bos, S., Bates, R.H., Barros, D., Meijer, A.H.*, et al.* (2015). Testing Tuberculosis Drug Efficacy in a Zebrafish High-Throughput Translational Medicine Screen. In Antimicrob Agents Chemother, pp. 753-762.

Osterod, M., Hollenbach, S., Hengstler, J.G., Barnes, D.E., Lindahl, T., and Epe, B. (2017). Age-related and tissue-specific accumulation of oxidative DNA base damage in 7,8-dihydro-8-oxoguanine-DNA glycosylase (Ogg1) deficient mice. Carcinogenesis *22*, 1459-1463.

Ouyang, K.J., Woo, L.L., Zhu, J.M., Huo, D.Z., Matunis, M.J., and Ellis, N.A. (2009). SUMO Modification Regulates BLM and RAD51 Interaction at Damaged Replication Forks. Plos Biology *7*.

Pandey, A., Andersen, J.S., and Mann, M. (2000). Use of mass spectrometry to study signaling pathways. Sci STKE *2000*, pl1.

Panier, S., and Boulton, S.J. (2014). Double-strand break repair: 53BP1 comes into focus. Nature Reviews Molecular Cell Biology *15*, 7-18.

Panula, P., Chen, Y.C., Priyadarshini, M., Kudo, H., Semenova, S., Sundvik, M., and Sallinen, V. (2010). The comparative neuroanatomy and neurochemistry of zebrafish CNS systems of relevance to human neuropsychiatric diseases. Neurobiol Dis *40*, 46-57.

Park, H.C., Kim, C.H., Bae, Y.K., Yee, S.Y., Kim, S.H., Hong, S.K., Shin, J., Yoo, K.W., Hibi, M., Hirano, T.*, et al.* (2000). Analysis of upstream elements in the HuC promoter leads to the establishment of transgenic zebrafish with fluorescent neurons. Developmental Biology *227*, 279-293.

Park, J.W., and Ames, B.N. (1988). 7-METHYLGUANINE ADDUCTS IN DNA ARE NORMALLY PRESENT AT HIGH-LEVELS AND INCREASE ON AGING - ANALYSIS BY HPLC WITH ELECTROCHEMICAL DETECTION. Proceedings of the National Academy of Sciences of the United States of America *85*, 7467-7470.

Pattanayak, V., Lin, S., Guilinger, J.P., Ma, E., Doudna, J.A., and Liu, D.R. (2013). High-throughput profiling of off-target DNA cleavage reveals RNA-programmed Cas9 nuclease specificity. Nat Biotechnol *31*, 839-843.

Pei, D.-S., and Strauss, P.R. (2013). Zebrafish as a model system to study DNA damage and repair. Mutation Research-Fundamental and Molecular Mechanisms of Mutagenesis *743*, 151-159.

Perrino, F.W., Harvey, S., Shaban, N.M., and Hollis, T. (2009). RNaseH2 mutants that cause Aicardi-Goutieres syndrome are active nucleases. J Mol Med (Berl) *87*, 25-30.

Pinna, L.A. (1990). CASEIN KINASE-2 - AN EMINENCE-GRISE IN CELLULAR-REGULATION. Biochimica Et Biophysica Acta *1054*, 267-284.

Pinna, L.A. (2002). Protein kinase CK2: a challenge to canons. Journal of Cell Science *115*, 3873-3878.

Plaut, I. (2000). Effects of fin size on swimming performance, swimming behaviour and routine activity of zebrafish Danio rerio. Journal of Experimental Biology *203*, 813-820.

Podlutsky, A.J., Dianova, II, Wilson, S.H., Bohr, V.A., and Dianov, G.L. (2001). DNA synthesis and dRPase activities of polymerase beta are both essential for single-nucleotide patch base excision repair in mammalian cell extracts. Biochemistry *40*, 809-813.

Pommier, Y., Barcelo, J.A., Rao, V.A., Sordet, O., Jobson, A.G., Thibaut, L., Miao, Z.H., Seiler, J.A., Zhang, H., Marchand, C*., et al.* (2006). Repair of topoisomerase I - Mediated DNA damage. Progress in Nucleic Acid Research and Molecular Biology, Vol 81 *81*, 179-+.

Pommier, Y., Sung, Y.L., Huang, S.Y.N., and Nitiss, J.L. (2016). Roles of eukaryotic topoisomerases in transcription, replication and genomic stability. Nature Reviews Molecular Cell Biology *17*, 703-721.

Pouliot, J.J., Yao, K.C., Robertson, C.A., and Nash, H.A. (1999). Yeast gene for a Tyr-DNA phosphodiesterase that repairs topoisomerase I complexes. Science *286*, 552-555.

Poulton, C., Oegema, R., Heijsman, D., Hoogeboom, J., Schot, R., Stroink, H., Willemsen, M.A., Verheijen, F.W., van de Spek, P., Kremer, A*., et al.* (2013). Progressive cerebellar atrophy and polyneuropathy: expanding the spectrum of PNKP mutations. Neurogenetics *14*, 43-51.

Pourquier, P., and Pommier, Y. (2001). Topoisomerase I-mediated DNA damage. Advances in Cancer Research, Vol 80 *80*, 189-216.

Quek, H., Luff, J., Cheung, K., Kozlov, S., Gatei, M., Lee, C.S., Bellingham, M.C., Noakes, P.G., Lim, Y.C., Barnett, N.L*., et al.* (2017). A rat model of ataxia-telangiectasia: evidence for a neurodegenerative phenotype. Human Molecular Genetics *26*, 109-123.

Rabe, B. (2013). Aicardi-GoutiSres syndrome: clues from the RNase H2 knock-out mouse. Journal of Molecular Medicine-Jmm *91*, 1235-1240.

Ramesh, T., Lyon, A.N., Pineda, R.H., Wang, C., Janssen, P.M.L., Canan, B.D., Burghes, A.H.M., and Beattie, C.E. (2010). A genetic model of amyotrophic lateral sclerosis in zebrafish displays phenotypic hallmarks of motoneuron disease.

Rasouli-Nia, A., Karimi-Busheri, F., and Weinfeld, M. (2004). Stable down-regulation of human polynucleotide kinase enhances spontaneous mutation frequency and sensitizes cells to genotoxic agents. Proceedings of the National Academy of Sciences of the United States of America *101*, 6905-6910.

Rass, U., Ahel, I., and West, S.C. (2007). Defective DNA repair and Neurodegenerative disease. Cell *130*, 991-1004.

Reijns, M.A.M., Bubeck, D., Gibson, L.C.D., Graham, S.C., Baillie, G.S., Jones, E.Y., and Jackson, A.P. (2011). The Structure of the Human RNase H2 Complex Defines Key Interaction Interfaces Relevant to Enzyme Function and Human Disease. Journal of Biological Chemistry *286*, 10530-10539.

Reijns, M.A.M., Rabe, B., Rigby, R.E., Mill, P., Astell, K.R., Lettice, L.A., Boyle, S., Leitch, A., Keighren, M., Kilanowski, F.*, et al.* (2012). Enzymatic Removal of Ribonucleotides from DNA Is Essential for Mammalian Genome Integrity and Development. Cell *149*.

Rena, G., Bain, J., Elliott, M., and Cohen, P. (2004). D4476, a cell-permeant inhibitor of CK1, suppresses the site-specific phosphorylation and nuclear exclusion of FOXO1a. Embo Reports *5*, 60-65.

Reya, T., and Clevers, H. (2005). Wnt signalling in stem cells and cancer. Nature *434*, 843-850.

Reynolds, J.J., Walker, A.K., Gilmore, E.C., Walsh, C.A., and Caldecott, K.W. (2012). Impact of PNKP mutations associated with microcephaly, seizures and developmental delay on enzyme activity and DNA strand break repair. Nucleic Acids Research *40*, 6608-6619.

Reyon, D., Tsai, S.Q., Khayter, C., Foden, J.A., Sander, J.D., and Joung, J.K. (2012). FLASH assembly of TALENs for high-throughput genome editing. Nat Biotechnol *30*, 460-465.

Rice, G.I., Duany, Y.D., Jenkinson, E.M., Forte, G.M.A., Anderson, B.H., Ariaudo, G., Bader-Meunier, B., Baildam, E.M., Battini, R., Beresford, M.W.*, et al.* (2014). Gain-of-function mutations in IFIH1 cause a spectrum of human disease phenotypes associated with upregulated type I interferon signaling. Nature Genetics *46*, 503-509.

Rihel, J., and Schier, A.F. (2012). Behavioral screening for neuroactive drugs in zebrafish. Developmental Neurobiology *72*, 373-385.

Robberecht, W. (2000). Oxidative stress in amyotrophic lateral sclerosis. Journal of Neurology *247*, 1-6.

Roberts, B.L., Vanrossem, A., and Dejager, S. (1992). THE INFLUENCE OF CEREBELLAR LESIONS ON THE SWIMMING PERFORMANCE OF THE TROUT. Journal of Experimental Biology *167*, 171-178.

Robu, M.E., Larson, J.D., Nasevicius, A., Beiraghi, S., Brenner, C., Farber, S.A., and Ekker, S.C. (2007). p53 activation by knockdown technologies. Plos Genetics *3*, 787-801.

Rodriguez-Mari, A., Wilson, C., Titus, T.A., Canestro, C., BreMiller, R.A., Yan, Y.L., Nanda, I., Johnston, A., Kanki, J.P., Gray, E.M.*, et al.* (2011). Roles of brca2 (fancd1) in Oocyte Nuclear Architecture, Gametogenesis, Gonad Tumors, and Genome Stability in Zebrafish. Plos Genetics *7*.

Rossi, A., Kontarakis, Z., Gerri, C., Nolte, H., Holper, S., Kruger, M., and Stainier, D.Y.R. (2015). Genetic compensation induced by deleterious mutations but not gene knockdowns. Nature *524*, 230-+.

Rouleau, M., Patel, A., Hendzel, M.J., Kaufmann, S.H., and Poirier, G.G. (2010). PARP inhibition: PARP1 and beyond. Nature Reviews Cancer *10*, 293-301.

Ruhl, T., Jonas, A., Seidel, N.I., Prinz, N., Albayram, O., Bilkei-Gorzo, A., and von der Emde, G. (2016). Oxidation and Cognitive Impairment in the Aging Zebrafish. Gerontology *62*, 47-57.
Rulten, S.L., Fisher, A.E.O., Robert, I., Zuma, M.C., Rouleau, M., Ju, L., Poirier, G., Reina-San-Martin, B., and Caldecott, K.W. (2011). PARP-3 and APLF Function Together to Accelerate Nonhomologous End-Joining. Molecular Cell *41*, 33-45.

Russell, W.L., Kelly, E.M., Hunsicker, P.R., Bangham, J.W., Maddux, S.C., and Phipps, E.L. (1979). SPECIFIC-LOCUS TEST SHOWS ETHYLNITROSOUREA TO BE THE MOST POTENT MUTAGEN IN THE MOUSE. Proceedings of the National Academy of Sciences of the United States of America *76*, 5818-5819.

Rutherford, N.J., Heckman, M.G., DeJesus-Hernandez, M., Baker, M.C., Soto-Ortolaza, A.I., Rayaprolu, S., Stewart, H., Finger, E., Volkening, K., Seeley, W.W.*, et al.* (2012). Length of normal alleles of C9ORF72 GGGGCC repeat do not influence disease phenotype. Neurobiology of Aging *33*.

Rydberg, B., and Lindahl, T. (1982). NON-ENZYMATIC METHYLATION OF DNA BY THE INTRACELLULAR METHYL-GROUP DONOR S-ADENOSYL-L-METHIONINE IS A POTENTIALLY MUTAGENIC REACTION. Embo Journal *1*, 211-216.

Sager, J.J., Bai, Q., and Burton, E.A. (2010). Transgenic zebrafish models of neurodegenerative diseases. Brain Structure & Function *214*, 285-302.

Samaee, S.M., Seyedin, S., and Varga, Z.M. (2017). An Affordable Intraperitoneal Injection Setup for Juvenile and Adult Zebrafish. Zebrafish *14*, 77-79.

Sambrook, J., and Russell, D.W. (2001). Molecular cloning : a laboratory manual (Cold Spring Harbor, N.Y.: Cold Spring Harbor Laboratory Press).

Sancar, A. (2003). Structure and function of DNA photolyase and cryptochrome blue-light photoreceptors. Chem Rev *103*, 2203-2237.

Sander, J.D., Dahlborg, E.J., Goodwin, M.J., Cade, L., Zhang, F., Cifuentes, D., Curtin, S.J., Blackburn, J.S., Thibodeau-Beganny, S., Qi, Y.*, et al.* (2011). Selection-free zinc-finger-nuclease engineering by context-dependent assembly (CoDA). Nat Methods *8*, 67-69.

Santhakumar, K., Judson, E.C., Elks, P.M., McKee, S., Elworthy, S., van Rooijen, E., Walmsley, S.S., Renshaw, S.A., Cross, S.S., and van Eeden, F.J. (2012). A zebrafish model to study and therapeutically manipulate hypoxia signaling in tumorigenesis. Cancer Res *72*, 4017-4027.

Sarkander, H.I., and Dulce, H.J. (1978). STUDIES ON REGULATION OF RNA-SYNTHESIS IN NEURONAL AND GLIAL NUCLEI ISOLATED FROM RAT-BRAIN. Experimental Brain Research *31*, 317-327.

Sarkander, H.I., and Uthoff, C.G. (1976). COMPARISON OF NUMBER OF RNA INITIATION SITES IN RAT-BRAIN FRACTIONS ENRICHED IN NEURONAL OR GLIAL NUCLEI. Febs Letters *71*, 53-56.

Sarno, S., Vaglio, P., Meggio, F., Issinger, O.G., and Pinna, L.A. (1996). Protein kinase CK2 mutants defective in substrate recognition - Purification and kinetic analysis. Journal of Biological Chemistry *271*, 10595-10601.

Sasagawa, S., Nishimura, Y., Kon, T., Yamanaka, Y., Murakami, S., Ashikawa, Y., Yuge, M., Okabe, S., Kawaguchi, K., Kawase, R*., et al.* (2016). DNA Damage Response Is Involved in the Developmental Toxicity of Mebendazole in Zebrafish Retina. Frontiers in Pharmacology *7*.

Schmid, B., Hruscha, A., Hogl, S., Banzhaf-Strathmann, J., Strecker, K., van der Zee, J., Teucke, M., Eimer, S., Hegermann, J., Kittelmann, M*., et al.* (2013). Loss of ALS-associated TDP-43 in zebrafish causes muscle degeneration, vascular dysfunction, and reduced motor neuron axon outgrowth. Proc Natl Acad Sci U S A *110*, 4986-4991.

Schoenfeld, A.R., Apgar, S., Dolios, G., Wang, R., and Aaronson, S.A. (2004). BRCA2 is ubiquitinated in vivo and interacts with USP11, a deubiquitinating enzyme that exhibits prosurvival function in the cellular response to DNA damage. Molecular and Cellular Biology *24*, 7444-7455.

Schottlaender, L.V., Polke, J.M., Ling, H.L., MacDoanld, N.D., Tucci, A., Nanji, T., Pittman, A., de Silva, R., Holton, J.L., Revesz, T*., et al.* (2015). The analysis of C9orf72 repeat expansions in a large series of clinically and pathologically diagnosed cases with atypical parkinsonism (vol 36, 1221.e1, 2015). Neurobiology of Aging *36*, 1768-1768.

Setini, A., Pierucci, F., Senatori, O., and Nicotra, A. (2005). Molecular characterization of monoamine oxidase in zebrafish (Danio rerio). Comparative Biochemistry and Physiology Part B: Biochemistry and Molecular Biology *140*, 153-161.

Shaban, N.M., Harvey, S., Perrino, F.W., and Hollis, T. (2010). The structure of the mammalian RNase H2 complex provides insight into RNA:DNA hybrid processing to prevent immune dysfunction. Faseb Journal *24*.

Shen, J., Gilmore, E.C., Marshall, C.A., Haddadin, M., Reynolds, J.J., Eyaid, W., Bodell, A., Barry, B., Gleason, D., Allen, K*., et al.* (2010). Mutations in PNKP cause microcephaly, seizures and defects in DNA repair. Nat Genet *42*, 245-249.

Shiloh, Y. (2003). ATM and related protein kinases: Safeguarding genome integrity. Nature Reviews Cancer *3*, 155-168.

Silva, I.A.L., Cancela, M.L., and Conceicao, N. (2012). Molecular cloning and expression analysis of xpd from zebrafish (Danio rerio). Molecular Biology Reports *39*, 5339-5348.

Simsek, D., and Jasin, M. (2010). Alternative end-joining is suppressed by the canonical NHEJ component Xrcc4-ligase IV during chromosomal translocation formation. Nature Structural & Molecular Biology *17*, 410-U443.

Sinha, R.P., and Hader, D.P. (2002). UV-induced DNA damage and repair: a review. Photochemical & Photobiological Sciences *1*, 225-236.

Sliwinska, A., Sitarek, P., Toma, M., Czarny, P., Synowiec, E., Krupa, R., Wigner, P., Bialek, K., Kwiatkowski, D., Korycinska, A.*, et al.* (2017). Decreased expression level of BER genes in Alzheimer's disease patients is not derivative of their DNA methylation status. Prog Neuropsychopharmacol Biol Psychiatry *79*, 311-316.

Songyang, Z., Lu, K.P., Kwon, Y.T., Tsai, L.H., Filhol, O., Cochet, C., Brickey, D.A., Soderling, T.R., Bartleson, C., Graves, D.J.*, et al.* (1996). A structural basis for substrate specificities of protein Ser/Thr kinases: Primary sequence preference of casein kinases I and II, NIMA, phosphorylase kinase, calmodulin-dependent kinase II, CDK5, and Erk1. Molecular and Cellular Biology *16*, 6486-6493.

Sordet, O., Redon, C.E., Guirouilh-Barbat, J., Smith, S., Solier, S., Douarre, C., Conti, C., Nakamura, A.J., Das, B.B., Nicolas, E.*, et al.* (2009). Ataxia telangiectasia mutated activation by transcription- and topoisomerase I-induced DNA double-strand breaks. Embo Reports *10*, 887-893.

Stainier, D.Y., Fouquet, B., Chen, J.N., Warren, K.S., Weinstein, B.M., Meiler, S.E., Mohideen, M.A., Neuhauss, S.C., Solnica-Krezel, L., Schier, A.F.*, et al.* (1996). Mutations affecting the formation and function of the cardiovascular system in the zebrafish embryo. Development *123*, 285-292.

Steffan, J.S., Bodai, L., Pallos, J., Poelman, M., McCampbell, A., Apostol, B.L., Kazantsev, A., Schmidt, E., Zhu, Y.Z., Greenwald, M.*, et al.* (2001). Histone deacetylase inhibitors arrest polyglutamine-dependent neurodegeneration in Drosophila. Nature *413*, 739-743.

Stemple, D.L. (2004). TILLING - a high-throughput harvest for functional genomics. Nature Reviews Genetics *5*, 145-U119.

Stetson, D.B., Ko, J.S., Heidmann, T., and Medzhitov, R. (2008). Trex1 prevents cell-intrinsic initiation of autoimmunity. Cell *134*, 587-598.

Stewart, A.M., Braubach, O., Spitsbergen, J., Gerlai, R., and Kalueff, A.V. (2014). Zebrafish models for translational neuroscience research: from tank to bedside. Trends in Neurosciences *37*, 264-278.

Stingele, J., Schwarz, M.S., Bloemeke, N., Wolf, P.G., and Jentsch, S. (2014). A DNA-Dependent Protease Involved in DNA-Protein Crosslink Repair. Cell *158*, 327-338.

Stoll, G., Pietilainen, O.P.H., Linder, B., Suvisaari, J., Brosi, C., Hennah, W., Leppa, V., Torniainen, M., Ripatti, S., Ala-Mello, S.*, et al.* (2013). Deletion of TOP3beta, a component of FMRP-containing mRNPs, contributes to neurodevelopmental disorders. Nat Neurosci *16*, 1228-1237.

Strahl, B.D., and Allis, C.D. (2000). The language of covalent histone modifications. Nature *403*, 41-45.

Strumberg, D., Pilon, A.A., Smith, M., Hickey, R., Malkas, L., and Pommier, Y. (2000). Conversion of topoisomerase 1 cleavage complexes on the leading strand of ribosomal DNA into 5 '-phosphorylated DNA double-strand breaks by replication runoff. Molecular and Cellular Biology *20*, 3977-3987.

Stuart, G.W., McMurray, J.V., and Westerfield, M. (1988). REPLICATION, INTEGRATION AND STABLE GERM-LINE TRANSMISSION OF FOREIGN SEQUENCES INJECTED INTO EARLY ZEBRAFISH EMBRYOS. Development *103*, 403-412.

Sturtz, L.A., Diekert, K., Jensen, L.T., Lill, R., and Culotta, V.C. (2001). A fraction of yeast Cu,Zn-superoxide dismutase and its metallochaperone, CCS, localize to the intermembrane space of mitochondria - A physiological role for SOD1 in guarding against mitochondrial oxidative damage. Journal of Biological Chemistry *276*, 38084-38089.

Sun, Y., Zhang, G., He, Z.Z., Wang, Y.J., Cui, J.L., and Li, Y.H. (2016). Effects of copper oxide nanoparticles on developing zebrafish embryos and larvae. International Journal of Nanomedicine *11*, 905-918.

Suster, M.L., Kikuta, H., Urasaki, A., Asakawa, K., and Kawakami, K. (2009). Transgenesis in zebrafish with the tol2 transposon system. Methods Mol Biol *561*, 41-63.

Suzuki, H., Watkins, D.N., Jair, K.W., Schuebel, K.E., Markowitz, S.D., Chen, W.D., Pretlow, T.P., Bin, Y., Akiyama, Y., van Engeland, M.*, et al.* (2004). Epigenetic inactivation of SFRP genes allows constitutive WNT signaling in colorectal cancer. Nature Genetics *36*, 417-422.

Swenberg, J.A., Lu, K., Moeller, B.C., Gao, L., Upton, P.B., Nakamura, J., and Starr, T.B. (2011). Endogenous versus Exogenous DNA Adducts: Their Role in Carcinogenesis, Epidemiology, and Risk Assessment. Toxicological Sciences *120*, S130-S145.

Takahashi, H., Hatakeyama, S., Saitoh, H., and Nakayama, K.I. (2005a). Noncovalent SUMO-1 binding act ivity of thymine DNA glycosylase (TDG) is required for its SUMO-1 modification and colocalization with the promyelocytic leukemia protein. Journal of Biological Chemistry *280*, 5611-5621.

Takahashi, N., Dawid, I.B. (2005b). Characterization of zebrafish Rad52 and replication protein A for oligonucleotide-mediated mutagenesis. Nucleic Acids Research *33*.

Takashima, H., Boerkoel, C.F., John, J., Saifi, G.M., Salih, M.A.M., Armstrong, D., Mao, Y.X., Quiocho, F.A., Roa, B.B., Nakagawa, M.*, et al.* (2002). Mutation of TDP1, encoding a topoisomerase I-dependent DNA damage repair enzyme, in spinocerebellar ataxia with axonal neuropathy. Nature Genetics *32*, 267-272.

Tamai, T.K., Vardhanabhuti, V., Foulkes, N.S., and Whitmore, D. (2004). Early embryonic light detection improves survival. In Curr Biol (England), pp. R104-105.

Tatham, M.H., Jaffray, E., Vaughan, O.A., Desterro, J.M.P., Botting, C.H., Naismith, J.H., and Hay, R.T. (2001). Polymeric Chains of SUMO-2 and SUMO-3 Are Conjugated to Protein Substrates by SAE1/SAE2 and Ubc9.

Taylor, J.P., Hardy, J., and Fischbeck, K.H. (2002). Biomedicine - Toxic proteins in neurodegenerative disease. Science *296*, 1991-1995.

Taylor, J.S., Braasch, I., Frickey, T., Meyer, A., and Van de Peer, Y. (2003). Genome duplication, a trait shared by 22000 species of ray-finned fish. Genome Res *13*, 382-390.

Taylor, J.S., Van de Peer, Y., Braasch, I., and Meyer, A. (2001). Comparative genomics provides evidence for an ancient genome duplication event in fish. Philos Trans R Soc Lond B Biol Sci *356*, 1661-1679.

Thermes, V., Grabher, C., Ristoratore, F., Bourrat, F., Choulika, A., Wittbrodt, J., and Joly, J.-S. (2002). I-SceI meganuclease mediates highly efficient transgenesis in fish. Mechanisms of Development *118*, 91-98.

Torres, J., and Pulido, R. (2001). The tumor suppressor PTEN is phosphorylated by the protein kinase CK2 at its C terminus - Implications for PTEN stability to proteasome-mediated degradation. Journal of Biological Chemistry *276*, 993-998.

Tresini, M., Warmerdam, D.O., Kolovos, P., Snijder, L., Vrouwe, M.G., Demmers, J.A., van, I.W.F., Grosveld, F.G., Medema, R.H., Hoeijmakers, J.H.*, et al.* (2015). The core spliceosome as target and effector of non-canonical ATM signalling. Nature *523*, 53-58.

Truong, L., Saili, K.S., Miller, J.M., Hutchison, J.E., and Tanguay, R.L. (2012). Persistent adult zebrafish behavioral deficits results from acute embryonic exposure to gold nanoparticles. Comparative Biochemistry and Physiology C-Toxicology & Pharmacology *155*, 269-274.

Tu, P.H., Raju, P., Robinson, K.A., Gurney, M.E., Trojanowski, J.Q., and Lee, V.M.Y. (1996). Transgenic mice carrying a human mutant superoxide dismutase transgene develop neuronal cytoskeletal pathology resembling human amyotrophic lateral sclerosis lesions. Proceedings of the National Academy of Sciences of the United States of America *93*, 3155-3160.

Turowec, J.P., Duncan, J.S., French, A.C., Gyenis, L., Denis, N.A.S., Vilk, G., and Litchfield, D.W. (2010). PROTEIN KINASE CK2 IS A CONSTITUTIVELY ACTIVE ENZYME THAT PROMOTES CELL SURVIVAL: STRATEGIES TO IDENTIFY CK2 SUBSTRATES AND MANIPULATE ITS ACTIVITY IN MAMMALIAN CELLS. Methods in Enzymology, Volume 484: Constitutive Activity in Receptors and Other Proteins, Part A *484*, 471-493.

Ulrich, H.D. (2008). The Fast-Growing Business of SUMO Chains. Molecular Cell *32*, 301-305.

Valton, J., Dupuy, A., Daboussi, F., Thomas, S., Marechal, A., Macmaster, R., Melliand, K., Juillerat, A., and Duchateau, P. (2012). Overcoming transcription activator-like effector (TALE) DNA binding domain sensitivity to cytosine methylation. J Biol Chem *287*, 38427-38432.

Van Der Schans, G.P. (1978). Gamma-ray induced double-strand breaks in DNA resulting from randomly-inflicted single-strand breaks: temporal local denaturation, a new radiation phenomenon? Int J Radiat Biol Relat Stud Phys Chem Med *33*, 105-120.

van Gent, D.C., Hoeijmakers, J.H.J., and Kanaar, R. (2001). Chromosomal stability and the DNA double-stranded break connection. Nature Reviews Genetics *2*, 196-206.

Vance, J.R., and Wilson, T.E. (2002). Yeast Tdp1 and Rad1-Rad10 function as redundant pathways for repairing Top1 replicative damage. Proceedings of the National Academy of Sciences of the United States of America *99*, 13669-13674.

Vaz, B., Popovic, M., Newman, J.A., Fielden, J., Aitkenhead, H., Halder, S., Singh, A.N., Vendrell, I., Fischer, R., Torrecilla, I.*, et al.* (2016). Metalloprotease SPRTN/DVC1 Orchestrates Replication-Coupled DNA-Protein Crosslink Repair. Mol Cell *64*, 704-719.

Vierck, J., O'Reilly, B., Hossner, K., Antonio, J., Byrne, K., Bucci, L., and Dodson, M. (2000). Satellite cell regulation following myotrauma caused by resistance exercise. Cell Biology International *24*, 263-272.

Vierstraete, J., Willaert, A., Vermassen, P., Coucke, P.J., Vral, A., and Claes, K.B.M. (2017). Accurate quantification of homologous recombination in zebrafish: brca2 deficiency as a paradigm. Scientific Reports *7*, 16518.

Vilk, G., Saulnier, R.B., St Pierre, R., and Litchfield, D.W. (1999). Inducible expression of protein kinase CK2 in mammalian cells. Evidence for functional specialization of CK2 isoforms. J Biol Chem *274*, 14406-14414.

Virag, L., and Szabo, C. (2002). The therapeutic potential of poly(ADP-ribose) polymerase inhibitors. Pharmacol Rev *54*, 375-429.

Walker, C., Herranz-Martin, S., Karyka, E., Liao, C., Lewis, K., Elsayed, W., Lukashchuk, V., Chiang, S.-C., Ray, S., Mulcahy, P.J.*, et al.* (2017). C9orf72 expansion disrupts ATM-mediated chromosomal break repair. Nat Neurosci *advance online publication*.

Wallace, S.S. (2014). Base excision repair: A critical player in many games. DNA Repair *19*, 14-26.

Wang, G., Rajpurohit, S.K., Delaspre, F., Walker, S.L., White, D.T., Ceasrine, A., Kuruvilla, R., Li, R., Shim, J.S., Liu, J.O.*, et al.* (2015). First quantitative high-throughput screen in zebrafish identifies novel pathways for increasing pancreatic β-cell mass. In eLife.

Wang, Q.E., Zhu, Q.Z., Wani, G., El-Mahdy, M.A., Li, J.Y., and Wani, A.A. (2005). DNA repair factor XPC is modified by SUMO-1 and ubiquitin following UV irradiation. Nucleic Acids Research *33*, 4023-4034.

Wang, Y., Shupenko, C.C., Melo, L.F., and Strauss, P.R. (2006). DNA repair protein involved in heart and blood development. Molecular and Cellular Biology *26*, 9083-9093.

Watanabe, K., Nishimura, Y., Oka, T., Nomoto, T., Kon, T., Shintou, T., Hirano, M., Shimada, Y., Umemoto, N., Kuroyanagi, J.*, et al.* (2010). In vivo imaging of zebrafish retinal cells using fluorescent coumarin derivatives. In BMC Neurosci, p. 116.

Watchon, M., Yuan, K.C., Mackovski, N., Svahn, A.J., Cole, N.J., Goldsbury, C., Rinkwitz, S., Becker, T.S., Nicholson, G.A., and Laird, A.S. (2017). Calpain Inhibition Is Protective in Machado-Joseph Disease Zebrafish Due to Induction of Autophagy. Journal of Neuroscience *37*, 7782-7794.

Weisiger, R.A., and Fridovich, I. (1973). MITOCHONDRIAL SUPEROXIDE DISMUTASE - SITE OF SYNTHESIS AND INTRAMITOCHONDRIAL LOCALIZATION. Journal of Biological Chemistry *248*, 4793-4796.

Weissman, L., Jo, D.G., Sørensen, M.M., de Souza-Pinto, N.C., Markesbery, W.R., Mattson, M.P., and Bohr, V.A. (2007). Defective DNA base excision repair in brain from individuals with Alzheimer's disease and amnestic mild cognitive impairment. Nucleic Acids Res *35*, 5545-5555.

Wells, O.S. (2014). Cellular and Biochemical Analyses of TDP1 mediated chromosomal break repair. In Biochemistry Department (University of Sussex).

Whitehouse, C.J., Taylor, R.M., Thistlethwaite, A., Zhang, H., Karimi-Busheri, F., Lasko, D.D., Weinfeld, M., and Caldecott, K.W. (2001). XRCC1 stimulates human polynucleotide kinase activity at damaged DNA termini and accelerates DNA single-strand break repair. Cell *104*, 107-117.

Wienholds, E., van Eeden, F., Kosters, M., Mudde, J., Plasterk, R.H., and Cuppen, E. (2003). Efficient target-selected mutagenesis in zebrafish. Genome Res *13*, 2700-2707.

Wiltshire, T.D., Lovejoy, C.A., Wang, T., Xia, F., O'Connor, M.J., and Cortez, D. (2010). Sensitivity to Poly(ADP-ribose) Polymerase (PARP) Inhibition Identifies Ubiquitin-specific Peptidase 11 (USP11) as a Regulator of DNA Double-strand Break Repair. Journal of Biological Chemistry *285*, 14565-14571.

Wood, A.J., Lo, T.W., Zeitler, B., Pickle, C.S., Ralston, E.J., Lee, A.H., Amora, R., Miller, J.C., Leung, E., Meng, X.*, et al.* (2011a). Targeted genome editing across species using ZFNs and TALENs. Science *333*, 307.

Wood, L.M., Sankar, S., Reed, R.E., Haas, A.L., Liu, L.F., McKinnon, P., and Desai, S.D. (2011b). A Novel Role for ATM in Regulating Proteasome-Mediated Protein Degradation through Suppression of the ISG15 Conjugation Pathway. Plos One *6*.

Worgul, B.V., Smilenov, L., Brenner, D.J., Junk, A., Zhou, W., and Hall, E.J. (2002). Atm heterozygous mice are more sensitive to radiation-induced cataracts than are their wild-type counterparts. Proceedings of the National Academy of Sciences of the United States of America *99*, 9836-9839.

Wright, G.J., Leslie, J.D., Ariza-McNaughton, L., and Lewis, J. (2004). Delta proteins and MAGI proteins: an interaction of Notch ligands with intracellular scaffolding molecules and its significance for zebrafish development. Development *131*, 5659-5669.

Wu, H.Y., Shyy, S., Wang, J.C., and Liu, L.F. (1988). TRANSCRIPTION GENERATES POSITIVELY AND NEGATIVELY SUPERCOILED DOMAINS IN THE TEMPLATE. Cell *53*, 433-440.

Wu, M.G., Guan, J., Li, C., Gunter, S., Nusrat, L., Ng, S., Dhand, K., Morshead, C., Kim, A., and Das, S. (2017). Aberrantly activated Cox-2 and Wnt signaling interact to maintain cancer stem cells in glioblastoma. Oncotarget *8*, 82217-82230.

Wu, X., Feng, J., Komori, A., Kim, E.C., Zan, H., and Casali, P. (2003). Immunoglobulin Somatic Hypermutation: Double-Strand DNA Breaks, AID and Error-Prone DNA Repair. J Clin Immunol *23*, 235-246.

Xie, J., Farage, E., Sugimoto, M., and Anand-Apte, B. (2010). A novel transgenic zebrafish model for blood-brain and blood-retinal barrier development. BMC Dev Biol *10*, 76.

Xu, D., Shen, W., Guo, R., Xue, Y., Peng, W., Sima, J., Yang, J., Sharov, A., Srikantan, S., Fox, D., 3rd*, et al.* (2013). Top3beta is an RNA topoisomerase that works with fragile X syndrome protein to promote synapse formation. Nat Neurosci *16*, 1238-1247.

Yan, Z. (2017). Skeletal Muscle Adaptation and Cell Cycle Regulation. : Exercise and Sport Sciences Reviews.

Yang, M., Hsu, C.-T., Ting, C.-Y., Liu, L.F., and Hwang, J. (2006). Assembly of a Polymeric Chain of SUMO1 on Human Topoisomerase I in Vitro.

Yang, S.H., Jaffray, E., Hay, R.T., and Sharrocks, A.D. (2003). Dynamic interplay of the SUMO and ERK pathways in regulating Elk-1 transcriptional activity. Molecular Cell *12*, 63-74.

Yang, Y.H., Fu, W., Chen, J.D., Olashaw, N., Zhang, X.H., Nicosia, S.V., Bhalla, K., and Bai, W.L. (2007). SIRT1 sumoylation regulates its deacetylase activity and cellular response to genotoxic stress. Nature Cell Biology *9*, 1253-U1280.

Yang, Y.Z., McBride, K.M., Hensley, S., Lu, Y., Chedin, F., and Bedford, M.T. (2014). Arginine Methylation Facilitates the Recruitment of TOP3B to Chromatin to Prevent R Loop Accumulation. Molecular Cell *53*, 484-497.

Yaung, S.J., Esvelt, K.M., and Church, G.M. (2014). CRISPR/Cas9-Mediated Phage Resistance Is Not Impeded by the DNA Modifications of Phage T4. In PLoS One.

Yeh, F.L., Wang, S.Y., Hsu, L.Y., Wang, D.Y., and Hsu, T. (2004). Cloning of the mismatch recognition protein MSH2 from zebrafish (Danio rerio) and its developmental stage-dependent mRNA expression. Biochimica Et Biophysica Acta-Gene Structure and Expression *1680*, 129-136.

Yeh, F.L., Yan, H.L., Wang, S.Y., Jung, T.Y., and Hsu, T. (2003). Molecular cloning of zebrafish (Danio rerio) MutS homolog 6(MSH6) and noncoordinate expression of MSH6 gene activity and G-T mismatch binding proteins in zebrafish larvae. Journal of Experimental Zoology Part a-Comparative Experimental Biology *297A*, 118-129.

Yu, L.L., Tucci, V., Kishi, S., and Zhdanova, I.V. (2006). Cognitive Aging in Zebrafish. Plos One *1*.

Yu, M., Liu, K., Mao, Z.B., Luo, J.Y., Gu, W., and Zhao, W.H. (2016). USP11 Is a Negative Regulator to gamma H2AX Ubiquitylation by RNF8/RNF168. Journal of Biological Chemistry *291*, 959-967.

Yu, S.L., Lee, S.K., Johnson, R.E., Prakash, L., and Prakash, S. (2003). The stalling of transcription at abasic sites is highly mutagenic. Molecular and Cellular Biology *23*, 382-388.
Zeng, Z., Richardson, J., Verduzco, D., Mitchell, D.L., and Patton, E.E. (2009). Zebrafish have a competent p53-dependent nucleotide excision repair pathway to resolve ultraviolet B-induced DNA damage in the skin. Zebrafish *6*, 405-415.
Zeng, Z., Sharma, A., Ju, L., Murai, J., Umans, L., Verme
ire, L., Pommier, Y., Takeda, S., Huylebroeck, D., Caldecott, K.W*., et al.* (2012). TDP2 promotes repair of topoisomerase I-mediated DNA damage in the absence of TDP1. Nucleic Acids Research *40*, 8371-8380.

Zhang, D., Iyer, L.M., He, F., and Aravind, L. (2012). Discovery of Novel DENN Proteins: Implications for the Evolution of Eukaryotic Intracellular Membrane Structures and Human Disease. Front Genet *3*, 283.

Zhang, F., Cong, L., Lodato, S., Kosuri, S., Church, G.M., and Arlotta, P. (2011a). Efficient construction of sequence-specific TAL effectors for modulating mammalian transcription. Nat Biotechnol *29*, 149-153.

Zhang, Y.B., Yuan, F.H., Presnell, S.R., Tian, K.L., Gao, Y., Tomkinson, A.E., Gu, L.Y., and Li, G.M. (2005). Reconstitution of 5 '-directed human mismatch repair in a purified system. Cell *122*, 693-705.

Zhang, Y.W., Regairaz, M., Seiler, J.A., Agama, K.K., Doroshow, J.H., and Pommier, Y. (2011b). Poly(ADP-ribose) polymerase and XPF-ERCC1 participate in distinct pathways for the repair of topoisomerase I-induced DNA damage in mammalian cells. Nucleic Acids Research *39*, 3607-3620.

Zhdanova, I.V., Yu, L., Lopez-Patino, M., Shang, E., Kishi, S., and Gueling, E. (2008). Aging of the circadian system in zebrafish and the effects of melatonin on sleep and cognitive performance. Brain Research Bulletin *75*, 433-441.

Zheng, L., Zhou, M., Chai, Q., Parrish, J., Xue, D., Patrick, S.M., Turchi, J.J., Yannone, S.M., Chen, D., and Shen, B.H. (2005). Novel function of the flap endonuclease 1 complex in processing stalled DNA replication forks. Embo Reports *6*, 83-89.

Zhou, T., Akopiants, K., Mohapatra, S., Lin, P.S., Valerie, K., Ramsden, D.A., Lees-Miller, S.P., and Povirk, L.F. (2009). Tyrosyl-DNA phosphodiesterase and the repair of 3 '-phosphoglycolate-terminated DNA double-strand breaks. DNA Repair *8*, 901-911.

Zhou, T., Lee, J.W., Tatavarthi, H., Lupski, J.R., Valerie, K., and Povirk, L.F. (2005). Deficiency in 3′ -phosphoglycolate processing in human cells with a hereditary mutation in tyrosyl-DNA phosphodiesterase (TDP1). Nucleic Acids Research *33*, 289-297.

Ziv, L., Muto, A., Schoonheim, P.J., Meijsing, S.H., Strasser, D., Ingraham, H.A., Schaaf, M.J., Yamamoto, K.R., and Baier, H. (2013). An affective disorder in zebrafish with mutation of the glucocorticoid receptor. Mol Psychiatry *18*, 681-691.